Editors:
Meho Sasa Kovacevic
Lovorka Libric
Mario Bacic

EUROENGEO 2024

Engineering Geology & Geotechnics: Building for the Future

Book of Extended abstracts

4th European regional conference of IAEG

Dubrovnik, Croatia, 8-12 October 2024

Engineering Geology and Geotechnics: Building for the Future

- Book of Extended Abstracts -

4th European Regional Conference of IAEG
Dubrovnik, Croatia, 8-12 October 2024

Editors:
Meho Sasa Kovacevic
Lovorka Libric
Mario Bacic

University of Zagreb, Faculty of Civil Engineering
Zagreb, 2024.

Publisher:

University of Zagreb, Faculty of Civil Engineering, fra Andrije Kačića Miošića 26, Zagreb, Croatia

Editors:

Meho Sasa Kovacevic, Lovorka Libric, Mario Bacic

Conference:

4th European Regional Conference of IAEG (EUROENGEO 2024)

Date and location:

8-12 October 2024, Dubrovnik, Croatia

Organizer:

University of Zagreb, Faculty of Civil Engineering

Croatian Geological Survey

Croatian Geotechnical Society

Croatian Geological Society

Under auspices of:

Ministry of Physical Planning, Construction and State Assets, Republic of Croatia

University of Zagreb, Republic of Croatia

Croatian Academy of Engineering, Republic of Croatia

Organization

CHAIRMEN

Ivan Kosović, Croatian Geological Survey
Lovorka Librić, University of Zagreb, Faculty of Civil Engineering

ORGANIZING COMMITTEE

Meho Saša Kovačević, University of Zagreb, Faculty of Civil Engineering
Danijela Jurić Kaćunić, University of Zagreb, Faculty of Civil Engineering
Lovorka Librić, University of Zagreb, Faculty of Civil Engineering
Mario Bačić, University of Zagreb, Faculty of Civil Engineering
Ivan Kosović, Croatian Geological Survey
Stratis Karantanellis, University of Michigan
Staša Borović, Croatian Geological Survey
Laszlo Podolszki, Croatian Geological Survey
Kosta Urumović, Croatian Geological Survey
Helen Reeves, Jacobs
Janusz Wasowski, National Research Council – Research Institute for Geo-hydrological Protection
Leo Matešić, University of Rijeka, Faculty of Civil Engineering
Alan Vranjković, INA d.d.
Ines Vlahov, INA d.d.
Nikša Marković, IN Stria d.o.o.

Content

Site Investigation and Characterization for Sustainable Infrastructure Development

QUANTIFYING URBAN DAMAGE DUE TO SLOW-MOVING LANDSLIDES: A MULTI-INSTRUMENT AND MULTI-DISCIPLINARY APPROACH 2

SINKHOLE HAZARD ASSESSMENT ON DOLOMITE LAND: A CASE STUDY OF KHUTSONG NORTH, CARLETONVILLE – GAUTENG PROVINCE IN SOUTH AFRICA 5

GEOMECHANICAL CHARACTERIZATION AND GEOTECHNICAL INPUTS FOR SARIÇAY DAM 7

EVALUATION OF THE STABILITY OF THE DIKE SYSTEM OF THE ŠPANIA DOLINA TAILINGS POND, SLOVAKIA 9

INVESTIGATIONS IN MINING PROJECTS – INNOVATION CHALLENGES 11

DESIGN OPTIMIZATION OF PILES IN WEAK CARBONATE ROCKS - A VALUE ENGINEERING CASE STUDY OF DUBAI – UAE 13

CHARACTERISATION OF EMBANKMENT ON SOFT GROUND IN THE NETHERLANDS 15

ABOUT GEOTECHNICAL INVESTIGATIONS OF A SALT DOME IN THE FOUNDATION GROUND OF A MOTORWAY BRIDGE 17

IMPORTANCE OF ENGINEERING GEOLOGICAL INVESTIGATION FOR CONSTRUCTION OF INFRASTRUCTURAL PROJECTS 19

DETECTION OF FRACTURED ZONES AND CAVERNS IN KARST USING GEOPHYSICAL METHODS AT THE LOCATION OF VIZINADA IN ISTRIA 21

SINKHOLE HAVOC TO A STATE OF DISASTER: CASE STUDY INTO A RESETTLEMENT PLAN FOR KHUTSONG NORTH COMMUNITY, GAUTENG PROVINCE – SOUTH AFRICA 23

DEM SUPER-RESOLUTION FOR PHOTOVOLTAIC SITE SUITABILITY ASSESSMENT 25

ASSESSING MECHANICAL PROPERTIES OF QUARTZITIC MATERIALS AND SHEAR BEHAVIOR OF QUARTZITIC JOINTS WITH REFERENCE TO THEIR WEATHERING GRADES 27

IDENTIFICATION OF GOAF AREAS AND DEFORMATION CHARACTERISTICS IN ORDOS 30

UNSTABLE SEEPAGE CHARACTERISTICS OF UNDERLYING SOFT CLAY ASSOCIATED WITH MICROSCOPIC MECHANISM IN RECLAMATION AREA: A CASE STUDY 32

HIGH-SPEED IDENTIFICATION OF COMPLEX DISCONTINUITIES IN LARGE-SCALE ROCK OUTCROPS 34

Engineering Geology and Cultural Heritage Protection

PORE STRUCTURE EVOLUTION IN ANDESITE ROCKS INDUCED BY FREEZE-THAW CYCLES EXAMINED BY NON-DESTRUCTIVE METHODS 39

ROCKFALL HAZARD EVALUATION IN A CULTURAL HERITAGE SITE: CASE STUDY OF AGIA PARASKEVI MONASTERY, MONODENDRI, GREECE 42

ARE OUR MONUMENTS MELTING AWAY? EXPLORING THE IMPACT OF CLIMATE CHANGE ON STONE SURFACE FINISHES OF BELGIAN HERITAGE BUILDINGS 44

CLIMATE CHANGE ADAPTATION AND CULTURAL HERITAGE: THE CASE STUDY OF THE ARCHAEOLOGICAL SITE OF ANCIENT MESSENE, GREECE 48

QUALITATIVE ASSESSMENT OF THE ROCKFALL RISK; CASE STUDY ARCHAEOLOGICAL SITE OF DELPHI, IN GREECE 51

THE VERSAILLES GRAND CANAL: A GEOTECHNICAL ENQUIRY, III 53

STABILITY OF THE HISTORICAL MONUMENTS: THE PHANTOM MENACE? 55

SAFEGUARDING “SHIPWRECK”: ASSESSING ROCKFALL RISKS ON THE WORLD-FAMOUS BEACH IN ZAKYNTHOS ISLAND, GREECE 58

Emerging Technologies and Applications in Engineering Geology and Geotechnics

A NON-PARAMETRIC CHANGE DETECTION METHOD FOR ROCKFALL MONITORING 61

FLUID FLOW CAPABILITY OF INCIPIENT FOLIATION, NATURAL FRACTURE ALONG FOLIATION, AND TENSILE FRACTURES OF SLATE 63

CASE STUDY ON USING OPTICAL SENSORS TO INVESTIGATE GROUNDWATER FLOW VELOCITY AND DIRECTION 65

GEOHYDROLOGICAL MONITORING OF SLOPE USING ADVANCED DISTRIBUTED FIBRE-OPTIC SENSING: FROM LABORATORY STUDY TO FIELD APPLICATIONS 67

ADVANCEMENTS IN LANDSLIDE VOLUME ESTIMATION: INSIGHTS FROM THE 2016 Mw7.8 KAIKOURA EARTHQUAKE 69

REFINING HYDRAULIC CONDUCITIVITY ESTIMATION IN FRACTURED MEDIA USING X-RAY TOMOGRAPHY, DISCRETE FRACTURE NETWORKS AND FLEXIBLE WALL PERMEAMETER 72

Geohazard Assessment and Risk Mitigation for Infrastructure Projects

EMERGENCY MANAGEMENT (MITIGATION, PREPAREDNESS, AND RAPID RESPONSE) OF LANDSLIDE DAM HAZARDS – A REVIEW 75

EVALUATION OF FAILURE TYPES AND EVOLUTION OF A DEEP-SEATED LANDSLIDE, TAICHUNG CITY, TAIWAN 77

ROTENFELS: ANALYSIS OF THE ROCKFALL HAZARD ON THE HIGHEST ROCK FACE NORTH OF THE ALPS 79

LARGE-SCALE LANDSLIDE SUSCEPTIBILITY ZONATION: CLASSIFICATION METHODS AND INFLUENCE ON A FURTHER APPLICATION IN SPATIAL PLANNING SYSTEM 81

REMEDIATION WORKS ON AN ACTIVE LANDSLIDE IN SVÄTÝ ANTON, SLOVAKIA 83

STABILITY ASSESSMENT OF HIGH CLIFF SLOPES IN CARBONATE ROCKS - A CASE STUDY, KINGDOM OF SAUDI ARABIA 85

A GEOTECHNICAL APPROACH FOR ENHANCING THE COASTAL VULNERABILITY INDEX (CVI) METHODOLOGY: APPLICATION IN THE GULF OF PATRAS, GREECE 88

BACK ANALYSIS OF CUT SLOPES ALONG THE FAST TRACK ROAD OF NEPAL 90

IMPACT OF DEEP-SEATED ROCK SLIDES ON INFRASTRUCTURE 92

SFM PHOTOGRAMMETRY FOR ROCKFALL MONITORING AND HAZARD ASSESSMENT ALONG ROAD NETWORKS. THE CASE IN AGRAFA REGION, CENTRAL GREECE 94

LANDSLIDE SUSCEPTIBILITY TO RAINFALL AT A NATIONAL SCALE IN NEPAL WITH EMPHASIS ON EARLY WARNING 96

LANDSLIDE HAZARD MANAGEMENT IN GREECE: THE NATIONAL LANDSLIDE DATABASE AS A MITIGATION TOOL 98

CYCLONE DANIEL'S SCARS: A LANDSLIDE ANALYSIS IN METEORA, GREECE 100

LANDSLIDE MAPPING AND MODEL DEVELOPMENT FROM MULTI-LEVEL REMOTE SENSING TECHNOLOGIES DATA, HRVATSKA KOSTAJNICA CASE STUDY, CROATIA 102

ASSESSING ROCKFALL HAZARDS POST-WILDFIRES: A CASE STUDY IN EVROS, GREECE 104

STREAMLINING ROCKFALL ANALYSIS: A DIGITAL PARADIGM FOR EFFICIENCY, COLLABORATION AND RISK MANAGEMENT 106

GEOMORPHIC EFFECTIVENESS OF FLOOD DISCHARGE AND ITS IMPORTANCE FOR RIVER-BED ENGINEERING CONSTRUCTIONS: A CASE OF THE GODAVARI, INDIA 108

MINING-INDUCED SUBSIDENCE SUSCEPTIBILITY MODELLING OF THE WITWATERSRAND BASIN USING WEIGHTS OF EVIDENCE (WOE) APPROACH IN GIS 111

FOLD-CONTROLLED ROCK SLIDING DETERMINED FROM STRUCTURE AND 2D INSAR PRESENTS A LOW HAZARD: THE CASE OF DUSNJÁRGA, NORTHERN NORWAY 113

AN EVIDENCE BASED APPROACH TO QUANTIFYING GEOLOGICAL UNCERTAINTY 115

Engineering Geology for the Society

GEOLOGICAL ENGINEERING FOR SOCIETAL & SUSTAINABLE DEVELOPMENT----BANGLADESH A CASE STUDY 118

THE INTEGRAL ROLE OF ENGINEERING GEOLOGISTS IN DISASTER RISK COMMUNICATION 120

EXPLORING THE EFFECT OF TEMPERATURE ON A CASCADING HAZARD: PROJECTING THE 2021 MELAMCHI FLOOD TO A WARMER CLIMATE 123

LABORATORY RAINFALL TEST ON PISTON FLOW PHENOMENA INVOLVING PORE AIR PRESSURE IN LANDSLIDE MASS 125

RESILIENCE 127

FAILURE MECHANISMS OF SOFT ROCK CLIFFS DUE TO SEA WAVE MOTION: A NUMERICAL INSIGHT 129

THE IMPORTANCE OF TOPOGRAPHIC POSITION ON LANDSLIDE FORMATION NEAR KUTINA 131

ENGINEERING GEOLOGY FOR THE SOCIETY: EXAMPLES FROM ZAGREB CITY AREA, CROATIA 133

INTEGRATION OF LOCAL RELIEF INTO SMALL-SCALE LANDSLIDE SUSCEPTIBILITY MAPPING 135

ENGINEERING GEOLOGY: A CORNERSTONE OF INFRASTRUCTURAL AND ECONOMIC ADVANCEMENT IN ALGERIA 137

Geological and Geotechnical Challenges in Urban Development and Construction

COASTAL AREAS UNDER THE THREAT OF LAND SUBSIDENCE AND FLOODING - THE CASES OF MESSOLONGHI AND AITOLIKON, GREECE 140

EVALUATING THE EFFECTIVENESS OF LANDSLIDE MITIGATION MEASURES USING MCDA METHODS AND SNAP SOFTWARE 142

EXPERIMENTAL METHOD FOR TESTING THIXOTROPIC PROPERTIES OF SOILS 144

OPTIMIZING URBAN MANAGEMENT, PLANNING, AND RESILIENCE THROUGH AN ENGINEERING GEOLOGICAL DATABASE: THESSALONIKI'S EXPERIENCE 146

FORMATION OF TALUS DEPOSITS IN SOFT ROCK MASS AND ITS IMPACT TO INFRASTRUCTURE: SOME EXAMPLES OF LOW COST MITIGATION MEASURES 148

INIO – A GLOBAL INSAR SERVICE, PROVIDING GEOTECHNICAL ANALYSIS FROM SPACE 150

Environmental Geology and Geotechnical Engineering for Natural Resource Management

EXPERIMENTAL STUDY ON TURBIDITY CURRENTS TRANSPORTING MICROPLASTICS IN DIFFERENT CANYON TOPOGRAPHIES 154

MULTI-HAZARD ASSESSMENT OF SOIL EROSION AND LANDSLIDE SUSCEPTIBILITY IN THE DRAINAGE BASIN OF THE PINIOS DAM IN GREECE 156

DAMAGE EVOLUTION OF GRANITE-ENCASED- CONCRETE STRUCTURE UNDER STEPWISE CYCLIC TRIAXIAL LOADING 158

HYDROGEOCHEMICAL MODELLING OF $CaCO_3$ SCALING FROM THE SERPENTINIZATION-DRIVEN HYPERALKALINE SRPINGS 160

INVESTIGATION OF THE ABSORBING PROPERTIES OF MODIFIED SANDY SOIL TO CREATE A GEOCHEMICAL BARRIER FOR STORAGE LANDFILLS MUNICIPAL SOLID WASTE 163

DISTRICT-SCALE SEASONAL UNDERGROUND THERMAL ENERGY STORAGE: CHALLENGES AND OPPORTUNITIES IN THE CZECH REPUBLIC 165

Advances in Geological Modelling for Engineering Applications

COMBINED IMPACT OF INHERENT AND STRESS-INDUCED ANISOTROPY ON ROCK PERMEABILITY AND SLOPE STABILITY: ODA'S EQUATION SOLUTION AND FLAC3D SIMULATION ANALYSIS 168

MULTI-TEMPORAL EVALUATION OF LANDSLIDES IN A DAM RESERVOIR AREA WITH THE INTEGRATION OF MULTIPLE METHODS 170

3D-NUMERICAL SIMULATION OF GEOMECHANICAL FRACTURE PROCESSES IN THE VICINITY OF DEEP GEOTHERMAL DRILLINGS IN SE BAVARIA, GERMANY 172

VIRTUAL OUTCROP RECONSTRUCTION FOR HYDROGEOLOGICAL PARAMETRIZATION (DARUVAR, CROATIA) 174

SURFACE GEOPHYSICAL INVESTIGATION OF NATURAL THERMAL SPRING AREA IN DARUVAR, CROATIA 176

3D RANDOM FIELD MODELLING OF SUBSURFACE STRATIGRAPHY AND GEOTECHNICAL PARAMETERS IN THE TAIPEI BASIN: IMPLICATIONS FOR MAPPING V_{S30} 178

FROM DATA TO DEPTHS: A JOURNEY INTO 3D GEOLOGICAL MODELLING 181

Geo-Aspects of Earthquake Engineering

DETAILED STUDY OF A LATERAL SPREADING FOLLOWING THE 2020 PETRINJA EARTHQUAKE (MW = 6.4) - KUPA RIVER (CROATIA) 184

MACROSEISMIC DATA TO CHARACTERIZE LOCALIZED TOPOGRAPHICAL DAMAGE PATTERNS IN NORTHERN CROATIA AFTER 2020 ZAGREB AND PETRINJA EARTHQUAKES 186

ACCOUNTING FOR SITE EFFECTS IN THE ASSESSMENTS OF SUSCEPTIBILITY TO CO-SEISMIC SLOPE FAILURES IN HILLTOP TOWNS OF THE SOUTHERN APENNINES 188

ASSESSING THE LIQUEFACTION EJECTA POTENTIAL BASED ON CPTu; CASE STUDY PINIADA VALLEY, GREECE 190

NATIONAL SCALE EARTHQUAKE SUSCEPTIBILITY MAPPING UTILIZING EXPLAINABLE ARTIFICIAL INTELLIGENCE IN THE NEPAL HIMALAYA 192

A GEOLOGICAL AND GEOPHYSICAL INTERPRETATION OF GRAVEL LIQUEFACTION SITE EFFECTS FOLLOWING THE Mw 6.4 PETRINJA (CROATIA) EARTHQUAKE 194

In the Path of Progress AI Innovations in Landslide and Engineering Geological Research

ON THE DEEP-SEATED BEDROCK LANDSLIDE TRIGGERED BY THE 2018 HOKKAIDO EASTERN IBURI EARTHQUAKE: A CASE STUDY 198

POINT CLOUDS AND MACHINE LEARNING IN ROCK SLOPE MODELING 200

EFFECTIVE ROCKFALL RISK MITIGATION TECHNIQUES BASED ON DIACHRONIC CLOSE-RANGE REMOTE SENSING DATASETS. CASE STUDY: KALYMNOS ISL. WORLD-RENOWNED CLIMBING TERRAIN (GREECE) 202

UNVEILING COASTAL CLIFF VULNERABILITIES BY INTEGRATING LIDAR, UAS, AND AI TECHNOLOGIES. CASE STUDY: NAVAGIO SHIPWRECK BEACH, ZAKYNTHOS (GREECE) 204

ADVANCING LANDSLIDE MAPPING: INTEGRATING MACHINE LEARNING AND OBJECT-BASED ANALYSIS WITH UAV-DERIVED DATA 206

ENVIRONMENTAL SEISMOLOGY WITH AI 208

Topic 1

Site Investigation and Characterization for Sustainable Infrastructure Development

QUANTIFYING URBAN DAMAGE DUE TO SLOW-MOVING LANDSLIDES: A MULTI-INSTRUMENT AND MULTI-DISCIPLINARY APPROACH

DAVIDE NOTTI[1], MARTINA CIGNETTI[1], DAVIDE CARDONE[1], DARIO PEDUTO[2], GIANFRANCO NICODEMO[2], DAVIDE LUONGO[2], ROSSELLA BOVOLENTA[3], BIANCA FEDERICI[3], DIEGO REALE[4], SIMONA VERDE[4], FABIANA CALÒ[4], EUGENIO SANSOSTI[4], GIANFRANCO FORNARO[4], DANIELE GIORDAN[1]

[1] *National Research Council of Italy, Research Institute for Geo-Hydrological Protection (CNR-IRPI),Torino, Italy, daniele.giordan@irpi.cnr.it*

[2] *Department of Civil Engineering, University of Salerno, Fisciano, Italy, dpeduto@unisa.it*

[3] *Department of Civil, Chemical and Environmental Engineering, University of Genova, Genova, Italy, rossella.bovolenta@unige.it*

[4] *National Research Council of Italy, Institute for Electromagnetic Sensing of the Environment (CNR-IREA), Napoli, Italy, fornaro.g@irea.cnr.it*

Introduction

Slow-moving landslides are impactful phenomena in mountainous regions, affecting buildings and infrastructure with critical economic and social consequences. Nowadays, the use of integrative approaches is increasing to obtain a comprehensive assessment of these complex phenomena, as well as the evaluation of their impact (Cardone et al., 2023; Notti et al., 2021; Peduto et al., 2018). This strategy allows for a proper definition of risk mitigation policies, ensuring the safety of citizens and urban areas (Cignetti et al., 2022; Peduto et al., 2021). In this context, we introduce a methodology to temporally and spatially characterize large slow-moving landslides and assess the related evolution and impact on anthropic elements, through the combined analysis of multi-source and multi-sensor data. We apply this methodology to Mendatica, Arroscia Valley (Ligurian Alps, northwestern Italy), affected by large relict and dormant landslides, with an active landslide portion impacting the village (Pepe et al., 2021). By exploiting the progressive installation of on-site instruments associated with SAR data processing and damage level investigation on buildings, we operated an overall historical reconstruction of the evolution of this slow-movement phenomenon and related impact.

Methodology

The proposed methodology consists of a multi-instrument and multi-disciplinary approach that merges geological-geomorphological ancillary data, on-site instruments measurements, satellite monitoring and building damage survey to improve the comprehension of the relation between the morphology and kinematics of landslides and the induced effects on the built-up environment (Figure 1).

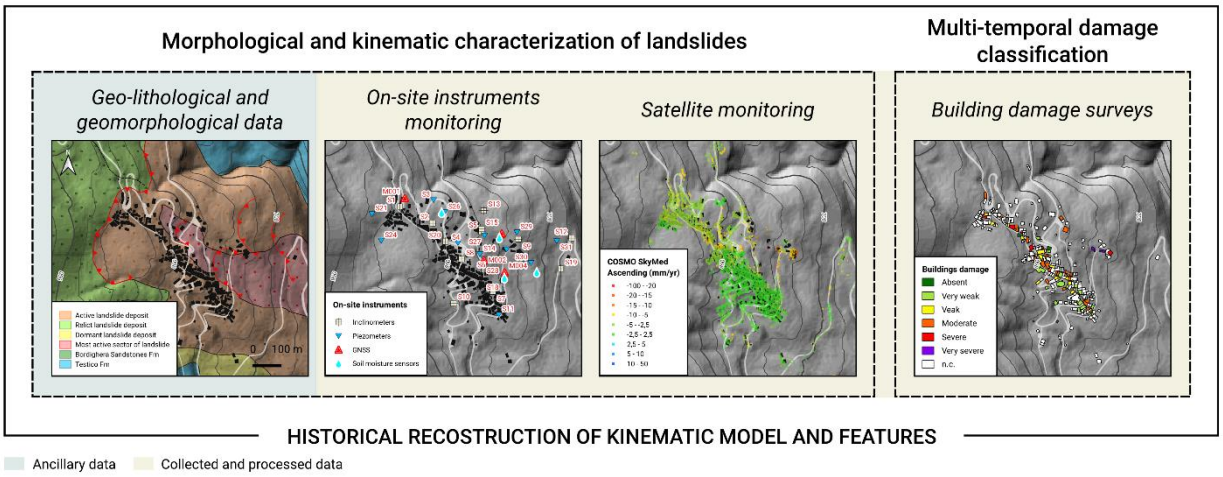

Figure 1. Outline of the materials and methodology used.

An investigation and collection of multi-source and multi-temporal data was carried out. Ancillary data were derived from national and regional web-portals (Federici et al., 2007; Trigila et al., 2008). In situ monitoring data, i.e., soil moisture measures (Bovolenta et al., 2020), borehole data (inclinometer and piezometer), and GNSS were analysed. An integration with SAR satellite images collected, processed and interpreted, including the multi-frequency SAR data (X-, C- and L-bands) and multi-temporal ranging in 2014-2022 (Noviello et al., 2020), has been carried out. A damage severity map was obtained from a field survey of buildings and infrastructures. Damage severity classification was performed using a ranking scale of five classes, ranging from 0 (negligible damage) to 5 (very severe damage) (Peduto et al., 2017). The kinematic characterization coupled with damage classification allows us to investigate the influence of landslide movement, allowing a complete reconstruction of its evolution and impact.

Results

Preliminary results reveal that most of the buildings examined during the field survey have negligible damage levels in the portion of the village built on relict/dormant landslides. In contrast, diffuse moderate to severe damage is located in the reactivations in the northeast sector. Buildings with very severe damage are concentrated in the eastern sector of the Mendatica village, which corresponds to the area with the most significant landslide activity. Within this sector, COSMO-SkyMed line-of-sight deformation registered the highest values, exceeding 10 mm/yr. In general, there is a good match between the CSK measurements and the building damage severity levels recorded during the last field survey in May 2023 (Figure 2). Nevertheless, many interacting factors (object of ongoing study) create a heterogeneous damage pattern. Field measurements of soil water content and piezometric level, automatically processed within the LAndslide Monitoring and Predicting (LAMP) system (Viaggio et al., 2022), confirmed critical areas of rain-induced slope instability, especially at Borgata Piano and allowed real-time analysis of landslide susceptibility with which urban damage is related.

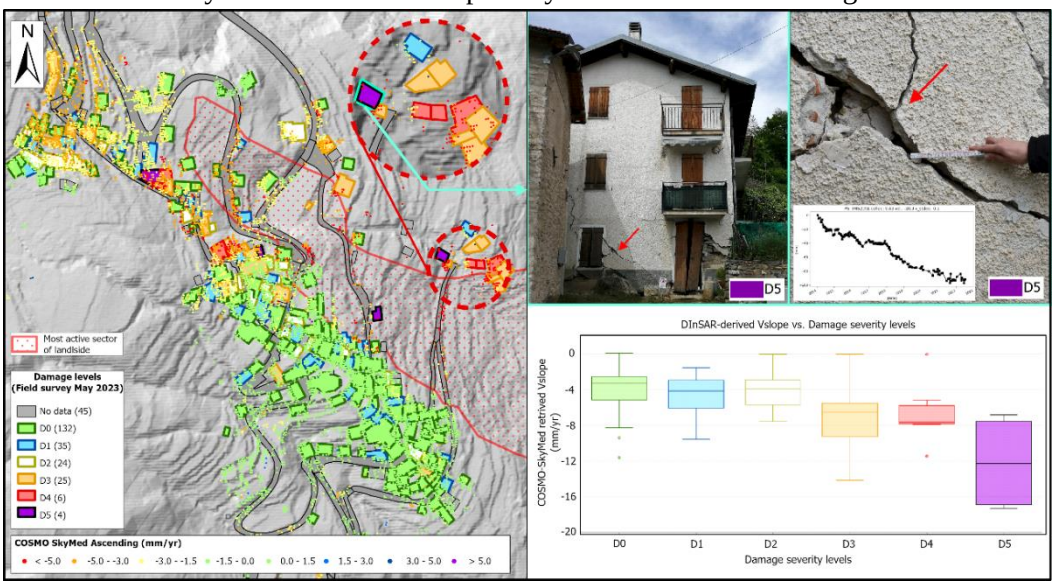

Figure 2. Comparison of damage levels recorded by the field survey and deformation data from CSK ascending geometry.

Conclusion

The multidisciplinary approach proposed is a way to understand better the complex relationship between landslide kinematics and damage to buildings and infrastructure. The coupled information given by the spatial diffuse monitoring given by multi-temporal SAR, combined with in-depth measures (e.g., moisture and inclinometers), is essential for understanding kinematics. At the same time, a detailed and rigorous building damage survey (engineering approach) helps to assess the effect of landslide movement. The same approach could be a model for many slow-moving landslides that affect villages

in many mountain areas, representing a suitable approach in risk assessment and proper land use planning.

References

Bovolenta, R., Iacopino, A., Passalacqua, R., Federici, B., 2020. Field Measurements of Soil Water Content at Shallow Depths for Landslide Monitoring. Geosciences 10, 409. https://doi.org/10.3390/geosciences10100409

Cardone, D., Cignetti, M., Notti, D., Godone, D., Giordan, D., Calò, F., Verde, S., Reale, D., Sansosti, E., Fornaro, G., 2023. Slope-Scale Evolution Categorization of Deep-Seated Slope Deformation Phenomena with Sentinel-1 Data. Remote Sensing 15, 5440. https://doi.org/10.3390/rs15235440

Cignetti, M., Godone, D., Notti, D., Zucca, F., Meisina, C., Bordoni, M., Pedretti, L., Lanteri, L., Bertolo, D., Giordan, D., 2022. Damage to anthropic elements estimation due to large slope instabilities through multi-temporal A-DInSAR analysis. Natural Hazards 1–30. https://doi.org/10.1007/S11069-022-05655-7/FIGURES/15

Federici, P.R., Chelli, A., Biagioni, F., Rapetti, F., 2007. Atlante dei centri abitati instabili della Liguria - IV Provincia di Imperia. Regione Liguria pag. 163.

Notti, D., Wrzesniak, A., Dematteis, N., Lollino, P., Fazio, N.L., Zucca, F., Giordan, D., 2021. A multidisciplinary investigation of deep-seated landslide reactivation triggered by an extreme rainfall event: a case study of the Monesi di Mendatica landslide, Ligurian Alps. Landslides 18, 2341–2365. https://doi.org/10.1007/s10346-021-01651-3

Noviello, C., Peduto, D., Verde, S., Zamparelli, V., Fornaro, G., Pauciullo, A., Reale, D., Nicodemo, G., Ferlisi, S., Gulla, G., 2020. Monitoring Buildings at Landslide Risk With SAR: A Methodology Based on the Use of Multipass Interferometric Data. IEEE Geoscience and Remote Sensing Magazine 8, 91–119. https://doi.org/10.1109/MGRS.2019.2963140

Peduto, D., Ferlisi, S., Nicodemo, G., Reale, D., Pisciotta, G., Gullà, G., 2017. Empirical fragility and vulnerability curves for buildings exposed to slow-moving landslides at medium and large scales. Landslides 14, 1993–2007. https://doi.org/10.1007/s10346-017-0826-7

Peduto, D., Nicodemo, G., Caraffa, M., Gullà, G., 2018. Quantitative analysis of consequences to masonry buildings interacting with slow-moving landslide mechanisms: a case study. Landslides 15, 2017–2030. https://doi.org/10.1007/s10346-018-1014-0

Peduto, D., Santoro, M., Aceto, L., Borrelli, L., Gullà, G., 2021. Full integration of geomorphological, geotechnical, A-DInSAR and damage data for detailed geometric-kinematic features of a slow-moving landslide in urban area. Landslides 18, 807–825. https://doi.org/10.1007/s10346-020-01541-0

Pepe, G., Cevasco, A., Piazza, M., Macciò, R., Arrighetti, F., Casagli, N., 2021. On the efficiency and effectiveness of automatic deep drainage systems during an extreme rainfall event: the Mendatica landslide case study (western Liguria, Italy). Landslides 18, 3799–3820. https://doi.org/10.1007/s10346-021-01740-3

Trigila, A., Iadanza, C., Spizzichino, D., 2008. IFFI Project (Italian landslide inventory) and risk assessment, in: First World Landslide Forum. pp. 18–21.

Viaggio, S., Iacopino, A., Bovolenta, R., Federici, B., 2022. Landslide susceptibility assessment: soil moisture monitoring data processed by an automatic procedure in GIS for 3D description of the soil shear strength. The International Archives of the Photogrammetry, Remote Sensing and Spatial Information Sciences XLVIII-4-W1-2022, 517–523. https://doi.org/10.5194/isprs-archives-XLVIII-4-W1-2022-517-2022

COSMO-SkyMed and SAOCOM images have been provided by ASI under license to use agreements in the framework of the MEFISTO Project (ASI contract n. 2021-10-U.0 CUP F65F21000630005). Product produced from Original SAOCOM Product - ©CONAE – Comisión Nacional de Actividades Espaciales (2021).

SINKHOLE HAZARD ASSESSMENT ON DOLOMITE LAND: A CASE STUDY OF KHUTSONG NORTH, CARLETONVILLE – GAUTENG PROVINCE IN SOUTH AFRICA

SIFISO NGUBELANGA[1], GOODMAN CHILIZA[2], BONGANI MSANE[3], MAKGARI SEBESHO[4]

[1] *Council for Geoscience, South Africa, sngubelanga@geoscience.org.za*

[2] *Council for Geoscience, South Africa, gchiliza@geoscience.org.za*

[3] *Council for Geoscience, South Africa, bmsane@geoscience.org.za*

[4] *Council for Geoscience, South Africa, msebesho@geoscience.org.za*

Introduction

Hazard assessment is a key component within the broader risk analysis process, including the risk analysis for geological hazards. Jennings (1966a) described hazards on dolomite land as taking place in one of two ways, i.e. as a gradual or caving "subsidence" or a rapid and catastrophic subsidence defined as "sinkhole". In his analysis of the problem of building on dolomite, Jennings (1966a) concluded that any structure built on dolomitic subsoil, be it house, office block, industrial plant, road, railway line, dam, etc. might be exposed to danger of subsidence. Variability of ground conditions in karst terrains, nature of earth materials and urbanization are critical factors contributing to the problem.

Increased urbanization of dolomite "karst" land around major metropolitan (City of Ekurhuleni, City of Johannesburg and City of Tshwane) areas of the Gauteng Province, have resulted in densely populated townships like Khutsong, thereby exacerbating the risk posed by dolomite related ground instability events. These events occur primarily due to the loss of roof support and eventual collapse of the final roof arch into subsurface cavities. In South Africa, sinkholes and subsidences do occur, and is mostly ascribed to concentrated ingress of water eroding material into subsurface cavities, or regional groundwater lowering or dewatering resulting in loss of roof support of the cavity (Dippenaar et al., 2019). The frequency and severity of the problem is much increased in areas where the water table is lowered (Jennings et al., 1965), or where it naturally occurs at greater depths.

The greatest challenge in hazard assessment is represented by lack of any data, poor quality or limited availability because only the most destructive events are captured in public media platforms including literature. It is in this context that the research team selected three of the most destructive events for analysis and linked these to the natural setting and influence of the anthropogenic activities to determine (1) the hazard rating and (2) estimate the probability (using a formular by Kirsten *et al.*, 2014) of any sinkhole event causing damage to a house/ building, road and water or sewer pipeline.

Methods

Hazard assessment process requires that complete data sets be available to characterize the identified hazard. Lack of any data, poor quality or limited availability of crucial information in the data set may prohibit a credible hazard assessment process regardless of the adopted method. The method for dolomite land hazard assessment in South Africa is described by Buttrick *et al*., (2001), expanded in Buttrick *et al.,* (2011), and incorporated into the South African National Standard (SANS) 1936. It requires that geological, geotechnical, geophysical and geohydrological data gathered during site investigation be collated and analysed to formulate a perspective on the stability of a dolomite site.

Subsequently, this method requires that a site be zoned in terms of inherent hazard class (IHC – 1 to 8), which is ultimately expressed in three broad inherent hazard categories, i.e. low, medium, and high. Buttrick *et al*., (2001), also defined sinkhole diameter of surface manifestation into four sizes, i.e. small (<2m), medium (2-5m), large (5-15m) and very large (>15m).

Results

The results of the current study and the discernible trends or observation maybe summarized as follows:

- IHC and zonation – the study area is dominated by high hazard with pockets of medium hazard.
- Events distribution and data quality – the study area is dominated by large to very-large (72%) size events and 78% of the sinkhole data lack details on the cause of events.
- Determination of hazard rating – in confirming the hazard zonation, the study area is characterized by over 80% of the events occurring in the high hazard category area.
- Probability of any sinkhole causing damage – the preliminary calculations indicate proportional increase in the *"probability of coincidence"* as well as the *"probability of damage"* with increasing diameter of a circumscribing sinkhole circle.

Data set analysis and insights suggest that the current hazard rating of the study area is *"intolerable"* and housing development is not sustainable.

Conclusion

Quantitative estimations for sinkhole events which occur in the urban environments are critical. One of the most important aspects in the hazard assessment process is data quality, and therefore, lack of data inventory, which is a crucial step in the process, makes it impossible to compile a hazard map. The greatest challenge is access to archives at relevant authorities or when accessed, available data sets are incomplete to allow for credible retrospective analysis and the quantitative estimation of the problem.

If in the future local authorities, private property developers, national agencies (housing, roads, etc.), bulk service providers and individual home/ property owners, are mandated to report all dolomite related ground instability events into a central databank, the risk assessment practitioners and engineering geologists will have a starting point when trying to assess dolomite sinkhole hazard. Therefore, implementation of appropriate risk mitigation measures, legislated basic sinkhole inspection (initial event dimensions, location, date, cause, etc.) and reporting requirements are needed.

References

Alcantara-Ayala, I. Geomorphology, natural hazards, vulnerability and prevention of natural disasters in developing countries. *Geomorphology Volume 47*. Elservier Science (2002), pp 107-124.

Buttrick, D.B.; Van Schalkwyk, A.; Kleywegt, R.J.; Watermeyer, R. Proposed method for dolomite land hazard and risk assessment in South Africa. *South African Institution of Civil Engineering Journal*. Volume 43 (2) 2001, pp 27-36, Paper 462.

Buttrick, D.B.; Trolip, N.Y.G.; Watermeyer, R.B.; Pieterse, N.D.; Gerber, A.G. A performance based approach to dolomite risk management. *Environmental Earth Sciences*. 2011 (64), pp 1127-1138.

Dippennar, M.A.; van Rooy, J.L.; Diamond, R.E. Engineering, hydrogeological and vadose zone hydrological aspects of Proterozoic dolomites (South Africa). *Journal of African Earth Sciences.* Volume 150 (2019), pp 511-521.

Jennings, J.E.; Brink, A.B.A.; Louw, A.; Gowan, G.D. Sinkholes and subsidences in the Transvaal dolomites of South Africa. *Procedures of VI th International Conference on Soil Mechanics & Foundation Engineering*, Montreal. Volume 1/11, 1965, pp 51– 54.

Jennings, J.E. Building on Dolomites in the Transvaal. *South African Institute of Civil Engineering – Commemorative Journal.* Geotechnical Division, February 1966a.

Kirsten, H.A.D.; Heath, G.J.; Venter, I.S.; Oosthuizen, A.C. The issue of personal safety on dolomite: Update of a probability-based evaluation with respect to singlestorey residential houses. *Journal of the South African Institute of Civil Engineering.* Vol 56 No. 2, August 2014, pp 78-87, Paper 719.

South African National Standards. Development of dolomite land – SANS 1936:2012 – PART 1 to 4. *Editions 1 Published by SABS Standards Division.* Pretoria 0001.

GEOMECHANICAL CHARACTERIZATION AND GEOTECHNICAL INPUTS FOR SARIÇAY DAM

GÖRKEM BAŞER[1], AYHAN KOÇBAY[2], YALÇIN ŞENTÜRK[3]

[1] *State Hydraulic Works, Turkey, gorkembaser@dsi.gov.tr*

[2] *State Hydraulic Works, Turkey, akocbay@dsi.gov.tr*

[3] *State Hydraulic Works, Turkey, ysenturk@dsi.gov.tr*

Introduction

In this study, the efforts made to determine the ground strength parameters of Sarıçay Dam will be explained. Sarıçay Dam (western Turkey) is a 125 m high, Roller Compacted Concrete (RCC) dam founded on Precambrian aged gneisses of the Menderes Massive, being built to meet the drinking water needs of the region. In-situ test data and rock mass classification systems were utilized to determine the strength parameters.

Methods

The variety of in-situ test methods provided important data in order to characterize Precambrian aged foundation rock, subjected to tectonic phases and various degrees of metamorphism. Engineering geology map prepared and strength parameters were evaluated via in-situ tests such as Probex Dilatometer, Goodman Jack, seismic refraction and downhole seismic. After ground stripping and removal of alluvium and highly weathered rock in the foundation, mapping and site studies carried out at dam site and it provided important data for the geomechanical modeling.

While creating the geomechanical model, laboratory and in-situ test data and observations on site were evaluated together in order to determine the shear strength and deformation modulus parameters which are the most important input parameters in the static and dynamic design of a concrete dam. The in-situ deformation moduli determined by in-situ tests using loading and unloading behaviour of rock and they evaluated together to suggest input parameters separately for each geomechanical class.

Table 1. Suggested rock mass parameters

Parameter	Right bank	Thalweg	Left bank	Conduit
Angle of internal friction, Φ (°)	38	39	33	33
Cohesion, c (MPa)	700	750	450	500
Deformation modulus (GPa)	2,2	2,5	1,7	2

Results

As a result of the findings; the stripping excavation on the left bank was deepened by approximately 30 m, and the dam face slope was changed to 1H/4V with the revised parameters. In addition, it was decided to perform consolidation grouting at 3 m intervals at a depth of 20 m due to the low strength zones encountered at shallow depths. Due to the changes in dam design and stripping excavation depth, the dam body was lengthened by 40 m and the volume of the dam body increased by 30 percent.

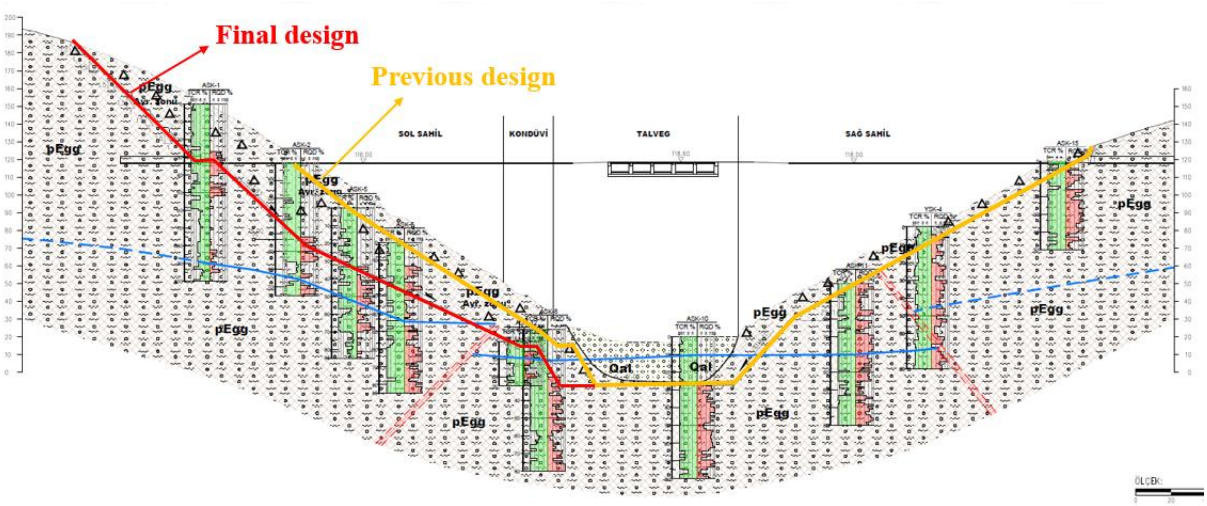

Figure 1. Stripping modification after geomechanical characterization

Conclusion

Metamorphic rocks show heterogeneous structure due to both the effect of metamorphism and intense tectonic movements. Increasing the number of in-situ experiments and the variety of methods in places with such heterogeneous mechanical properties provides important contributions to the classification of geomechanical properties.

EVALUATION OF THE STABILITY OF THE DIKE SYSTEM OF THE ŠPANIA DOLINA TAILINGS POND, SLOVAKIA

MARTIN BEDNARIK[1], RENÉ PUTIŠKA[1], BIBIANA BRIXOVÁ[1], RUDOLF TORNYAI[1], RÓBERT CSIZMADIA[2]

[1]*Comenius University Bratislava, Faculty of Natural Sciences, Department of Engineering Geology, Hydrogeology and Applied Geophysics, Slovakia; mbednarik@uniba.sk*

[2]*GEOFOS, Ltd., Žilina, Slovakia, robert.csizmadia@geofos.sk*

Introduction

In 1983, the tailings pond was in a state of emergency with water seepage and a breach in the stability of the dam. The rehabilitation of the tailings pond consisted of the reconstruction of the drainage system, the construction of an embankment weight bench made from the heap material, the filling of the created lagoon and the construction of additional monitoring probes. The Špania Dolina tailings pond was used from 1977 to 1999 to capture solid substances contained in the wastewater from the flotation treatment plant, which processed several types of raw materials. Initially, it processed copper ores, later Hg ores and finally talc-magnesite raw material. The assessment of the stability of the dam using the deformation method showed the relative strength of the tailings body, with the exception of the stability on the shear surfaces above the dark sludge. As a remedial measure, the berm was drained with a subsurface and surface drainage system and a gravity embankment was constructed. No further drainage systems were constructed until the tailings pond was closed. In 2000, the stability of the tailings dam was assessed as part of its reclamation and the condition of the tailings pond was continuously monitored. In 2021, a comprehensive assessment of the safety elements of the Špania Dolina tailings pond was required, including an assessment of the stability conditions of the dam based on variant stability calculations and the construction of a modern monitoring network (Putiška et al., 2022).

Methods

Geotechnical, engineering geological, drilling, laboratory and geophysical work was undertaken to provide a comprehensive assessment of the stability of the tailings dam system. This work included the installation of inclinometric and piezometric boreholes, dynamic penetration probes (DPP), surface geophysical measurements (electrical resistivity tomography - ERT, seismic refraction tomography - SRT, MASW, electromagnetic induction - EMI) and borehole logging. The condition of the drainage system was assessed using camera surveys and a comprehensive reconnaissance of the area surrounding the sludge pond. In order to assess the influence of the relief on water inflows into the body of the tailings pond, a map of relief slope vectors was created (Fig. 1). Above the level of the tailings pond are the steep slopes of the surrounding hills, forming a relatively large area of the imaginary micro-watershed of the tailings pond plain. On the area of the tailings pond and its surroundings, the inspection revealed several deficiencies regarding the drainage of the tailings pond area and the drainage of water from the surrounding slopes. Due to the saturation of the deposited material with water, seepage of the dam occurs at the level of the foot of the bottom berm of the tailings pond. The occurrence of leaks in the vicinity of drainage measures points to their poor efficiency and the need to dewater the tailings pond.

Results

The stability conditions of the tailings dike system were evaluated based on the q_{dyn} results from the DPP point to a state related to the saturation of the tailings pond during the period of conducting the penetration tests (April 2022). According to the defined criteria, the environment of the embankment system was divided into quasi-homogeneous layers. The first group (red colour) with a q_{dyn} value of 0 to 3 MPa represents an unstable environment, the second group (yellow colour) with a q_{dyn} value of 3 to 7 MPa represents a conditionally stable environment, the third group (green colour) with a q_{dyn} value greater than 7 MPa represents a stable environment (Fig. 2).

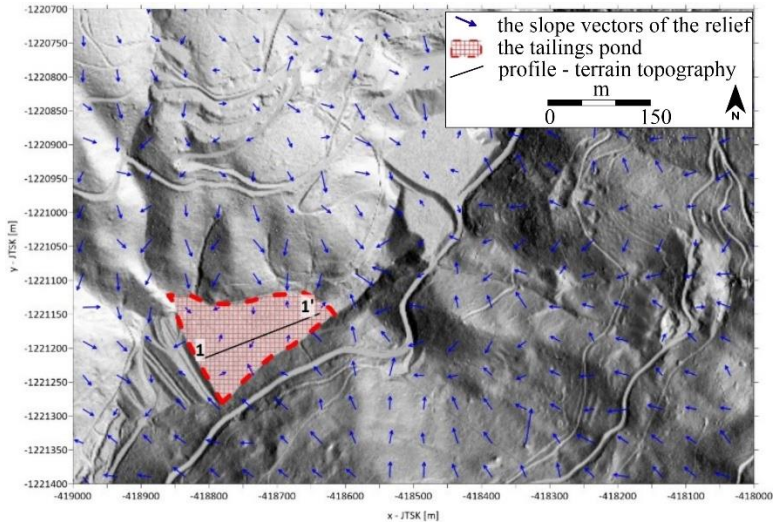

Figure 1. Map of the slope vectors of the relief

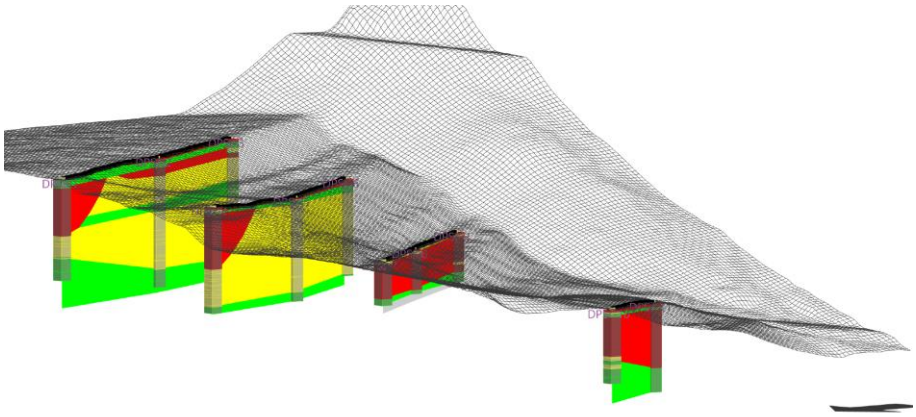

Figure 2. Visualization of continuous q_{dyn}

Conclusion

The results of the monitoring system observations and stability calculations indicate that the saturation of the tailings pond responds to seasonal variations and associated precipitation. This analysis suggests that, under the most unfavourable conditions, the tailings dam system is a system with stable conditions close to equilibrium over virtually its entire length and height. Based on a comprehensive evaluation of the safety elements of the tailings pond, a modern monitoring network has been designed and built with continuous on-line collection of information and warning conditions.

Acknowledgments:

This research was partly funded by the Agency of the Ministry of Education, Science, Research and Sport of the Slovak Republic, VEGA, grant project No. 1/0182/23 "Quantification of landslide risk in urbanized areas of Slovakia threatened by the devastating effects of slope movements" and VEGA 1/0180/24 „Application and evaluation of the results of multifunctional analysis of surface seismic waves (MASW) in geological engineering and geotechnical tasks".

References

Putiška, R., Bednarik, M., Ciszmadia, R., Solčiansky., Jurčák, S., Dostál, I., Brixová, B. *Zhodnotenie bezpečnostných prvkov odkaliska Špania Dolina – nové a možnosti recyklácie uložených banských odpadov. Záverečná správa.* AEGEO, s.r.o., Bratislava, 2022.

INVESTIGATIONS IN MINING PROJECTS – INNOVATION CHALLENGES

MARCIO LEÃO [12], SIMMON SOUZA[1], LUIZ MOTA[1], EDUARDO MARQUES[2]

[1] *Tractebel Engineering, Brazil,* marcio.leao@tractebel.engie.com , simmon.souza@tractebel.engie.com , luiz.mota@tractebel.engie.com

[2] *Federal University of Viçosa, Brazil,* eduardo.marques@ufv.br

Introduction

Geotechnical projects in mining, compared to geotechnical projects in civil engineering, have similar characteristics of data acquisition, such as geological-geotechnical investigations, *in situ* tests, and sampling for laboratory tests. Strategic changes in mining allow basic studies (hydrological, geological, and geotechnical) to occur eventually untimely, creating obstacles to bypassing already disposed materials or constructed structures, and limiting investigation methods, especially at depth. In terms of challenges in the investigation, we can also mention the restriction of the use of pressurized water, the adoption of drilling fluids (when performing permeability studies) and knowledge of their influence on the environment, the tooling composition of the equipment used for deep geotechnical holes, the use of special samplers, the choice of appropriate samples, and the execution of *in situ* tests. Despite good engineering practices guiding procedures in widely known standards, these are not enough for obtaining this information, requiring adjustments or even modifications; however, these alternative techniques must be validated (MARQUES & LEÃO, 2023). This extend abstract discusses the operational methodology of soil infiltration tests using the wireline system as an alternative to the conventional method in deep soils in mining projects in Brazil.

Methods

The methodology was based on the authors' observations in fieldwork and kick-off meetings with drilling service companies, in addition to evaluating the procedure, as an alternative to the conventional method for evaluating the soil permeability test (MARQUES & LEÃO, 2023).

Results

Figure 1 illustrates the permeability test conducted with a non-conventional diameter (BWL). In this representation, it is possible to observe a higher probability of leakage between the outer wall of the BWL rod and the inner wall of the HQ rod. This system is seldom used in engineering projects due to the lack of studies on the application of diameter reductions of *in situ* permeability tests, raising questions about the efficacy of the test and the driving of the rods. It is worth noting that the shoe is formed by a thin cutting piece, approximately 0.8 mm thick, while the annular space between the HQ crown and the BWL is 8 mm. It is also emphasized that due to the absence of rod centralizers and calibrators, there may be non-linearity of the BWL rod, and therefore the results may present uncontrolled variables due to the variation of the perforated space. Moreover, as the hydraulic load of the drilling column increases (as a result of deeper tests), the probability of water return increases.

By physical principle, the size of the contact area is directly proportional to the resistance, meaning that the wider the tool wall, the greater the difficulty of driving the tool without causing wall collapse. In locations without prior knowledge, tests may not be conducted at the desired depth but rather at a deeper position (necessitating telescoping). In stratified materials of thin thickness, this procedure becomes more critical, making it impossible to conduct the test in the section drilled with HQ. Given the absence of technical-scientific studies on the presented methodology, it is not possible to assess the influence of subsurface variables or the procedure itself.

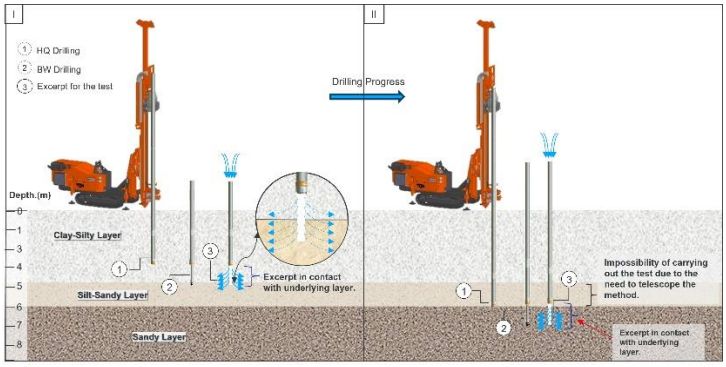

(a)

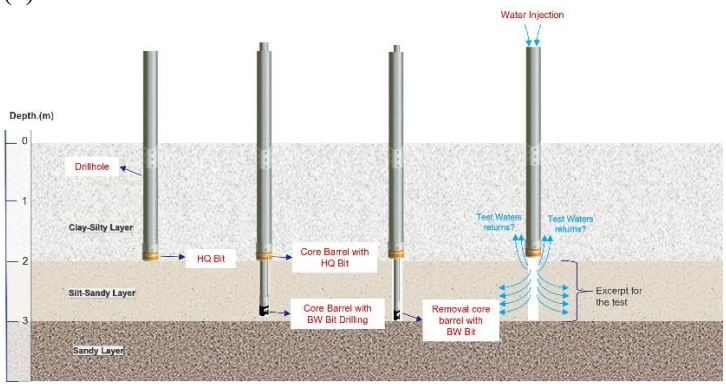

(b)

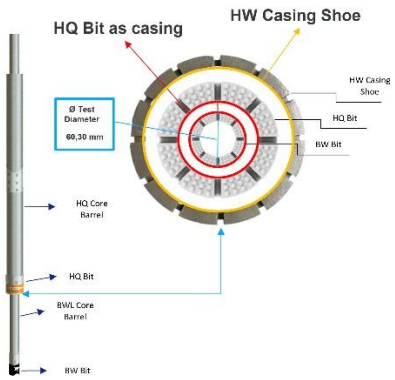

(c)

In (a), the methodology for performing the infiltration test using the wireline system:(1) Drill with the HQ rod to the desired depth. (2) Use the BWL rod to perform a telescoping operation, advancing over the underlying layer. In this way, the HQ rod would function as a casing. (3) The BWL rod is retracted to the same level as the HQ rod, thus freeing the section for the test. In (b), a detail of the procedure, and in (c), a comparison between the conventional methodology and the wireline system.

Figure 1. Execution Procedure of Soil Infiltration Test Using the Wireline System.

The evaluation of permeability values should be correlated with geological conditions (BUREAU OF RECLAMATION, 1995). It is a highly variable parameter, especially in tropical residual soils with extensive granulometry, where the finer particles are generally aggregated in their natural state. The comparison between methods and variables must have statistical support (LÓPEZ-ACOSTA et al. 2019). Ununderstood hypotheses, such as flow geometry, measurement scales, and test methodology, hinder the understanding of the results obtained by the procedure. It is important to note that the larger the volume of the tested section, the greater the influence of the massif's characteristics. This characteristic is valid for both shallow and deep tests, due to the soil's maturity.

Conclusion

For the adoption of new procedures, it is necessary for these methodologies to undergo critical evaluation to assess the influence of changing factors associated with the modification of conventional tools in different geological materials and with a higher number of tests. Therefore, research must evolve by considering the variables that influence the results.

References

López-Acosta, N.P.; Espinosa-Santiago, A.L.; Barba-Galdámez, D.F. *Characterization of soil permeability in the former Lake Texcoco, Mexico*. Open Geosciences, 2019.

Marques E.A.G; Leão, M.F. *Descomplicando a Geologia de Engenharia*. São Paulo, ABGE, 316 p., 2023 (in portuguese).

U.S. Department of the Interior, Bureau of Reclamation. *Ground Water Manual*, 690 p., 1995

DESIGN OPTIMIZATION OF PILES IN WEAK CARBONATE ROCKS - A VALUE ENGINEERING CASE STUDY OF DUBAI - UAE

MOHAMMED MUSTHAFA KHALEEL[1], MOHAMMED JALALUDDIN AHMED[2], KURIAN JACOB[3]

[1] *Arab Centre for Engineering Studies Dubai, United Arab Emirates, k.musthafa@aces-int.com*

[2] *Arab Centre for Engineering Studies Dubai, United Arab Emirates, m.ahmed@aces-int.com*

[3] *Arab Centre for Engineering Studies Dubai, United Arab Emirates, k.jacob@aces-int.com*

Introduction

Deep foundations in weak rock formations are typically designed, with sockets in the rock mass. The design of such foundations is based on the loading magnitude, geometry, elastic properties and the side frictional resistance of the socket length. In the designs, it is a common trend to overestimate the pile capacities, which leads to needless and inefficient use of materials such as concrete and reinforcement. Most of the published correlations of fs (skin friction) to UCS (Unconfined compressive strength) are developed based on the load tests on low-capacity piles in specific geological conditions, and the UCS values which are not necessarily representative of the test depths, resulting in large variations in the calculated foundation design depths. To overcome the problem, value engineering method- Preliminary Test Pile (PTP) can be used to optimise the pile lengths, while meeting effectively the acceptable load carrying capacities.

Methodology

As per Dubai building code (DBC) 2021 requirement, for obtaining allowable working capacity of pile based on site investigation data a global safety factor of not less than 2.5 needs to be considered, however in case of verification by static load test on piles are performed then partial safety factors as per Eurocode to be applied. Accordingly, in order to estimate insitu skin friction in weak rocks, 3 high-capacity bidirectional load tests were performed. The value engineering exercise was carried out, using Eurocode approach, through back analysis of the data to optimize the design lengths of the piles. The theoretical pile capacity was estimated based on William and Pell's method (ref. 5) was found to be 8900kN for a length of 30m. It was anticipated that a minimum a reduction +20% in pile length was considered.

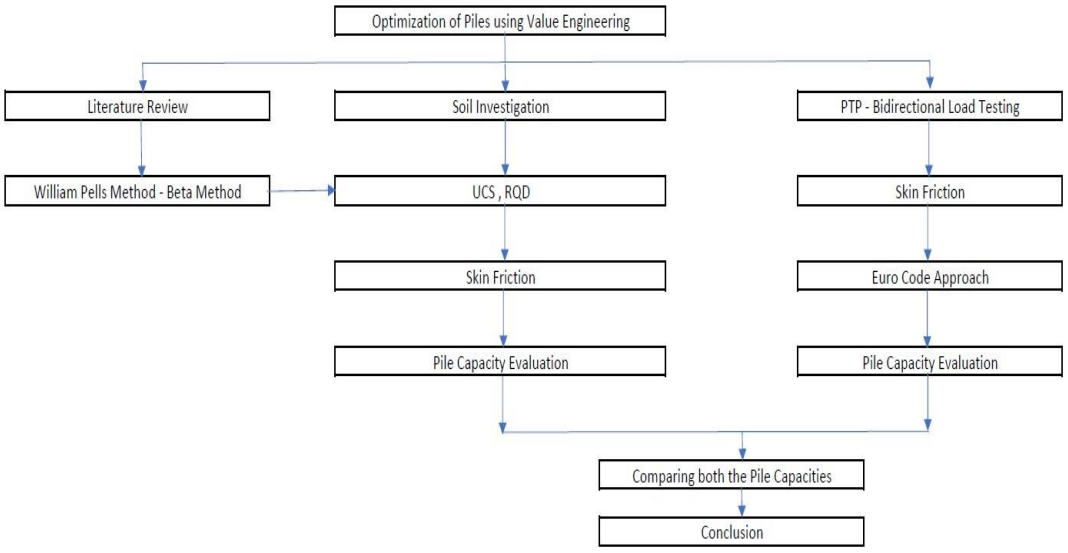

Figure 1. Methodology adopted for value engineering

Geology

The reclaimed land site in Dubai was explored with 24 boreholes depth ranges from 30 to 60m. The exploration reveals a subsurface profile with 12 to 19m thick sand, underlain by 27m of Sandstone followed by 17 m thick Conglomerate bed, and was further underlain by Siltstone up to 60m depth.

Analysis with Eurocode approach based on PTP

Eurocode 7 (ref. 1) describes three procedures for obtaining the characteristic compressive resistance Rc;k of a pile. The Rc;k is to be determined directly (i.e. not estimated) from the measured pile resistance Rc;m values (ultimate limit state resistances) by applying correlation factors ξ1 and ξ2 (related to number of piles tested), to the mean and minimum measured resistances according to below equation and values of ξ1 and ξ2 .

$$R_{c;k} = Min\left\{\frac{(R_{c;m})_{mean}}{\xi_1}; \frac{(R_{c;m})_{min}}{\xi_2}\right\}$$

n	1	2	3	4	≥ 5
ξ_1	1,4	1,3	1,2	1,1	1,0
ξ_2	1,4	1,2	1,05	1,0	1,0

Considering Design Approaches: DA1.C1: A1 + M1 +R1 ; A1=1.35,M1=1 and R1=1 ; DA1.C2: A2 + M1 +R4(Governing) ; A2=1,M1=1 and R4=1.4, Design Approach-1, combination 2 is mostly governing; hence, was considered for this case study. Based on the above estimated skin frictions the allowable skin frictions were recommended. The below figure 2 shows the estimated skin frictions from PTP as well as through the theoretical estimates.

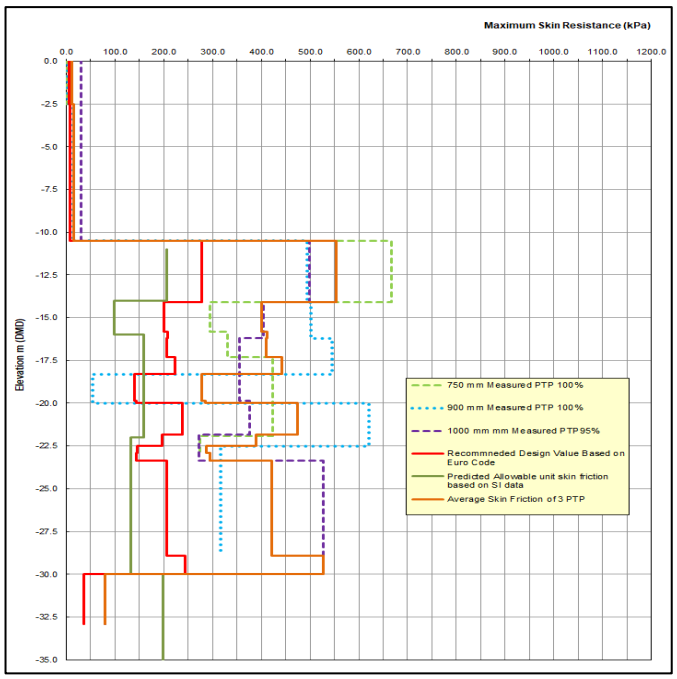

Figure 2. Graphical presentation of skin friction values from PTP

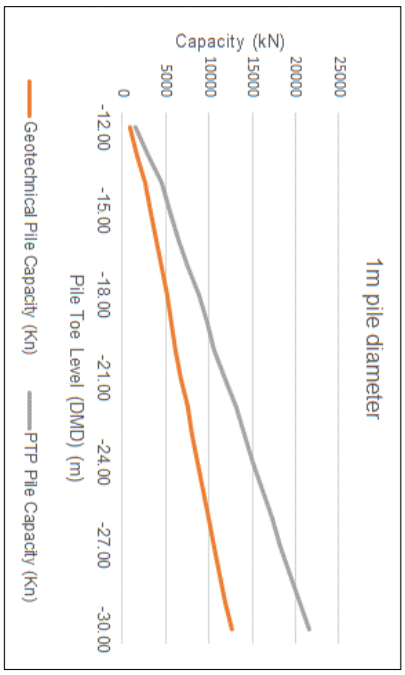

Figure 3. Pile capacities vs Toe Level

Conclusion and Recommendations:

The above value engineering method/ exercise as shown in figure 3 helped in optimising the pile lengths by over 30%. Hence, it is recommended to carry out the estimations of rock socket frictions in Intermediate Geomaterials based on the pile load tests (PTP) and optimize the design length of deep foundations. The value engineering exercise brought in substantial impact on the cost, time schedule, safety and performance of the structure.

References

1. BS EN 1997-1, *Eurocode 7, Geotechnical Design, Part 1 General Rules*, 2004
2. Deep Foundation, *A contribution for Improving current Design Practice in Dubai UAE*
3. Rowe, R.K. & Armitage, H.H., *A design method for drilled piers in soft rock.* Canadian Geotechnical Journal, Volume 24, No. 1: pp. 126-142, 1987.
4. Tomlinson, M. & Woodward, J. (5th ed.). *Pile Design and Construction Practice,* New York: Taylor & Francis, 2008.
5. William's A.F & Pells P.J.N. *Side resistance rocksocket in sandstone, mudstone and shale*. Canadian geotechnical journal, Volume 18 ,1981.

CHARACTERISATION OF EMBANKMENT ON SOFT GROUND IN THE NETHERLANDS

KEN GAVIN [1], TOM DE GAST [1], MARIO BACIC[2], SASA MEHO KOVACEVIC[2], CORMAC REALE[3]

[1] *TU Delft, The Netherlands,* k.g.gavin@tudelft.nl, t.degast@tudelft.nl

[2] *The University of Zagreb, Croatia,* mbacic@grad.hr, msk@grad.hr

[3]*The University of Bath, United Kingdom,* cr760@bath.ac.uk

Introduction

The case study area "Oostmolendijk" is located between the towns of Ridderkerk and Hendrik-Ido-Ambacht, along the river Noord in the Zuid-Holland province of the Netherlands. Oostmolendijk is a small part of the greater dyke ring IJssel-monde also known as dijkring 17. As a primary dijk, Oostmolendijk is critically important for the protection of people and infrastructure in dijkring 17. Whilst most of the dyke ring is considered stable, Oostmolendijk considered here is affected by continuous ground settlement and cracking of the road surface resulting in ongoing maintenance problems. This excessive settling and spreading relative to neighbooring dijks, leads to widespread cracking in the embankment face and the road upon it (Reale et al., 2023). The dyke has a height of approximately +4.7m NAP (Amsterdam Datum Level) with a small berm providing support at approximately +2m NAP.

The investigation consists of geophysical techniques (MASW and ERT) and geotechnical methods including additional CPTs and Borehole to obtain soil samples. An important focus of the investigation is to consider both the vertical and horizontal scales of fluctuation of the soil layers. Cone penetration tests (CPT) were carried out along the embankment at regular intervals, both on the dyke and in the field adjacent. These show a relatively uniform profile consisting of Holocene era soft soil deposits to a depth of 12 m below NAP overlying Pleistocene era coarse sands to great depth. Investigation boreholes at the site indicate that there are three different soft soil layers present within the Holocene deposits. An upper organic silty clay layer overlying a peat layer, which is in turn underlain by a lower clay. The aim of the survey was to improve geotechnical knowledge of the substratum and understand the material spatial variability, partiularly in the horizontal direction in order to identify areas of critical concern and design a suitable stabilisation method.

Methodology

The CPT programme was designed to enhance the identification of the horizontal scale of fluctuation. The CPT layout ensured multiple CPTs were positioned at each lag distance (e.g. 1m, 2m, … etc.), see Figure 1. Repeated close range measurements are crucial for accurate determination of the scale of fluctuation, as they help ensure consistent peak and trough detection. This approach maximises the efficiency of data collection while enhancing the reliability of the spatial variability analysis.

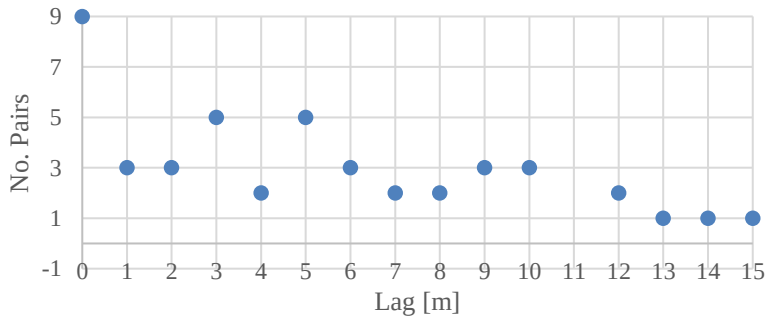

Figure 1 CPT pairs versus lag distance, ensuring repeated measurement at close lag distances.

The CPTs were broken into layers for spatial analysis before being decomposed to investigate the underlying spatial structure. A Gauss-Markov correlation function was then fitted to the underlying structure using a least squares approach (Reale et al., 2022). The results were then interpreted vertically and horizontally to determine the scales of fluctuation.

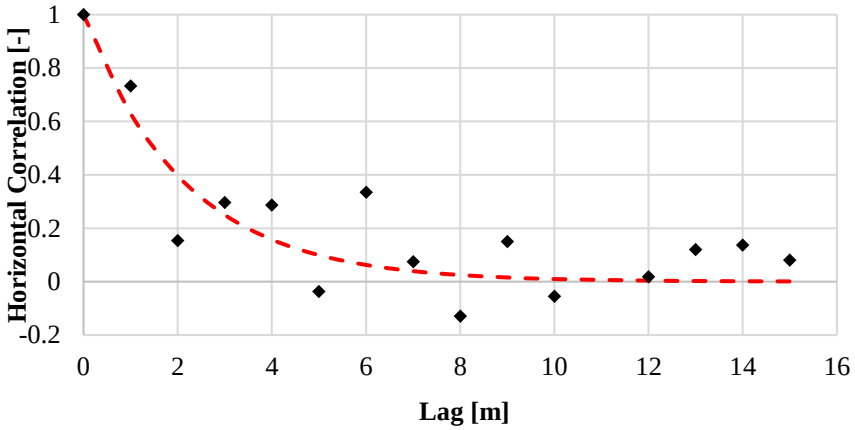

Figure 2 Horizontal correlation for the peat layer, red dashed line indicates fitted Gauess Markov model, showing a horizontal scale of fluctation of 5.14m

Results and Conclusion

Initial results at Oostmolendijk show a significant difference in the horizontal scale of fluctuation between the layers, with the deeper Pleistocene sand layers having reasonably small horizontal scales of fluctuation less than 1m. While the Holocene soft soil deposits exhibit far larger horizontal scales of fluctuation of up to 5.14m, see Figure 2. This indicates that across the linear dijk there is likely to be zones of high relative weakness in the soft clay and peat layers. Designing the CPT layout to maximise the number of CPTs at close range lag spacings enhanced data collection and ensured accurate horizontal scales of fluctuation could be obtained from all layers The next steps at the site are to interpret the laboratory testing and geophysical surveys and correlate them with the CPT results to build a full ground model to identify potential zones of weakness.

Acknowledgement

This research was funded by European Union Horizon Europe Programme, GA 101104283, CIRCUIT project (Holistic approach to foster circular and resilient transport infrastructures and support the deployment of green and innovation public procurement and innovative engineering practices.).

References

Reale, C., Kovačević, M.S., Bacic, M. and Gavin, K.G., 2022. Assessment of the spatial variability of a Croatian flood embankment using the cone penetration test. In Cone Penetration Testing 2022 (pp. 1053-1057). CRC Press.

Reale, C., Gupta, A., De Gast, T. and Gavin, K., 2023. Assessing the vulnerability of a Dutch river dyke to rising water levels. In 14th International Conference on Applications of Statistics and Probability in Civil Engineering 2023.

ABOUT GEOTECHNICAL INVESTIGATIONS OF A SALT DOME IN THE FOUNDATION GROUND OF A MOTORWAY BRIDGE

EMILIA ELENA MILUTINOVICI [1], ERBIL BALLIKAYA [2], DANIEL MIHAILESCU [3], GABRIELA DRAGOMIR [4]

[1] *AGIM, Romania,* emiliamilutinovici@gmail.com
[2] *AGIM, Romania,* erbilballikaya@gmail.com
[3] *PROSPECT TECHNICAL STUDIES, Romania,* daniel.mihailescu75@gmail.com
[4] *PROSPECT TECHNICAL STUDIES, Romania,* gabriela.dragomir@prospects.ro

Introduction

The EU's trans-European transport network policy, the TEN-T policy, aims to develop a more efficient and high-quality transport infrastructure across the EU. Romania has the privilege to develop during this period many infrastructure projects to ensure the implementation of the TEN-T framework on its territory. These projects are in different stages of implementation, from feasibility studies to design and execution. In the southern part of Transylvania, in-situ investigations were carried out for the design of a motorway sector. The section is known to be an area with a good foundation ground, comprising a covering formation made up of alternating fine or coarse stiff, uncohesive deposits, and a marly bedrock. Following the site investigations, a body of salt was identified underground that extends along the length of the highway for about 500 m. The salt body occurs at depths between 17.00 and 23.00 m, down to depths of 40.00-45.00 m. It is much thicker in its eastern part, of about 20.0 m, thinning to the west, where its thickness is reduced to 5.00 m. Salt does not appear over as a massive body and is dispersed with in the marly formation that constitutes bedrock.

Methods

The salt body is associated with other types of soils that can be constituted as difficult foundation soils. Thus, around the salt body there is a typical formation, called "salt brecia" (also described in point 8), but also "sinkhole" areas (depression, collapse or suffocation), of circular or semicircular shapes, in a depression form, sometimes as a water hole (with fresh water), surrounded by typical hydrophilic vegetation. Following the information collected from the nearest City Hall, it was confirmed that there were no salt exploitations that used water injection and saline extraction, so from this point of view, theoretically, there is no risk of the existence of caverns due to salt exploitation. However, the formation is crossed by groundwater, also in the area being historically known a well (it has not been identified at this time on the ground), from which the locals used to extract salt water for food preservation. The existence of sink-hole water accumulations in the area shows that in the past there have been collapses at the level of the salt deposit. Cracked soils appear, also called "salt brecia", associated with the salt body. Their cracking is due to the geological growth of the salt body. It can occur in the upperside or bedside area of the salt body, or can be interspersed with it, and is made up of centimetric fragments of marl or marl sites mixed with centimetric fragments of crystalline or recrystallized salt. The existence of salt bodies can also be associated with faults or anticline zones.

A number of investigations were perfomed in-situ the area.

- 20 boreholes with depth between 30.00 and 80.00 m
- in some of the boreholes, SPT test were performed
- Menard presiometer test were performed in 3 level of depth
- An exhaustive geophysical survey consisting by electric sounding and seismic refraction

Results

In general, the stratification found in geotechnical drilling is made up of covering formation and base rock. The covering formation is of Pleistocene age and is mainly made up of fine or coarse non-cohesive deposits, medium dense up to average depths of -10.00 m, which rest on thick non-cohesive deposits. At the top of them there are also clayey-dusty intercalations. The base rock, of Miocene age, is made up

of marly clays, clayey marls, marls, with some thin intercalations of sandstones or cemented sands.
At the top of the base rock was found the salt deposit, with thicknesses between 5.00-25.00 m, in the eastern part with thicknesses of 25.0 m, tapering to the west, where it reaches thicknesses of 5.0 m or even less. The salt deposit appears both as a finely disseminated salt, mixed with the mass of marly clay, especially in its edge areas, but also as a massive salt. In the western part, the salt has a migrated nature, on the layer surface, recrystallized. The depth at which the salt deposit was found is as follows:

Table 1. Salt formation limits

Borehole	Salt formation upperside depth (m)	Salt formation bedside depth (m)
F739	-	-
BH13_1	21.50	22.00
F740	20.00	20.50
BH13_2	20.00	20.50
F741	17.00	23.00
BH13_3	18.70	22.30
F742	19.50	24.00
BH13_4	24.30	26.00
F743	20.00	26.00
F744	24.00	25.00
BH13_5	25.50	41.00
BH13_5a	22.00	37.00
F745	-	-
BH13_6	24.10	38.40
F746	20.50	38.50
BH13_6a	16.90	41.00
BH13_7	16.50	40.00
BH13_7a	15.70	39.80

As a result of the geophysical investigations, the contour of the salt body was determined, the propagation speeds of the seismic waves were identified, and the values for dynamic parameters and the Poisson coefficient were established for the analyzed strata. The quality class of the soils encountered was also established, in accordance with the provisions of Eurocode 8.

Conclusion

Considering the fact that this salt body is part of the foundation ground of a future viaduct, whose project involved indirect foundation, on piles, it became extremely important to know the geometry and its properties, in order to choose a feasible foundation method.
The in-situ investigation program involved geotechnical drilling, in-situ tests (penetration and presyometric tests) and geophysical investigations. The result of the interpretations of field and laboratory investigations will lead to the choice of a design solution that will ensure the stability and integrity of the future construction.

References

ASRO. (2008, iulie). SR EN 1997-1 Eurocod 7: Proiectarea Geotehnica; Partea 1: Reguli generale. *ASRO Standard Roman*, pg. 18-19.

MDRAP. (2014). Normativ privind documentatiile geotehnice pentru constructii - NP074-2014. *Monitorul Oficial, partea I*, 1-14.

IMPORTANCE OF ENGINEERING GEOLOGICAL INVESTIGATION FOR CONSTRUCTION OF INFRASTRUCTURAL PROJECTS

MARKO COPIĆ [1]

[1] *Croatian Geological Survey, dept. of Hydrogeology and Engineering Geology, Zagreb, Croatia, mcopic@hgi-cgs.hr,*

Introduction

A project for the construction of high voltage overhead transmission lines (OHTL) in Norway started in 2016. Typical high voltage line consists of 3 main parts: foundations, steel lattice towers, and electrical conductors (wires). In this project every tower had 4 "legs", each connected to its foundation. Two general foundation types (Statnett SF 2016) were designed: 1) rock foundation with steel rebars vertically anchored into the bedrock, and 2) soil foundation with a concrete foot plate buried at designed depth (2 - 4.5 m). This work presents the events occurred during the construction of foundations for 6 towers located in an agricultural area and the conducted geological and geotechnical investigations. Construction works had to be executed when the ground was frozen to prevent damage made by vehicles. Soil excavations started in February 2017. After approx. 1.5 m of humus, a layer of light grey material appeared. Based on visual check, material was classified as silty clay with significant amount of water content, relatively soft at surface, but it didn't seem like a concern. Designed excavation depth was more than 3 m and excavator started to excavate this material. Immediately after, the material started to change its properties significantly. It became extremely soft, almost liquid, with tendency to flow, excavated pit walls were collapsing and the excavator was sinking in it, but undisturbed parts of the material were still relatively stiff. According to behaviour of this material it was assumed to be sensitive or quick clay. Construction of six foundations within the time schedule in this material was a challenge.

Methods

Geological data consisted of geological maps of bedrock (Norges geologiske undersøkelse (NGU)), description of the line route, (geological setting, definition of rock type and drillability parameters) (Statnett SF 2016), rock foundations design rules (Statnett SF 2016) and instructions for classification of the rock ground (Statnett SF 2016). Rock classification and soil type determination were conducted prior to construction. There was a concern that designed foundations were not suitable due to very poor physical-mechanical properties of the material. Differential settlements were expected and waiting for laboratory testing for calculating foundation design would take too long. Therefore, it was decided to try with in-situ experimental solutions. In situ and laboratory tests were conducted later (Table 1) at tower site where the material was so soft that calculated piled foundations had to be built.

Results

According to geological maps 1:50,000 and geological description of the line route, heterogeneous migmatitic gneisses covered with quaternary deposits (moraine, gravel, sand clay) were expected in the area. Excavation showed presence of soft and sensitive material at all 6 tower sites but with different properties.

Soft sensitive clays like quick clays are well known in Scandinavia and in some regions in Canada. The salt pore water of these marine clays has been leached out since last glaciations and left a brittle mineral structure. Norwegian quick clay has a very low permeability and hence pore water pressure becomes a crucial parameter that can affect the stability of material. Soft sensitive clays, also termed quick clays, usually exhibit sensitivity greater than 30 and have remoulded shear strength less than 0.5 kPa. Sensitivity is defined as a ratio of undisturbed undrained shear strength to the remoulded undrained shear strength of the material (Thakur et al., 2006).

Some excavation pits were performed 1 - 2 weeks earlier and thin layer of ice was formed at surface of the material. At these sites the material was not extremely soft. In more recent excavation pits, material was still very soft. Fortunately, the terrain was flat and there was no danger of landslides, so the main concern was how to build foundations within required geometric tolerances as foundations settlement

Figure 1. Two excavators spreading crushed stone into the excavation pit

was expected. Accordingly, two foundation methods were tested: 1) soil improvement by compacting crushed stone in layers and construction of foundations according to the original design. Method was chosen at tower sites excavated earlier and according to the design (four separate excavation pits for each foundation) as the material seemed relatively stiff, and 2) at later excavated tower sites, change in foundation geometry was chosen. Instead of four separate and deep foundations, one big and shallower foundation foot plate was applied, with geonet and layer of uncompacted crushed stone beneath the foundation (Figure 1). Method 1) was partially successful. Compacting crushed stone made the material softer at some spots so it wasn't compacted evenly. Most of foundations built with this method had differential settlements but inside tolerances. Foundations at one tower spot built with this method had to be demolished and rebuilt due to differential settlements caused by heavy rain during concreting. Method 2) was successful at all applied tower spots. At one tower spot material was so soft that people were sinking in it so rapidly that it wasn't possible to work in it. At this tower site foundation piles were applied. Figure 1 shows laboratory and in situ test results conducted at this tower site.

Table 1. Laboratory testing results showed changes in sensitivity with depth

Depth (m)	W (%)	Remoulded Cu (kPa)	Undisturbed Cu (kPa)	$St=\frac{Cu(undisturbed)}{Cu(remoulded)}$
3	30 - 33	7	35	5
6	35 - 41	~ 0.5	8-9	16 - 19
9	35 - 37	<=0.5	13-23	25 - 40

Conclusion

It is not a rare case in OHTL industry that economic feasibility of geotechnical or engineering geological investigations are questioned due to their high costs (a lot of tower spots, difficult terrain, environmental restrictions etc). This case presents one of many possible consequences of unexpected and rare material occurrence in construction projects and emphasizes importance of detailed preliminary investigations. Fortunately, in this case the consequences were only of financial nature. Inclined terrain, higher air temperatures or lack of good planning and cooperation would probably endanger the whole project. Multidisciplinary investigations, optimised for specific project, should be part of planning process for important infrastructural projects. Engineering geological and geotechnical investigations shouldn't be considered as an expense but rather as an investment in safer construction.

References

Statnett SF *09-06-01 - AC Suspension Tower Foundation Rock %96 Tender drawing*. Statnett internal document, 2016.

Statnett SF *09-06-02 - AC Suspension Tower Foundation Soil %96 Tender drawing.* Statnett internal document, 2016.

Norges geologiske undersøkelse (NGU) (Geologiske kart). Available online: https://www.ngu.no/geologiske-kart

Statnett SF *08-01-02 - Exh E -TN Geological description 420 kV Namsos-Hofstad-Afjord.* Statnett internal document, 2016.

Statnett SF *08-03-01 Anchorage of Tower Foundations in Rock - Classification of Rock Ground_SDOK-82-14_R2.* Statnett internal document, 2016.

Statnett SF *08-03-02 Anchorage of Tower Foundations in Rock - Design Rules_SDOK-82-3_R2*. Statnett internal document, 2016.

Thakur, V., Grimstad, G., Nordal, S. *Instability in Soft Sensitive Clays,* 2006 ECI Conference on Geohazards, Lillehammer, Norway

DETECTION OF FRACTURED ZONES AND CAVERNS IN KARST USING GEOPHYSICAL METHODS AT THE LOCATION OF VIZINADA IN ISTRIA

BOŽO PADOVAN [1], VALENTINO MEJRUŠIĆ [1], MARKO MARIČIĆ [1], JOSIP MIKŠIĆ [1]

[1] *Terra Compacta d.o.o., Croatia,* bpadovan@terra-compacta.hr

[1] *Terra Compacta d.o.o., Croatia,* vmejrusic@terra-compacta.hr

[1] *Terra Compacta d.o.o., Croatia,* mmaricic@terra-compacta.hr

[1] *Terra Compacta d.o.o., Croatia,* jmiksic@terra-compacta.hr

Introduction

Geotechnical designing in Karst is often challenging because of many unknown parameters related to materials, composition and current condition of field of research. To get comprehensive picture of underground, geophysical methods presents fast and reliable solution to identify important features of underground that are later used during geotechnical designing (Yilmaz, 2015). Construction of luxurious mansion is planned in village Žudetići, municipality of Vižinada. Location of the construction site is at the edge of Pazin flysch basin where Eocene flysch is in contact with Cretaceous limestone.

Methods

During field prospecting, indications of fractured and hollow zones have been observed. In that zones during rainy periods a flow of water can be heard. This flow of water is unlike characteristic underground water flows in karst areas and instead it is represented as water pockets that sporadically move through smaller fractures and possibly small caves. Local residents describe sound of flow as “crunching” or “gurgling”.

Figure 1. Distribution of geophysical profiles.

Geophysical profiles were set along main axes of the building, perpendicular to flysch and limestone contact and along all locations with presumed fractures and caves. Geophysical methods included seismic refraction tomography and geoelectric tomography. Combination of such methods provides key parameters needed to differentiate materials and to detect fractured zones with positions of main fractures and caverns (Gebrande & Miller, 1985.) (Gibson, Odegard, & Sutton, 1979).

Results

Boundary between flysch and limestone as well as their volume and thickness were determined through electrical resistance propagation. By observing only electrical resistance propagation it is not possible to unequivocally detect fractured zones. Elastic P-waves propagation in seismic tomography confirmed forementioned boundary and showed many zones with inversion of velocity of seismic waves. Inversion in elastic P-waves velocities, which is gained by seismic inversion modelling, is significant indicator of fractured zones and caverns underground. During initial phase of construction, zones with inverted

seismic velocities and increases in electrical resistivities have been confirmed as fractured zones with significant fractures and caverns.

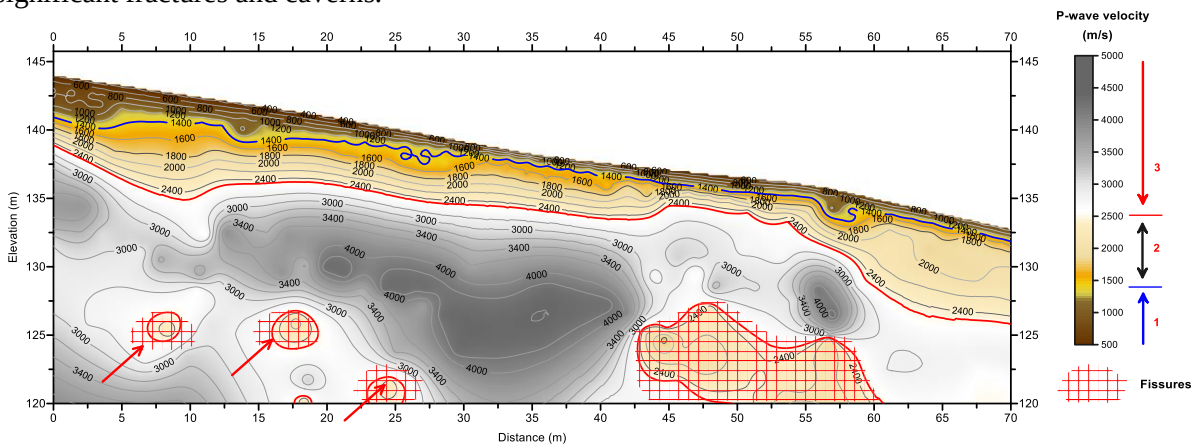

Figure 2. Seismic refraction profile.

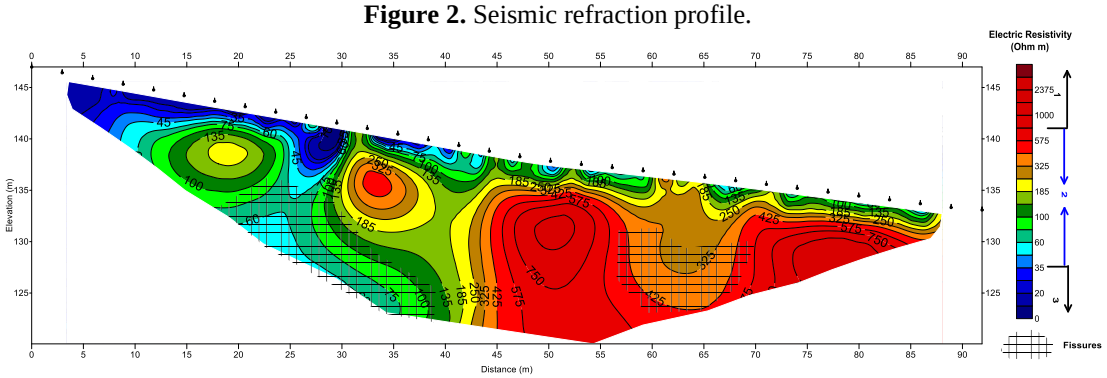

Figure 3. Electric tomography profile.

Conclusion

In order to establish as reliably as possible the existence of geological phenomena such as caverns, cavities, fractured zones, cracks, contacts between different lithological members, it is necessary to avoid the ambiguity of geophysical methods (Yilmaz, 2015). Geoelectrical tomography can distinguish between materials if they have different electrical conductivity (Loke & Dahlin, 2002), but the results can easily be affected by a number of factors such as, for example, a change in the water level (or the absence of water) underground. On the other hand, using refraction tomography, it is often impossible to distinguish between materials (Gardner, Gardner, & Gregory, 1974) due to their similar velocities (ie, compacted marl and weathered limestone), even if they have significantly different electrical conductivities. Therefore, the combination of seismic refraction tomography and geoelectric tomography increases the reliability of distinguishing materials and successfully determining phenomena such as fracture zones and caverns.

References

Gardner, G. H., Gardner, L. W., & Gregory, A. R. (1974, December). *Formation velocity and density - the diagnostic basics for stratigraphic traps*. Geophysics, 39(6), 770 - 780.

Gebrande, H., & Miller, H. (1985.). *Refraktionsseismik*. In F. Bender (Ed.), Angewandte Geowissenschaften II (pp. 226 - 260). Stuttgart.

Gibson, B. S., Odegard, M. E., & Sutton, G. H. (1979). *Nonlinear least-squares inversion of traveltime data for a linear velocity-depth relationship*. Geophysics, 44, 185-194.

Loke, M. H. (2011). *Electrical resistivity surveys and data interpretation*. In Encyclopedia of Solid Earth Geophysics (pp. 276-283).

Yilmaz, O. (2015). *Engineering Seismology with Applications to Geotechnical Engineering. Society of Exploration Geophysicists*.

SINKHOLE HAVOC TO A STATE OF DISASTER: CASE STUDY INTO A RESETTLEMENT PLAN FOR KHUTSONG NORTH COMMUNITY, GAUTENG PROVINCE – SOUTH AFRICA

BONGANI MSANE [1], SIFISO NGUBELANGA [2],

[1] *Infrastructure and Land Use, Council for Geoscience, South Africa, E-mail: bmsane@geoscience.org.za*

[2] *Infrastructure and Land Use, Council for Geoscience, South Africa, E-mail: sngubelanga@geoscience.org.za*

Introduction

Karst-related sinkholes and subsidences occur on areas underlain by Chuniespoort Group dolomite bedrock in the Gauteng Province, South Africa. Although dolomite land occurs across five of the nine South African provinces, the sinkhole problem has considerably been more severe in Gauteng than in other provinces (Constantinou and van Rooy, 2019).

Khutsong township was established in the late 1950s, as a result of the gold mining history has been a source of migrant labour for areas around South Africa and neighbouring countries, such as Mozambique, Swaziland, etc (Kirshner, 2012, *in* Tune, 2016). At the time of establishment, no geological surveys were conducted to determine the suitability of the area for urban development.

Despite the ever-increasing ground instabilities in the region, Khutsong contunued to develop until 1980 when a private firm was comissioned to conduct a first geotechnical study. From this date until at least the year-2013, several dolomite stability surveys have been conducted by various engineering geological firms and a Dolomite Risk Management Plan (DRMP) was compiled in 2004 (HDA, 2020). Inspite of these intervesions and the formation of disaster management team of the Westrand District Municipality by the then newly established Merafong City Local Municipality (MCLM), new sinkhole events continued to cause havoc across Khutsong and even in areas previously classified as safe. From 2016 to date, the situation has drastically deteriorated resulting in several house being demolished, roads closed, and the wet services network destroyed creating a local state of emergency. As a result of the intolerable rate of new sinkholes and in line with the Disaster Management Act, 57 of 2002 (DMA), a State of Local Disaster was declared on Khutsong North during November 2016.

The dolomite risk assessment study is aimed at gathering data relevant to re-assess the current situation and provide details on any additional areas for inclusion into the Khutsong North Re-settlement Plan.

Methods

The ultimate objective of the project is to align the existing development with the technical requirements as stipulated in South African National Standard (SANS) 1936:2012 for development on dolomite land and the National Home Builders Registration Council (NHBRC) 2015 Manual. Data and information were collated from a few sources for review: MCLM, ENGEODE Database of the Council for Geoscience (CGS), including site visits and stakeholder engagement meetings. Reference was also made to various published sources (maps) and previous media reports addressing the issue of dolomite risk.

Using the available reports, percussion boreholes and ground instability events occurring within the area of Khutsong North Extensions (Khutsong Proper & Extension 1 – 6), the stability of the area was re-assessed in terms of the current Method of Scenario Supposition – statistical occurrence of eight inherent hazard classes as described in SANS 1936-2:2012.

Results

The available record of ground instability events combined with geological maps, geotechnical and geohydrological data was used to assist the MCLM to outline the necessary measures and implement the Khutsong North Re-settlement Plan. The current dolomite stability risk assessment broadly subdivided the study area into two composite inherent hazard class (IHC) zones, namely: Zone 1: IHC

3 - 4//1 and Zone 2: IHC 5 – 8//1. This zonation largely reflects medium to high susceptibility of medium to very large size events with respect to ingress of water, and a low susceptibility of all-size events with respect to groundwater level drawdown. Based on the current study, the existing resettlement plan was revised, and new priority area were added to make a total of nine (9) priority areas, Figure 1.

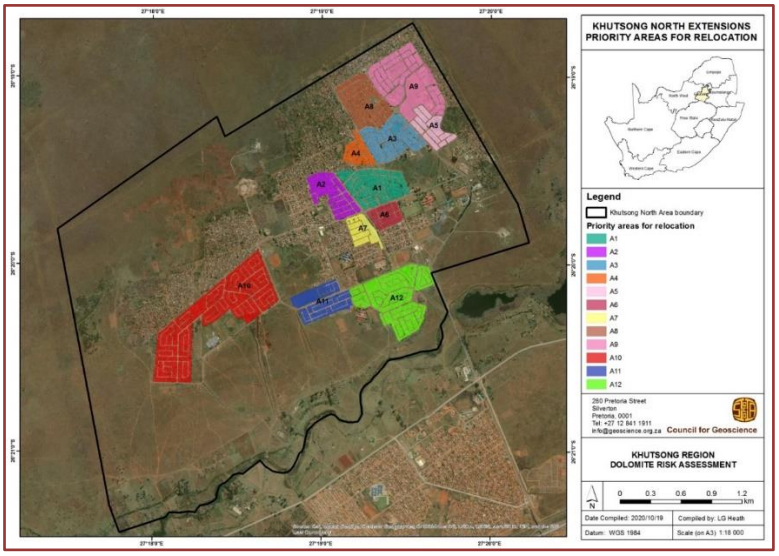

Figure 3. Priority areas identified for re-settlement, (CGS Report, 2020)

Conclusion

The regional dolomite risk assessment on Khutsong North Extensions confirmed that the area is predominantly characterised by high hazard (IHC 5 – 8), i.e. over 58% of the boreholes reveal these conditions. Furthermore, the available ground instability events (sinkholes & subsidences) recorded reveal an area dominated by larger (5-15m) to very-large size events (>15m). Most of these events are directly attributed to poor stormwater management and leaking water-bearing infrastructure. The situation has led to the demolition of many houses, closure of roads and collapse of the wet services systems, and has necessitated the consideration of an expensive re-settlement option.

In conclusion, the area is deemed generally unsuitable for residential development and at least, the upgrade of the wet services infrastructure must be implemented in the non-priority areas.

References

Buttrick, D B, Van Schalkwyk, A, Kleywegt, R J & Watermeyer, R B. Proposed method for dolomite land hazard and risk assessment in South Africa. Journal of the South African Institution of Civil Engineering, 2001, 43(2): 27–36.

Constantinou, S., Van Rooy, J.L. Sinkhole and subsidence size distribution across dolomitic land in Gauteng. SAICE Journal. 2019, Paper 1373.

Council for Geoscience. Phase A – Dolomite Stability Risk Assessment of Khutsong Proper & Khutsong North Extension 1 – 6. 2020, Report number: 2020-0129.

National Home Builders Registration Council. Home Building Manual and Guide. 2015, NHBRC Communications, Sunninghill, Johannesburg.

Tune, L. The Dynamics of Mining Towns: The Case of Khutsong Township, Carletonville. Master Thesis, University Of The Witwatersrand, Johanneburg, South Africa, 2016.

The Housing Development Agency (HDA). Review and finalisation of Programme Implementation Plan: Khutsong Sinkhole Intervention 2020, RFP/JHB/2020/011.

South African National Standard. Development of dolomite land – SANS 1936 – Parts 1-5. 2012, SABS Standards Division, Pretoria 0001.

DEM SUPER-RESOLUTION FOR PHOTOVOLTAIC SITE SUITABILITY ASSESSMENT

JIYOON KU [1], HYEONG-DONG PARK [2, 3]

[1] *Department of Energy Systems Engineering, Seoul National University, Korea, rnldbs9808@snu.ac.kr*

[2] *Department of Energy Resources Engineering, Seoul National University, Korea, hpark@snu.ac.kr*

[3] *Research Institute of Energy Systems, Seoul National University, Korea, hpark@snu.ac.kr*

Introduction

To ensure a sustainable economic return over a 20-year period, the deployment of photovoltaic (PV) installations necessitates the critical consideration of solar irradiance and site suitability. Developing solar power on unstable sites can lead to significant damage from landslides, making it essential to assess ground stability in advance. A Digital Elevation Model (DEM) serves as a crucial tool in this assessment, representing terrain surfaces through elevation data contained in each pixel. Topographic analysis using DEMs provides critical site parameters such as slope gradients and hydrological systems, essential for selecting stable sites for solar installations. High-resolution (HR) DEMs, offering more detailed analyses, are preferable but may be difficult to acquire or limited in area and scope. Evaluating the accuracy and cost-effectiveness of HR data is necessary. This study aims to compare how three critical geological parameters for photovoltaic site suitability—slope, aspect, and distance from streams—change with different DEM resolutions and how these changes affect the identification of suitable areas for PV installations. Should significant disparities between low and high-resolution DEM data emerge, future research could utilise super-resolution techniques to synthesise HR data from existing lower-resolution (LR) datasets. This study serves as a preliminary study, analysing existing DEMs of varying resolutions.

Methods

This study evaluates the impact of DEM resolution on the suitability of sites for PV installations, focusing on three distinct geographic regions in South Korea: flatlands, mountains, and mixed terrain, each spanning 2000 km². Two types of DEMs are utilised: a low-resolution DEM with a spatial resolution of 30 m (ASTER, 2023) and a high-resolution DEM with 12.5 m (ASF, 2024). The study concentrates on 3 critical topographic factors that significantly affect the viability of PV installations: slope, aspect, and distance from streams. Land stability increases with a slope inclination angle of less than 10° (Nebey et al., 2020). Unstable slope affects both the construction feasibility and risk of land movement. Solar panels in the northern hemisphere generate optimal energy on south-facing slopes (157.5°–202.5°), and sites more than 1 km from streams are preferred to mitigate flooding risks (Nebey et al., 2020). Using ArcGIS, a Geographic Information Systems (GIS) platform, three topographic factors were extracted from both the LR and HR DEMs. A detailed comparison was then conducted to evaluate how DEM resolution influences the assessment of each parameter and the sensitivity of site suitability assessments.

Results

Across all topographic factors and regions, HR DEM showed a decreased area suitable for PV installations (Table 1). For slope, HR DEMs have steeper slopes than LR DEMs, resulting in a smaller area suitable for PV installations, particularly in mountainous regions with the greatest difference in suitability. Aspect exhibited the least change between LR and HR data, implying that it is less sensitive to resolution. However, HR DEMs detected significantly more streams in all regions, reducing suitable areas due to the 1 km safety buffer requirement. Figure 1 shows that LR detects main streams (primary and secondary) comparable to HR, but has limitations in detecting detailed tributaries. The Flatlands area revealed the greatest difference, with 243 more streams identified via HR data, greatly limiting suitable sites.

Table 1. Suitable areas for PV installations based on topographic factors using LR and HR DEMs in flatlands, mountains, and mixed terrain.

Criteria	Flatlands (km²)		Mountains (km²)		Mixed terrain (km²)	
	LR	HR	LR	HR	LR	HR
Slope (under 10°)	1631.15	1564.56	221.52	195.15	773.3	744.94
Azimuth (south facing)	249.21	223.56	249.41	249.16	252.7	235.59
Distance from streams (> 1 km)	1568.32	1067.19	1616.06	1145.67	1636.72	1169.66
Combined	155.83	15.3	18.12	1.55	66.2	5.84

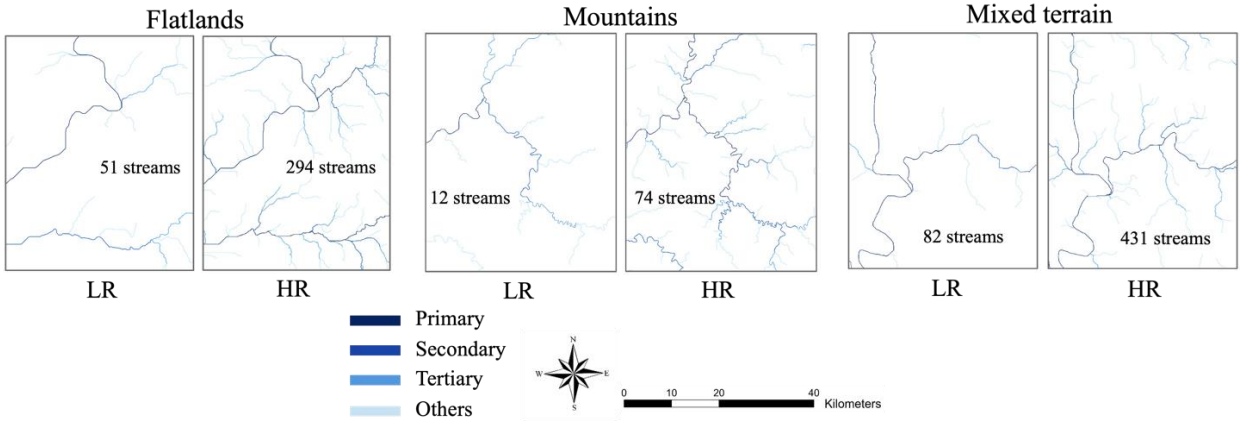

Figure 1. Stream networks identified using LR and HR DEMs in flatlands, mountains, and mixed terrain.

Conclusion

This study assessed the impact of LR and HR Digital DEMs on the identification of suitable sites for PV installations. HR DEMs identified 73 km² less suitable sites across all terrains, a 3.6% difference over the total area (2000 km²). This discrepancy arises from HR DEMs' superior ability to delineate stream networks, highlighting significant advantages of fine-resolution data, particularly in identifying areas less susceptible to flooding. Consequently, HR DEMs provide a more detailed assessment, enabling more accurate and sustainable site selection for solar installations. The findings emphasise the benefits of HR data for terrain analysis, recommending the use of existing high-quality resolution data where available or generating such data through super-resolution techniques in future research. This contributes to the strategic planning and optimisation of solar energy projects, emphasising environmental considerations and long-term sustainability.

Acknowledgement

This study was supported by Energy & Mineral Resources Development Association of Korea (EMRD) grant funded by the Korea government (MOTIE) (2021060003, Training Program for Specialists in Smart Mining).

References

ASF (Alaska Satellite Facility). available online: https://asf.alaska.edu/datasets/daac/alos-palsar-radiometric-terrain-correction/ (accessed on 11 March 2024).

ASTER GDEM 003 (Advanced Spaceborne Thermal Emission and Reflection Radiometer Global Digital Elevation Model Version 3). available online: https://asterweb.jpl.nasa.gov/gdem.asp (accessed on 7 May 2023).

Nebey, A. H.; Taye, B. Z.; Workineh, T. G. Site suitability analysis of solar PV power generation in South Gondar, Amhara Region. Journal of Energy, 2020, 1, 3519257.

ASSESSING MECHANICAL PROPERTIES OF QUARTZITIC MATERIALS AND SHEAR BEHAVIOR OF QUARTZITIC JOINTS WITH REFERENCE TO THEIR WEATHERING GRADES

ARINDAM BASU [1]

[1] *Indian Institute of Technology Kharagpur, India, abasu@gg.iitkgp.ac.in*

Introduction

The ongoing process of weathering in nature produces progressive but intricate changes in rock microstructure. The common 6-fold weathering classification scheme for uniform materials proposed by ANON (1995) is applicable for categorizing weathering grades of most polymineralic rocks. However, capturing the intricate gradational change of quartzite in response to weathering is a challenging task as quartz, the most resistant mineral to weathering, is the chief mineral constituent of quartzite. Subsequently, assessing mechanical properties of quartzitic materials with reference to weathering grades becomes difficult in an engineering environment encountering weathered profiles.

It is likely that the degree of weathering of the joint surface materials would influence the shear behavior of quartzitic joints. However, quantitative assessment of shear behavior of quartzitic joints with reference to weathering grades does not seem to have gained much attention.

This extended abstract first presents the author's experience in categorizing weathering grades of quartzitic materials from the Chaibasa Formation (India) and evaluating their mechanical properties with reference to the categorized grades. Subsequently, the shear behavior of quartzitic joints with regard to the degree of weathering of joint surface materials, which has got tremendous implications to shallow-depth rockslides in quartzitic terrains of tropical/sub-tropical regions, is also evaluated.

Methods

Quartzitic rock materials from the Chaibasa Formation (India) were investigated by the author and his co-workers (Basu et al., 2011; 2012). An attempt was made to categorize weathering grades of these materials using the 6-fold weathering classification scheme (ANON, 1995). In order to capture the gradational variations of the quatzitic materials, observations pertaining to discoloration/staining, grain luster, intactness of grain boundaries, relative strength and slaking were utilized to discriminate weathering-induced gradational changes of the quartzite materials. It is to note that quartzite dominantly consists of quartz grains which hardly show any discoloration and the weathered appearance of the quartzitic rocks is attributed mainly to the alteration of biotite and other iron bearing minerals that are present in a small proportion (< 5% of the rock volume). Such macroscopic categorization of weathering grades was also substantiated by microstructural study as well as by rock index tests (e.g. rebound hammer test). Uniaxial compression and Brazilian tensile tests were performed on the drilled core specimens of the quartzite.

Only a handful of studies explored the influence of weathering on the shear behavior of rock joints. With regard to quartzitic joints, this issue did not seem to have been explored. The author along with his co-workers (Ram and Basu, 2019) investigated shear behavior of unfilled-planar qurtzitic joints with reference to weathering grades of joint surfaces. The weathering grades were determined exactly in compliance with the method demonstrated by (Basu et al., 2011; 2012). Multistage CNL (constant normal load) direct shear tests were performed at three different consecutively increasing normal stresses within a range of 0.22–0.70 MPa under dry condition. Since quartzite is virtually a monominerallic rock and joints with different weathering grades but with comparable joint roughness coefficient were selected for the study, the shear behavior observed in the laboratory were likely to be a direct function of weathering grade of the joint surfaces.

Results

Uniaxial compressive strength, Young's modulus and Brazilian tensile strength of the quartzitic materials were determined in the laboratory. The ranges of these values with reference to weathering grades are presented in Table 1 which broadly demonstrates an adverse effect of weathering on the mechanical behaviors. Table 1 also shows some overlap of these ranges particularly in adjacent grades.

Table 1. Mechanical properties of quartzitic materials with reference to weathering grades (from Basu et al., 2011; 2012)

Weathering grade	Uniaxial compressive strength (MPa)	Young's modulus (GPa)	Brazilian tensile strength (MPa)
I	-205.76-	-45.56-	11.35-8.99
II	114.75-51.71	15.88-6.07	8.50-2.54
III	80.00-42.46	5.22-3.45	4.79-1.87
IV	-42.44-	-1.08-	2.29-1.65

Representative shear stress-shear displacement plots of the quartzitic joints are shown in Figure 1. It should be noted that finding fresh rocks at the ground surface is unusual as reported by previous researchers. The omission/absence of Grade I joint surface in Figure 1 is attributed to the unavailability of those rocks on the investigated outcrops. A clear adverse effect of degree of weathering on the shear behavior of joints becomes apparent (Figure 1). The strength of the joint surface materials which is a function of weathering grade plays a key role in controlling the shear behavior of the joints with minimal asperities. The nature of the shear behavioural patterns of Grade II and Grade III joints are, however, similar whereas Grade IV joint shows a completely different shear stress-shear displacement pattern (Figure 1). It was not possible to carry out multistage CNL direct shear tests on Grade IV joint surfaces as the test specimens got broken after the first phase of shearing (Figure 1). Another interesting feature Figure 1 depicts is that the difference of peak strength between two dissimilar grades is maximum at the highest normal stress. This can be attributed to the crushing of asperities which is more likely to happen at relatively higher normal stresses in case of higher weathering grade. From the peak shear strength vs. normal stress plots, the peak friction angle could be determined. The ranges of peak friction angle for Grade II and Grade III joints were found to be 38°–40° and 31°–35°, respectively.

Conclusions

- The conventional 6-fold weathering classification for uniform materials is capable of capturing gradational weathering induced changes of quartzitic materials.
- As weathering intensifies, deterioration of mechanical properties of quartzite becomes apparent. The ranges of mechanical properties of quartzitic materials, however, do depict some overlaps particularly in adjacent grades.
- As weathering of quartzitic joints intensifies, both peak shear strength and peak friction angle get reduced.
- At higher normal stresses, the adverse effect of joint surface weathering on the peak shear strength becomes more prominent than at lower normal stresses.

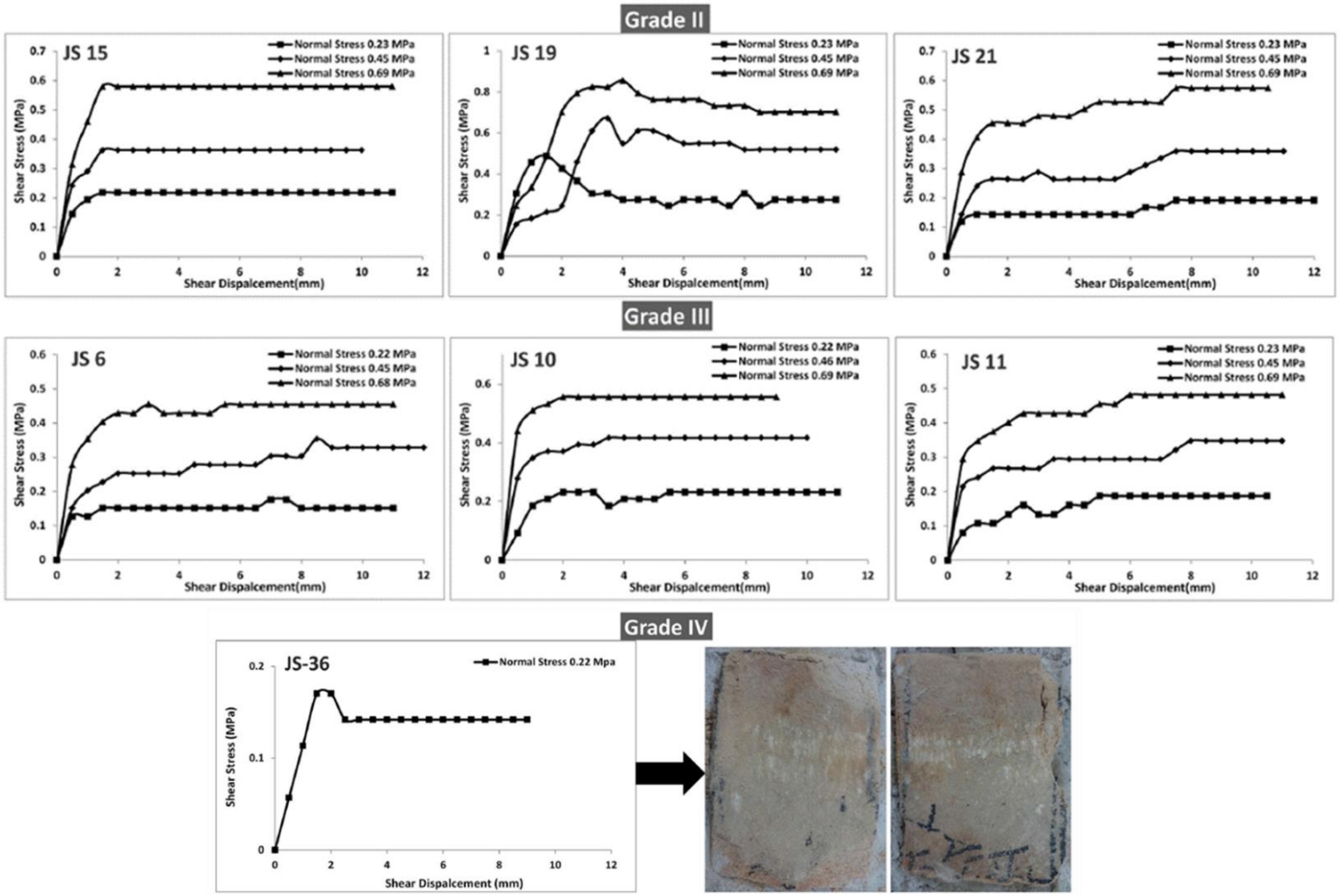

Figure 1. Representative **s**hear stress-shear displacement plots with reference to weathering grades of quartzitic joints (from Ram and Basu, 2019)

References

ANON. The description and classification of weathered rocks for engineering purposes:

Geological Society Engineering Group Working Party Report. *Quarterly Journal of Engineering Geology and Hydrogeology.* 1995, 28, 207–242.

Basu, A.; Ghosh, N.; Das, M. Weathering grade categorization and subsequent evaluation of compressive and tensile strengths of quartzite. *Journal of Engineering Geology.* 2011, XXXVII, 1–4.

Basu, A.; Ghosh, N.; Das, M. Categorizing weathering grades of quartzitic materials and assessing Brazilian tensile strength with reference to assigned grades. *International Journal of Rock Mechanics & Mining Sciences.* 2012, 49, 148–155.

Ram, B. K.; Basu, A. Shear behavior of unfilled-planar quartzitic rock joints with reference to weathering grade of joint surfaces. *Rock Mechanics and Rock Engineering.* 2019, 52, 4113–4121.

IDENTIFICATION OF GOAF AREAS AND DEFORMATION CHARACTERISTICS IN ORDOS

CHEN CAO [1], QING WANG [1], JIANPING CHEN [1], ZONGZHENG LI [1], QINGKUN YANG [1], LIANJING ZHENG [1]

[1] *Jilin University, China, ccao@jlu.edu.cn*

Introduction

Ordos City is a significant coal production base in China, with frequent mining activities that have led to the formation of numerous goaf areas.By analyzing the deformation rate values and distribution characteristics from SBAS-InSAR results, the range of subsidence areas caused by coal mining in Ordos City can be identified. The deformation characteristics of these subsidence areas are further examined by focusing on typical subsidence zones based on their deformation rates.

Methods

In this research, SBAS-InSAR technology is employed to monitor surface deformation in the coal mines of Ordos City and obtain detailed deformation information for the study area. The deformation rate is then estimated using the singular value decomposition method, allowing for the characterization of the temporal variation in the study area.

Results

A total of 142 coal mine goaf subsidence areas were identified within the study area, covering a total of 833.83 km², with a maximum deformation of -778.362 mm.

The subsidence rate in these areas is negative, exhibiting a pattern of multi-layered circular nesting. According to the timing analysis results, subsidence in the goaf areas occurs continuously.The subsidence rate is significantly influenced by mining activities, leading to a sharp increase in settlement rates.

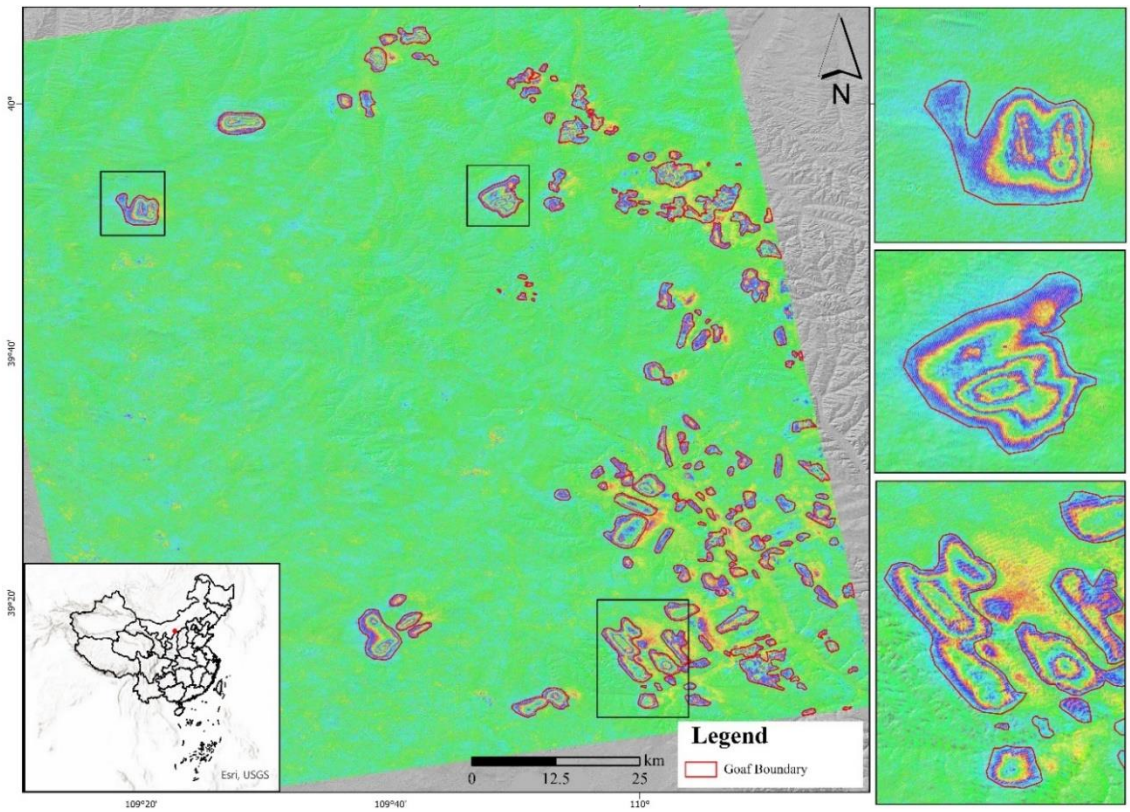

Figure 1. Annual deformation rate of Ordos and enlarged views of typical ereas

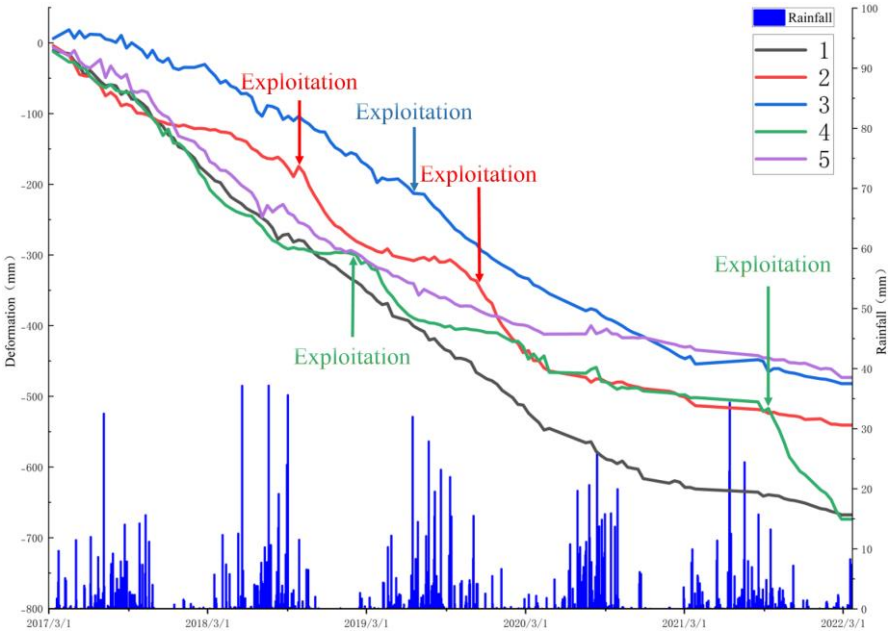

Figure 2. Deformation results from the time series curve of characteristic points in the subsidence zone

Conclusion

To mitigate the threats to personal safety and property loss caused by geological disasters in large subsidence areas resulting from extensive mining activities in Ordos City, it is crucial to accurately determine the subsidence zones within goaf areas.

By analyzing surface deformation rates and distribution patterns, along with temporal analysis of deformation characteristics, these hidden geological dangers can be effectively identified and addressed, reducing the risks associated with subsidence areas.

References

Baek, et al. "Analysis of ground subsidence in coal mining area using SAR interferometry." Geosciences Journal 12 (2008): 277-284.

Du, Yuling, et al. "Investigation of deformation patterns by DS-InSAR in a coal resource-exhausted region with Spaceborne SAR imagery." Journal of Asian Earth Sciences: X 5 (2021): 100049.

Hooper, Andrew, and Howard A. Zebker. "Phase unwrap** in three dimensions with application to InSAR time series." JOSA A 24.9 (2007): 2737-2747.

Li, Lu, et al. "An Automatic Spatial-Temporal Evolution Inversion Method of Mining Goaf Based on the Improved Hotspot Analysis and Probability Integral Method." IEEE Journal of Selected Topics in Applied Earth Observations and Remote Sensing (2023).

Li, Menghua, et al. "Detection of coal-mining-induced subsidence and map** of the resulting deformation using time series of ALOS-PALSAR data." Remote Sensing Letters 7.9 (2016): 855-864.

Liu, Lin, et al. "Accelerated glacier mass loss (2011–2016) over the Puruogangri ice field in the inner Tibetan Plateau revealed by bistatic InSAR measurements." Remote Sensing of Environment 231 (2019): 111241.

Zhang, Yonghong, et al. "Monitoring of urban subsidence with SAR interferometric point target analysis: A case study in Suzhou, China." International Journal of Applied Earth Observation and Geoinformation 13.5 (2011): 812-818.

Zhao, Changjun, et al. "A ground surface deformation monitoring InSAR method using improved distributed scatterers phase estimation." IEEE Journal of Selected Topics in Applied Earth Observations and Remote Sensing 12.11 (2019): 4543-4553.

UNSTABLE SEEPAGE CHARACTERISTICS OF UNDERLYING SOFT CLAY ASSOCIATED WITH MICROSCOPIC MECHANISM IN RECLAMATION AREA: A CASE STUDY

MENG YAO [1], QING WANG [1], QINGBO YU [1], JIANPING CHEN [1]

[1] *College of Construction Engineering, Jilin University, Changchun 130026, China, yuqb@jlu.edu.cn*

Introduction

Artificial reclamation is one of the main means of land expansion for many coastal cities around the world. However, the permeability of underlying soft clay (USC), derived from the dredged load, has not been paid enough attention, although it is closely related to the long-term deformation and stability of foundation soil. Hence, this paper analyzes the relationship between time-varying permeability characteristics and microscopic pore characteristics of USC in reclamation area. This paper may provide a scientific basis for explaining the long-term differential subsidence in different reclamation areas and other similar areas.

Methods

Chongming East Shoal located at the eastern end of Chongming Island, is one of the typical multi-phase reclamations in Shanghai. Five boreholes were arranged from west to east to obtain the property change of soft clay in different reclamation periods.A series of indoor tests, including the variable head permeability test, mercury intrusion porosimetry, and scanning electron microscope, were carried out to reveal the micro-mechanism of differential permeability.

Results

The results revealed that the seepage process of clay showed a transition from unstable seepage to relatively stable seepage. Meanwhile, the permeability coefficient (PC) attenuated with time cyclically, indicating the alternating effect of the closed and opened unstable seepage channels. During seepage, clay particles could be entrained by pore water and intercepted by pores, thus clogging seepage channels. Then, the increased pore water pressure could break through new seepage channels. The degree of pore clogging was positively correlated with the average cycle period of PCs, and this was also present in the relatively stable stage of PCs.

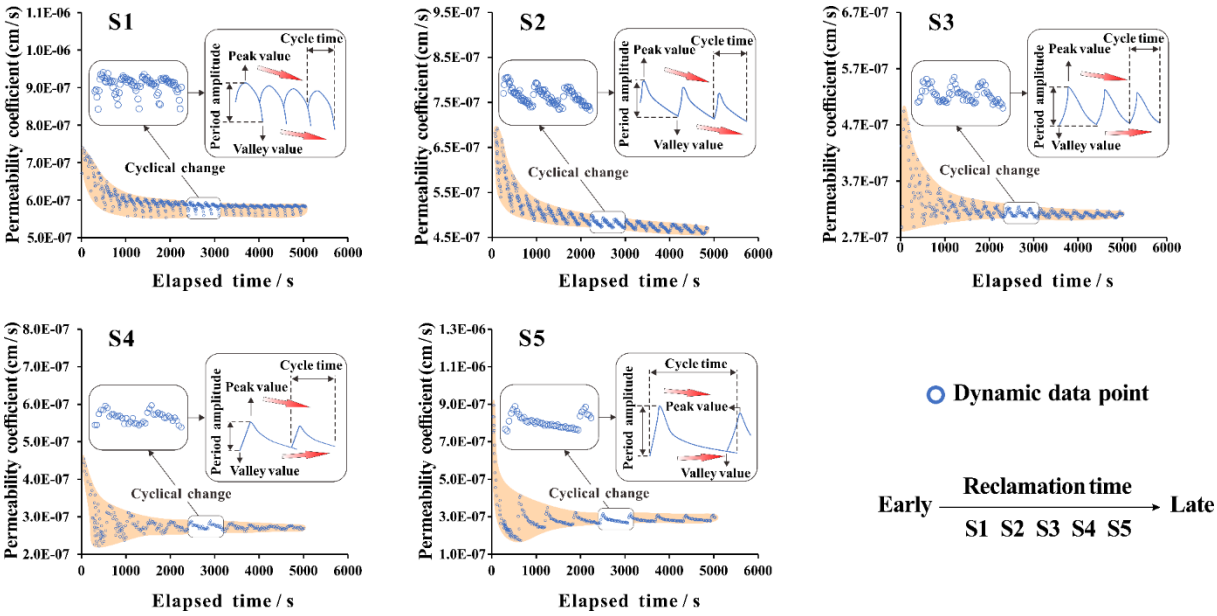

Figure 1. Evolution and statistics (per 1000 s) of representative permeability coefficients of soil samples S1-S5.

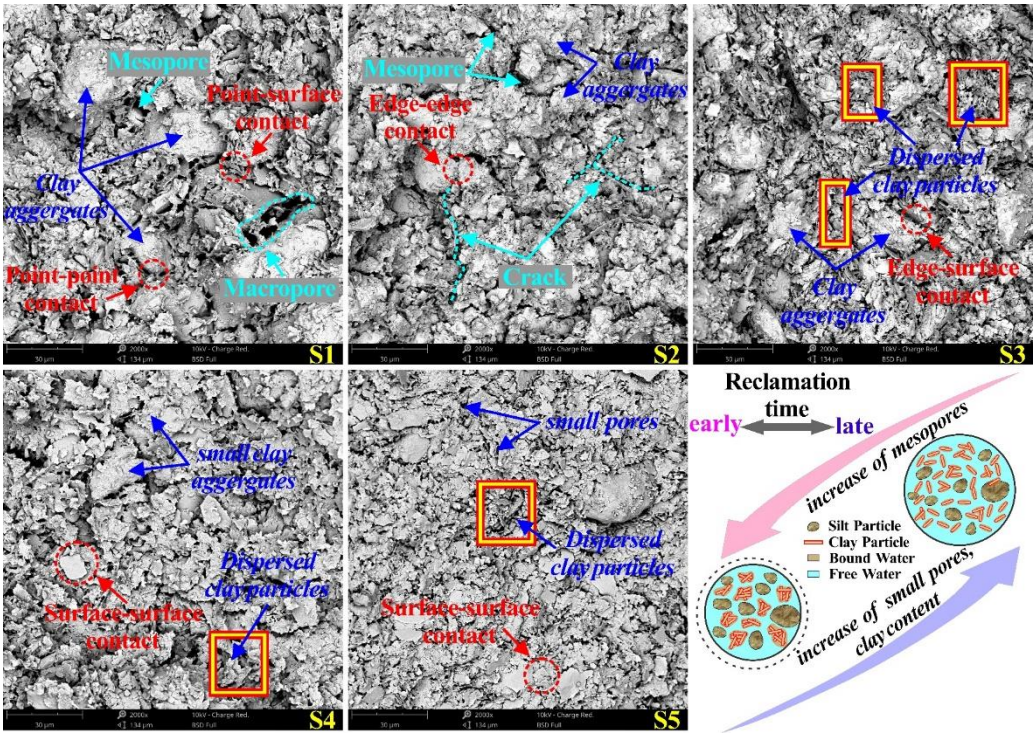

Figure 2. Microstructure characteristics of USC in different reclamation areas

Conclusion

A lower mesopores content, higher fractal dimension, and aggregated flocculate microstructure could promote the clogging effect and result in lower permeability efficiency. Affected by unstable seepage channels, soft clay may face long-term potential deformation in the future, which needs further investigation.

References

Yuan, X.Q.; Wang, Q.; Lu, W.X.; Zhang, W.; Chen, H.E.; Zhang, Y. Indoor simulation test of step vacuum preloading for high-clay content dredger fill. *Marine Georesources & Geotechnology*. 2018, 36, 83–90.

Horikoshi, K.; Takahashi, A. Suffusion-induced change in spatial distribution of fine fractions in embankment subjected to seepage flow. *Soils and Foundations*. 2015, 55, 1293–1304.

Zhang, M.X.; Zhu, X.W.; Yu, G.L.; Yan, J.M.; Wang, X.B.; Chen, M.L.; Wang, W.M. Permeability of muddy clay and settlement sim-ulation. *Ocean Engineering.* 2015, 104, 521–529.

Han, Y.; Wang, Q.; Xia, W.T.; Liu, J.; Wang, J.Q.; Chen, Y.T.; Shen, J.J. Experimental study on the hydraulic conductivity of un-saturated dispersive soil with different salinities subjected to freeze-thaw. *Journal of Hydrology*. 2020, 583, 124297.

HIGH-SPEED IDENTIFICATION OF COMPLEX DISCONTINUITIES IN LARGE-SCALE ROCK OUTCROPS

WEN ZHANG [1], JIALI HAN [2], JIANPING CHEN [3], QING WANG [4]

[1] *Jilin University, China, zhang_wen@jlu.edu.cn*

[2] *Jilin University, China, Jlhan21@mails.jlu.edu.cn*

[3] *Jilin University, China, chenjp@jlu.edu.cn*

[4] *Jilin University, China, wangqing@jlu.edu.cn*

Introduction

Discontinuities on slopes typically exhibit lower mechanical strength compared to the intact rock, making rockfalls and landslides slide along them. As a result, accurately identifying discontinuities on high and steep slopes is crucial for determining the boundaries of engineering geohazards.

Point cloud data is widely used in automatic identification research. Traditional methods for automatic identification based on point cloud data can be broadly classified into two categories: clustering methods and region growing methods. While these algorithms have produced significant results in academic research, previous studies have predominantly focused on simpler scenarios. These scenarios often involve smaller point cloud datasets, and more regularly developed discontinuities with distinct variations among different groups of discontinuities.

In contrast, practical large-scale applications present more challenging conditions, with discontinuities that are numerous, and highly disordered with complex orientations non-smooth surfaces. These complexities place greater demands on the ability of the algorithm to accurately process and efficiently identify discontinuity.

The objective of this paper is to develop an algorithm capable of efficiently processing point clouds containing tens of millions of points while ensuring high recognition accuracy for complex discontinuities.

Methods

This paper proposes an edge-first connection algorithm, which first identifies all discontinuity edge points in the point cloud without considering their specific association with any particular discontinuity. The next step is to merge the non-edge points belonging to the same discontinuity through a connectivity operation, thereby completing the identification process. This approach differs from traditional algorithms that sequentially identify one discontinuity at a time before moving on to the next. The advantage of the edge-first connection algorithm is that it simplifies complex logical operations during computation, significantly improving computational efficiency.

The first step of the proposed method based on point cloud data is to identify discontinuity edges within the neighbourhood. The method identifies edge points by analyzing the deviation of normal vectors. Specifically, the normal vector for each point is calculated by fitting a plane to its nearest neighbouring points. If the angle between the normal vector of a point and its neighbours exceeds a set threshold, the point is classified as an edge point. This process is repeated for all points, effectively identifying the edge points in the point cloud.

The second step of the method involves merging non-edge points belonging to the same discontinuity by checking for shared neighbouring points. Closely located non-edge points within the same discontinuity tend to have overlapping neighbourhoods, while points from different discontinuities do not share neighbours due to edge points separating them. This process is facilitated by applying

connectivity principles from graph theory, where points and their neighbours are treated as subsets of nodes. The algorithm identifies and merges connected subsets until it forms maximal connected subsets, representing complete discontinuities.

Results

The edge-first connection algorithm was applied to identify discontinuities on the Xulong slope located in the Jinsha River suture zone. The slope, measuring 280 meters in length and 200 meters in height, comprises a point cloud with 13 million points. The algorithm efficiently identified 2780 discontinuities on the slope within just 3 hours, demonstrating excellent recognition efficiency. A comparison between the discontinuities identified by the automatic method and those identified manually on the model revealed that the pole plots from both methods had highly similar pole distributions and high-density centres (Figure 1). Furthermore, both methods identified three dominant groups of discontinuities, with their orientations shown in Table 1. The differences in orientations between the dominant groups identified by the two methods ranged from 2° to 8°. This result demonstrates that the edge-first connection algorithm also delivers highly satisfactory accuracy in recognizing complex fractures over large areas.

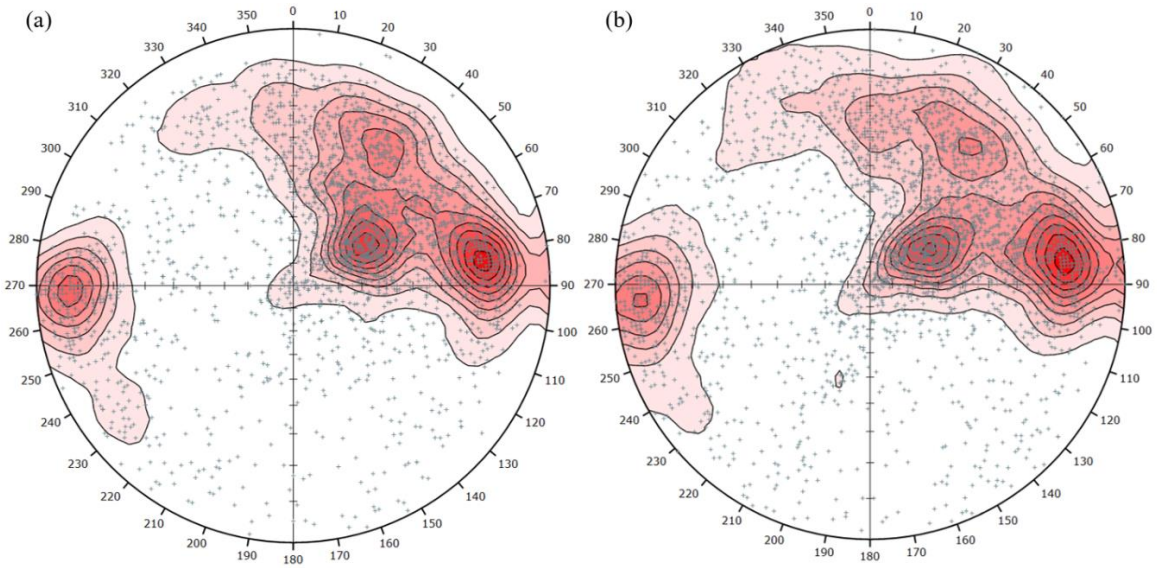

Figure 1. The comparison of pole charts from automatic method (a) and manual method (b).

Table 1. The comparison of the dominant groups from automatic and manual method

Method	Group 1	Group 2	Group 3
Automatic	46°∠30°	84°∠74°	23°∠63°
Manual	51°∠32°	76°∠72°	20°∠60°

Conclusion

This paper presents an edge-first connection algorithm that uses a computational approach distinct from traditional methods, significantly reducing complex logical operations. When applied to identifying discontinuities on the Xulong slope in the Jinsha River suture zone, the algorithm delivered outstanding results, showcasing both high computational efficiency and impressive accuracy. These outcomes demonstrate the feasibility of rapidly identifying complex discontinuities across large-scale rock slopes.

References

Assali, P., Grussenmeyer, P., Villemin, T., Pollet, N. & Viguier, F. Surveying and modeling of rock discontinuities by terrestrial laser scanning and photogrammetry: Semi-automatic approaches for linear outcrop inspection. Journal of Structural Geology. 2014, 66:102-114.

Battulwar, R., Zare-Naghadehi, M., Emami, E. & Sattarvand, J. A state-of-the-art review of automated extraction of rock mass discontinuity characteristics using three-dimensional surface models. Journal of Rock Mechanics and Geotechnical Engineering. 2021, 13(4):920-936.

Brideau, M.-A., Yan, M. & Stead, D. (2009) The role of tectonic damage and brittle rock fracture in the development of large rock slope failures. Geomorphology. 2009, 103(1):30-49.

Chen, J., Zhu, H. & Li, X. Automatic extraction of discontinuity orientation from rock mass surface 3D point cloud. Computers & Geosciences. 2016, 95:18-31.

Chen, N., Cai, X., Li, S., Zhang, X. & Jiang, Q. Automatic extraction of rock mass discontinuity based on 3D laser scanning. Quarterly Journal of Engineering Geology and Hydrogeology. 2020, 54(1):qjegh2020-054.

Daghigh, H., Tannant, D. D., Daghigh, V., Lichti, D. D. & Lindenbergh, R. A critical review of discontinuity plane extraction from 3D point cloud data of rock mass surfaces. Computers & Geosciences. 2022, 169:105241.

Ding, L., Kapp, P. & Wan, X. Paleocene-Eocene record of ophiolite obduction and initial India-Asia collision, South central Tibet. Tectonics. 2005, 24:TC3001.

Drews, T., Miernik, G., Anders, K., Höfle, B., Profe, J., Emmerich, A. & Bechstädt, T. Validation of fracture data recognition in rock masses by automated plane detection in 3D point clouds. International Journal of Rock Mechanics and Mining Sciences. 2018, 109:19-31.

Ferrero, A. M., Forlani, G., Roncella, R. & Voyat, H. I. (2009) Advanced Geostructural Survey Methods Applied to Rock Mass Characterization. Rock Mechanics and Rock Engineering. 2009, 42(4):631-665.

Ge, Y., Cao, B. & Tang, H. (2022) Rock Discontinuities Identification from 3D Point Clouds Using Artificial Neural Network. Rock Mechanics and Rock Engineering. 2022, 55(3):1705-1720.

Ge, Y., Tang, H., Xia, D., Wang, L., Zhao, B., Teaway, J. W., Chen, H. & Zhou, T. Automated measurements of discontinuity geometric properties from a 3D-point cloud based on a modified region growing algorithm. Engineering Geology. 2018, 242:44-54.

Gigli, G. & Casagli, N. Semi-automatic extraction of rock mass structural data from high resolution LIDAR point clouds. International Journal of Rock Mechanics and Mining Sciences. 2011, 48(2):187-198.

Gomes, R. K., De Oliveira, L. P. L., Gonzaga, L., Tognoli, F. M. W., Veronez, M. R. & De Souza, M. K. An algorithm for automatic detection and orientation estimation of planar structures in LiDAR-scanned outcrops. Computers & Geosciences. 2016, 90:170-178.

Hu, L., Xiao, J. & Wang, Y. Efficient and automatic plane detection approach for 3-D rock mass point clouds. Multimedia Tools and Applications. 2020, 79(1):839-864.

Kong, D., Wu, F. & Saroglou, C. Automatic identification and characterization of discontinuities in rock masses from 3D point clouds. Engineering Geology. 2020, 265:105442.

Menegoni, N., Giordan, D., Perotti, C. & Tannant, D. D. Detection and geometric characterization of rock mass discontinuities using a 3D high-resolution digital outcrop model generated from RPAS imagery–Ormea rock slope, Italy. Engineering Geology. 2019, 252:145-163.

Olariu, M. I., Ferguson, J. F., Aiken, C. L. V. & Xu, X. Outcrop fracture characterization using terrestrial laser scanners: Deep-water Jackfork sandstone at Big Rock Quarry, Arkansas. Geosphere. 2008, 4(1):247-259.

Riquelme, A., Cano, M., Tomás, R. & Abellán, A. Identification of Rock Slope Discontinuity Sets from Laser Scanner and Photogrammetric Point Clouds: A Comparative Analysis. Procedia Engineering. 2017, 191:838-845.

Riquelme, A. J., Abellán, A., Tomás, R. & Jaboyedoff, M. A new approach for semi-automatic rock mass joints recognition from 3D point clouds. Computers & Geosciences. 2014, 68:38-52.

Singh, S. K., Raval, S. & Banerjee, B. P. Automated structural discontinuity mapping in a rock face occluded by vegetation using mobile laser scanning. Engineering Geology. 2021, 285:106040.

Sturzenegger, M. & Stead, D. Close-range terrestrial digital photogrammetry and terrestrial laser scanning for discontinuity characterization on rock cuts. Engineering Geology. 2009, 106(3):163-182.

Sun, W., Wang, J., Yang, Y. & Jin, F. Rock Mass Discontinuity Extraction Method Based on Multiresolution Supervoxel Segmentation of Point Cloud. IEEE Journal of Selected Topics in Applied Earth Observations and Remote Sensing. 2021, PP:1-1.

Wang, S., Zhang, W., Zhao, X., Sun, Q. & Dong, W. Automatic identification and interpretation of discontinuities of rock slope from a 3D point cloud based on UAV nap-of-the-object photogrammetry. International Journal of Rock Mechanics and Mining Sciences. 2024, 178:105774.

Wang, W., Zhao, W., Chai, B., Du, J., Tang, L. & Yi, X. Discontinuity interpretation and identification of potential rockfalls for high-steep slopes based on UAV nap-of-the-object photogrammetry. Computers & Geosciences. 2022, 166:105191.

Wang, X., Zou, L., Shen, X., Ren, Y. & Qin, Y. A region-growing approach for automatic outcrop fracture extraction from a three-dimensional point cloud. Computers & Geosciences. 2017, 99:100-106.

Wasantha, P. L. P., Ranjith, P. G., Xu, T., Zhao, J. & Yan, Y. L. (2014) A new parameter to describe the persistency of non-persistent joints. Engineering Geology. 2014, 181:71-77.

Wilkinson, M. W., Jones, R., Woods, C. E., Gilment, S., Mccaffrey, K., Kokkalas, S. & Long, J. A comparison of terrestrial laser scanning and structure-from-motion photogrammetry as methods for digital outcrop acquisition. Geosphere. 2016, 12:GES01342.1.

Wu, Q. & Kulatilake, P. H. S. W. (2012) REV and its properties on fracture system and mechanical properties, and an orthotropic constitutive model for a jointed rock mass in a dam site in China. Computers and Geotechnics. 2012, 43:124-142.

Wu, Q., Liu, Y., Tang, H., Kang, J., Wang, L., Li, C., Wang, D. & Liu, Z. Experimental study of the influence of wetting and drying cycles on the strength of intact rock samples from a red stratum in the Three Gorges Reservoir area. Engineering Geology. 2023, 314:107013.

Yan, J., Chen, J., Zhan, J., Song, S., Zhang, Y., Zhao, M., Liu, Y. & Xu, W. Automatic identification of rock discontinuity sets using modified agglomerative nesting algorithm. Bulletin of Engineering Geology and the Environment. 2022, 81(6):229.

Yi, X., Feng, W., Wang, D., Yang, R., Hu, Y. & Zhou, Y. An efficient method for extracting and clustering rock mass discontinuities from 3D point clouds. Acta Geotechnica. 2023, 18(7):3485-3503.

Zeng, Y., Lei, Q., Wang, Z., Ding, S., Liu, K., Huang, X., Huang, Z. & Wang, X. Numerical simulation of fluid injection-induced fault slip in heterogeneous shale formations. Computers and Geotechnics. 2021, 134:104120.

Zhang, S.-L., Yin, Y.-P., Hu, X.-W., Wang, W.-P., Zhu, S.-N., Zhang, N. & Cao, S.-H. Initiation mechanism of the Baige landslide on the upper reaches of the Jinsha River, China. Landslides. 2020, 17:2865-2877.

Zhang, W., Han, J., Lu, C., Liu, H., Chen, J., Wang, J., Li, T. & Chen, J. Geometric searching of 3D critical slip surface of a non-persistent fracture-dominated rock slope. Computers and Geotechnics. 2024, 173:106493.

Zhang, W., Zhao, X., Pan, X., Wei, M., Yan, J. & Chen, J. Characterization of high and steep slopes and 3D rockfall statistical kinematic analysis for Kangyuqu area, China. Engineering Geology. 2022, 308:106807.

Topic 2

Engineering Geology and Cultural Heritage Protection

PORE STRUCTURE EVOLUTION IN ANDESITE ROCKS INDUCED BY FREEZE-THAW CYCLES EXAMINED BY NON-DESTRUCTIVE METHODS

MARTIN MAĽA [1], VLADIMÍR GREIF [2], MARTIN ONDRÁŠIK [3]

[1] *Department of Engineering Geology, Hydrogeology and Applied Environmental Geophysics, Faculty of Natural Sciences, Comenius University in Bratislava, Slovakia, mala26@uniba.sk*

[2] *Department of Engineering Geology, Hydrogeology and Applied Environmental Geophysics, Faculty of Natural Sciences, Comenius University in Bratislava, Slovakia, vladimir.greif@uniba.sk*

[2]) *Department of Geotechnics, Faculty of Civil Engineering, Slovak University of Technology in Bratislava, Slovakia, martin.ondrasik@stuba.sk*

Introduction

Mechanical or physical weathering (physical rock breakdown) is a key process that influences the appearance of geo-relief, especially at high altitudes or in polar periglacial regions. It is closely related to the regional and global climate (Grossi et al. 2007). Physical rock breakdown mainly stems from the propagation of cracks in the rock matrix (Eppes and Keanini, 2017). The sources of stresses induced by freezing and thawing (F-T cycling) and causing deterioration of rock material are still under discussion[3]. Frost damage may include a combination of several mechanisms, with crystallization pressure (Everett, 1961; Scherer, 1999; Steiger, 2005a, 2005b; Steiger et al., 2014; Walder and Hallet, 1985) currently being the main contributor. This is followed by subsequent hydraulic (Powers, 1945) or volumetric expansion (Hirschwald, 1908). The relative importance of these mechanisms varies depending on the material properties, moisture conditions, and thermal conditions (Hall, 1999).

In this study, we compare the values of petrophysical properties before and after 100 freeze-thaw (F-T) cycles, as well as the recorded length change behavior and temperature development on a vacuum-saturated fractured andesite rock sample taken from the Babina Quarry in Slovakia. This was done using a specially-constructed thermodilatometer, VLAP 04, equipped with two HIRT-LVDT sensors. Additionally, we employed non-destructive visualization of the rock pore network via μCT imaging to investigate the evolution of the pore structure and fracture network in pyroxene andesites throughout the freeze-thaw process.

Methods

Initial Properties of Rock Fabric

The basic hypothesis underlying our experimental approach is that the pressures induced by ice crystallization caused microcrack growing a this correlates with increase in pore volume, level of pore connectivity and changes in pore size distribution that are made possible through water supply to growing ice front. Rock deterioration induced by the effects of frost weathering results from the combined action of processes mainly linked to rocks' pore network system parameters (initial petrophysical parameters). In this study, we worked with fractured andesite core sample of a cylinder shape with a size of 5.0 cm in length and 3.2 cm in diameter. The solid phase, which controls mechanical strength of rocks and building materials by extent of cementation and mineral phase bonding was analyzed by scanning electron microscopy- SEM, of standard polished thin section.

Quantification of changes in pore system network before and after F-T cycling was performed repeatedly by set of nondestructive techniques, with emphasis on:

- pore interconnectivity by spontaneous imbibition method according to Hu et al.[13] and Maľa and Greif;
- pore size distribution by newly developed experimental method for identifying the pore structure of rocks according to Ondrášik et al. [15]. Results of representative pore radii distribution pattern was also verified by mercury intrusion porosimetry.

Non-destructive visualizations

Visualization and quantification of microcrack propagation before and after repeated freezing and thawing was performed on industrial μCT Phoenix | tome | x L 240 according to Maľa et al. (2022). Image processing was carried out in AVIZO 2019.1 software by several image visualization techniques.

Freeze-Thaw tests

To understand the internal structural changes of the sample induced by damage mechanisms during ice crystallization we simulated freeze thaw conditions by custom designed thermodilatometer VLAP 04 [14]. VLAP 04 is capable of controlling the temperature change in the range -17°C to +60°C and we simulated temperature change in the range from -10°C to +10°C with cooling rate of -0.18°C/min and subsequent heating rate of 0,21°C/min to avoid thermal shock. Porosity change induced by excessive pressure during F-T cycle results in a residual strain. A damage quantification can thus be derived from monitoring the length and temperature changes during the ice crystallization. This was measured by two linear variable differential transformer sensors (HIRT-LVDT-T101 F) of VLAP 04.

Results

Our results showed that the tested andesite from Babiná is a rock with extremely low porosity and a bimodal pore size distribution pattern which consists mainly of nanometric sized micropores, as well as a macropores. This corresponds to the results from the indicative rock pore structure method. Based on those results, the rock pore structure of Babina andesite predominantly contains hardly-accessible macropores, which are interconnected by micropores and mesopores. A part of this specimen's matrix contains a large amount of blind and isolated pores. Pore interconnection determined by the imbibition curve slope C(I) is also extremely low, but with a significant increase after F-T cycling. Non-destructive visualization by μCT showed only a slight increase in macroporosity of the sample after 100 F-T cycles. On the other hand, significant fracture opening corresponds to a 31 pp. increase of fracture volume. The largest dimensional changes of porous structures are also bound to the locations near the fracture. The physical breakdown of rock necessarily stems from the propagation of fractures. Freeze-thaw induced cracking of a brittle-elastic solid like pyroxene- andesite is caused by ice crystallization and hydraulic pressure build-up which led to rock fatigue failure. Subcritical cracking of the tested andesite results in total residual strain of 8x10-5 recorded after 100 F-T cycles.

Conclusion

Andesites from Babiná, which are rocks with very low total and effective porosity, as well as a high proportion of weakly interconnected micro- and mesopores, exhibit relatively good structural cohesion and high resistance to the effects of frost weathering. The main disintegration process of such volcanic rocks is subcritical fracture growth, which is induced by both crystallization and hydraulic pressures in the pore space. This process can lead to long-term deterioration of the rock material.

References

Deprez, M., De Kock, T., De Schutter, G., Cnudde, V. A review on freeze-thaw action on weathering of rocks. *Earth Sci Rev* **203**, 103143 (2020).

Eppes, M. C., Keanini, R Mechanical weathering and rock erosion by climate dependent subcritical cracking. *Rev. Geophys*. **55**, 470–508 (2017).

Everett, D.H. Thermodynamics of frost damage to porous solids. *Trans Farday Soc* **57(7)**, 1541–1551 (1961).

Grossi, C. M., Brimblecombe, P., Harris, I. Predicting long term freeze-thaw risks on Europe built heritage and archaeological sites in a changing climate. *Sci. Total Environ.* **377**, 273-281 (2007).

Hall, K. The role of thermal stress fatigue in the breakdown of rock in cold regions. Geomorphology **31**, 47–63 (1999).

Hirschwald, J. DiePrüfung der naturlichen Bausteineaufihre Verwitterungs beständigkeit, Verlag Wilhelm Ernst & Sohn, Berlin, [In German]; (1908).

Hu, M.Q., Persoff, P., Wang, J.S.Y., (2001). Laboratory measurement of water imbibition into low-permeability welded tuff. J Hydrol 242, 64–78.

Maľa, M., Greif, V. (2021). Effect of frost damage on the pore interconnectivity of porous rocks by spontaneous imbibition method. Bull. Eng. Geol. *Environ.* 80(11), 8789–8799.

Maľa, M., Greif, V. & Ondrášik, M. (2022) Pore structure evolution in andesite rocks induced by freeze–thaw cycles examined by non-destructive methods. Sci Rep 12, 8390

Powers, T.C. The air requirements of frost-resistant concrete. *Portland Cement Association, Chicago* (1949).

Steiger, M., Crystal growth in porous materials I: the crystallization pressure of large crystals. *J. Cryst. Growth* **282**, 455–469 (2005a.).

Steiger, M., Crystal growth in porous materials—II: Influence of crystal size on the crystallization pressure. J. *Cryst. Growth* **282**, 470–481 (2005b).

Steiger, M., Charola, A.E., Sterflinger, K., Stone in Architecture. In: Siegesmund, S., Snethlage, R. (Eds.), Stone in Architecture: Properties. *Springer-Verlag, Durability*, 225–315 (2014).

Walder, J., Hallet, B., A theoretical model of the fracture of rock during freezing. *Geol Soc Am Bull* **96 (3)**, 336–346 (1985).

ROCKFALL HAZARD EVALUATION IN A CULTURAL HERITAGE SITE: CASE STUDY OF AGIA PARASKEVI MONASTERY, MONODENDRI, GREECE

SPIROS PAPAIOANNOU [1], *GEORGE PAPATHANASSIOU* [2], VASILIS MARINOS [3]

1 Department of Geology, Aristotle University of Thessaloniki, Greece, spapaioan@geo.auth.gr

[2] Department of Geology, Aristotle University of Thessaloniki, Greece, gpapatha@geo.auth.gr

[2] School of Civil Engineering, National Technical University of Athens, Greece, marinosn@civil.ntua.gr

Introduction

The methodology that is usually followed for the evaluation of rockfall hazard within an area is discriminated in several stages, including a detailed engineering geology field survey and analysis of the data obtained during this survey, identification of the failure type mechanism, e.g., wedge, planar slide, toppling, and the assessment of the rockfall trajectory and the evaluation of critical parameters like the kinetic energy and the bounce height of the detached rock.

The study area concerns the rocky slope defined by Monastery of St. Paraskevi (northeast of Monodendri village) up to the natural entrance of the Vikos gorge in the Region of Epirus (northwest Greece). The structures of St. Paraskevi Monastery, including the Temple, were built more than 600 years ago, right under a nearly vertical limestone slope of more than 100m high. In the past, rockfall phenomena have occurred in the slope of the study region triggered by earthquake and rainfall resulting in the construction of protection measures.

The goal of this study is twofold: (i) to evaluate the rockfall potential, and (ii) to simulate the trajectories of likely to fail blocks in order to examine their run-out distance and to assess the rockfall hazard in terms of kinetic energy and bounce height.

Methods

For the purposes of this study, we used a geological compass to measure the orientation of the discontinuities, in terms of dip and dip direction, while a Schmidt hammer was used for estimating the uniaxial compressive strength (UCS) of the intact rock and the joint compressive strength (JCS). Furthermore, the roughness of the joints was assessed based on a profilometer. Finally, the filling material and the weathering conditions at the area were also assessed.

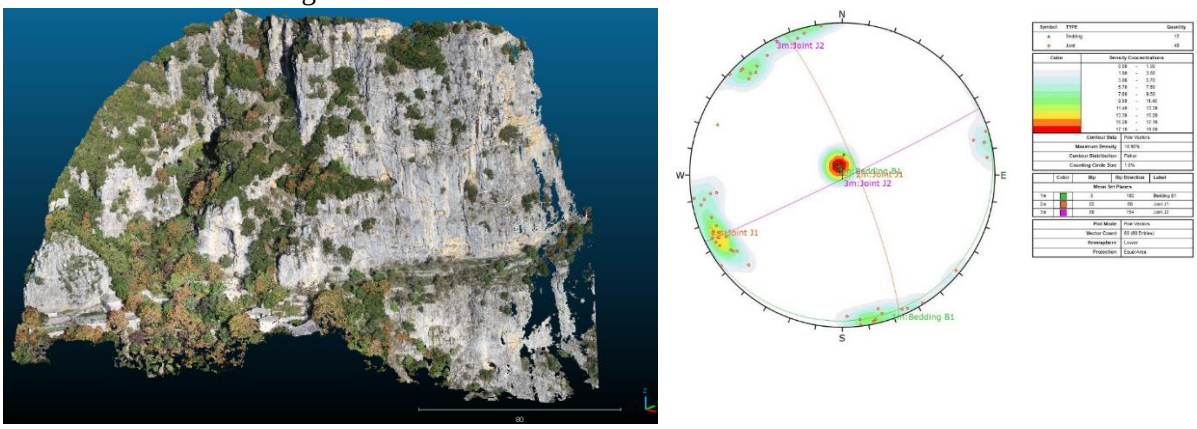

Figure 1. Left. 3D model of the slope face. Right. Stereographic projection of concentration lines of discontinuity poles from field survey based on geological compass.

Furthermore, considering the steep morphology of the rock slope, it was decided to conduct a RPAS survey in October 2021 as well as in May 2023 to reconstruct an accurate and detailed 3D model of the studied area. The RPAS imagery was collected using a DJI Phantom 4 Pro V2.0 In order to detect the

discontinuity sets and measured their orientation at the studied area, the generated on CloudCompare™ point cloud was analyzed by applying recently developed SfM-based methodologies (proposed by Riquelme et al. 2014 and described by Valkaniotis et al. 2018, Papathanassiou et al. 2021 among others). Supervised analysis using the open source software Discontinuity Set Extractor (DSE) (developed by Riquelme et al. 2014), and manually oriented (CloudCompare™) approaches were applied in the developed 3D model.

Results

The outcome arisen from the comparison of the information regarding the discontinuity sets obtained by the DSE, as well as from the field survey based on geological compass is shown in Table 1.

Table 1. Comparison of major discontinuity levels (dip/dip direction) of tectonic diagram by the DSE as well as the traditional tectonic diagram at different locations on the slope face

Set	Field Survey Measurements	DSE		
	Site D	Site A	Site B	Site C
	Dip/Dip Direction	Dip/Dip Direction	Dip/Dip Direction	Dip/Dip Direction
B1	5°/160°	23°/144°	08°/162°	08°/135°
J1	82°/068°	77°/081°	76°/088°	85°/093°
J2	88°/154°	86°/150°	83°/141°	88°/148°

Following this step, we assessed the mean volume of the likely to be detached rock boulders from slope face as 1.18m, while the maximum volume was estimated as 3.3m³. After that step, we estimated the parameters of the trajectory, kinetic energy, impact, distance and bounce height for three critical profiles. The trajectories were extracted from the developed point cloud with the open-source software CloudCompare™ and imported on the software Rocfall of Rocscience for estimating their parameters. Considering the results of the simulation, it is concluded that rockfall phenomena can threat the zone between Monastery of St. Paraskevi and natural entrance of Vikos gorge.

Conclusion

By comparing the results of traditional field survey with those provided based on the developed 3D point-cloud, using open-source software, i.e., Discontinuity Set Extractor (DSE), we found out that are in agreement. Regarding the rockfall hazard, it is pointed out that construction of rockfall barriers is necessary. In additional, scaling is suggested as the primary mitigation measure that should be realized in advance in order to minimize the risk.

References

Papathanasiou, G., Riquelme, A., Tzevelekis, T., Evaggelou, E. Rock Mass Characterization of Karstified Marbles and Evaluation of Rockfall Potential Based on Traditional and SfM-Based Methods; Case Study of Nestos, Greece. Geosciences 2020, 10, 389; doi:10.3390/geosciences10100389.

Riquelme, A.; Tomàs, R.; Cano, M.; Pastor, J.L.; Abellán, A. Automatic Mapping of Discontinuity Persistence on Rock Masses Using 3D Point Clouds. Rock Mech. Rock Eng. 2018, 51, 3005–3028.

Valkaniotis, S.; Papathanassiou, G.; Ganas, A. Mapping an earthquake-induced landslide based on UAV imagery; case study of the 2015 Okeanos landslide, Lefkada, Greece. Eng. Geol. 2018, 245, 141–152.

ARE OUR MONUMENTS MELTING AWAY? EXPLORING THE IMPACT OF CLIMATE CHANGE ON STONE SURFACE FINISHES OF BELGIAN HERITAGE BUILDINGS

MORGANE FANFONE [1], FANNY DESCAMPS [3], ANNE-LISE HANTSON [4], LAURENT DEBAILLEUX [2]

[1] University of Mons, Faculty of Engineering, Belgique, Morgane.FANFONE@umons.ac.be

[2] University of Mons, Faculty of Engineering, Belgique, Laurent.DEBAILLEUX@umons.ac.be

[3] University of Mons, Faculty of Engineering, Belgique, Fanny.DESCAMPS@umons.ac.be

[4] University of Mons, Faculty of Engineering, Belgique, Anne-Lise.HANTSON@umons.ac.be

Introduction

With the climate change and its ensuing challenges, we fear adverse repercussions for the materials and structures of our heritage buildings. These concerns include increased rainfall in European countries combined with acidification due to pollution, primarily caused by the rise in CO_2 and the presence of SO_X and NO_X compounds from human activities (IPCC 2023; Saiz-Jimenez et al. 2004). This acidic environment particularly impacts limestone, which is sensitive to the interaction of calcium carbonate ($CaCO_3$) with acid solutions (Basu et al. 2020).

Investigating material alteration involves understanding of phenomena affecting the intrinsic properties of rocks and plays an essential role in the diagnosis and preservation of stone masonry heritage buildings (Trudgill and Viles 1998). This analysis helps us to better understand the behaviour of these limestones and serves as a reference for further investigation in other acidic environment expositions.

Weathering of ashlar, especially in historic buildings, has been observed for several decades (Brimblecombe 2000; Cartwright et al. 2008; MEDISTONE and Bromblet 2010). By controlling independent parameters, it is possible to understand how the material behaves under controlled weathering conditions (pH solution, period cycling). In particular, exposure to acidic atmospheres is a concern that has been studied by many scientists (De Kock et al. 2017; Gibeaux et al. 2018; Menéndez 2018; Rodríguez et al. 2023; Salvini et al. 2022; Vagnon et al. 2021; Vázquez et al. 2015; Yan et al. 2022), with repetitive cycles enabling the correlation of various parameters such as porosity, water absorption rate, roughness, mass loss, pH values...

Methods

Two ornamental limestones were subjected to short artificial exposure: Belgian Blue Stone (BBS - Carboniferous in age) and Gobertange Stone (GS - Lutetian in age). Both rocks are found on historical monuments and newly built constructions in Belgium. BBS is composed of approximately 96% calcite, 1-10% magnesium carbonate, less than 2% quartz, others iron minerals and numerous fossils, mainly crinoids (De Barquin 2001). GS is principally composed of 73-87% calcite, 11-25% quartz and others iron minerals (Pierre et Marbres de Wallonie asbl 2024)

30 x 30 x 31mm cubes have been used for the tests. Density and porosity of samples are first determined. Two test conditions were chosen: exposure to urban synthetic rainwater composed of a mixed solution of 600 ml of HNO_3 (10-5 mol/l) and 400ml of H_2SO_4 (5.10-6 mol/l) carried at pH 5 (Eyssautier et al. 2016; Gibeaux et al. 2016); and to an exaggerated exposure of a stone kitchen worktop with an acid source like vinegar (acetic acid CH_3COOH 7% - pH 2.44). The experiments were carried out during 5 cycles of immersion and drying, without continuous agitation. (Bureau de Normalisation 2003; Xie et al. 2004). Between each cycle, the solution is renewed, starting from a known pH, and measured at the end of each phase. To ensure that the pH remains almost constant during the test, the stone specimens are alternatively immersed in approximately 130mL solutions for 24 hours (passive immersion) and then dried in a ventilated oven for 24h at 100°C.

These tests focus on the characterizing the evolution of exposed surfaces in terms of surface roughness and specific area, by using 3D optical profilometry in laboratory (Nikiema 2024). Other indicators, such as mass loss and porosity variation, are also explored.

Results

Both rocks have different initial properties: porosity less than 1% for BBS and 6-10% for GS. There is a general increase in porosity for all tested samples. Concerning the mass, each phase is characterised by a mass loss, especially with the acetic acid test. Nonetheless, GS seems to lose mass more significantly (rate of cumulative mass lost compared to initial mass after 5 cycles: BBS – 38% / GS – 43 %). After 5 cycles in immersion with acetic acid, each face of the cubes reduced by approximately 2.5mm for BBS and 4mm for GS (Figure 1-a).

A change in texture is observed for the test with acetic acid test during which partial dissolution of the rock matrix occurs. For BBS, the predominantly calcite matrix around the fossils in the rock dissolves first, revealing the fossils and increasing roughness (Phase 1 Surface roughness, all the irregularities characterising the surface, Sa = 3.843µm (std. DV 0.343) - Phase 5 Sa = 105.611 µm (std. DV 14.721)). For GS, the alteration process appears different, with more selective dissolution, revealing quartz grains (Phase 1 Sa = 11.225µm (std. DV 3.801) - Phase 5 Sa = 57.777 µm (std. DV 7.245)).

The tests in the synthetic acid rain do not show a significant trend in mass loss or change in roughness over just 5 cycles, for both rocks (Figures 1,2).

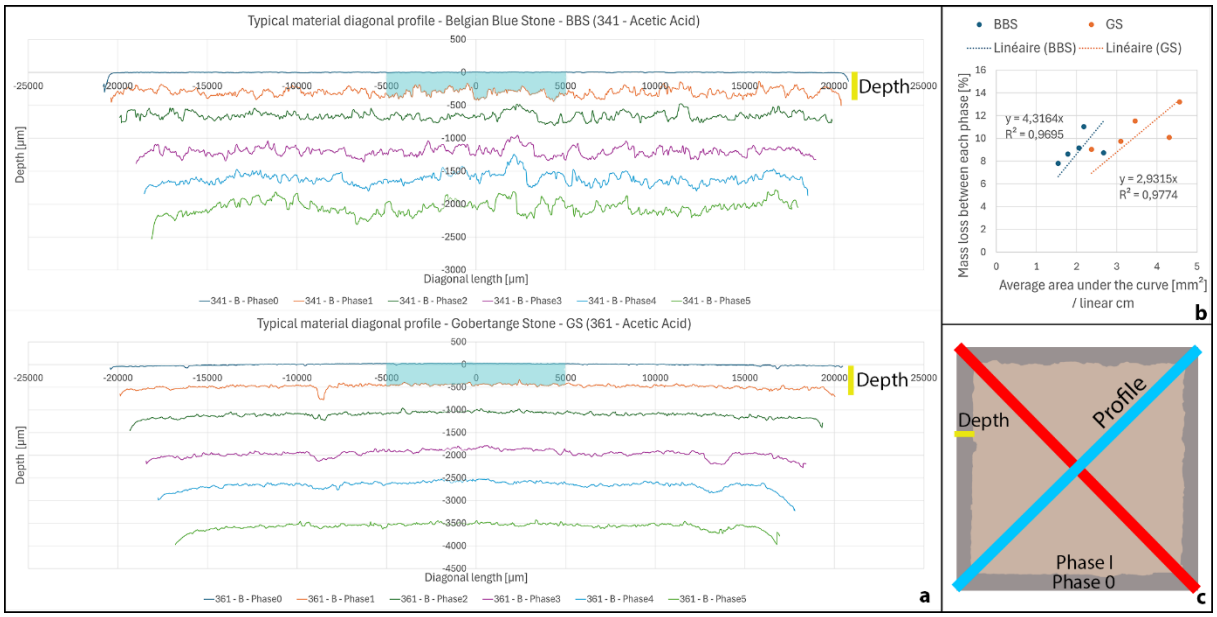

Figure 1. (a, c) Set of typical profiles for immersion of the two stones studied in acetic acid - (b) Correlation between mass loss and area under the curve per phase

Conclusion

These preliminary tests highlight key parameters, such as porosity and main matrix composition to analyse and help to understand the weathering mechanisms of building stones under cyclic acid rains attack.

Results highlight the five immersion/drying cycles had a greater impact with 7% dilute acetic acid (pH 2.44) than with synthetic acid rain (pH 5). This underscores the importance to pursue the efforts of industrialized countries to reduce polluting gases and to protect stone surfaces from household acid attacks, which are irreversible for our stone thresholds and worktops. However, the study, which involved a limited test campaign, does not allow to emphasize the aggressive nature of pH=5 rain. Further tests are necessary on these materials to determine the long-term impact of these pollutants.

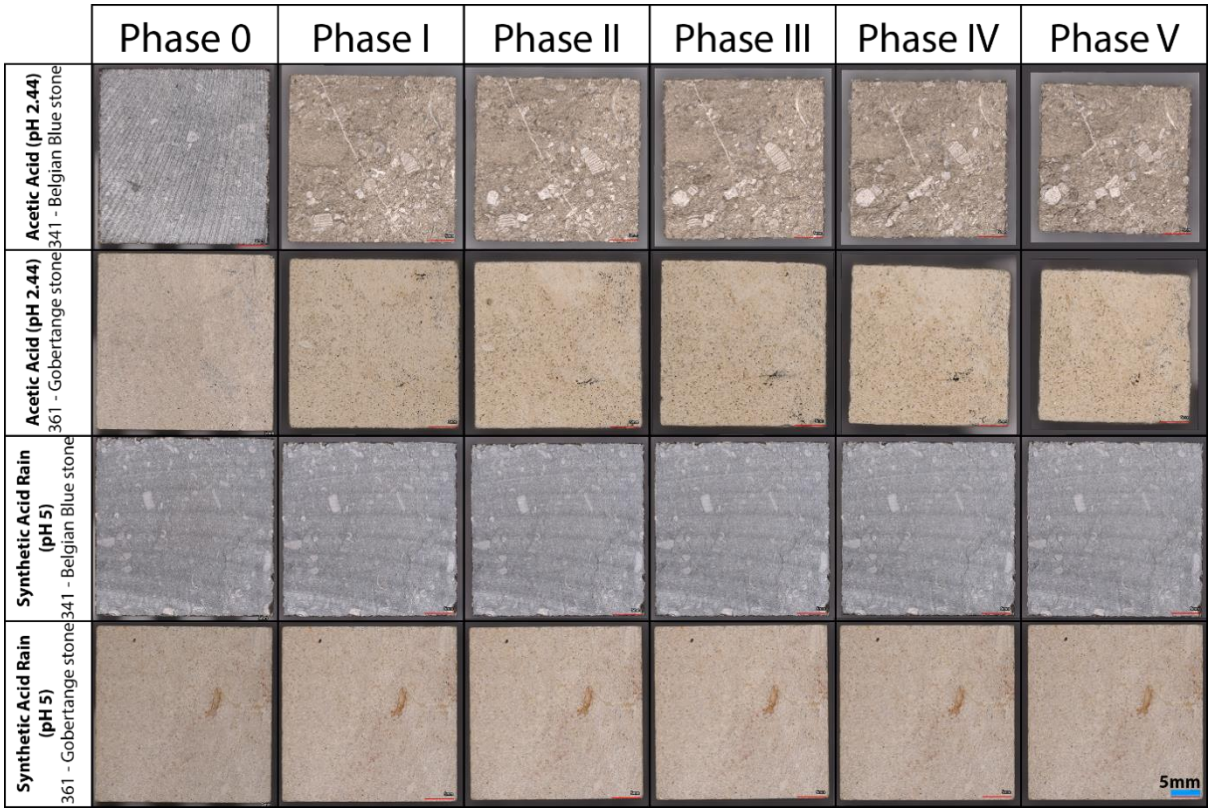

Figure 2 - Appendix. Mapping and evolution of surface finishes following the test phases. There is a noticeable reduction in the size of the samples and a change in texture for both stones following immersion in an acetic acid solution. The surface almost does not change when immersed in a synthetic acid rain solution.

References

Basu, A.; Ram, B.; Nanda, N.; 'Subhadeep Nayak, S. Deterioration of Shear Strength Parameters of Limestone Joints under Simulated Acid Rain Condition.' *International Journal of Rock Mechanics and Mining Sciences* 135, 2020. doi:10.1016/j.ijrmms.2020.104508

Brimblecombe, P. 'Air Pollution and Architecture: Past, Present and Future'. *Journal of Architectural Conservation* 6: 30–46, 2000. doi:10.1080/13556207.2000.10785268.

Bureau de Normalisation. *NBN EN 13919 NBN EN 13919 : Méthodes d'essai Pour Éléments En Pierre Naturelle - Détermination de La Résistance Au Vieillissement Accéléré Au SO_2 En Présence d'humidité.* 2003. Available online: https://www.boutique.afnor.org/fr-fr/norme/nf-en-13919/methodes-dessai-pour-elements-en-pierre-naturelle-determination-de-la-resis/fa111434/22723 (accessed on January 25, 2024).

Cartwright, A.; Bourguignon, E.; Bromblet, P.; Cassar, J.; Charola, A; Witte, E; Rodrigues, J. et al. *ICOMOS-ISCS: Illustrated Glossary on Stone Deterioration Patterns Glossaire Illustré Sur Les Formes d'altération de La Pierre.* 2008.

De Barquin, F.; Buildwise. NIT 220, 58 p., 2001/06/00. *NIT 220 : La pierre bleue de Belgique dite petit granit d'âge géologique tournaisien.* 2001. Available online: https://www.buildwise.be/fr/publications/notes-d-information-technique/220/ (accessed on January 25, 2024).

De Kock, T.; Van Stappen, J.; Fronteau, G.; Boone, M.; De Boever, W.; Dagrain, F.; Silversmit, G.; Vincze, L.; Cnudde, V. 'Laminar Gypsum Crust on Lede Stone: Microspatial Characterization and Laboratory Acid Weathering'. *Talanta 162: 193–202,* 2017. doi:10.1016/j.talanta.2016.10.025.

Eyssautier, S.; Marin, B.; Thomachot-Schneider, C. ; Fronteau, G.; Schneider, A.; Gibeaux, S.; Vázquez, P. 'Simulation of Acid Rain Weathering Effect on Natural and Artificial Carbonate Stones'.

Environmental Earth Sciences 75, 2016. doi:10.1007/s12665-016-5555-z.

Gibeaux, S.; Thomachot-Schneider, C.; Schneider, A.; Cnudde, V.; De Kock, T.; Barbin, V.; Vázquez, P. *'EXPERIMENTAL STUDY OF THE AGEING OF BUILDING STONES EXPOSED TO SULFUROUS AND NITRIC ACID ATMOSPHERES'*. 2016.

Gibeaux, S.; Vázquez, P.; De Kock, T.; Cnudde, V.; Thomachot-Schneider, C. 'Weathering Assessment under X-Ray Tomography of Building Stones Exposed to Acid Atmospheres at Current Pollution Rate'. *Construction and Building Materials* 168: 187–98, 2018. doi:10.1016/j.conbuildmat.2018.02.120.

IPCC. *'AR6 Synthesis Report: Climate Change 2023 — IPCC'*. 2023. Available online: https://www.ipcc.ch/report/sixth-assessment-report-cycle/ (accessed on June 16, 2024).

Nikiema, T.; Gonze, N.; Descamps, F. 'Correlation between Joint Roughness Coefficient (JRC) and statistical roughness parameters'.2024.

MEDISTONE, Association; Bromblet, P. *'Guide « Altérations de La Pierre »'.* 2010. Available online: chrome-extension://efaidnbmnnnibpcajpcglclefindmkaj/https://www.pierres-info.fr/biblio-taille_de_pierre/alteration-pierre-naturelle.pdf (accessed on November 27, 2023).

Menéndez, B. 'Estimators of the Impact of Climate Change in Salt Weathering of Cultural Heritage'. *Geosciences* 8(11): 401, 2018. doi:10.3390/geosciences8110401.

Pierre et Marbres de Wallonie asbl. 'Calcaire gréseux de Gobertange'. Pierres et Marbres de Wallonie. 2024. Available online: https://www.pierresetmarbres.be/fr/votre-projet/pierres/calcaire-greseux-de-gobertange/ (accessed on June 16, 2024).

Rodríguez, I.; Ortiz, A.; Caldevilla, P.; Giganto, S.; Búrdalo Salcedo, G.; Fernández-Raga, M. 'Comparison between the Effects of Normal Rain and Acid Rain on Calcareous Stones under Laboratory Simulation'. *Hydrology* 10, 2023. doi:10.3390/hydrology10040079.

Saiz-Jimenez, C.; Brimblecombe, P.; Camuffo, D.; Lefèvre, R.-A.; Van Grieken, R. 'Damages Caused to European Monuments by Air Pollution: Assessment and Preventive Measures'. *Air Pollution and Cultural Heritage, Chapter: Damages caused to European monuments by air pollution: assessment and preventive measures.* Taylor and Francis Group, London, 91–109, 2004. doi:10.1201/b17004-15

Salvini, S.; Bertoncello, R.; Coletti, C.; Germinario, L.; Maritan, L.; Massironi, M.; Pozzobon, M.; Mazzoli, C. 'Recession Rate of Carbonate Rocks Used in Cultural Heritage: Textural Control Assessed by Accelerated Ageing Tests'. *Journal of Cultural Heritage* 57: 154–64, 2022. doi:10.1016/j.culher.2022.08.010.

Trudgill, S. T.; Viles, H. A. 'Field and Laboratory Approaches to Limestone Weathering'. *Quarterly Journal of Engineering Geology* 31(4): 333–41, 1998. doi:10.1144/GSL.QJEG.1998.031.P4.06.

Vagnon, F.; Costanzo, D.; Ferrero, A. M.; Migliazza, M. R.; Pastero, L.; Umili, G. 'Simulation of Temperature and Chemical Weathering Effect on Marble Rocks'. IOP *Conference Series: Earth and Environmental Science* 833(1): 012068, 2021. doi:10.1088/1755-1315/833/1/012068.

Vázquez, P.; Menéndez, B.; Denecker, M.; Thomachot-Schneider, C. 'Comparison between Petrophysical Properties, Durability and Use of Two Limestones of the Paris Region'. *In Geological Society*, London, Special Publications, 2015. doi:10.1144/SP416.15.

Xie, S.; Qi, L.; Zhou, D. 'Investigation of the Effects of Acid Rain on the Deterioration of Cement Concrete Using Accelerated Tests Established in Laboratory'. *Atmospheric Environment - ATMOS ENVIRON* 38: 4457–66, 2004. doi:10.1016/j.atmosenv.2004.05.017.

Yan, Z.; Wang, Z.; Su, G.; Wu, Z.; Liu, F.-T. 'Experimental Investigation on Influence of Acidic Dry-Wet Cycles on Karst Limestone Deterioration and Damage'. *Geofluids* 2022: 1–12, 2022. doi:10.1155/2022/8562226.

CLIMATE CHANGE ADAPTATION AND CULTURAL HERITAGE: THE CASE STUDY OF THE ARCHAEOLOGICAL SITE OF ANCIENT MESSENE, GREECE

VASILIKI POUGKAKIOTI[2], GIANNA KITSARA[1], ELENI MAISTROU[2], MILTIADIS LAZOGLOU[2], CHRISTOS GIANNAKOPOULOS[1]

[1] Institute for Environmental Research and Sustainable Development, National Observatory of Athens, I. Metaxas and Vasileos Pavlou, PC.15236 Old Penteli Athens, Greece, gkitsara@noa.gr

[2]ELLINIKI ETAIRIA-Society for the Environment and Cultural Heritage, 28 Tripodon St., 105 58, Athens, Greece, vaspoug@gmail.com

Introduction

‘’The majority of heritage sites in the Mediterranean are vulnerable to an increasing rate of threats from man-made global warming and extreme events’’ (Kapsomenakis et al., 2022). This study contributes to relatively few studies that examine the effects of climate change on individual sites, specifically tangible heritage (Orr et al., 2021). To bridge the gap between climate change science and the planning of climate change adaptation for cultural assets, it is necessary to analyse climate data and cultural heritage information. Several research efforts are devoted in analyzing a single scenario and a single climate model without considering the potential uncertainties (Sesana et al., 2021). In this study we use climate projections (of e.g. temperature, precipitation) from a selected (after evaluation) regional climate model for two future periods (2031-2060, 2071-2100) under three different emission scenarios (Representative Concentration Pathways RCPs) to estimate and analyse relative climate indices identifying the most significant risks to the study site: the archaeological site of Ancient Messene in South Greece. The IPCC 2001 vulnerability assessment analysis follows, in our methodological approach, for assessing the impacts of climate indices changes or extreme climate events, on the case study site. Through this process, it was presumed that it is possible to identify the sites needs as efficiently as possible and propose adaptation measures or policies.

Methods

The archaeological site of Ancient Messene was chosen, as the case study site, because of its monumental nature, historical significance, documented vulnerability to extreme climate events and susceptibility to the anticipated effects of climate change. To identify the most significant risks to the study site, an analysis of related climate indices, was conducted using climate projections (of e.g. temperature, precipitation, relative humidity, wind speed) from a selected regional climate model for two future periods (2031-2060, 2071-2100) under three different emission scenarios (RCPs). The GCM/RCM pair used in this study (MPI-ESM-LR_RCA4) was selected out of 5 GCM/RCM pairs (regional climate models hereafter) after evaluation with temperature/precipitation station observations. The 1971-2000 period served as a reference /control period for estimating changes of the climate indices (e,g hot days, dry days, fire weather index). The RCPs (https://climate.copernicus.eu/sites/default/files/2021-01/infosheet3.pdf) examined here were namely the: RCP2.6 (very low future emissions, severe mitigation), RCP4.5 (intermediate scenario with mitigations measures and moderate future emissions), and RCP8.5 (very high future emissions, no mitigation policies). Statistical analysis using the z-test and t-test assessed the significance of differences in climate values. For the vulnerability assessment of the study site to the impacts of climate change, the risk assessment methodology from IPCC, 2001 was used based on the analysis of the climate projections and indices. This approach is based on exposure, sensitivity, and adaptive capacity McCarthy et al. (2001). High vulnerability arises from high exposure and sensitivity combined with limited adaptability, whereas increased adaptive capacity and reduced exposure and sensitivity decrease vulnerability. In this study, vulnerability assessment was viewed as an essential step in assessing the impacts of extreme climate events on the study site and proposing measures or policies to address them on all human activity sectors.

Results

The analysis indicated a warmer, drier future with an increased frequency of hot and dry days and decreased annual precipitation across all scenarios. Under RCP8.5, hot days and consecutive dry days

could rise by up to 60 and 20 days by 2100 respectively, significantly elevating the fire risk and droughts

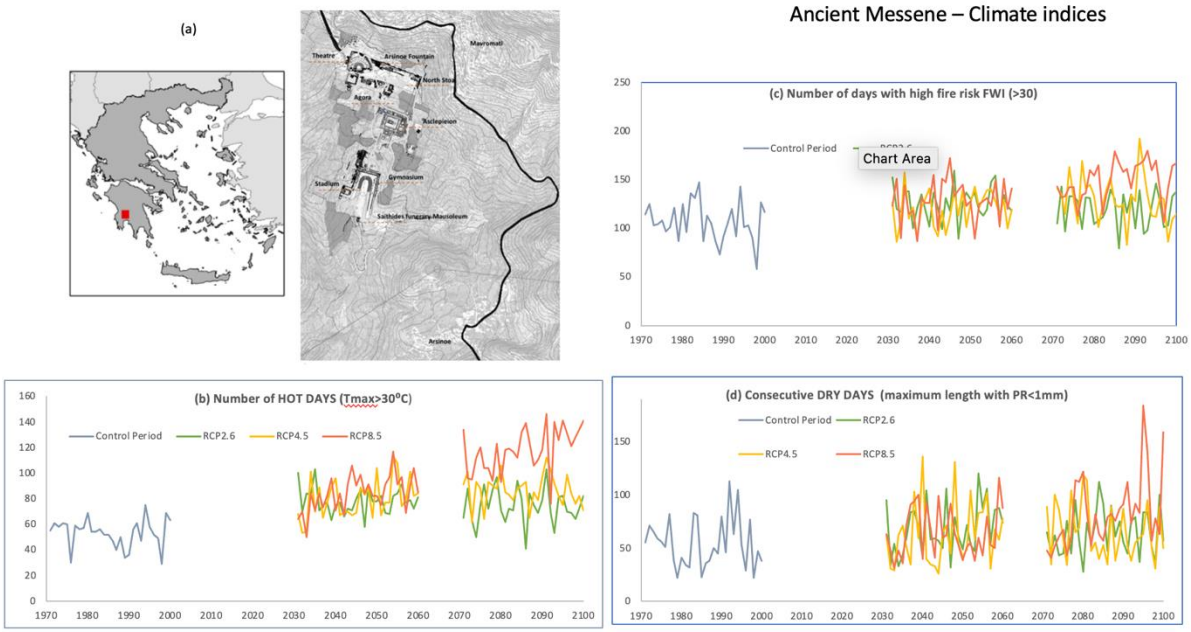

Figure 1. (a) The geographical location of the archaeological site and the topographical plan of the archaeological site of Ancient Messene (ELLET, 2021); (b),(c),(d) Climate indices for 2 future periods (2031-2060, 2071-2100) under 3 RCPs-1971-2000 is the reference period.

(Figure 1b,d). A notable increase in days (60) with high fire risk (FWI fire weather index >30), with extreme values under RCP8.5 was shown (Figure 1c). These findings highlight fire risk, drought conditions as primary threats to Ancient Messene, underscoring the urgent need for adaptation measures and policies addressing their impacts on the archaeological site. The vulnerability analysis approach outlined by IPCC in 2001 was employed to assess the impact of these threats on the study site. This approach also facilitated the identification of priorities for adaptation measures.

Conclusion

The analysis revealed the site's moderate-to-high risk exposure due to its location, prone to warm, drought conditions, wildfire. The site's adaptability is hindered by inadequate infrastructure, including a poor drainage network, lack of comprehensive fire protection, and insufficient emergency vehicle access. The incomplete legal framework for protection zones further exacerbates the site's vulnerability, highlighting the need for significant improvements in infrastructure, management, and legal protection to enhance resilience to climate change. Priorities for adaptation measures include developing a fire protection study and implementing necessary measures, as well as improving road infrastructure and internal routes for safe access and evacuation. These steps, along with enhanced management and legal protection, are vital to bolster the site's resilience against climate change impacts (ELLET, 2021).

References

Elliniki Etairia Society for the Environment and Cultural Heritage (ELLET), *Development of Pilot Assessments and Adaptation Guidelines for Cultural HeritageCase Study: The Archaeological Site of Ancient Messene* (7-108), 2021.

Intergovernmental Panel on Climate Change (IPCC), Climate Change 2001: *The Scientific Basis, Contribution of Working Group I to the Third Assessment Report of the IPCC*, United Kingdom and Cambridge University Press, 2001.

Kapsomenakis, J., Douvis, C., Poupkou, A., Zerefos, S., Solomos, S., Stavraka, T., Melis, N.S., Kyriakidis, E., Kremlis, G., & Zerefos, C. *Climate Change Threats to Cultural and Natural Heritage UNESCO Sites in the Mediterranean*. Environment, Devel opment and Sustainability . 2022

McCarthy, J., Canziani, O. F., Leary, N. A., Dokken, D. J., & White, K. S. Climate Change 2001: Impacts, Adaptation and Vulnerability. Contribution of Working Group II to the Third Assessment Report of the IPCC. Cambridge University Press. 2001

Orr, S. A., Richards, J., & Fatorić, S. Climate Change and Cultural Heritage: A Systematic Literature Review (2016-2020). The Historic Environment: Policy & Prac- tice, 12, 434-477. 2021

Pougkakioti, V., Lazoglou, M., & Maistrou, E. (2023). Climate Change vs Cultural Heritage: An Adaptation Strategy for the Archaeological Site of Ancient Messene. American Journal of Climate Change, 12, 456-488.

Sesana, E., Gagnon, A. S., Ciantelli, C., Cassar, J., & Hughes, J. J. Climate Change Impacts on Cultural Heritage: A Literature Review. Wiley Interdisciplinary Reviews: Climate Change, 12, e710. 2021

Themelis, P. Ancient Messene. History-Monuments-People, Militos Editions, 2010.

QUALITATIVE ASSESSMENT OF THE ROCKFALL RISK; CASE STUDY ARCHAEOLOGICAL SITE OF DELPHI, IN GREECE

DEVLIOTI KYRIAKI[1], PAPATHANASSIOU GEORGE[1], CHRISTARAS BASILE[1], VOUVALIDIS KONSTANTINOS[1]

[1] *Aristotle University of Thessaloniki, Greece, kdevliot@geo.auth.g*

[1] *Aristotle University of Thessaloniki, Greece, gpapatha@geo.auth.gr*

[1] *Aristotle University of Thessaloniki, Greece, christar@geo.auth.gr*

[1] *Aristotle University of Thessaloniki, Greece, vouval@geo.auth.gr*

Natural hazards, such as rockfalls are often caused by extreme and intense weather and climate phenomena, endangering human life and impacting society, economy and tourism, worldwide. Monumental areas near steep rocky slopes are frequently threatened by this type of geological phenomena. Rockfall hazard varies in terms of their intensity, severity, extent, as well as in terms of their effects to the elements exposed at risk, including visitors safety and Monumental Sites sustainability. In the present work, the Archaeological Site of Delphi, in Greece was studied. This Site is facing rockfall phenomena from ancient times till nowadays. Modelling rockfalls, in 3D environment contribute to avoid loss of human life and property damage, so, many factors should be taken into account, such as the distribution and calculation of rock block volumes, their geometric and mechanical characteristics, the mechanisms of failure etc. Alongside, UAV systems constitute an innovative technology for obtaining three-dimensional (3D) data and aerial photographs, they reduce time and cost of work, compared to classic conventional field working and they provide the possibility of creating high-resolution data. This study aims at an initial qualitative risk assessment. This was achieved by creating tables (Risk matrix) and spatial distribution maps, in ArcGIS environment, both for Direct Material and Direct Intangible loss, through three-dimensional trajectometric analyses, by calculating the intensity (kJ), the probability of reaching the Monumental area (Ppropag) and the simultaneous determination of rock blocks trajectory termination (stop points).

Introduction

In mountainous areas rockfalls are a major threat causing serious damage to infrastructure and buildings, Cultural Heritage Sites and loss of human life (Scavia et al. 2020). Understanding the severity of the rockfall phenomena and the social and economic impacts, many researchers have developed risk assessment techniques, for rocky slopes, based on visual monitoring, simple calculations and estimating rock mass properties, through systems classification and evaluation (Pantelidis 2009). Risk assessment can be achieved, either qualitatively or quantitatively. For the qualitative characterization of Risk, the descriptive and qualitative elements of the area being studied are taken into account, as well as the expected social effects of the natural phenomena under consideration. The qualitative assessment of the risk includes the subjective criterion of each researcher, with the designation "High", "Medium" and "Low", through a table of qualitative assessment of the risk (Risk matrix).

Methods-Results

In the present work, an initial approach for qualitative risk assessment (Risk) was carried out, by creating tables (Risk matrix) and maps, in ArcGIS environment, both for Intangible (Fig. 1) and Material loss that might be caused, based on the colour gradation of the 3D spatial visualization of the probability of propagation (Ppropag) of rock blocks at the elements of Risk in the Site, also considering rock blocks trajectories termination (stop points). So, according to the 3D spatial distribution map of Fig. 1 the degree of Risk seems to be high in the entirety of the Monuments of the Site, as well as in the Kastalia Spring (red colour), while medium appears at the Entrance of the Archaeological Area, the visitors corridor, the road network and the Archaeological Museum (yellow colour). Finally, it appears small at the Parking area (green colour). In order to export the above results, a four-step methodology was followed including the following steps: 1) assessment of the rockfall susceptibility, 2) evaluation of the rockfall hazard through 3D trajectrometric analysis, in 2D and 3D environment, 3) examination of the

degree of Risk according to the spatial allocation of the selected critical zones on the rocky cliff, which were used for Hazard determination.

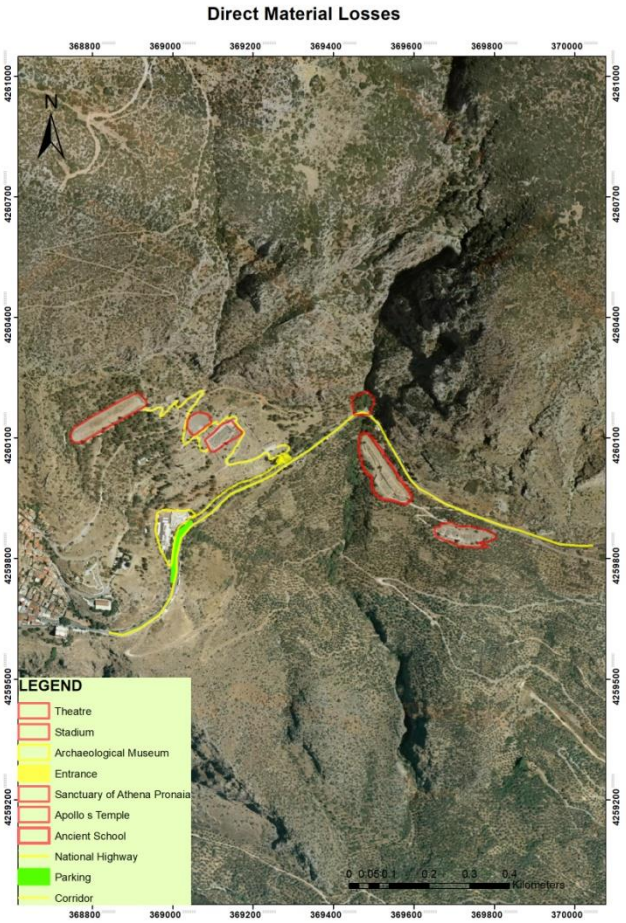

Figure 1. Distribution map of qualitative Risk assessment (Risk matrix), based on the rockfall probability in the Archaeological Site of Delphi, as well as its Direct Material Losses-effects.

Conclusion

The aim of this study was the development of a detailed rockfall hazard assessment and a preliminary rockfall qualitative Risk assessment methodology in the Archaeological Site of Delphi, the results of which can be used in proposing the appropriate rockfall interventions in the examined Area. This UNESCO World Heritage Site, is a symbol and the center of Greek culture, the sustainability of which, as well as staff and thousands of visitors safety constitute the main objective of the present work.

References

Pantelidis, L. Rock slope stability assessment through rock mass classification systems, International Journal of Rock Mechanics & Mining Sciences, 2009, 46, 315–325.

Scavia, C.; Barbero, M.; Castelli, M.; Marchelli, M.; Peila, D.; Torsello, G. and Vallero G. Evaluating Rockfall Risk: Some Critical Aspects. Innovative Strategies for Sustainable Mitigation of Landslide Risk. Geosciences, 2020. https://doi.org/10.3390/geosciences10030098.

THE VERSAILLES GRAND CANAL: A GEOTECHNICAL ENQUIRY, III

JEAN-DAVID VERNHES [1], RÉJANNE LE BIVIC [2], ANNICK HEITZMANN [3]

[1] *UniLaSalle, France, jean-david.vernhes@unilasalle.fr*

[2] *UniLaSalle B2R (GeNumEr) U2R 7511, France, rejanne.lebivic@unilasalle.fr*

[3] *Etablissement Public du Château de Versailles, France, annick.heitzmann@chateauversailles.fr*

Introduction

The Versailles castle park planning needed important geotechnical works. The park's masterpiece, the Grand Canal (Figure 1), was built over a period of almost fifteen years in the last third of the XVIIth century. The principal results of an archive investigation focused on this basin were communicated at the 17th ECSMGE (Vernhes and Heitzmann, 2019) and completed at the 3rd ISSMGE TC301 International Symposium (Vernhes *et al*., 2022), with field and coarse GIS data. The archives proved to be sufficient to determine phases in the construction of the basin but with almost no spatial details. The current and original terrain topography then became the main target to assess the earthworks overall volume and thus decipher the planners' strategy.

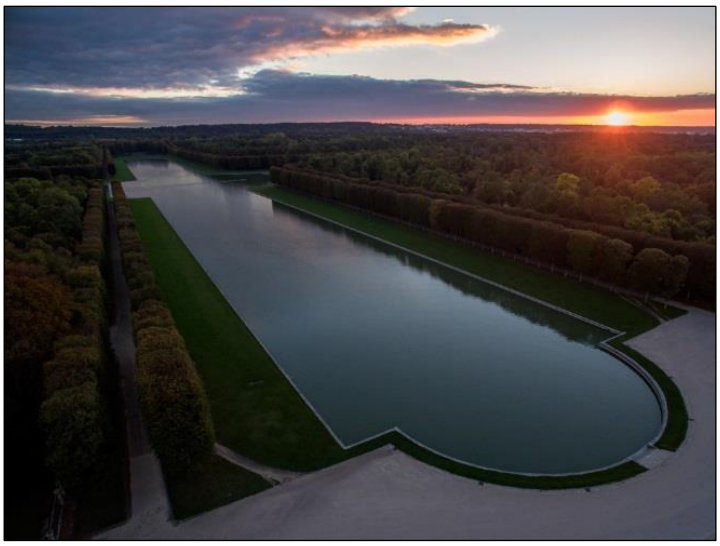

Figure 1. Aerial view of the *Grand Canal*'s Northern branch (© Th. Garnier)

Methods

The geological data constraint for such an objective, based on field surveys, proved to be tricky. According to the most recent geological map, issued by Jean Goguel in 1967, the grounds in which the two meters deep and 230,000 m² canal had been dug are tabular late Eocene to Oligocene layers, what could have helped to offer clues on earth movements through geophysical and light geotechnical field investigations. However, boreholes (Lablaude, 1997) revealed that the topographical depression in that area is filled with recent mixed Eocene and Oligocene origin colluvia.

Relying on the former coarse GIS data entailed a high level of uncertainty in the 2022's conclusions. The present extended abstract aims at showing the scientific potential of the French National Geographical Institute (IGN) Lidar covering of France's surface, coincidently available since 2022. Its processing by the authors now offers a finer Digital Elevation Model of the Grand Canal area. As an example, the previous 1-meter topographical model had made it impossible to get rid of the artifacts due to the many trees all around the canal. The 2022 LiDAR dataset being classified, a 75 cm DEM was created excluding the vegetation from the pointcloud, revealing unseen ground details.

Results

As an example, Figure 2 shows a map with a range of heights and a shading mode meant to visualise the Gally creek hydraulic trenches (see e.g. landmark 'c'), necessary to prevent higher flooding risk in the park provoked by the canal's barrier effect on the local hydrographic and hydrogeological natural regimes. This map also makes obvious the extent of the fine fill layers near the canal, originally particularly hard to see towards the West of the Southern arm.

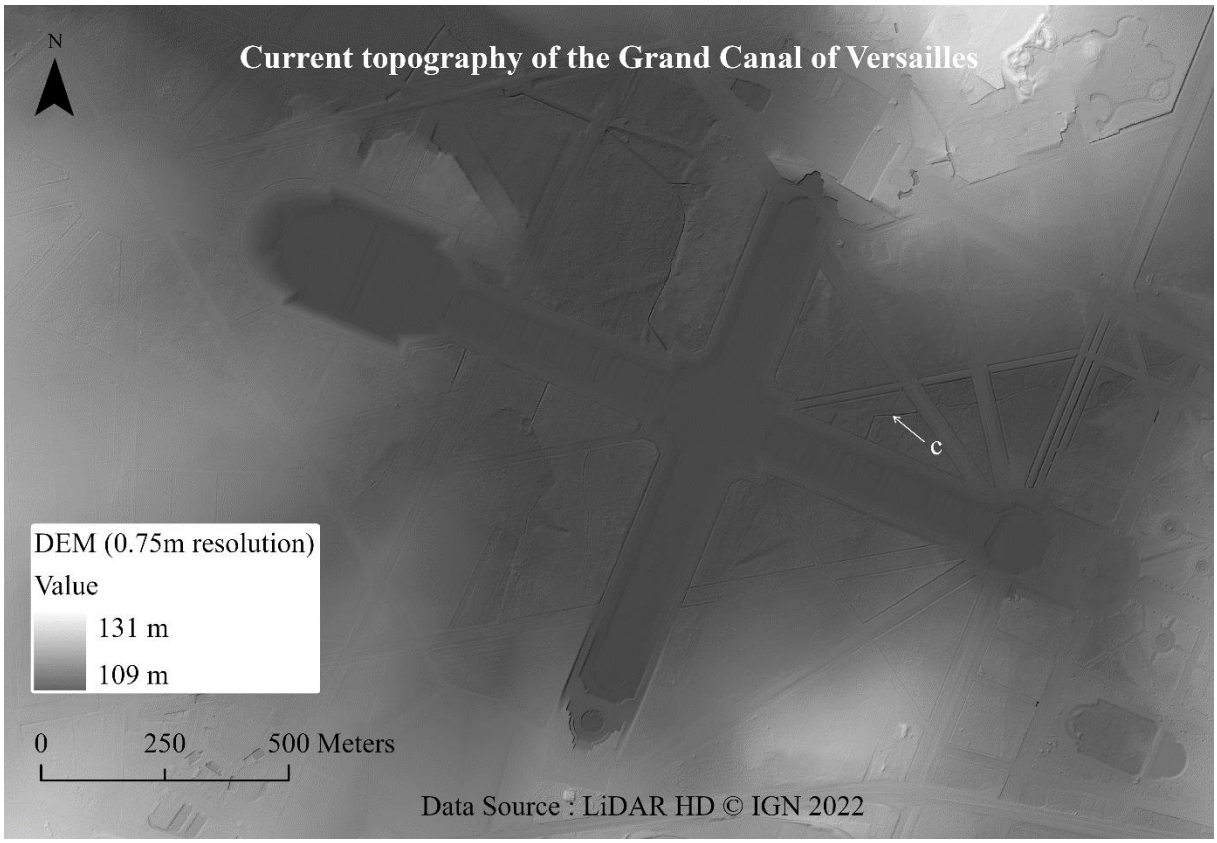

Figure 2. Digital Elevation Model of the Grand Canal in Versailles, computed from LiDAR aerial data acquired by the French Geographical Institute (IGN) in 2022. The heights reference is the average sea level at Marseille.

Conclusion

After full exploitation of today's new DEM, the next step will be to enhance the original topography DEM hypothesis, now easier to assume. An idea to give better foundations and realism to the solution will be to use computer-assisted (AI) characterization of natural vs. man-modified topography, using as an input IGN data in areas recognised to be with similar geomorphological conditions.

References

Goguel, J. Versailles, carte géologique de la France à 1/50000, n°182, Orléans, Bureau de Recherches géologiques et minières. 1967.

Lablaude, P.-A. Etude préalable à la restauration des berges et margelles du grand canal, rapport destiné à l'Etablissement Public du Musée et du Domaine National de Versailles. 1997, 145 p. Unpublished.

Vernhes, J.-D.; Heitzmann, A. Le Grand Canal à Versailles : enquête géotechnique. *Proceedings of the XVIIth European Conference on Soil Mechanics and Geotechnical Engineering*, Reykjavik, Iceland, 2019. ISBN 978-9935-9436-1-3

Vernhes, J.-D.; Saulet, P.; Heitzmann, A. Le Grand Canal à Versailles : enquête géotechnique, II. *Proceedings of the 3rd ISSMGE TC301 International Symposium*, Naples, Italy, 2022. ISBN 978-1-003-30886-7

STABILITY OF THE HISTORICAL MONUMENTS: THE PHANTOM MENACE?

FILIP HARTVICH[1], JANA MAŘÍKOVÁ-KUBKOVÁ[2]

[1] *Dpt. of Engineering Geology, Institute of Rock Structure and Mechanics, Czech Academy of Sciences, Czech Republic,* hartvich@irsm.cas.cz

[2] *Dpt. of Historical Archaeology, Institute of Archaeology in Prague, Czech Academy of Sciences, Czech Republic,* jana.marikova.kubkova@gmail.com

Introduction

The Prague and Vyšehrad castle are two main dominants of historical UNESCO site of Prague, one of the most beautiful and well-preserved medieval cities. However, as the originally medieval fortifications are naturally built on the prominent hilltops, they did not avoid problems with the long-term stability of numerous buildings. As both castle complexes are more than 1000 years old, the stability issues go deep into history and literally deep into many meters of the aggravated anthropogenic deposits. Therefore, it was decided to monitor the displacement to observe the stability of the site for their protection. Various monitoring systems were considered (Klimeš et al. 2011, Greif et al 2017, Fantini et al. 2016).

Figure 1. Three monitored sites in the underground of the Prague Castle

Methods

In August 2020, the monitoring was established at the Prague castle, and in February 2022 at the Vyšehrad castle. The monitoring was initiated by the archeologists and heritage sites´ authorities, who observed indications of movements at several places of the monuments. Several pairs of automatic extensometers Gefran supplemented with dataloggers Tertium Beacon (Racek et al. 2021, Crosta et al 2017, Tertium 2017) were installed across the most prominent open cracks in the walls. The devices were set to measure once every hour, with the dilatation accuracy of 0,05 mm and temperature accuracy

of 0,1 °C.

Results

The results of the 3 years monitoring (2 years at Vyšehrad) were analysed. The largest movements at Prague castle exceeded 1 mm at the most significant opening. Generally, data from Prague castle show combination of thermal expansion with a significant trend for opening of the cracks. The largest clear trends reached 1 mm (1A) and 0,52 mm (1B) for the observed period. At the Vyšehrad castle, the largest movements were observed on the brick wall at the viewpoint, with the clean trend exceeding 3 mm in 2 years. This magnitude of movements is considered a significant potential threat for the stability.

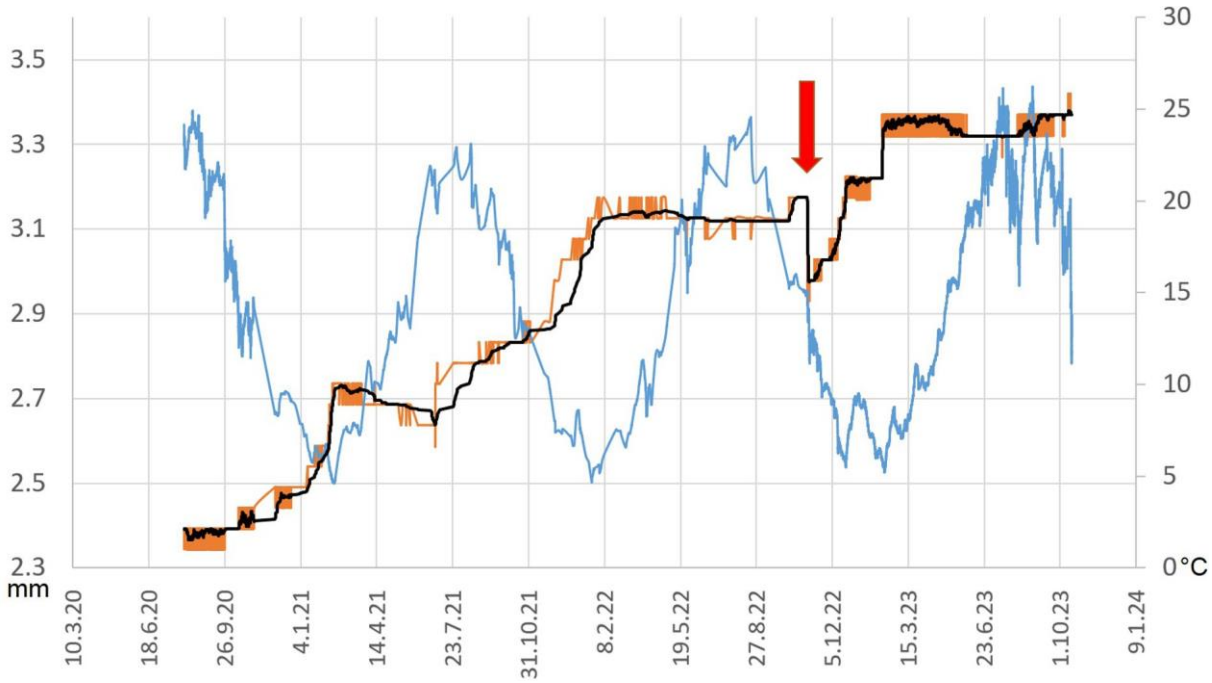

Figure 2. Displacement chart of the fastest moving 1A measurement (see Fig. 1). Orange line: measured displacement, black line - 1 day running average, blue line - temperature. The red arrow indicates prominent reverse impulse

Conclusion

The monitoring shows distinct and clear irreversible displacement trends, at some monitored cracks exceeding 1 mm per year. The influence of temperature can be distincly observed as cyclic phases with yearly period. The causes of the movements are currently being investigated, however, most likely they are connected to the underground seeping of water, causing erosion in the anthropogenic deposits, which leads to subsidence and consequent opening of the cracks.

References

Crosta, G.B., Agliardi, F., Rivolta, C., Alberti, S., Dei Cas, L., (2017). Long-term evolution and early warning strategies for complex rockslides by real-time monitoring. *Landslides* 14, 1615-1632..

Fantini, A., Fiorucci, M., Martino, S., Marino, L., Napoli, G., Prestininzi, A., Salvetti, O., Sarandrea, P., Stedile, L. (2016). Multi-sensor system designed for monitoring rock falls: the experimental test-site of Acuto (Italy). *Rendiconti Online Societa Geologica Italiana* 41, 147-150.

GEFRAN (2020). Position Transducers, 1st ed. 25050 PROVAGLIO D'ISEO (BS) ITALY.

Greif, V., Brcek, M., Vlcko, J., Varilova, Z., Zvelebil, J., (2017). Thermomechanical behavior of Pravcicka Brana Rock Arch (Czech Republic). *Landslides* 14, 1441-1455.

Klimeš, J., Rowberry, M.D., Blahůt, J., Briestenský, M., Hartvich, F., Košťák, B., Rybář, J., Stemberk, J., Štěpančíková, P. (2011): The monitoring of slow moving landslides and assessment of stabilisation

measures using an optical-mechanical crack gauge. *Landslides*,. Vol. 9, Issue 3, p. 407-415

Racek, O., Blahůt, J., Hartvich, F. (2021): Observation of the rock slope thermal regime, coupled with crackmeter stability monitoring: initial results from three different sites in Czechia (central Europe). *Geoscientific instrumentation methods and data systems*, vol. 10, issue 2, 203-218

Tertium technology (2019). Gego Crack meter. Pisa Italy.

Vaziri, A., Moore, L., Ali, H., (2010). Monitoring systems for warning impending failures in slopes and open pit mines. *Nat Hazards* 55, 501-512.

SAFEGUARDING "SHIPWRECK": ASSESSING ROCKFALL RISKS ON THE WORLD-FAMOUS BEACH IN ZAKYNTHOS ISLAND, GREECE

VASSILIS MARINOS[1], THEMISTOKLIS CHATZITHEODOSIOU [1], IOANNIS FARMAKIS [2], DIMITRA PAPOULI [1], ATHINA TSIROGIANNI[1]

[1] *National Technical University of Athens, Greece, marinosv@civil.ntua.gr*

[2] *University of Newcastle, Australia, i.farmakis@icloud.com*

Introduction

This research focuses on the engineering geological hazard and risk assessment of rockfalls and proposes protection measures for the cliffs surrounding the Shipwreck beach in Zakynthos and its safer accessibility. Located in the north-western part of Zakynthos Island in the Ionian Sea, Shipwreck Beach is a significant tourist destination in Greece. The area's characteristics include a high volume of visitors, exceptional natural beauty, steep and high slopes, and significant rockfalls, presenting technical challenges for protection measures (Figure 1 & Figure 2). The key requirements for risk management are preserving the aesthetic environment, maintaining tourist appeal with acceptable risk, and providing economically and technically feasible risk reduction solutions. In the study area, the rock mass is composed of thin-bedded blocky limestone, which generally exhibits high strength but is affected by various systems of discontinuities and fractures. Rockfalls have occurred due to factors such as steep slopes, strong earthquakes, marine erosion undercutting the steep slopes developing subvertical tensile cracks, and weather-induced discontinuities. These rockfalls involve fragments of various sizes, impacting the beach zone and the sea. Many overhanging rock blocks pose a high risk, threatening beach access, the surrounding marine zone, and viewing areas at the top of the slopes.

Figure 1. The world famous "Shipwreck" beach in Zakynthos island, Greece (left photo). Numerous overhanging rock blocks, from the vertical and high (up to 200m) slopes, present a significant danger, jeopardizing beach access, the nearby marine area, and the viewpoints at the top of the slopes (right photo)

Methods

Engineering geological surveys mapped rock mass qualities, main structural features, and evaluated the rock, discontinuity and rock mass properties along with on-site and laboratory tests. A 3-d point cloud, generated by thousands of images captured from two UAVs from a team of team of surveying engineers, was used in the geospatial analysis and 3D reconstruction programs. Automated (Riquelme ets al., 2014) and conventional measurements assessed joint systems and blocks. Dangerous overhanging blocks were mapped and analyzed using 3D risk analysis, with geotechnical software RocSlope3 by Rocscience Inc.

determining critical volumes and detachment locations. Rockfall analyses, including static and seismic conditions, were performed using Rocfall 3 (Figure 2).

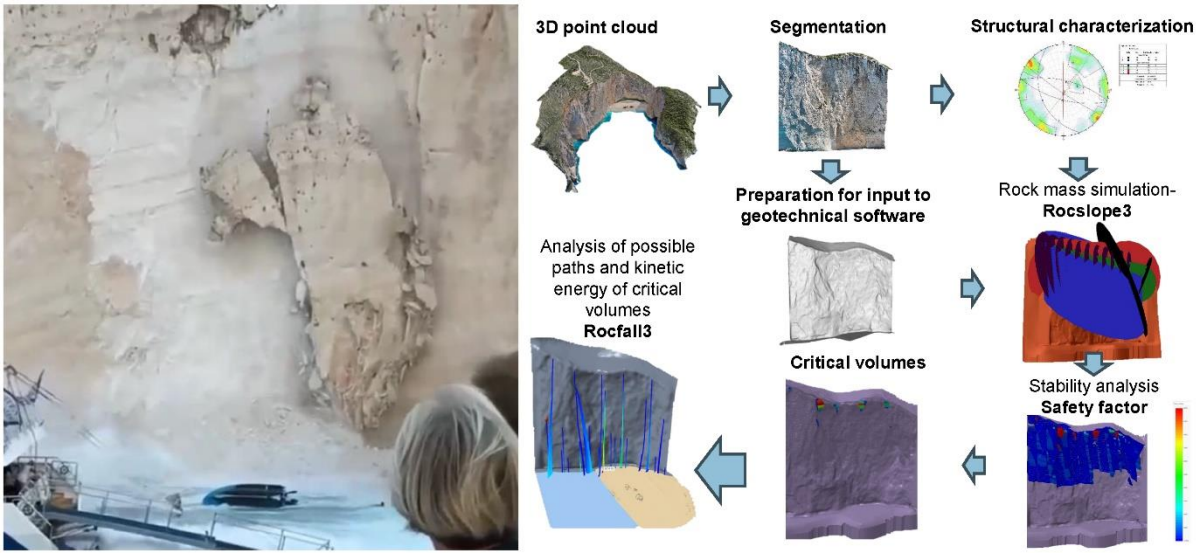

Figure 2. Rockfall risk analysis methodoly. A recent rockfall (~300 m^3), occured in summer 2018 under static conditions, is shown in the left photo.

Results

The study found a very high risk of falling blocks from various locations on the slopes. The main failure mechanism is block toppling due to undercutting and stress relief. Access zones were delineated based on a 3D analysis. Risk reduction can be achieved through protection measures, including unobtrusive interventions and observation points if unstable zones are avoided or stabilized. The study proposes installing a long-term geotechnical monitoring system for the slopes.

Acknowledgments

This study is an integral part of the interdisciplinary original research titled "Research-Documentation and Proposals by the National Technical University of Athens for the Preservation of the Shipwreck and Safe Visitor Access to the Area.". The detailed results of the research can be downloaded from the website: https://navagio-zakynthou.ntua.gr/

References

Azzoni, A., & de Freitas, M. H. (1995). Experimentally gained parameters, decisive for rock fall analysis. Rock Mechanics and Rock Engineering, 28(2), 111–124. https://doi.org/10.1007/BF01020064.

Pfeiffer, T.J., and Bowen, T.D.," ""Computer Simulation of Rockfalls." Bulletin of Association of Engineering Geologists. Vol. 26", No. 1. 1989. pp135-146 @ Glenwood Canyon, Colorado, USA

Riquelme, A.J., Abelian, A., Tomas, R., Jaboyedoff, M., 2014. A new approach for semi-automatic rock mass joints recognition from 3D point clouds. Comput. Geosci. 68, 38-52.

Robotham, M.E., and Wang, H., and Walton, G.," "Assessment of risk from rockfall from active and abandoned quarry slopes."" Institution of mining and Metallurgy", Section A. 1995.104(Jan-April), pp A25-A33. @ Limestone quarry in England.

Westoby, M. J., Brasington, J., Glasser, N. F., Hambrey, M. J., Reynolds, M. J. (2012). Structure-from motion photogrammetry: a low-cost, effective tool for geoscience applications. Geomorphology 179, pp. 300 – 314.

Topic 3

Emerging Technologies and Applications in Engineering Geology and Geotechnics

A NON-PARAMETRIC CHANGE DETECTION METHOD FOR ROCKFALL MONITORING

IOANNIS FARMAKIS [1], DAVIDE ETTORE GUCCIONE [1], KLAUS THOENI [1], ANNA GIACOMINI [1]

[1] *Centre for Geotechnical Science and Engineering, The University of Newcastle, Australia,* i.farmakis@icloud.com

Introduction

Rockfall monitoring defines the process of recording rockfall activity patterns along a given rock slope. With 3D data capturing techniques, a typical digital change detection methodology for rockfalls includes three steps – distance computation, spatial clustering, and shape reconstruction (Abellan et al. 2009). Distance computation refers to the computation of distances between two point clouds. A statistical limit of detection at 95% confidence (LoD_{95}) applies to extract significant changes (DiFrancesco et al. 2020). In the second step, the significant distances point cloud should be clustered in space to form individual rockfall point clouds. The third step of the 3D rockfall state-of-the-art methodology includes the computation of the loss volume represented by each individual rockfall point cloud as extracted by spatial clustering (DiFrancesco et al. 2021). This state-of-the-art methodology includes some user-defined input parameters at each step that can significantly influence the result. The selection of appropriate input parameter values within the individual steps of the process poses specific challenges associated with the nature of the problem and the data type. This is mainly because rockfalls as phenomena can occur in any size and arrangement and thus configurations made for specific block sizes and patterns may not always apply to the entire extent of the monitored rock slope. Considering the several challenges associated with user-defined parameter selection within the distance-based state-of-the-art 3D rockfall detection methodology, this paper presents a non-parametric method specifically designed for 3D rockfall monitoring.

Methods

The new method, VoxFall (voxelized rockfall), does not rely on any distance computation and its objective is to eliminate user subjectivity and present a new tool for rockfall monitoring that would only be controlled by the quality of the input data. VoxFall's development was based on the following three conceptual principles: a) in rockfall detection the interest is not in the magnitude or the direction of the displacement of each point but in the volume that has been detached (not displaced), b) as in an image, where anything below the resolution is not visible, VoxFall uses a voxel (volumetric pixel) grid – a 3D image of the scene – which's resolution is defined by the quality properties of the input models, and c) often in rockfall cases model coverage is challenged by the survey setting where it is apparent that volume computations require shape reconstruction of the extracted clusters with hole-filling.

The algorithm treats the two input models as a single scene and conforming with the realization that this is an unavoidable operation, 3D mesh models are used as input. After the required pre-processing the two models are merged and the rockfall volumes are enclosed between the "before" and "after" surfaces (Figure 1a, b). However, it is important to make sure that the detected clusters of the empty space satisfy a minimum degree of confidence and do not include the effects of potentially insufficient data quality. To achieve that, we apply a two-step process:

1) **Fitting an occupancy grid:** To extract the empty space from the input scene we use a voxel (volumetric pixel) grid (Figure 1c). VoxFall is a non-parametric method where the resolution of the analysis (voxel size) – which is the only factor that could influence the result – is defined by the quality of the input data, and specifically by the registration error. To extract the empty space between the two models, we need to make sure that there are no empty voxels between stable parts. Therefore, the quality of the input data decides the ability of VoxFall to reliably only "see" the empty space that corresponds to rockfalls and confidently avoid false positives.
2) **Empty space clustering and volume computation:** By using the voxel grid data structure, we cluster the extracted continuous 3D space without relying on any input parameter. Spatial clustering in VoxFall is simple and neighbor search is facilitated by grid indexing. For each

rockfall cluster, the volume is computed as a function of the voxels it includes.

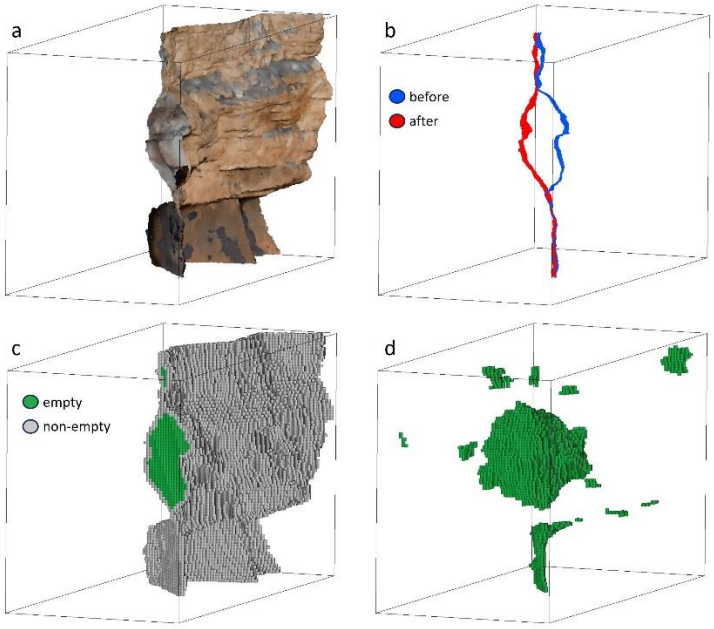

Figure 1. VoxFall detection method.

Results and Conclusions

To validate the reliability of the new algorithm a synthetic seting and real rock slope dataset were used. VoxFall performance was compared to the existing distance-based methodologies. The results across all the experimental settings prove the sensitivity of the distance-based methods and the dependency of the detections on the input parameters compared to VoxFall detections. Specifically, distance-based rockfall detection workflows appear to be highly sensitive to not only the spatial clustering tuning but also their distance computation input parameters. In the original dataset, VoxFall almost perfectly predicts the rockfall volume (0.3% difference) within an arrangement of recorded rockfall events.

The study conludes that distance-based rockfall monitoring as it is used today is highly sensitive to multiple input parameters and requires pre-existing knowledge of rockfall activity to tune them. The new method – VoxFall – provides a unified framework that enables for direct volume detection and clustering amongst them. VoxFall results depend only on the input data quality and no user intervention is required. The study's comprehensive experiments support that VoxFall can provide high quality results in terms of both segmentation/detection and volume estimation introducing the method as an efficient and effective tool for 3D rockfall monitoring.

References

Abellán, A., Jaboyedoff, M., Oppikofer, T., Vilaplana, J.M., 2009. Detection of millimetric deformation using a terrestrial laser scanner: experiment and application to a rockfall event. Nat. Hazards Earth Syst. Sci. 9, 365–372. https://doi.org/10.5194/nhess-9-365-2009

DiFrancesco, P.-M., Bonneau, D., Hutchinson, D.J., 2020. The Implications of M3C2 Projection Diameter on 3D Semi-Automated Rockfall Extraction from Sequential Terrestrial Laser Scanning Point Clouds. Remote Sens. 12, 1885. https://doi.org/10.3390/rs12111885

DiFrancesco, P.-M., Bonneau, D.A., Hutchinson, D.J., 2021. Computational Geometry-Based Surface Reconstruction for Volume Estimation: A Case Study on Magnitude-Frequency Relations for a LiDAR-Derived Rockfall Inventory. ISPRS Int. J. Geo-Information 10, 157. https://doi.org/10.3390/ijgi10030157

FLUID FLOW CAPABILITY OF INCIPIENT FOLIATION, NATURAL FRACTURE ALONG FOLIATION, AND TENSILE FRACTURES OF SLATE

XUAN-XINH NGUYEN [1], CHE-WEI YEH [2] TAN-MINH LE [2], JIA-JYUN DONG [2,3]

[1] *Institute of Rock Structure and Mechanics, the Czech Academy of Sciences, Prague, Czech Republic, nguyen@irsm.cas.cz*

[2] *Graduate Institute of Applied Geology, National Central University, Taoyuan, Taiwan, n111624006@g.ncu.edu.tw*

[2] *Graduate Institute of Applied Geology, National Central University, Taoyuan, Taiwan, minhpro84@gmail.com*

[2] *Graduate Institute of Applied Geology, National Central University, Taoyuan, Taiwan, jjdong@geo.ncu.edu.tw*

[3] *Earthquake-Disaster & Risk Evaluation and Management Center, National Central University, Taoyuan, Taiwan*

Introduction

Slate host rock relying on induced fractures for enhanced fluid flow in a low permeability system are investigated as a potential CO_2 sequestration and geothermal site. The permeability properties of incipient foliations, fractures along foliation are assessed using slate samples from the Hungyeh Formation in Taiwan. Hydraulic and mechanical apertures (e, E) of both natural and artificial tensile fractures along incipient foliations were measured simultaneously using the pulse-decay-balance (PDB) method based on the YOKO2 system (Nguyen et al., 2023). Stress-dependent hydraulic and mechanical apertures are then applied to determine rock mass permeability using Snow's model (Snow, 1965). The results are compared to the stress-dependent permeability of the matrix to understand the influence of fractures along incipient foliations on reservoir fluid flow behavior.

Methods

Intact slate samples oriented perpendicular and parallel to incipient foliations were drilled from rock cores. Samples drilled parallel to incipient foliations were used to determine natural fracture along foliation (NFF), and create artificial tensile fracture (ATF) using the Brazilian tensile test.

The matrix permeability of intact samples was determined using a pulse decay method (Brace et al., 1968), while stress-dependent matrix permeability was assessed using a power law (Dong et al., 2010). Additionally, the e and E of fractures were measured simultaneously by the pulse-decay-balance method (PDB) based on the YOKO2 system (Nguyen et al., 2023). The E was determined from fracture volume measurements, and the e was derived from an analysis of the pressure decay curve. The stress dependence of the apertures was determined using an exponential function (Liu et al., 2004), and the results were used to calculate the equivalent permeability of rock mass using Snow's model. These findings were then compared to the permeability of intact slate (Fig. 1).

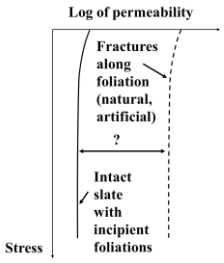

Figure 1. Schematic diagram of stress-dependent permeability of intact slate and fractures along foliation.

Results

Matrix permeability decreases with increasing stress, and anisotropic permeability is observed for incipient foliations. The matrix permeability oriented parallel to incipient foliations (black open circles) is ten times larger than that oriented perpendicular to incipient foliations (gray solid squares) (Fig. 2a).

Permeability of the rock mass increases with decreasing fracture spacing (Snow, 1965). We used an average fracture spacing of 0.1 m, observed from the rock core, to determine the equivalent permeability of rock mass using Snow's model. With smooth joint roughness (joint roughness coefficient, $JRC < 4$) of fractures along foliation, the equivalent permeability of rock mass calculated by the mean stress-dependent e is roughly 0.01–0.1 mD (blue solid curve in Fig. 2d). The contribution of fractures to the permeability is 100 times larger than the matrix permeability. However, the equivalent permeability of rock mass remains within the low permeability range of geothermal reservoirs (light grey region in Fig. 2d). Additionally, assuming the e equals the E for open fractures due to high fluid pressure injection, the equivalent permeability calculated based on the mean stress-dependent E (green solid curve) is approximately 2×10^2–2×10^3 mD (Fig. 2d). The contribution of open fractures to the permeability is 10^4 times greater than that of the matrix permeability (red curve). This significant increase in equivalent permeability places it within the high permeability range (dark gray region in Fig. 2d).

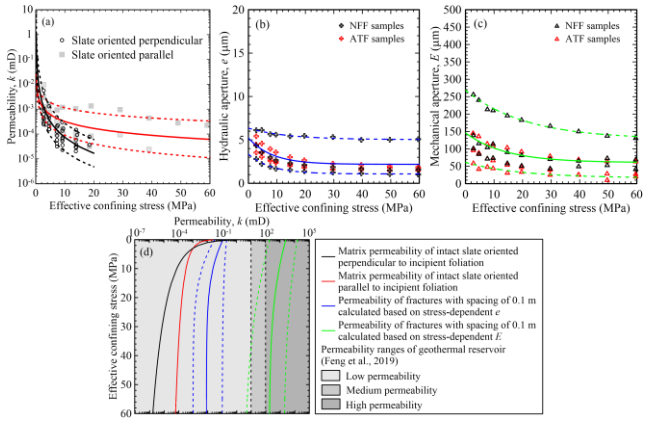

Figure 2. Stress dependency of (a) matrix permeability and (b) $\boldsymbol{e}$ and (c) $\boldsymbol{E}$ of fractures along foliation. (d) The equivalent permeability of rock mass is determined using the Snow's model with spacing of 0.1 m.

Conclusion

Slate host rock with induced fractures for enhanced fluid flow in a low permeability system is a potential site for CO_2 sequestration and geothermal applications. Fluid flow occurs in fractures along incipient foliation under effective stress up to 60 MPa. The equivalent permeability of rock mass with open fractures can increase significantly based on the stress-dependent mechanical aperture.

References

Brace, W. F.; Walsh, J. B.; Frangos, W. T. Permeability of granite under high pressure. *Journal of Geophysical research*. 1968, 73, 2225–2236.

Dong, J. J.; Hsu, J. Y.; Wu, W. J.; Shimamoto, T.; Hung, J. H.; Yeh, E. C.; Wu, Y. H.; Sone, H. Stress-dependence of the permeability and porosity of sandstone and shale from TCDP Hole-A. *International Journal of Rock Mechanics and Mining Sciences*. 2010, 47, 1141–1157.

Feng, J. Y.; Zhang, Y.; He, Z. L.; Sun, Z. M.; Luo, J. Discussion on evaluation methodology of hydrothermal geothermal reservoir. *Journal of Groundwater Science and Engineering*. 2019, 7.

Liu, H. H.; Rutqvist, J.; Zhou, Q.; Bodvarsson, G. S. Upscaling of normal stress-permeability relationships for fracture networks obeying fractional Levy motion. *Elsevier Geo-Engineering Book Series*. 2004, 2, 263–268.

Nguyen, X. X.; Tai, P. L.; Dong, J. J.; Yu, C. W. A novel pulse-decay-balance method for smooth rock joint aperture measurement. *International Journal of Rock Mechanics and Mining Sciences*. 2023, 170, 105504.

Snow, D. T. *A parallel plate model of fractured permeable media*. Ph.D. Thesis, University of California, Berkeley, California, USA, 1965.

CASE STUDY ON USING OPTICAL SENSORS TO INVESTIGATE GROUNDWATER FLOW VELOCITY AND DIRECTION

CHIHPING KUO [1], CHENYU YANG [2]

[1] *National Yunlin University of Science and Technology, Taiwan, Taiwan, cpkuo@yuntech.edu.twl*

[2] *National Yunlin University of Science and Technology, Taiwan, Taiwan, M11216009@yuntech.edu.tw*

Abstract

Detecting groundwater flow velocity and direction is an important work for hydrogeological and geotechnical engineering. Many methods were developed and are used now, such as thermal sensors, electromagnetic sensors, ultrasonic sensors, impeller sensors, and so on. In this study, optical sensors were used to investigate the situation of in-situ groundwater. The methodology of such kinds of sensors is to detect the suspended particles in the fluid and count their velocity and velocity. The results of the sensors compared with the customized environmental conditions in the test site were discussed here. A field test was discussed in this study as well.

Study Area

A construction requires dewatering wells for deep excavation. The location of the site is close to the left shore of Keelung River and showed in Figure 1. The average flow of the river is about 3,690cms and the average velocity for normal days is about 0.53m/s. According to geological investigation data, the upper stratum near surface contains interlayers of sandy soil and clayey soil, called Songshan stratum with an average thickness about 40m around the study area. The low stratum beneath Songshan stratum contains gravels, called Chingmei stratun. Chingmei stratum is a confining aquifer containing saturated groundwater. For the deep excavation, the permeability parameter (*K*) of the gravel, as showen in Figure 2, in Chingmei stratum is required to acquire by in-situ investigation and laboratorial test.

Methods

The permeability parameter is crucial for the design of the pumping wells. However, the permeability parameters were not easy to evaluated by the sample from drilled boreholes because they were disturbed. The boreholes, named #AH-1 and #AH-2, were performed to observe the soil samples and groundwater. The casing pipes with screen at GL-40m to -43m were installed in the boreholes to be observing wells. The outer gap around the depth of screen was filled with fine sands and other area was sealed with bentonite. The sensor uses optical camera to catch motion of particles was employed to evaluate velocity and direction of groundwater flow. According to Darcy's Law, the permeability parameter can be evaluated by velocity (*V*) and hydraulic gradient (*i*).

Results

The evaluated velocities of each location is listed in Table 1. The hydraulic gradient (*i*) was 0.00035, thus the converted permeability parameter (*K*) is listed in Table 1. As well. The range of permeability parameter (*K*) is from 1.311 cm/sec to 4.658 cm/sec, the values from #AH-2 is larger than from #AH-1. The value coordinates to the permeability of GP that defined in USCS, say Poorly graded gravel, sandy gravel, with little or no fines.

The direction of groundwater flow is majorly toward north-east as from observing well#AH-2 to #AH-1. The result of the detection of direction matched the evaluation of velocity.

Conclusion

To use optical sensors to investigate groundwater flow velocity and direction is efficient and useful to evaluated permeability parameter (*K*).

However, the groundwater body that too turbid or too clear is disincentive to this method.

References

Geotech Environmental Equipment, Inc., Introuduction Website of Geotech Colloidal Borescope , https://www.geotechenv.com/geotech_colloidal_borescope.html

Peter M. Kearl, Observations of Particle Movement in a Monitoring Well Using the Colloidal Borescope. *Joumnal of Hydrology*. 1997, 200:323-344.

Kearl, P. M. and Roemer, K., Evaluation of Groundwater Flow Directions in a Heterogencous Aquifer Using the Colloidal Borescope. *Advances in nvironmental Research*. 1998, 2(1), 12-23.

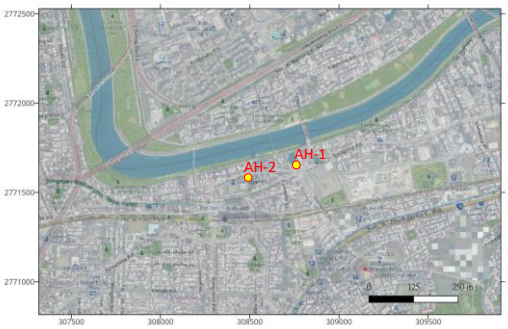

Figure 1. The map of study area and the borehole for observing groundwater

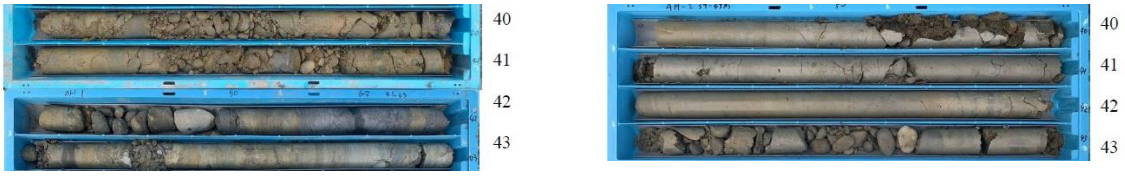

(a) the bored soil and rock samples from BH#AH-1 (b) the bored soil and rock samples from BH#AH-2

Figure 2. The borehole samples of borehole #AH-1 and #AH-2 in Figure 1

(a) the probe of optical camera and lights (b) the performance of the test

Figure 3. The equipment used in this study

Table 1. Measured results of velocity of groundwater and evaluated permeability of the stratum

AH-1			AH-2		
GL-[m]	V(um/sec)	K(cm/sec)	GL-[m]	V(um/sec)	K(cm/sec)
40	466.94	1.311	40	1345.32	3.776
41	648.11	1.819	41	1659.73	4.658
42	635.96	1.785	42	920.73	2.584
43	515.73	1.447	43	1650.35	4.632

GEOHYDROLOGICAL MONITORING OF SLOPE USING ADVANCED DISTRIBUTED FIBRE-OPTIC SENSING: FROM LABORATORY STUDY TO FIELD APPLICATIONS

ASHIS ACHARYA[1,*], DAIKI TANIMURA[2], CHAO ZHANG[3], FUMIHIKO ITO[3], TOSHIHIRO SAKAKI[4], MITSURU KOMATSU[5], ISSEI DOI[6], AND TETSUYA KOGURE[7,8,9]

[1]*Major in Science of Environmental Systems, Graduate School of Natural Science and Technology, Shimane University, 1060 Nishikawatsu-cho, Matsue, Shimane 690-8504, Japan*
[2]*Major in Science and Engineering, Graduate School of Natural Science and Technology, Shimane University, 1060 Nishikawatsu-cho, Matsue, Shimane 690-8504, Japan*
[3]*Interdisciplinary Faculty of Science and Engineering, Shimane University, 1060 Nishikawatsu-cho, Matsue, Shimane 690-8504, Japan*
[4]*ESE Consulting, LLC, 6-10-101 Midorigaokacho, Ashiya, Hyogo 659-0014, Japan*
[5]*Graduate School of Environmental and Life Science, Okayama University, 3-1-1 Tsushimanaka, Kita-ku, Okayama 700-8530, Japan*
[6]*Disaster Prevention Research Institute, Kyoto University, Gokasho, Uji, Kyoto 611-0011, Japan*
[7]*Institute of Environmental Systems Science, Shimane University, 1060 Nishikawatsu-cho, Matsue, Shimane 690-8504, Japan*
[8]*Centre for Natural Disaster Reduction Research and Education, Shimane University, 1060 Nishikawatsu-cho, Matsue, Shimane 690-8504, Japan*
[9]*Disaster Prevention Research Institute, Geodisaster Research Division, Kyoto University, Gokasho, Uji, Kyoto 611-0011, Japan*

Introduction

The development of novel distributed fibre-optic sensing (DFOS) techniques has made significant technological advancements, from traditional slope monitoring tools to real-time measurements of multiple parameters such as strain or temperature (Shi et al. 2021). These sensing methods fulfil the demands of extensive and distributed monitoring of geological structures across vast distances, offering measurements with excellent resolution (Acharya and Kogure 2023). DFOS-based fibre-optic sensors, when embedded into sliding masses, function akin to the nerves in the human body, adeptly capturing extensive information to assess the health condition of the landslide (Acharya and Kogure 2024).

This study evaluated the effectiveness of the Rayleigh-based phase-noise compensated optical frequency-domain reflectometry (PNC-OFDR) method in offering valuable insights into thermal mapping, groundwater flow monitoring, and strain monitoring. A series of experiments were designed and executed to create temperature maps along the length of a test specimen using the PNC-OFDR method, which boasts a fine spatial resolution and rapid measurement times. As a field application, this study attempts to monitor the strain (to examine the deformation characteristics of basement rocks) and temperature changes (to locate the seepage phenomenon) within a deep slope.

Methods

This study demonstrates the feasibility of the PNC-OFDR sensing method to monitor the distributed temperature field with an ultra-short data acquisition period of 2 ms, a spatial resolution of 2 cm, and a temperature resolution of 0.1 °C. Two FR PVC cables were used in the laboratory experiments. One was for heating (heating cable; H-cable), and the other for temperature sensing (temperature measurement cable; T-cable). Two cables were embedded within a cylindrical concrete mortar specimen and subjected to various heating powers. Two water-holding boxes were installed along the specimen at two positions to retain water. If the anomaly of temperature fields is identified with the fibre-optic sensing system by measuring the local spectral shift, the water-supplied position can be located and monitored.

Field deployment involved installing monitoring systems within a 50-meter-deep borehole, where optical cables for heating, temperature sensing, and strain sensing were embedded (Fig.1). The hardened anchorage formed by cement slurry backfill facilitates both seepage detection through actively heated DFOS (AH-DFOS) method and rock deformation monitoring via strain sensing. We have conducted the heating tests of boreholes at different electrical powers to locate the groundwater and other seepage phenomena. We continuously record strain and temperature within the borehole and delve into the relationship between bedrock deformation, seasonal variations, and groundwater flow levels.

Figure. 1 Methods of optical cables installation inside a borehole.

Results

The temporal evolution of temperature along the specimen during a heating period of 3 hrs at four different electrical powers was investigated. The study's results indicated that the PNC-OFDR technique demonstrated a high sensitivity to even small temperature changes, accurately pinpointing water locations at two distinct points. The research determined the minimal heating power required to successfully locate the water positions. The magnitude of the heating power exerted a significant impact on the temperature change. Three distinct phases of temperature increment were observed for a given heating period: rapid, fast, and gentle increase.

DFOS-based cables installed in a deep borehole enabled us to acquire spatially continuous temperature profiles. We measured groundwater dynamics and thermal parameters around a borehole, performing a heating test by heating the armour of a single fibre-optic cable and interpreting the resulting heating curves. We also demonstrated the seasonal effect of the AH-DFOS method on groundwater changes in the context of highly fractured rock.

Conclusion

The experimental study successfully demonstrated the precision of the PNC-OFDR sensing method in monitoring and identifying water position within a two-metre-long cement mortar specimen. Heating the copper wires caused a continuous temperature increase along the specimen, revealing a significant temperature difference between water-supplied and dry sections. Using the AH-DFOS method, we examined groundwater dynamics and the impact of seasonal variations on groundwater levels. Future work will involve continuous strain and temperature monitoring within the borehole, further exploring the relationship between bedrock deformation, seasonal changes, and groundwater flow. The insights and data gathered will benefit engineering geologists and geotechnical engineers in fibre-optic sensing applications for geotechnical monitoring.

References

Acharya, A., Kogure, T. Application of novel distributed fibre-optic sensing for slope deformation monitoring: A comprehensive review. *International Journal of Environmental Science and Technology*. 2023, 8217–8240. https://doi.org/10.1007/s13762-022-04697-5

Acharya, A., Kogure, T. Advances in fibre-optic-based slope reinforcement monitoring: A review, *Journal of Rock Mechanics and Geotechnical Engineering*. 2024 (Accepted on 17 March 2024 for publication)

Shi, B., Zhang, D., Zhu, H., Zhang, C., Gu, K., Sang, H., Han, H., Sun, M., Liu, J. DFOS Applications to geo-engineering monitoring. *Photonic Sensors.* 2021, 11(2):158–186. https://doi.org/10.1007/s13320-021-0620-y

ADVANCEMENTS IN LANDSLIDE VOLUME ESTIMATION: INSIGHTS FROM THE 2016 MW7.8 KAIKOURA EARTHQUAKE

EFSTRATIOS KARANTANELLIS [1], MARIN K. CLARK [1], DIMITRIOS ZEKKOS [2], MIKE J. WILLIS [3]

[1] *Department of Earth and Environmental Sciences, University of Michigan, USA*

[2] *Department of Civil and Environmental Engineering, University of California, USA*

[3] *Department of Geoscience, Virginia Tech, USA*

Introduction

Landslides are complex geological phenomena characterized by the downward movement of mass along a slope. Over the past decades, the frequency and intensity of landslides have been on the rise, primarily due to rapid urbanization, increased occurrence of extreme events, and poor land management practices (Corominas & Moya, 2008). Landslide susceptibility is influenced by factors such as topographical features and engineering geological properties of the rock masses involved (Petley, 2012). Climate change impacts, including changing rainfall patterns and increased weather extremes, have also introduced a new urgency for improving hazard assessment. A common approach involves mapping landslides in 2D using satellite or aerial imagery and estimating the volume by applying a volume-area (V/A) relationship (Larsen et al., 2010). However, the increasing deployment of satellites and the growing accessibility of high-resolution satellite imagery have ignited a new era for landslide volume assessment because of repeat measurements of topography. This study explores the application of satellite photogrammetric technology for landslide volume estimation using 3D change detection procedures. We present a case study of the 2016 Mw7.8 Kaikoura earthquake in New Zealand, which triggered extensive landslides. We utilized high-resolution Digital Surface Models (DSMs) derived from Worldview-3 satellite imagery acquired before and after the earthquake using the SETSM (Surface Extraction with TIN-based Search-space Minimization) algorithm. 3D change detection is employed to estimate landslide volumes across a selected area of interest in Hapuku area, NZ.

The 2016 Mw7.8 Kaikoura Earthquake

The 2016 Mw7.8 Kaikoura earthquake occurred on November 14, 2016, near the town of Kaikoura in the northeastern South Island of New Zealand. The complex earthquake ruptured more than 21 individual fault structures, leading to extensive landsliding (Hamling et al., 2017). The seismic shaking, combined with steep topography and friable geological formations, mobilized large volumes of rock, soil, and debris (Massey et al., 2018, 2020). The 29,557 landslides triggered by the Kaikoura earthquake ranged from shallow soil slips to deep-seated rock failures, causing widespread disruption to transportation networks and infrastructure.

Methods and Results

The SETSM algorithm is an automated object-space digital surface creation algorithm for rational function model imagery, optimized for high-resolution satellite imagery (Noh & Howat, 2015). It generates high-resolution DSMs from stereoscopic satellite imagery by detecting and matching corresponding image features in stereo image pairs to calculate parallax, which is then used to estimate elevation values for each pixel in the resulting DSM (Noh & Howat, 2017). In our study, a polygon-based landslide inventory was created for a subset area of the earthquake-affected region using high-resolution Worldview-3 imagery and SETSM-derived orthoimagery. Landslide identification involved visual analysis techniques on ortho-rectified optical imagery, focusing on features such as vegetation changes/removal, variations in reflectivity, and alterations in surface texture (Scaioni et al., 2014). First, we compared the pre- and post-event SETSM data with pre- and post-event LiDAR datasets in the coastal region where both datasets overlapped. Secondly, we compared the post-event SETSM topography with the post-event LiDAR data in the mountainous areas. We further classified sample regions into vegetated and non-vegetated to assess the influence of vegetation on the model comparisons. This analysis revealed a smaller average 3D distance for non-vegetated areas, indicating

a more precise alignment of data points for the LiDAR. The surface change detection model, created by differencing the pre- and post-event topography, was used to estimate the volume of displaced material for individual landslides. To ensure the accuracy of the volume estimates, we implemented several quality control measures. We established a threshold based on the maximum root mean square error (RMSE) from the point cloud alignment to identify areas with significant surface changes exceeding the 95% confidence level. Next, we differentiated the pre- and post-event point clouds within the validated surface change areas. This process involved separating points with negative elevation changes (representing loss of material) from points with positive changes (representing deposition). Subsequently, we performed a vertical difference analysis on each point cloud to determine the volume change associated with loss and deposition. Finally, we implemented a 0.3 volume-to-area (V/A) ratio threshold to distinguish between actual landslides and potential misinterpretations arising from factors like vegetation changes. The resulted V/A relationship between the mapped landslide area and the estimated volume from direct point cloud differencing was $VL = 1.82 \times AL^{1.16}$. The average loss area we identified was 1,178 m^2 and the maximum 130,494 m^2 (minimum 100 m^2). The analysis of the relationship between volume and area revealed a strong positive correlation between the two landslide variables (Pearson's $r = 0.89$, $p < 0.05$) in the AOI (Figure 1).

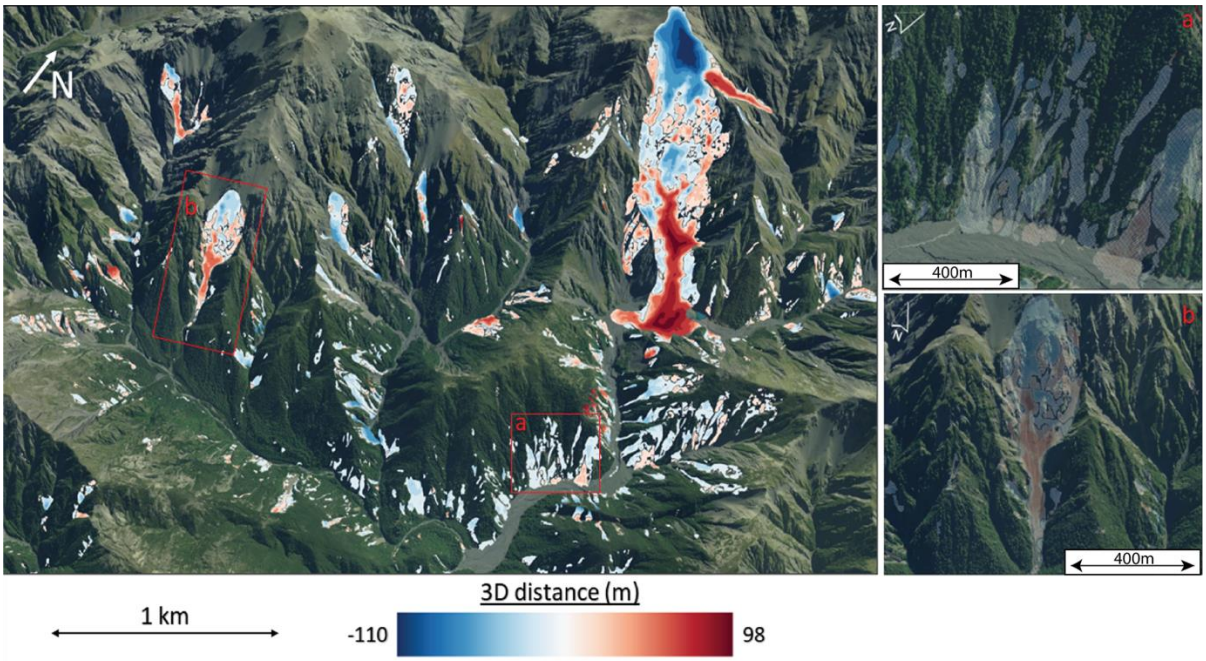

Figure 1. Map of the 3D signed distances from the geomorphic change detection phase between the pre-SETSM and the post-SETSM point clouds.

Conclusion

This study highlights the importance of topography in landslide modeling and proposes a comprehensive satellite-based approach for volume estimation, considering both frequent small landslides and impactful larger events. We identified 1,448 landslides, mostly narrow debris flows, with deep-seated landslides creating dam lakes. Topography registration accuracy varied between vegetated and non-vegetated areas, with the latter showing better alignment. 3D calculations revealed meter-scale erosion and deposition post-earthquake. We established a volume-to-area threshold to avoid overestimation and achieved meter scale volume calculations using pre- and post-event data. This research emphasizes the need for a holistic approach to landslide management, and innovations like SETSM and 3D distance mapping contribute to detailed analysis for rapid response and long-term planning. The findings stress the importance of continuous methodological development for accurate 3D landslide analysis, paving the way for improved preparedness and safety in landslide-prone areas.

References

Corominas, Jordi, and José Moya. "A review of assessing landslide frequency for hazard zoning purposes." *Engineering geology* 102.3-4 (2008): 193-213

Hamling, Ian J., et al. "Complex multifault rupture during the 2016 M w 7.8 Kaikōura earthquake, New Zealand." *Science* 356.6334

Massey, C., et al. "Landslides triggered by the 14 November 2016 Mw 7.8 Kaikōura earthquake, New Zealand." *Bulletin of the Seismological Society of America* 108.3B (2018): 1630-1648

Massey, C. I., et al. "Volume characteristics of landslides triggered by the MW 7.8 2016 Kaikōura Earthquake, New Zealand, derived from digital surface difference modeling." *Journal of Geophysical Research: Earth Surface* 125.7 (2020)

Petley, David. "Global patterns of loss of life from landslides." *Geology* 40.10 (2012): 927-930

Larsen, Isaac J., David R. Montgomery, and Oliver Korup. "Landslide erosion controlled by hillslope material." *Nature Geoscience* 3.4 (2010): 247-251

REFINING HYDRAULIC CONDUCITIVITY ESTIMATION IN FRACTURED MEDIA USING X-RAY TOMOGRAPHY, DISCRETE FRACTURE NETWORKS AND FLEXIBLE WALL PERMEAMETER

ELISA MAMMOLITI [1], DAVIDE FRONZI [1], MIRKO FRANCIONI [2], STEFANO MAZZOLI [3], JONATHAN DOMIZI[1], MATTEO RAPAZZETTI[1], ALESSIA CAPUTO[4], ALBERTO TAZIOLI[1], GIUSEPPE SCARPELLI[1], PAOLO CASTELLINI[4]

[1] *Department of Science, Matter Engineering, Environment and Urban Planning, Marche Polytechnics University, Italy, e.mammoliti@staff.univpm.it*

[2] *Department of Pure and Applied Sciences, University of Urbino, Italy*

[3] *School of Science and Technology, University of Camerino, Italy*

[4] *Department of Industrial Engineering and Mathematical Sciences, Marche Polytechnics University, Italy*

Introduction

Measuring hydraulic conductivity in fractured media is fundamental for several engineering applications including slope stability calculations and modelling of groundwater flow; however, it is also challenging due to varying discontinuities in aperture, roughness, and connectivity (Berkowitz, 2002; Mammoliti et al., 2023). Although traditional permeameter tests are able to capture data, they struggle with fracture complexity (Witherspoon et al., 1980). Recent advances in 3D X-ray tomography provide non-destructive, high-resolution imaging for detailed fracture analysis, precisely measuring discontinuity apertures and roughness to enhance fluid flow understanding (Glad et al., 2023). This study integrates 3D X-ray tomography with fracture analysis and DFN models to improve predictive accuracy of hydraulic conductivity in the Scaglia Rossa formation, a major fractured carbonate formation in the Umbria-Marche succession.

Methods

Standard flexible wall permeameter tests were used to measure the hydraulic conductivity of rock samples by imposing water flow and monitoring inflow, outflow, and differential pressure. High-resolution 3D X-ray tomography provided a 3D dataset of the fracture network, including fracture roughness and aperture. Discontinuities were classified from a geo-structural perspective, and aperture and roughness were manually measured using JRC (Barton, 1977) and an optical comparator to validate tomography data. Three DFN models were developed, using: (1) all identified discontinuities and manually extracted P21 values, (2) exclusively open discontinuities and manually extracted P21 values, and (3) open discontinuities and P32 values from 3D X-ray tomography (still under development).

Results

Fracture analysis revealed varying hydraulic conductivity essentially controlled by rock discontinuities (joints, veins, stylolites), with negligible flow within the matrix. Joints filled with clay, as well as pressure solution cleavage (tectonic stylolites) showed minimal enhancement in water flow due to reduced aperture and impervious filling. Conversely, open joints with favourable orientation for water flow exhibited higher hydraulic conductivity values, serving as preferential flow paths. Photogrammetric methods were used for fractures analysis using high-res photos processed into 3D models, to determine fracture intensity parameters (Figure 1a). Many fractures were closely spaced and filled with low-permeability materials, limiting groundwater flow. Clear-open joints exhibited pronounced water flow aligning coherently with their geometry. Detailed fracture characterization, integrating 3D X-ray tomography (Figure 1b), provided crucial insights into discontinuities pattern, aperture and roughness (Figure 1c), supporting permeameter results and allowing us to obtain improved physically based DFN models for water flow in fractured rock formations.

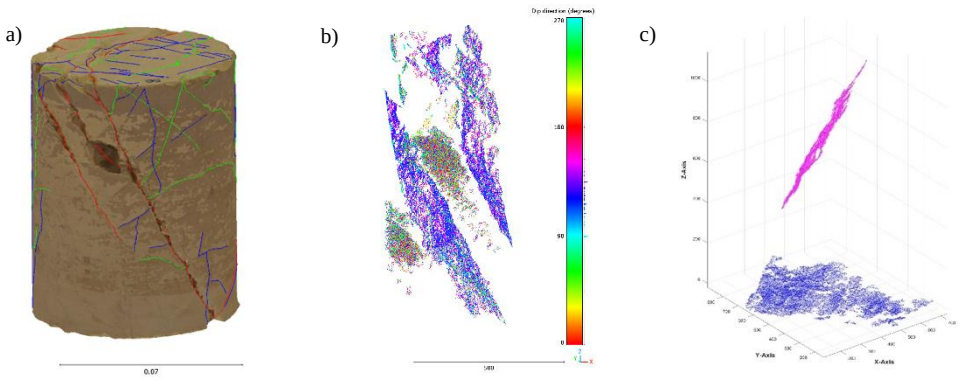

Figure 1. Example of discontinuity extraction and analysis. **(**a) Fracture network characterizing rock sample (used for fracture intensity calculation). (b) Extraction of rock discontinuities from 3D X-ray tomography. (c) Data post-processing for roughness calculation.

Conclusion

This study highlights the importance of combining standard testing with advanced imaging and modelling to accurately predict hydraulic conductivity in fractured rocks. Measuring roughness and aperture via 3D X-ray tomography enhances DFN models and hydraulic conductivity predictions. Flexible wall permeameter tests validate DFN-derived conductivity. Although currently ongoing, this research suggests that integrating 3D X-ray tomography could be crucial for groundwater management and engineering applications in fractured rock environments. Future work will focus on classifying rock bridges using tomographic methods.

References

Barton, N., & Choubey, V. The shear strength of rock joints in theory and practice. Rock mechanics. 1977, 10, 1-54.

Berkowitz, B. Characterizing flow and transport in fractured geological media: A review. Adv. Water Resour. 2002, 25 (8–12), 861–884.

Glad, A. C.; Afrough, A.; Amour, F.; Ferreira, C. A.; Price, N.; Clausen, O. R.; Nick, H. M. Anatomy of fractures: Quantifying fracture geometry utilizing X-ray computed tomography in a chalk-marl reservoir; the Lower Cretaceous Valdemar Field (Danish Central Graben). Journal of Structural Geology. 2023, 174, 104936

Mammoliti, E.; Pepi, A.; Fronzi, D.; Morelli, S.; Volatili, T.; Tazioli, A.; Francioni M. 3D Discrete Fracture Network Modelling from UAV Imagery Coupled with Tracer Tests to Assess Fracture Conductivity in an Unstable Rock Slope: Implications for Rockfall Phenomena. Remote Sensing. 2023, 15(5), 1222.

Witherspoon, P. A.; Wang, J. S.; Iwai, K.; & Gale, J. E. Validity of cubic law for fluid flow in a deformable rock fracture. Water resources research. 1980, 16(6), 1016-1024.

Topic 4

Geohazard Assessment and Risk Mitigation for Infrastructure Projects

EMERGENCY MANAGEMENT (MITIGATION, PREPAREDNESS, AND RAPID RESPONSE) OF LANDSLIDE DAM HAZARDS – A REVIEW

JIA-JYUN DONG[1]

[1] *Graduate Institute of Applied Geology, National Central University, Taiwan, jjdong@geo.ncu.edu.tw*

Introduction

Outburst flood from landslide barrier lakes is hazardous to the downstream of the nature dams. Inundation upstream of the landslide dams induced casualties and properties loss as well. Since the landslide dams are usually short-lived, emergency management is challenge because rapid responses are required. Costa (1985) published one USGS report "Floods from dam failures" (include landslide dams and constructed dams) in 1985. This is an important documentation from the hazard assessment view point of landslide dam hazards. The special publication of ASCE "Landslide Dams: Processes, Risk, and Mitigation" (Schuster, 1986), consisted of nine papers on landslide dams, could be one of the pioneer collections for landslide dam study. The landslide processes involved in forming landslide dams, the potential for catastrophic failure of the dams, and upstream/downstream effects of the dams are introduced. Case histories from the United States, Canada, Pakistan, Japan, and China are illustrated. Two years later, Costa and Schuster (1988) published a classical review paper of "The formation and failure of natural dams" (related to landslides, glacial-ice, and moraine), which using "an integrated view of the phenomenon as a whole". Soon after this review, Costa and Schuster (1991) documented 463 historical landslide dam cases from all around the world. This documentation is the most important landslide dam inventory in 90's. In 2002, Korup (2002) published an important review paper on geomorphic and hydrologic aspects of the formation, failure and geomorphic impact of landslide dams. Although this is a very comprehensive review of landslide dam study, the conclusions of this paper pointed out that there is a considerable lack of understanding of geomorphic forms and processes involved with landslide-dam formation, stability and failure.

For the past two decades, together with the increasingly understanding of landslide dam evolution, the technologies acquiring critical information for landslide dam hazard mitigation have been significantly improved. Many comprehensive books and review papers (e.g., Evans et al., 2011; Zhang et al., 2016; Zheng et al., 2021; Zhong et al., 2021; Fan et al., 2020; 2021) were published, based on the new database, numerical and experimental tests, and case histories of landslide dams. Worldwide landslide dam inventories are accumulated continuously as well. However, few review comprehensively gathering knowledge relevant to emergency management. Thorough reviews focusing on available technologies for emergency management is needed.

Methods

In this study, state of the art review focuses on the issues which are relevant to emergency management (McLoughlin, 1985) of possible short-live landslide dams including: predicting river blockage and providing scenarios (preparedness before the dam forming), early identifying the dam forming (secure more time for emergency response), rapidly evaluating the hazards (risk) of landslide dam (upstream and downstream), and short-term measures (hard and soft ones) to mitigate the hazards.

Results

Emergency management strategies before the landslide dam forming (preparedness) are illustrated, including (a) data collection (including landslide dam inventory), (b) susceptibility analysis, and (c) possible hazard scenarios development. Moreover, technologies for early identifying the occurrence, location, and characteristics of landslide dam and related lake are introduced, including (a) landquake, (b) abnormal hydrogeological response, and (c) remote sending data. Relevant information required for emergency management is indicated, too. Finally, rapid hazard evaluation methods are summarized, including (a) downstream (stability, breach process, and flood routing), and (b) upstream (predicting the temporal variation of lake surface elevation). Thanks to the quick development of new technologies,

preparedness and rapid assessment of the landslide dam hazards soon after the formation of a landslide dam is possible for decision-making to prevent or minimize the losses.

Conclusion

The author reviewed many review papers, books, and documentations and surprisingly found out few of them focused on comprehensively gathering knowledge relevant to emergency management. This review will be a useful reference for emergency management of landslide dam hazards.

References

Costa, J. E. Floods from Dam Failures, Open-File Report 85-560, US Geological Survey. 1985.

Costa, J.E.; Schuster, R.L. The formation and failure of natural dams. *Geol. Soc. Am. Bull.* 1988, 100 (7), 1054‑1068.

Costa, J. E.; Schuster, R. L. Documented Historical Landslide Dams from around the World, Open-File Report 91-239, US Geological Survey. 1991.

Evans, S. G. The maximum discharge of outburst floods caused by the breaching of man-made and natural dams. *Canadian Geotechnical Journal*, 1986, 23(3), 385-387.

Evans, S. G.; Hermanns, R. L.; Strom, A.; Scarascia-Mugnozza, G. (eds.). Natural and artificial rockslide dams (Vol. 133). Springer Science & Business Media. 2011.

Fan, X.; Dufresne, A.; Subramanian, S. S.; Strom, A.; Hermanns, R.; Stefanelli, C. T.; Hewitt, K.; Yunus, A.P.; Dunning, S.; Capra, L.; Geertsema, M.; Miller, B.; Casagli, N; Jansen, J.D.; Xu, Q. The formation and impact of landslide dams–State of the art. *Earth-Science Reviews*, 2020, 203, 103116.

Fan, X.; Dufresne, A.; Whiteley, J.; Yunus, A. P.; Subramanian, S. S.; Okeke, C.A.U.; Panek., T.; Hermanns., R.L.; Peng, M.; Strom, A.; Havenith, H.B.; Dunning, S.; Wang, G.; Stefanelli, C. T.. Recent technological and methodological advances for the investigation of landslide dams. *Earth-Science Reviews*, 2021, 218, 103646.

Korup, O. Recent research on landslide dams-a literature review with special attention to New Zealand. *Progress in Physical Geography*, 2002, 26(2), 206-235.

McLoughlin, D. A framework for integrated emergency management. *Public administration review*, 1985, 45, 165-172.

Zhang, L.M.; Peng, M.; Chang, D.S.; Xu, Y. Dam Failure Mechanisms and Risk Assessment. John Wiley & Sons Singapore Pte. Ltd., Singapore. 2016.

Zheng, H.; Shi, Z.; Shen D, Peng, M.; Hanley, K.J.; Ma, C.; Zhang, L. Recent Advances in Stability and Failure Mechanisms of Landslide Dams. *Front. Earth Sci.,* 2021, 9:659935. doi: 10.3389/feart.2021.659935

Zhong, Q.; Wang, L.; Chen, S.; Chen, Z.; Shan, Y.; Zhang, Q.; Ren, Q.; Mei, S.; Jiang, J.; Hu, L.; Liu, J. Breaches of embankment and landslide dams-State of the art review. *Earth-Science Reviews*, 2021, 216, 103597.

EVALUATION OF FAILURE TYPES AND EVOLUTION OF A DEEP-SEATED LANDSLIDE, TAICHUNG CITY, TAIWAN

CHE-MING YANG [1], CHIA-LUNG HSIEH [1]

[1] *Department of Civil and Disaster Prevention Engineering, National United University, Taiwan, stanleyyangcm@nuu.edu.tw*

Introduction

Deep-seated landslides typically exhibit complex failure patterns due to their considerable depth, area, and volume, often triggered by intense rainfall and seismic activity. The response of such landslides varies depending on the triggering and types of failure involved. The geological and geomorphological context plays a crucial role in the types of rock slope failures, particularly influenced by the orientations of discontinuities and slope surfaces (Korup et al., 2010). Rock slope failures can be classified into planar sliding, wedge sliding, toppling, and rockfall (Stead and Wolter, 2015), with some landslides showing a combination of two or more failure types. The distinct rock slope failure mechanisms result in different kinematic processes and consequences, affecting disaster prevention and mitigation strategies. Therefore, a comprehensive assessment of failure types and their magnitudes is essential for effective disaster. This study focuses on deep-seated landslide (4 ha in area, ~14.5m in depth) in Taichung City, central Taiwan with the aim of establishing its geological model. The landslide occurs within a flysch foreland sequence of the Miocene Cholan Formation, adjacent to the of wall the Chelungpu Fault. The cuesta landform predominant prevalent in this region.

Methods

Based on the regional geological map, high-resolution digital elevation model, digital surface model, and multi-period images, this study employs various methodologies: (a) field investigation involving analysis of discontinuity attitudes and observation of outcrops; (b) geomorphological analysis including topographic interpretation and slip surface trace; (c) geotechnical exploration through boreholes and underground monitoring; (d) orthoimage interpretation incorporating the landslide's failure history. As a result, this comprehensive approach enables the establishment of a geological model and evolution of a deep-seated landslide (Fig. 1).

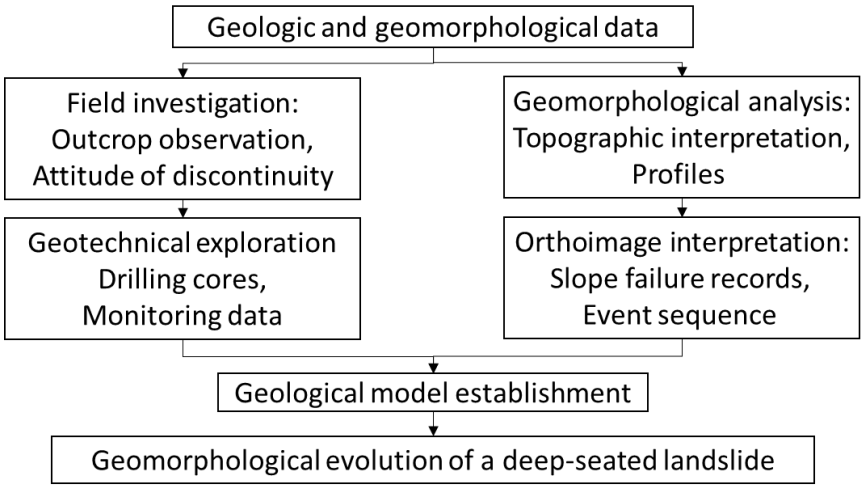

Figure 1. Flowchart of this study.

Results

The field investigation revealed the potential slip zone surrounding the landslide site, with a survey conducted on adjacent outcrops to analyze the lithology and attitudes of bedding planes and joint sets. The topographic features of landslide were identified, and the main scarp and right limb cliff corresponding to distinct two joint sets. Analysis of multi-temporal orthoimages depicting the slope

failure indicated the extent and locations of past failures, providing insights into the sequence of events and the relationships between different sections within the deep-seated landslide. However, orthoimages were found to be insufficient in identifying variations in the right limb cliff. Therefore, a combination of field surveys and aerial views obtained through the use of drones is deemed essential for this study. A 3D model was constructed to visualize and present the spatial information of the deep-seated landslide. The failure mechanisms were categorized into four types: (1) rockfalls occurring at the main scarp and the right limb cliff, (2) planar sliding along the bedding of the upper slope, (3) wedge failure at the intersection of the main scarp and right limb cliff and, (4) colluvium circular failure in the lower slope.

Based on the findings of investigation, it is observed that planar sliding along the bedding plane near the riverside is likely to initiate at the initial stages, leading to the elevation difference at the right limb, resulting in the formation of a high cliff. Over the long term, the uplift of the Chelungpu thrust fault has reduced the stability of inclined sedimentary rocks, causing the enlargement and thickening of the daylighted rock layers. The slope failures develope from the lower slope to the upper slope, the main scarp develops backward progressively due to planar failure. Additionally, rockfall events are noted to occur along the main scarp. Furthermore, the bedding plane dips to southeast and the right limb cliff faces to north with east-west strike. The intersection of two discontinuities form the wedges plunging to the east. The deposits of three failure zones mentioned above moves downslope, resulting in the accumulation of a thick colluvium.

Moreover, the deposits increase the loading and the toe erosion both worsen the stability of colluvium. The significant displacement of colluvium was identified by orthoimages, which induced by heavy rainfall. After colluvium descends, the daylighted rock layers and wedges on the upper slope become prone to instability. Consequently, dynamic interaction is likely to persist over the long term.

Conclusion

A geological model of deep-seated landslide has been developed, identifying four distinct failure types (rockfalls, planar failure, circular failure, and wedge failure) by field survey, analysis, and interpretation of orthoimages. Furthermore, the geomorphologic evolution of a deep-seated landslide can be clarified by examining the interplay of these four types of failure.

Acknowledgements

This research was supported by the National Science and Technology Council (NSTC- 112-2116-M-239-001) and National United University (project No. SM113004).

References

Korup, O.; Densmore, A. L.; Schlunegger, F. The role of landslides in mountain range evolution. *Geomorphology*. 2010, 120(1-2), 77-90.

Stead, D.; Wolter, A. A critical review of rock slope failure mechanisms: The importance of structural geology. *Journal of Structural Geology*. 2015, 74, 1-23.

ROTENFELS: ANALYSIS OF THE ROCKFALL HAZARD ON THE HIGHEST ROCK FACE NORTH OF THE ALPS

STEVE GRUSLIN [1], TIFFANY HENNEBAUT [2], ANAÏS ENDRÈS [3]

[1] *GEOCONSEILS, Luxembourg, steve.gruslin@geoconseils.lu*

[2] *GEOCONSEILS, Luxembourg, tiffany.hennebaut@geoconseils.lu*

[3] *ECOLE NATIONALE SUPERIEURE DE GEOLOGIE, France, anais.endres1@etu.univ-lorraine.fr*

Introduction

The Rotenfels rhyolitic rock face in Bad Münster am Stein-Ebernburg (Germany), the highest north of the Alps (over 200m high), presents a particular risk of falling and scattered boulders. In recent years, numerous blocks have fallen onto the road and railway below. Protection against geological hazards is complicated by the fact that the site is a protected natural area. It is therefore impossible to secure the rock face directly, and boulder barriers are the only possible solution. Boulder barriers already exist in various places, but they are currently insufficient to protect the road and railway effectively. The study we carried out had several objectives: identify the geological risks that could affect the road and railway, determine, where there is no fence, the rebound energies and heights that the fences to be installed will have to absorb, and, where there are already fences, to establish whether the current fences are suitable and which part requires additional fences. The safety measures to be implemented were determined by means of an in situ characterisation of the rock, a risk analysis and trajectometric studies.

Figure 4. Two views of Rotenfels, with the road and railway line to be protected clearly visible

Methodology

Based on field observations, the entire site was divided into 19 zones with similar characteristics in terms of topography, wall height, rock aspect, ground occupation at the foot of the wall, etc. For each of the zones thus defined, except few zones that were not accessible, the rock was characterised by a series of in situ measurements including stereographic measurements, a survey of the instabilities affecting the wall, Rockschmidt hammer measurements and a classification of the rock mass according to several internationally recognised systems (Q, RMR, GSI). All the measurements taken in the field were used for our risk analysis, enabling us to define the areas from which the blocks could have originated and the dimensions of the unstable boulders to be expected. The size of the critical blocks (plurimetric), and the blocks found on the ground (around $0.1m^3$), have been added to estimate a volume of blocks (between $0.1m^3$ and $1m^3$) that should be modelised in the trajectory modelisations. Small stones ($<0.1m^3$) have also been modelised, according to the volume of scree cone found on site.

Trajectometric study and rocfall simulations

Three main types of blocks have been defined. The volume of the blocks was defined by field assessment, i.e.: the critical volume of the block verified for each zone, the orientation of the various

joints and their persistence, and the volume of the block found on the ground or at the foot of the slope for each zone. These observations enable us to estimate two main scales of boulder, with a volume of around 0.1 – 0.2m^3, and a volume of around 1m^3. The small rocks (from 0.0005m^3 to 0.1m^3) have also been modelised by the interpretation of scree cone volume. The distribution has been changed in function of the zone classification: the most fractured areas present more 0.1m^3 blocks, and the more massive areas 0.2m^3 blocks. To a lesser extent, boulders with a volume of 5m^3 were also modelled to consider the collapse of the largest elements. This volume of 5m^3 is an average volume given the fragmentation of the block along the fall and the rebound. Some exceptional boulders, close to the foot of the cliff, have been modelled with a volume of 10m^3. But these events remain exceptional, and therefore have not been used to estimate the energy and rebound to be taken up by the barriers.
The 2D simulations with large boulders were made only for critical cuts or where large blocks were suspected on site. For the 3D simulations, the contour lines acquired by Lidar were imported and all the observations collected in the field were uploaded to the 3D model (weathered areas, critical blocks, scree cone, angle slope …). The 3D representation was used to model the propagation of the blocks in space. It also allowed to represent the ended point of each modelised block. The parameters used in the simulations were based on the Schmidt hammer when measurement have been possible (Rayudu, 1997), or from the Rocfall library.

Results

The simulations show that the ended point could reach the road and the train tracks. Thanks to these simulations, we have been able to converge the models results with the observations made on site. We were thus able to estimate the propagation hazard, which will draw the areas to be treated as a priority. Thanks to the 3D refined model, we were also able to precise the most critical areas where the fences should be installed or renewed. These results are limited to blocks with a 95% probability of occurrence, which means that the more extreme results (i.e. exceptional block size) are considered exceptional events with an acceptable occurrence rate for users.

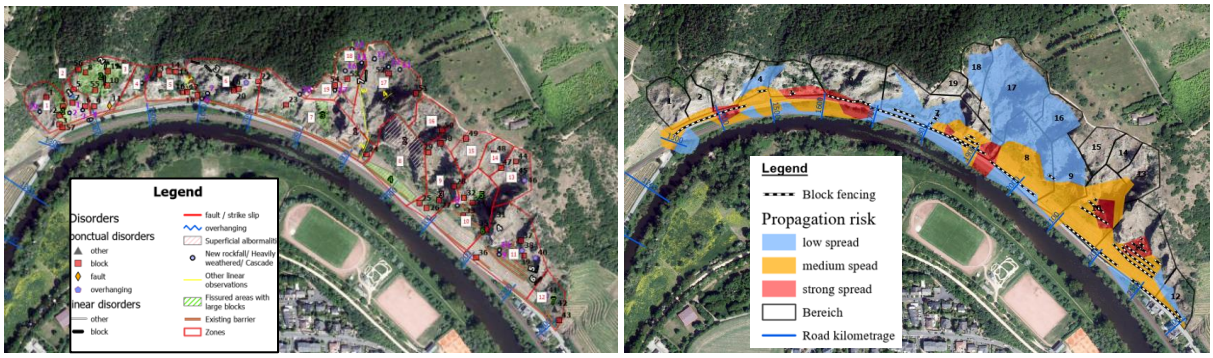

Figure 5. Zoning of the site studied into 19 zones with the diverse observations made on site (left**)** and map of the propagation hazard (right)

Conclusion

All the calculations have shown that the risk is very real for road and railway. The methodology put in place, enabling the acquisition of the field data's needed for the trajectometric calculations, made it possible to determine the input data's (energy and height of rebound) needed to dimension, in a second phase, the safety measures to be implemented to protect the road and the railway line.

References

Landsamt für Geologie und Bergbau Rheinland-Pfalz, *Geologie von Rheinland-Pfalz,* Stuttgart, E. Schweizerbart'sche Verlagsbuchhandlung (Nägele u. Obermillen), 2005.

Rayudu DNP, *Computer simulations of rockfalls – Application to rockfalls at fox glacier, West Coast, New Zealand*, Thesis, Lincoln University, 1997.

LARGE-SCALE LANDSLIDE SUSCEPTIBILITY ZONATION: CLASSIFICATION METHODS AND INFLUENCE ON A FURTHER APPLICATION IN SPATIAL PLANNING SYSTEM

SANJA BERNAT GAZIBARA [1], IVA ŠTEFIČAR [1], MARKO SINČIĆ [1], MARTIN KRKAČ [1], SNJEŽANA MIHALIĆ ARBANAS [1]

[1] *University of Zagreb, Faculty of Mining, Geology and Petroleum Engineering, Croatia, sanja.bernat@rgn.unizg.hr*

Introduction

Classification of landslide susceptibility maps (LSMs) is crucial for land use spatial planning and management, and it affects the possibilities of practical use of maps and the quality of information depicted by the map. Adopting one classification system or another will affect the map's readability, final appearance, and, most importantly, the decision-making tasks required for effective land management. This research compares and evaluates the reliability of the most commonly used classification methods and proposes a classification based on the Receiver Operating Characteristic (ROC) curve. The analyses were carried out on the landslide susceptibility model for the study area (20 km^2) in Hrvatsko zagorje (Croatia), which was derived in the frame of the LandSlidePlan project (Bernat Gazibara et al., 2022).

Methods

The landslide susceptibility model for the study area in Hrvatsko zagorje was derived from a detailed LiDAR-based landslide inventory (Krkač et al., 2022), high-resolution geoenvironmental causal factors and by applying the Random Forests method. Stable pixels were randomly generated in the same quantity as unstable pixels, outside the known landslide areas identified in the LiDAR-based inventory. For landslide susceptibility modelling, 50% of the landslide polygons in the inventory were randomly selected for the model training and the remaining 50% for model validation, while 100% of the mapped landslides were used for susceptibility zoning. Considering landslide causal factors, a set of eight maps grouped as geomorphological (slope, aspect, curvature), geological (engineering formations, proximity to engineering formations), hydrological (proximity to drainage network, proximity to permanent streams) and anthropogenic (proximity to land-use contact) were prepared from LiDAR DTM 5m resolution, engineering geological map in scale 1:5000 (Sinčić et al., 2022), and existing high-resolution land use data. The derived landslide susceptibility model showed high model verification AUC (85.1 %) and can be considered representative for further analysis. The classification methods used in this analysis were equal intervals, quantiles, natural breaks, geometrical intervals, standard deviation and classification based on the ROC curve expressed by cumulative landslide area and cumulative landslide susceptibility, i.e. probability. Furthermore, cut-off values for zonation using the ROC curve were set to different cumulative landslide area presence. Derived LSMs were classified into five zones: very low, low, medium, high and very high susceptibility zones.

Results

To analyse the influence of eight classification methods on landslide susceptibility zoning, the percentage of susceptibility zones in the study area and the percentage of landslide presence in each susceptibility zone were calculated (Figure 1). The criteria for choosing the optimal method is that the zonation results in a map with a low percentage of high and very high susceptibility zones containing a high landslide presence. On the contrary, low and very low susceptibility zones should contain low landslide presence. Considering the above, the method based on the ROC curve with different threshold values proved to be the most optimal method for landslide susceptibility zonation in the study area. The methods of equal intervals, natural breaks, and standard deviations resulted in LSMs with a low percentage of the study area in very high susceptibility zones with low landslide presence. The quantile

method and geometrical intervals resulted in a lower percentage of the study area in very low susceptibility zones compared to the LSMs classified based on the ROC curve.

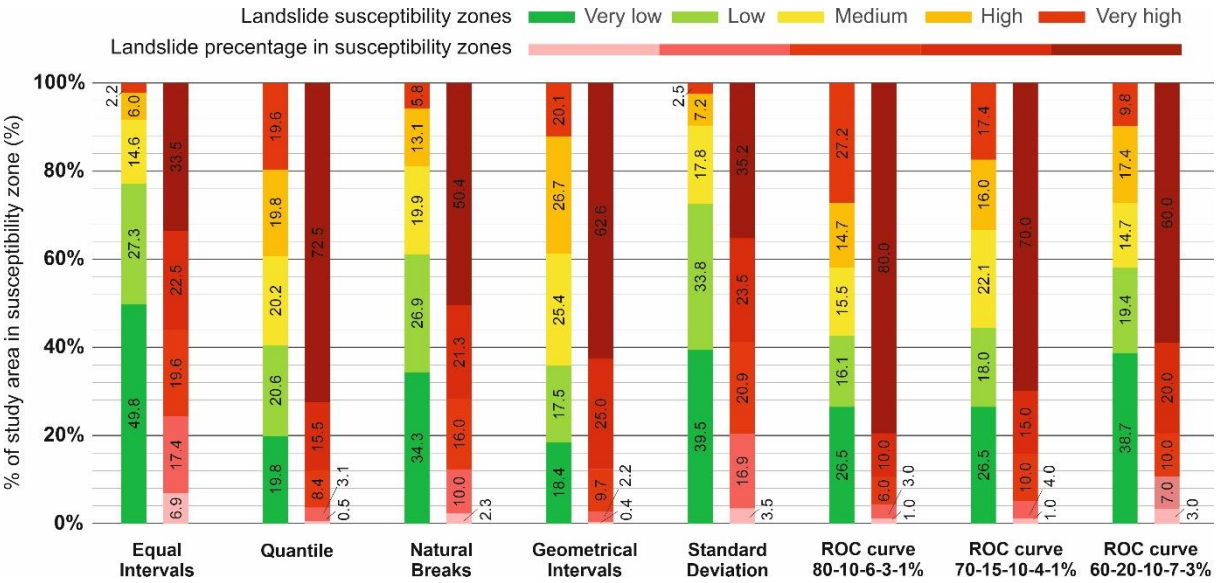

Figure 1. Distribution of landslide susceptibility zone areas and landslide presence based on eight different classification methods.

Conclusion

Derived landslide susceptibility zonation maps differ based on the area of susceptibility zones and the percentage of known landslides in susceptibility zones. Since the most effective and generally cheapest risk mitigation measures are non-structural measures based on land use planning, these large differences in the interpretation of landslide susceptibility zones can impact responsible and sustainable spatial planning and risk assessment at a local level. We conclude that landslide susceptibility zonation by applying the ROC curve enables the interpretation of smaller areas of high and very high susceptibility zones with high landslide presence; the only precondition is that landslide susceptibility modelling is based on representative and reliable LiDAR-based inventory.

References

Bernat Gazibara, S.; Mihalić Arbanas, S.; Sinčić, M.; Krkač, M.; Lukačić, H.; Jagodnik, P.; Arbanas, Ž. LandSlidePlan -Scientific Research Project on Landslide Susceptibility Assessment in Large Scale. *In Proceedings of the 5th ReSyLAB*, Rijeka, Croatia, 23-26 March 2022; pp. 99–106.

Krkač, M.; Bernat Gazibara, S.; Sinčić, M.; Lukačić, H.; Mihalić Arbanas, S. Landslide Inventory Mapping Based on LiDAR Data: A Case Study from Hrvatsko Zagorje (Croatia) *In Proceedings of the 5th ReSyLAB*, Rijeka, Croatia, 23-26 March, 2022; pp. 81–86.

Sinčić, M.; Bernat Gazibara, S.; Krkač, M.; Lukačić, H.; Mihalić Arbanas, S. The Use of High-Resolution Remote Sensing Data in Preparation of Input Data for Large-Scale Landslide Hazard Assessments. *Land*. 2022, 11, 1360, doi:10.3390/land11081360.

REMEDIATION WORKS ON AN ACTIVE LANDSLIDE IN SVÄTÝ ANTON, SLOVAKIA

MARTIN BEDNARIK[1], RÓBERT CSIZMADIA[2], RENÉ PUTIŠKA[1], BIBIANA BRIXOVÁ[1], RUDOLF TORNYAI[1] & ALEŠ HAVLÍN[3]

[1]*Comenius University Bratislava, Faculty of Natural Sciences, Department of Engineering Geology, Hydrogeology and Applied Geophysics, Slovakia; mbednarik@uniba.sk*

[2]*GEOFOS, Ltd., Žilina, Slovakia,* robert.csizmadia@geofos.sk

[3]*National Radiation Protection Institute, Brno, Czech Republic*

Introduction

Due to the increasing activity of slope movements, an emergency was declared in the village of Svätý Anton on February 8, 2021. The landslide in Svätý Anton posed an immediate risk to the main road no. I/51, its traffic, and the surrounding infrastructure. The landslide in Svätý Anton represents a reactivated form of an old landslide. The condition for its creation in the past was a favorable geological structure; Neogene fine-grained and sandy tuffs, which, due to weathering processes, acquired the character of fine-grained soils with unfavorable physical and mechanical properties and erosive activity of the Štiavnica stream. The current activity state is caused by anomalous precipitation in this environment.

Methods

In the first phase, comprehensive drainage of the landslide area was proposed and implemented, both surface and deep drainage. The second phase addressed permanent stabilization measures to secure the toe of the landslide slope along the road by constructing a retaining wall to achieve local stability on the specific shear surface and to ensure the required passable width of the first-class communication 1/51 and its drainage, which was non-functional before the commencement of the works. The rescue works in the second phase were designed as a two-stage steel anchored construction. A flexible, stabilizing, and simultaneously permeable construction was proposed. Both stages of security are formed from an anchored steel stabilization structure. The approach to the design of the second phase was initiated after analyzing the stability situation of the massif post-drainage and evaluating the effectiveness of the constructed drainage elements. The evaluation also included the results of measurements from geotechnical monitoring and geophysical measurements. The existing monitoring network was expanded as part of the rescue works.

Results

A surface drainage system was implemented to reduce the contribution of precipitation to the body of the landslide. To lower the level of the groundwater level, subhorizontal drainage wells and prefabricated drainage drains were designed and implemented at the foot of the slope deformation. ZUBOR prefabricated drainage geodrains (Fig. 1 left) were realized in the foot of the landslide body at an axial distance of 1.50 m with a slope of 3°. They were installed in the rock environment using mechanical vibration equipment. Horizontal drainage wells (Fig. 1 middle) were realized with a drilling rig using coreless technology with a full profile lost rolling chisel. The initial approx. 20 m was realized with a drilling diameter of Ø 156 mm, while the pipes were not perforated (wells below the road). The remaining length of the wells was perforated, min. 5% of the casing area (pipe diameter 89 mm). The outlet of the wells is in a low concrete wall, while the water is drained directly into the recipient - Štiavnica stream. Drainage branches 1 and 2 are located on the sides of the landslide body and branch off in the crown of the landslide, they are designed for the most efficient capture of water above the landslide body (Fig. 1 right). A control shaft is located on each drainage branch, used for the capture and sedimentation of fine-grained material in sludge pits, and for visual monitoring of the functionality of the system. As part of the first stage of immediate emergency measures, reconstruction works were also carried out - cleaning and modification of the outlet part of the culvert into the recipient of the Štiavnica stream, cleaning of the existing culvert under the road, repair of the inflow part of the culvert and reconstruction of the road ditch. The retaining wall was designed as a two-stage steel anchored

structure (Fig. 2 left). A flexible, stabilizing and at the same time permeable structure was designed, which does not prevent the drainage of the accumulation. Both levels of security are made of an anchored steel stabilization structure. The system consists of a spatial supporting steel structure. The front is a steel frame made of HEA100 elements with a protective net, the dimensions of the front are 2.50x2.00 m (40 pcs in total). In the body of the backfill, there is a hidden support tie rod - ground anchor. The stabilizing steel structure is completed in the lower floor at its beginning and end with the help of gravity gabion retaining walls (Fig. 2 right).

Figure 1. From left – outlet of prefabricated drains at the foot of the landslide; realization of horizontal drainage wells; surface rigol and control shaft

Figure 2. Left: View of the retaining wall - two-stage steel anchored structure; Right: The lower basket of the gabion retaining wall

Conclusion

Remedial works were carried out as part of immediately implemented emergency measures. The stabilization of the landslide area was solved comprehensively, starting with additional research works, which refined the engineering geological, hydrogeological, and geotechnical conditions of the area, through the design of remediation to their implementation. On the landslide, geotechnical monitoring consisting of inclinometric measurements, regime observations, geodetic measurements, and measurements of the yield of drainage wells was designed and is ongoing.

Acknowledgments:

This research was partly funded by the Agency of the Ministry of Education, Science, Research and Sport of the Slovak Republic, VEGA, grant project No. 1/0182/23 “Quantification of landslide risk in urbanized areas of Slovakia threatened by the devastating effects of slope movements“ and VEGA 1/0180/24 „Application and evaluation of the results of multifunctional analysis of surface seismic waves (MASW) in geological engineering and geotechnical tasks”.

STABILITY ASSESSMENT OF HIGH CLIFF SLOPES IN CARBONATE ROCKS - A CASE STUDY, KINGDOM OF SAUDI ARABIA

MOHAMMED MUSTHAFA KHALEEL[1], MOHAMMED JALALUDDIN AHMED[2], KURIAN JACOB[3]

[1] *Arab Centre for Engineering Studies Dubai, United Arab Emirates, k.musthafa@aces-int.com*

[2] *Arab Centre for Engineering Studies Dubai, United Arab Emirates, m.ahmed@aces-int.com*

[2] *Arab Centre for Engineering Studies Dubai, United Arab Emirates, k.jacob@aces-int.com*

Introduction

The proposed Project, spread over an area of 7km2, located in the Kingdom of Saudi Arabia, is bound by a 20 -25 m high, over 5 km long cliff section to the west of the high land. The stability of the cliff slopes have a bearing on the short-term safety and performance of the structures close to the cliff line. The study performed to ascertain the stability of the 'cliff/ escarpment' is considered in the design of the Emergency Vehicular Access (EVA) route and the utility corridor serving the open areas bounded by the Historical Walls along the top of the escarpment.

Methodology

The methodology included acquisition of field data, including geological mapping aided with the satellite imageries to decipher the presence of geological features like faults, shear zones, discontinuities with their orientation with respect to the escarpment. Mapping of cliff face and the area in a width of 100 m along the cliff line was carried out deploying suitable equipment's/ techniques like GPS with rover, terrestrial photography etc. The azimuthal data of the discontinuities/ joints were collected; besides, the joint parameters/ features and laboratory testing like direct shear tests along the identified potential discontinuities. The data was synthesized using the rocscience software's to check the kinematic admissibility, identify the failure modes and the potential blocks. Analytical checks for the for the potential blocks were carried out and global stability checks using slope/W programme, targeting a Safety Factor of 1.5 and 1.2 for static and dynamic conditions.

Geology

The veering cliff line and the high land areas exposes the Jurassic formations (ref 3) which includes the Jubaila Limestone (Ji)- a cream coloured compact limestone with interbeds of calcarenite and thin dolomitic units of Kimmeridgiam age near the top. The Hanifa Formation (Jh)- cream and tan soft limestone with minor interbedded marl and tan clay shale; several brown calcarenite beds, partly Oolitic in middle and upper parts are also noticed. The distinctive geo-structural features noticed are mostly the bandings/ beddings with continuity or discontinuity.

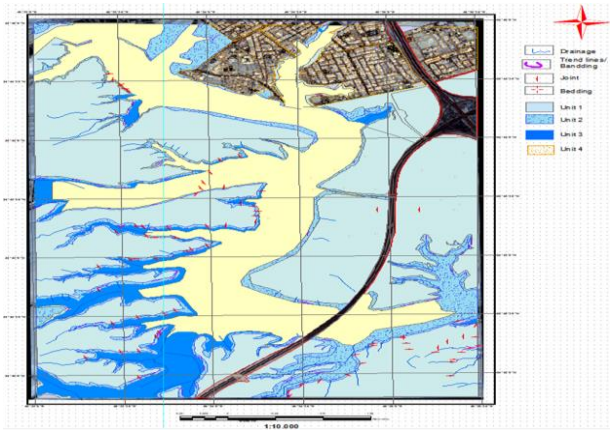

Figure 1. Satellite imagery based geological map of the area

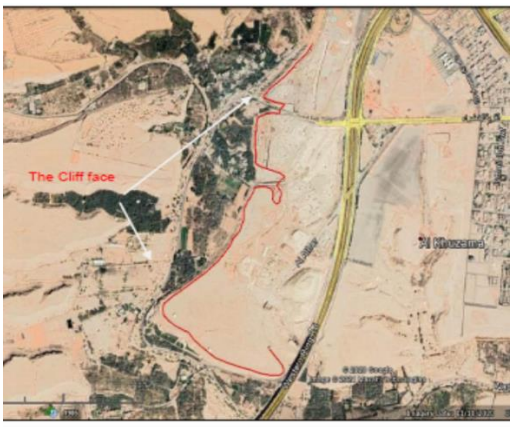

Figure 2. Aerial view of the project location

The valley/ wadi area to the west of the high land, could be a strong erosional feature along mega structural elements, but due to extensive anthropological interventions the elements are camouflaged. The structural elements delineated are Joints/ discontinuities and form lines of beddings. The Cliff line is broadly controlled by the differential erosion activity along the major joints/ fracture system in the area i.e. the N-S to NNE - SSW and E-W fracture systems at large. No such major fault lines / shear zones are discernible in the study area of the project. A 2 – 5 m wide highly destressed zone along the cliff line is manifested by dilated vertical joints with infillings of silt and sand, block movements/ rotations etc.

Rock mass characterisation

The rock mass on the surface in general are unweatherd to slightly weathered (Class-I/II). The effects of weathering are seen along the joints / discontinuities with coatings and in-fillings of clayey to silty material. The rock mass beyond a depth of 1 – 1.5 m are fresh (class I). The thin inter bedded siltstone in general is moderately to highly weathered (Class III/ IV) up to a depth of 5 m from surface (as noticed on the cliff face). Over 36 locations were identified (geopoints G1, G2, G3...etc.) along the cliff edge and the toe line for data collection. From each of these locations 20 – 70 Joint data with the specified parameters were collected. Based on the bore hole logs and the results of geological mapping/ study of the cliff sections, the rock mass was classified in to two categories as Rm1 and Rm2

Keeping in view the commonality of the joint sets, their surface characteristics and the potentiality/ vulnerability of the cliff edge, the locations were clubbed to form Seven structural zones (ZI, ZII...ZVII) for further assessments and analysis (table 1). Each zone covers the 25 m high cliff face and a width of 120 m from cliff edge, respectively.

Slope Stability Analysis: The data was synthesized using the Rocscience software's to the carry out the Kinematic admissibility check and identify the failure modes (ref 2).

Table 1. Kinematic admissibility checks

Structural Zone (Z)	Joint Set combination	Wedge No	Azimuth of joint sets (°)	Azimuth of slope (°)	Input parameters	Analysis remarks
Z-I	J1, J3	ZI/W1	031/72,007/84	075/80 (E-W cliff)	γ=2.5 t/m3 ϕ° Average=24 ucs= 40 MPa E=35 g=0.17 Water pressure =50% in tension cracks	
	J1, J4	ZI/W2	031/72,187/88			
	J5, JR1	ZI/W3	292/88,310/70			
	J6, JR1	ZI/W4	096/87,310/70			
	JR1	P1	060/81			
Z-II	No Failure Mode					
Z-III	J1, J3	ZIII/W1	306/17,185/80	300/40 (N-S Cliff)		
	J1	ZIII/P1	306/17			
Z-IV	Not considered for slope stability analysis					
Z-V	No wedge/planar failure found					
Z-VI	Not considered for slope stability analysis					
Z-VII	J1, J2	ZVII/W1	312/22,176/86	310/40 (N-S Cliff)		
	J1, J3	ZVII/W2	312/22,359/85			
	J1, J4	ZVII/W3	312/22,290/81			
	J1	ZVII/P1	312/22			

Table 2. Output of Analitical checks

Zone	Block No.	FoS (1)	Slope Protection/ Treatment Measures				FoS (2)	FoS (3)	Wedge weight. (t)	Wedge volume. (m3)	Remarks
			Rockbolt Length (m)	Ancr length (m)	Capacity (t)	Shotcrete (mm)					
Z -I	ZI-W1	1.48	-	-	-		1.48	1.44	2.62	1.04	Safe
	ZI-W2	2.12	-	-	-	-	2.12	2.08	2.07	0.87	Safe
	Z1-W3	2.39	-	-	-	-	2.39	2.05	23.80	9.55	Safe
	Z1-W4	1.45	-	-	-	100	22.0	21.17	16.34	6.53	Safe

Z-III	ZIII-W1	-	-	-	-	-					WnF(4)
	ZIII -P1	2.65	-	-	-	-	2.65	1.71	348	139	Safe
Z-VII	ZVII-W1, W2, W3 & W4	-	-	-	-	-	-	-	-	-	WnF(4)
	ZVII / P1	1.82	-	-	-	-	1.82	1.20	17	41	Safe

FoS (1) Static (without support or seismic effects), indicating the likely risk of instability under own wt, water pressure, and external loading without introducing support (Anchor).
FoS (2) Static with support, as necessary to achieve the target safety factor.
FoS (3) Dynamic EQ effects (with 0.17 g). T was adjusted, if required such that minimum target safety factor is satisfied
WnF (4) Wedge block not Formed

Analytical checks for the potential blocks and global stability checks using *Rocscience* and *slope/W* programmes were carried out respectively targeting a Factor of Safety of 1.5 and 1.2 (ref 1) for the respective static and dynamic conditions. The profiles (S1 - S8) were checked for global stability using a FEM model study by circular failure analysis- Morgenstern method using *slope/W* programme, with a surcharge load of 35 tons at the cliff top. A typical analysis of section Z-II/ S1 –17.5m slope height is given below.

Typical stability analysis for slope S1 – Z-II of 17.5m height

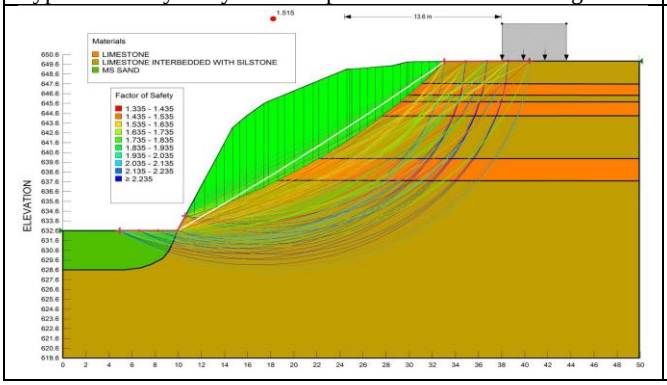

Summary of output from Global stability check

Section ID	*Factor of Safety*	
	Static	*Dynamic / Earthquake*
SECTION 1	*1.515*	*1.197*
SECTION 2	*1.516*	*1.210*
SECTION 3	*1.512*	*1.189*
SECTION 4	*1.491*	*1.223*
SECTION 5	*1.495*	*1.289*
SECTION 6	-	
SECTION 7	*1.491*	*1.198*
SECTION 8	*1.809*	*1.387*

Figure 3. Outputs of Global Analysis

Conclusion and Recommendations:

The above analytical check reveals that in general the wedges formed show high FoS (+2) and are expected to be stable due to their high shear strength characteristics and relatively low/ sub-horizontal beds. No such support system was required for the stabilization of the cliff slopes with foundation/ structural loadings of 35t. The cliff slopes have potential/ unstable wedges in the 2 – 3 m wide de-stressed zone along the cliff edge and locally on the slope face. These wedge blocks are likely to get dislodged/ slide down with time, due to the in fillings in the dilated joints and eventual charging with rain water. The natural slopes by virtue of it's gentle to moderate slope angles of 45 – 50º with the sub-horizontal/ gently dipping (2 – 5º) bedding planes (J2) provide relatively stable conditions for the cliff.

Keeping in view the compulsions of the heritage site, specific recommendations on slope stabilization (without shotcrete, guniting, mesh, anchors) like use of synthetic grouts or pinning the loose blocks locally with rock bolt were advised. Based on the evaluations and the manifestations of a 2 – 5 m wide distressed zone along the cliff line a safe set back distance of 5 - 8m from the escarpment edge has been recommended.

References

1. Duncan C. Wyllie**,** *Foundations on Rock (2nd Edition),* E&FN Spon. 1999
2. Hoek. E and Bray.J.W, *Rock Slope Engineering (Revised third edition)***,** Institution of Mining and Metallurgy, U.K, 1999.
3. Richard A. Bramkamp, Leon F. Ramirez, Geology of the Northern Tuwayq Quadrangle, KSA, USGS Publications Warehouse, 1958.

A GEOTECHNICAL APPROACH FOR ENHANCING THE COASTAL VULNERABILITY INDEX (CVI) METHODOLOGY: APPLICATION IN THE GULF OF PATRAS, GREECE

VASILEIOS BOUMPOULIS[1], NIKOLAOS DEPOUNTIS[1], GEORGE PAPATHEODOROU[1]
[1]Department of Geology, University of Patras, Greece, vasileios_boumpoulis@ac.upatras.gr

Introduction

Coastal zones are one of the most complex and dynamic systems since their landform changes rapidly due to the combined action of tidal flows, currents and waves on coastal sediments (Raper et al. 2005; Boumpoulis et al. 2023). One of the most common and diachronic problems in coastal zones is the coastal erosion. In Greece, more than 20% of its total shoreline (EC 2004; Boumboulis et al. 2021) is threatened by coastal erosion and rising sea levels. Coastal Vulnerability Index (CVI) is one of the most used methods to assess coastal vulnerability to sea-level rise (SLR) driven erosion. However, numerous methodological gaps in the CVI approach can be found in the literature, especially in local scale areas. For this reason, this study aims to construct a coastal vulnerability assessment conceptual framework to improve the outcomes of CVI in local scale areas. To achieve this, an index model named as Geotechnical Coastal Vulnerability Index (GCVI) is used, which incorporates two geotechnical variables in the calculations, the geotechnical identification and the median grain size distribution (D50), as well as the presence of P. Oceanica. The use of those parameters seems to improve the quantification of coastal resistance to erosion and seems to be more accurate in the calculations of CVI in local scale areas. As a local scale (pilot) area to apply this approach it was used the Gulf of Patras in Western Greece, which is suffering erosion problems due to climate change and human intervention.

Methods

The selected key variables of GCVI used in this study are: i) the geotechnical identification, ii) the median grain size distribution (D50) of coastal sediments, iii) the significant mean wave height, iv) the coastal slope, v) the presence of P. Oceanica and vi) the average tidal range.

To calculate the geotechnical variables, a thorough geotechnical investigation was carried out in the research area, including drilling of boreholes, laboratory and in-situ geotechnical tests (Standard Penetration Test-SPT), numerous coastal sediment sampling and field engineering–geological mapping. The synthesis of those collected data led to the creation of a local scale geotechnical map of the pilot area. This map classifies the geological formations of the coastal zone according to their geotechnical characteristics and their erosion resistance that is used in the GCVI model.

The final integration of geotechnical variables into the numerical calculation of the index for classifying the shoreline into different vulnerability classes, performed via the total number of blows SPT for the variable of geotechnical identification. While for the median grain size distribution (D50) variable, the spatial distribution of the D50 value estimated using the optimal spatial interpolator method, as it is described in Boumpoulis et al. (2023). For the weighting of each one of the six variables used in the GCVI model, the Principal Component Analysis (PCA) method was implemented. For the validation of the results, the rate of the historical shoreline movement (m/y) was used, by constructing the receiver operating characteristic (ROC) curve and computing its area under the curve (AUC) value.

Results

The spatial distribution of the GCVI along the shoreline of the pilot area (Figure 1) shows that the coastal Zone 1, the greater part of Zone 4 and half of Zone 8 have a very high vulnerability level. Moreover, the coastal Zone 5, the western part of Zone 4, small parts of Zone 7 and the central part of Zone 8 have a high vulnerability level. In addition, the coastal Zone 1, the western and eastern part of Zone 3, Zone 6 and a small part of Zone 7 have a moderate vulnerability status. Finally, the central part of Zone 3, Zone 5 and the western part of Zone 2 are characterized by very low and low vulnerability regime. The validation results, represented by ROC curves and AUC values, indicated that the parameter for the rate of historical shoreline movement and the PCA method achieved a 67.57% accuracy. This is considered as satisfactory percentage compared to similar coastal vulnerability models, which achieve around 68.9% (Fu et al. 2022).

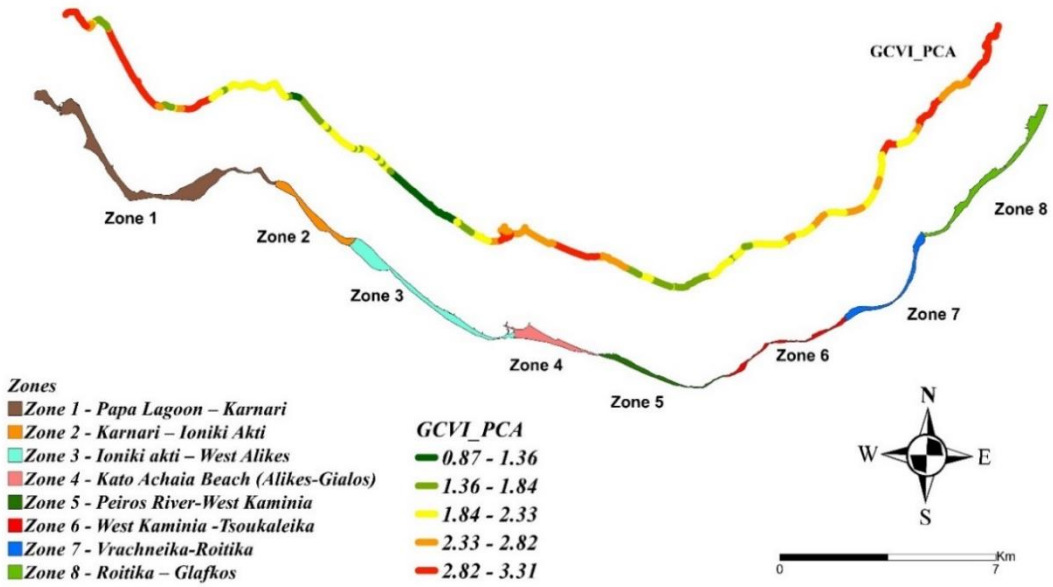

Figure 1. Spatial distribution of GCVI along the shoreline of the Gulf of Patras.

Conclusion

In the literature, several efforts have been made to improve coastal vulnerability models, especially the CVI, which is the best-known model to calculate vulnerability. A first attempt towards the improvement of those uncertainties, is the quantification of resistance to erosion variable with the use of geotechnical data instead of geological data in the CVI calculations for the research area (Boumboulis et al. 2021). Moreover, the classical formulation of CVI with the use of i) geological, ii) historical shoreline movement, iii) the significant mean wave height, iv) the coastal slope, v) sea level rise and vi) the average tidal range and the absence of weigh factors in the relvant calculations may underestimate the vulnerability and this fact is mentioned also in other papers (De Serio et al. 2018). In this study the use of six variables, with an emphasis given in the geotechnical variables and the presence of P. Oceanica, along with the introduction of weight factors using PCA, seems to increase the reliability and accuracy of the vulnerability model, as each variable has a different contribution to vulnerability assessment. Futhermore, a validation model was developed using the rate of the historical shoreline movement to assess how accurately the model values reflect to reality, since in most of the relevant research studies there is not proposed a standard procedure for verifying the predictions in CVI models.

References

Boumboulis V, Apostolopoulos D, Depountis N, Nikolakopoulos K (2021) The Importance of Geotechnical Evaluation and Shoreline Evolution in Coastal Vulnerability Index Calculations. J Mar Sci Eng 9:423. https://doi.org/10.3390/jmse9040423

Boumpoulis V, Michalopoulou M, Depountis N (2023) Comparison between different spatial interpolation methods for the development of sediment distribution maps in coastal areas. Earth Sci Informatics 16:2069–2087. https://doi.org/10.1007/s12145-023-01017-4

De Serio F, Armenio E, Mossa M, Petrillo AF (2018) How to define priorities in coastal vulnerability assessment. Geosci 8:1–20. https://doi.org/10.3390/geosciences8110415

EC [European Commission] (2004) Living with Coastal Erosion in Europe – Sediment and Space for Sustainability. OPOCE, Luxembourg. http://www.eurosion.org/project/eurosion_en.pdf (accessed July 2016).

Fu GW, Cao C, Fu KZ, et al (2022) Characteristics and evaluation of coastal erosion vulnerability of typical coast on Hainan Island. Front Mar Sci 9:1–19. https://doi.org/10.3389/fmars.2022.1061769

Raper J, Livingstone D, Bristow C, McCarthy T (2005) Constructing a Geomorphological Database of Coastal Change Using GIS. Coast Mar Geo-Information Syst 399–413. https://doi.org/10.1007/0-306-48002-6_28

BACK ANALYSIS OF CUT SLOPES ALONG THE FAST TRACK ROAD OF NEPAL

UJJWAL KRISHNA RAGHUBANSHA [1], RANJAN KUMAR DAHAL [2]

[1] *Central Department of Geology,Tribhuwan University, raghubanshiujjwal@gmail.com*

[2] *Central Department of Geology,Tribhuwan University, rkdahal@gmail.com*

Introduction

Slope stability is the major problem in mountainous country either natural or engineered slopes. The detailed study of topography, geology, shear strength, groundwater conditions, external loading and plan curvature of the slope are an important parameter for slope stability analysis. There are various challenges in making the Cut Slopes on landslide made landscape.

This study is mainly focused on the back analysis of cut slope failure, stability analysis and inventory mapping of cut slope/cut slope failures. Traditional slope stability analysis involves predicting the location of the critical slip surface of the slope and calculation of FOS at that location. Back analysis technique can be used in a deterministic and probabilistic analysis to find all possible failure mechanisms, FOS and reliability indices. Slope seepage analysis is modeled as the finite element through transient seep/w using different parameters such as hydraulic conductivity of soil and rock, grain size analysis, liquid limit, volumetric water content, and extreme monsoon rainfall. Similarly, soil slope stability is analyzed using slope/w limit equilibrium method using strength parameters, such as friction angle, cohesion and pore-water pressure from seep/w. kinematic analysis is carried out in discontinuous rock mass. Back analysis is carried out in cut slope failure assuming Factor of Safety (FOS) as 1 under consideration of trial values of strength parameters through probabilistic and sensitivity method.

Methods

The limit equilibrium analysis is a conventional method used for analyzing slopes assessing the balance between external forces acting on the slope and the internal forces resisting failure along the potential failure surface. This methodology yields findings that are reasonably accurate and dependable for simple material strength behavior with the calculation of a safety factor, which is important for assessing the sensitivity of potential future conditions of slope. However, a different method for studying slope stability known as finite element analysis preserves global equilibrium up until the slope fails while making fewer assumptions about the failure cause. This approach is helpful for providing precise and flexible information regarding deformation at operating stress levels and failure.

Geological sections are made based on drillings and various geophysical investigations and lab works for the back analysis of cut slope failure. Slide 2D software was used. The deterministic analysis was carried out using the mean of all the input parameters to find one critical failure surface. Among the available LE methods, Bishop Simplified Method (BSM) was used as it is the most suitable for a circular failure.

Results

The back analysis of geological parameters at failure portion considering the factor of safety 1.5 for dry condition. The reduced geological parameter at failure locations is taken based on the sensitivity analysis. In the sensitivity analysis among cohesion and friction angle, friction angle is more sensitive, it indicates that small changes in the value of friction angle can have a larger impact on the overall stability of the slope compared to small changes in the value of cohesion. This is because the shear strength of the slope is more influenced by friction angle than cohesion.

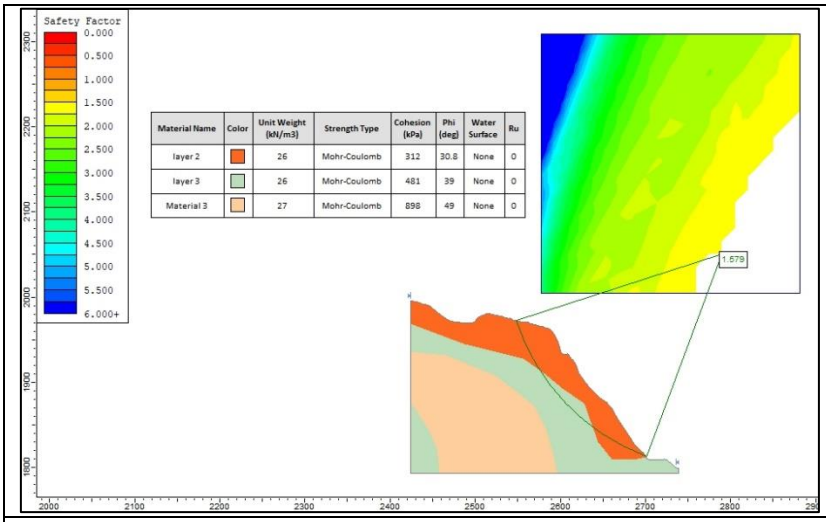

Figure 1: Back Analysis of profile

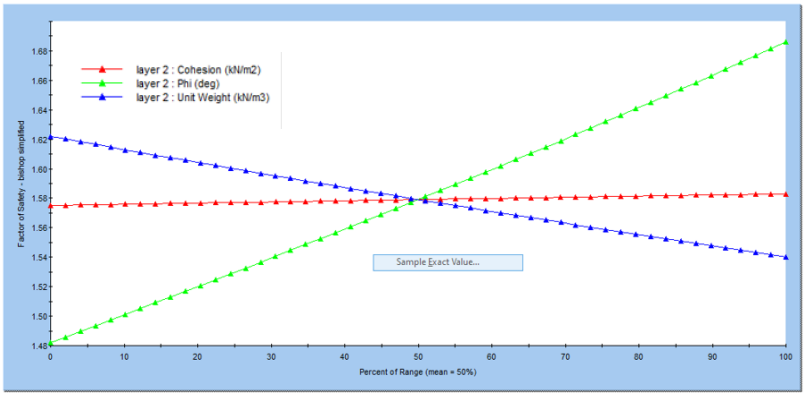

Figure2: Combined sensitivity plot of FOS vs friction angle cohesion and Unit weight

Conclusion

A comprehensive back analysis and stability assessment of the cut slopes were done for slope stability. Sensitivity analysis and probabilistic approach of stability analysis was used to analyze the slope failure. Limit Equilibrium method was used for stability analysis. Bishop Simplified Method (BSM) analysis was carried out to determine the factor of safety.

References

Abramson, L. W., Lee, T. S., Sharma, S., & Boyce, G. M. (2002). Slope stability and stabilization methods. John Wiley & Sons.

Barton, N. (1976). The Shear Strength of Rock and Rock Joints. In Int. J. Rock Mech. Min. $ci. & Geomech. Abstr (Vol. 13). Pergamon Press.

Bishop,A.W. (1955). The use of slip circles in the stability analysis of slopes. Géotechnique, 7-17.

Cheng, Y.-M., Wei, W.-B., & Wang, X.-M. (2007). Dynamic response of a high rockfill dam in an earthquake. Soil Dynamics and Earthquake Engineering, 27(8), 749-763

Duncan, J. M., Wright, S. G., & Brandon, T. L. (2008). Limit equilibrium and finite- element analysis of slopes. Geotechnique, 58(7), 537-546.

Edgers, L., & Nadim, F. (2004). Rainfall-induced slides of unsaturated slopes. InLandslides: evaluation and stabilization (pp. 1091-1096).

Fellunius, W. (1936). Calculations of the Stability of Earth Dams. Proceedings of the second Congress of Large Dams. Vol. 4, pp. 445-63, Washington D. C.

Hatheway, A. W. (1996). Slope Stability and Stabilization Methods. In Environmental & Engineering Geoscience: Vol. II (Issue 3, pp. 447–449).

Michalowski, R. L. (1995). Limit equilibrium method of stability analysis. In B. R. Singh (Ed.), Principles of geotechnical engineering (pp. 214-270). CRC Press.

IMPACT OF DEEP-SEATED ROCK SLIDES ON INFRASTRUCTURE

CHRISTIAN ZANGERL [1]

[1] BOKU University, Department of Civil Engineering and Natural Hazards, Institute of Applied Geology, Peter Jordan-Strasse 82. 1190 Vienna, Austria, christian.j.zangerl@boku.ac.at

Introduction

Deep-seated rock slides affecting entire valley slopes and reaching volumes of millions of m^3 are frequently observed in mountainous regions. This type of landslide displaces at velocities in the range from extremely slow to extremely rapid (Zangerl & Strauhal 2020) and the deformation is localised along one or several shear zones where most of the measured total slope displacement accumulates. These shear zones reach thicknesses in the range of a few decimetres to tens of meters and are composed of uncemented fault breccias and gouges, with a spatially heterogeneous arrangement (Strauhal et al. 2017). Concerning slow moving rock slides, if active or reactivated over longer periods of time, they can adversely affect settlements and infrastructure due to differential and localised displacements of the ground surface and subsurface. Even for very slow movements the damage can be considerable and the life-cycle of man-made structures can be reduced, accompanied with a great economic loss. In some rare cases there is also the danger of a sudden slope failure with acceleration to high velocities and the transition to long runout flow-type rock avalanches, in the worst case leading to a catastrophic event.
This study presents an overview and summary of mechanisms how slowly moving deep-seated rock slides can interact with infrastructure, such as dam reservoirs, high- and railway foundations and bridges, penstocks, headrace tunnels, water supply and transportation tunnels. Using selected, well-studied case studies from the Alps, the underlying interaction processes between infrastructure and deep-seated rock slides are shown in detail, emphasizing the role of cascading and interconnected processes (Mani et al. 2023), as well as the increasing relevance of climate change factors.

Methods

The case studies presented herein include comprehensive analyses of the failure and deformation processes in relationship to the infrastructure based on a broad spectrum of applied methods, comprising geological-geomorphological field surveys, GIS-based terrain analyses, in-situ investigation by core drilling, drift construction and geophysical exploration, surface and subsurface deformation and hydrogeological monitoring, and numerical modelling techniques. Results from these investigations and measurements are presented in the context, how the geological-hydrogeological situation, the geometry and kinematics, as well as the different influencing factors can affect the stability and the temporally variable deformation behaviour of a rock slide.

Results

Reactivation and/or acceleration of existing rock slides or slabs thereof are often observed in connection with the construction of infrastructure, leading to differential and localized displacements of the ground. The triggers for this can be based on natural or construction related factors, or a combination of both, including extreme rainfall and snow melt events, erosion at the foot by flooding, the initial infilling of a reservoir or the rapid drawdown, construction of a cut slope, loading of the slope by the infrastructure building itself, and others. In addition, frequently observed ongoing slope movements, even with an extreme low level of activity, can have an adverse impact on the structure over long periods of time and require early recognition, comprehensive planning, and if necessary, action.
Deep-seated rock slides can adversely affect dam reservoirs in various ways. One possibility is that an abutment of the dam is located in a rock slide mass which is moving (Schuster 2006). This results in a narrowing of the valley leading to a progressive deformation of the structure, often accompanied by the formation of cracks (Barla 2018). In this context, the movement of the rock slide can be triggered or accelerated by the initial impounding of the reservoir or its drawdown. Moreover, the progressive deformation of the abutments can lead to unfavourable seepage behaviour below the dam structure. The

instability of abutments and foundations, especially during the construction phase of a dam, is a further interaction mechanism that needs foresighted planning and mitigation measures (Dini et al. 2020). Impact also may occur when rock slides gradually reduce the storage space of the reservoir or threaten the infrastructure and its surroundings through sudden high-velocity rock slide events. In particular, the initial impoundment can lead to reactivation and/or acceleration of pre-existing rock slides, which requires measures such as continuous monitoring or even the construction of slope drainage drifts to maintain operational safety (Zangerl et al. 2024).

Deep-seated rock slides can affect penstocks, headrace and water supply tunnels, as well as highway and railway tunnels. Penstocks and headrace tunnels as essential components of hydropower plants or drinking water supplies can be impacted in their service life by very slow-moving rock slides due to localised shear deformation (Barla 2018, Leblhuber & Bonapace 2013, Poisel et al. 2015). On the one hand, very low movement rates of a few mm/year can accumulate over a long period of time and exceed the structural limits with regard to deformation, and on the other hand extreme meteorological and/or hydrological events can trigger reactivations or accelerations.

The impact of deep-seated rock slides on road/highway and bridge foundations mainly involve localized deformations of the slope flanks, leading to sliding and toppling mechanism of the structure. Inactive rock slides that are reactivated by extreme meteorological events or slope foot erosion due to flooding are particularly critical. In this context, a case study from Austria, where a flood event from 2005 triggered and reactivated pre-existing rock slides or slabs, causing damage of main roads and bridges as well as headrace drifts and penstock of a hydropower plant, will be presented.

Conclusion

The implications of this study are manifold and emphasize the high relevance of reliable feasibility studies and the consideration of overlapping cause and triggering factors, as well as cascading and compound effects in order to avoid subsequent problems during the construction and operation phase, and to achieve the planned service life and infrastructure safety.

References

Barla, G. Numerical modeling of deep-seated landslides interacting with man-made structures. Journal of Rock Mechanics and Geotechnical Engineering, 2018, 10(6), 1020-1036.

Dini, B.; Manconi, A.; Loew, S.; Chophel, J. The Punatsangchhu-I dam landslide illuminated by InSAR multitemporal analyses. Scientific reports, 2020, 10(1), 8304.

Leblhuber, P.; Bonapace, P. New penstock at the Kaunertal hydropower station–site investigation and grouting concept. Geomechanics and Tunnelling, 2013, 6(5), 446-455.

Mani, P.; Allen, S.; Evans, S.G.; Kargel, J.S.; Mergili, M.; Petrakov, D.; Stoffel, M. Geomorphic Process Chains in High-Mountain Regions—A Review and Classification Approach for Natural Hazards Assessment. Reviews of Geophysics, 2023, 61(4), e2022RG000791.

Poisel, R.; am Tinkhof, K.M.; Preh, A. Die Interaktion Großhangbewegungen–Tunnel am Beispiel eines Lehnenstollens in 370 m Seehöhe. Österreichische Ingenieur- und Architekten-Zeitschrift, 2015, 160, 221-230.

Schuster, R.L. Interaction of dams and landslides: case studies and mitigation. Reston, Virginia: US Geological Survey, Professional Paper, 2006, 1723, 107p.

Strauhal, T.; Zangerl, C.; Fellin, W.; Holzmann, M.; Engl, D. A.; Brandner, R.; Tropper, P.; Tessadri, R. Structure, mineralogy and geomechanical properties of shear zones of deep-seated rockslides in metamorphic rocks (Tyrol, Austria). Rock Mechanics and Rock Engineering, 2017, 50, 419-438.

Zangerl, C.; Strauhal, T. Investigations and monitoring of deep-seated rock slides in feasibility studies for dam reservoirs. AUC GEOGRAPHICA, 2020, 55(2), 210-217.

Zangerl, C.; Lechner, H.; Strauss, A. Influence of Rock Slide Geometry on Stability Behavior during Reservoir Impounding. Applied Sciences, 2024, 14(11), 4631.

SFM PHOTOGRAMMETRY FOR ROCKFALL MONITORING AND HAZARD ASSESSMENT ALONG ROAD NETWORKS. THE CASE IN AGRAFA REGION, CENTRAL GREECE

THEMISTOKLIS CHATZITHEODOSIOU [1], IOANNIS FARMAKIS [2], DIMITRA PAPOULI [1], GEORGE STOUMPOS [1], GEORGE PROUNTZOPOULOS[3], VASSILIS MARINOS [1]

[1] *National Technical University of Athens, Greece, chatzitheodosiou@mail.ntua.gr*

[2] *University of Newcastle, Australia, i.farmakis@icloud.com*

[3] *Independent Geotechnical Engineering Consultant, Greece, gproun@gmail.com*

Introduction

Rockfalls pose a major threat to transportation in mountainous regions, particularly in tectonically disturbed limestone areas like central Greece (Marinos, 2010). Remote sensing technologies, such as Structure-from-Motion (SfM) photogrammetry (Westoby et al., 2012) and Terrestrial Laser Scanning (TLS) LiDAR, have improved hazard assessment by providing high-resolution data for terrain and rockfall analysis (Kromer et al., 2019; Chatzitheodosiou et al., 2024). This study examines the Agia Varvara-Agrafa region in Evritania, Greece, where complex geology consisted of heterogenous and tectonised rock masses create conditions for frequent rockfalls along a critical mountain road. A large wedge-shaped rockslide in this area has exposed disturbed rock masses, resulting in continuous smaller rockfalls and new slides that pose significant risks to road safety.

Methods

Over a two-year period, with monitoring intervals of four months, SfM photogrammetry was utilized to capture the evolution of susceptible slopes through high-resolution UAV imagery. This method generated precise point clouds, enabling detailed analysis of geomorphological changes and creating a time series of terrain evolution. The M3C2 algorithm (Lague et al., 2013) was applied for accurate quantification of rockfalls and slope deformations. Additionally, spatial clustering through the DBSCAN algorithm (Ester et al., 1996) and volumetric measurements via the Iterative Alpha Shape algorithm (DiFrancesco et al., 2021) contributed to the development of a comprehensive digital rockfall database. This database enhanced the understanding of landslide dynamics in the region.

Results

The methodology identified potential rockfall sources, tracked failure kinematics, and estimated potential failure volumes. It provided essential data for designing effective rockfall mitigation strategies, improving safety on the Agia Varvara-Agrafa road. Potential failures ranged from 5 to 30 m^3 for occasional detachments from upper slopes, and 1 to 2 m^3 for more frequent smaller rockfalls. The accurate projection of failure locations and consistent post-failure assessments confirmed the effectiveness of this approach in managing rockfall hazards.

Conclusion

This study demonstrates that SfM photogrammetry and associated methods can significantly enhance the risk management of transportation corridors in geologically complex terrains by informing targeted mitigation strategies. The approach is broadly applicable to similar geological settings, contributing to improved infrastructure safety.

References

Chatzitheodosiou, T. "One rock at a time" 3D Geology Mini-Series. *Available online:* https://sketchfab.com/themisto123 *(accessed on February 2024).*

Chatzitheodosiou, T.; Farmakis, I.; Prountzopoulos, G.; Papouli, D.; Stoumpos, G.; Marinos, V. Addressing rockfall challenges in flysch environment - A case study from Greece. In *Proceedings of the 6th Regional Symposium on Landslides in the Adriatic-Balkan Region, ReSyLAB2024, Belgrade*, Serbia,

15–18 May 2024; pp. 283-289.
DiFrancesco, P.M.; Bonneau, D.A.; Hutchinson, D.J. Computational geometry-based surface reconstruction for volume estimation: a case study on magnitude-frequency relations for a LiDAR-derived rockfall inventory. *ISPRS International Journal of Geo-Information.* 2021, 10.
Ester, M.; Kriegel, H.P.; Sander, J.; Xu, X. A density-based algorithm for discovering clusters in large spatial databases with noise. In *Proceedings of the KDD-96 Conference*, Portland, Oregon, 2–4 August 1996.
Kromer, R.; Walton, G.; Gray, B.; Lato, M.; Group, R. Development and optimization of an automated fixed-location time lapse photogrammetric rock slope monitoring system. *Remote Sensing.* 2019, 11.
Lague, D.; Brodu, N.; Leroux, J. Accurate 3D comparison of complex topography with terrestrial laser scanner: application to the Rangitikei Canyon (New Zealand). *ISPRS Journal of Photogrammetry and Remote Sensing*. 2013, 82, 10–26.
Marinos, V. New proposed GSI classification charts for weak or complex rock masses. *In Proceedings of the 12th International Congress of Geological Society of Greece; Bulletin of Greek Geological Society*: Patra, Greece, 2010; Volume XLIII, pp. 1248–1259.
Westoby, M.J.; Brasington, J.; Glasser, N.F.; Hambrey, M.J.; Reynolds, J.M. Structure-from-Motion photogrammetry: a low-cost, effective tool for geoscience applications. *Geomorphology*. 2012, 179, 300–314.

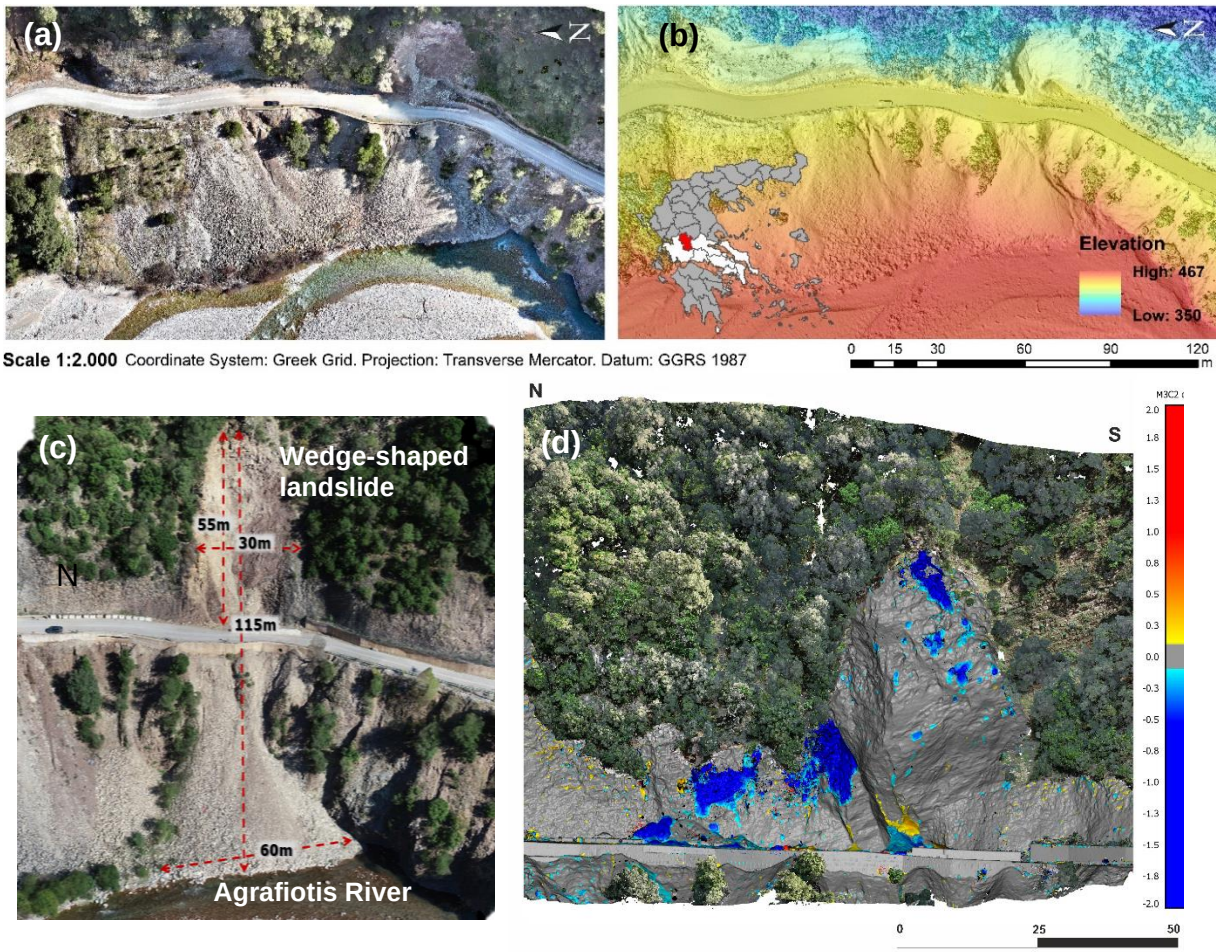

Figure 1. The Agia Varvara - Agrafa study site in Evritania, Central Greece, featuring: (a) an orthomosaic, (b) a Digital Surface Model (DSM) (surveyed on 03 Feb. 2020), (c) an aerial view of the landslide, (d) M3C2 change detection output, depicting negative (loss) and positive (gain) changes presented by cooler and warmer colours, respectively. [For an interactive exploration and detailed visual representation of the Agia Varvara - Agrafa slope, readers are encouraged to visit the latest digital twin online (Chatzitheodosiou, 2023)].

LANDSLIDE SUSCEPTIBILITY TO RAINFALL AT A NATIONAL SCALE IN NEPAL WITH EMPHASIS ON EARLY WARNING

ANANTA MAN SINGH PRADHAN [1], SUCHITA SHRESTHA [2], RENÉ KAHNT[3]

[1] *Ministry of Energy, Water Resources and Irrigation, Government of Nepal, Nepal, anantageo@hotmail.com*

[2] *Department of Mines and Geology, Ministry of Industry, Commerce and Supplies, Government of Nepal, Lainchour, Kathmandu, Nepal, suchitashrestha@gmail.com*

[3] *G.E.O.S Ingenieurgesellschaft mbH, Germany, r.kahnt@geosfreiberg.de*

Introduction

Landslides are becoming increasingly frequent in Nepal due to intensifying precipitation patterns and the expansion of rural road construction. These factors significantly enhance the risk to both lives and livelihoods in the affected areas. To address this pressing issue, this study presents an integrated methodology that combines two advanced modeling techniques aimed at predicting landslide probabilities. The first technique focuses on analyzing historical data and covariates to identify areas prone to landslides. The second technique employs real-time data collection and machine learning algorithms to continuously update and refine the predictions. By merging these two approaches, more accurate and timely forecasts of landslide occurrences can be provided. Additionally, the study proposes the establishment of a near-real-time warning system for landslides. This system is designed to alert communities and authorities about imminent landslide threats, allowing for swift evacuation and disaster response measures. The integration of these modeling techniques and the warning system aims to mitigate the adverse impacts of landslides, enhancing the resilience of communities in Nepal to such natural disasters. Through this comprehensive approach, we hope to safeguard lives and livelihoods against the growing threat of landslides. This research deals with landslide analysis and subsequent development and implementation of local and regional nowcast early warning systems in the Nepal Himalaya.

Methods

In this study, an integrated process based on two different modelling approaches has been applied. First, a probabilistic approach of landslide susceptibility modelling. The initial method employed a probabilistic, explainable artificial intelligence (XAI) strategy, amalgamating Generalized Additive Models with Structured Interactions (GAMI-Net), to forecast the probability of landslide events within geomorphic slope units. These models integrate various causative factors (CFs) and leverage data on geo-environmental factors associated with landslide occurrences. Second, developed a near-real-time landslide warning system coupling the result of landslide susceptibility and decision tree based selection criteria. Terrain analysis-derived independent variables were incorporated to bolster the modeling procedures in this study. Moreover, the adoption of a global Landslide Hazard Assessment model for Situational Awareness (LHASA) (Kirschbaum and Stanley, 2018) aided in pinpointing areas and timeframes with heightened landslide potential within the study region.

The modelling procedures have been supported throughout this research by including independent variables obtained from terrain analysis. All morphometric variables were derived from a detailed Digital Elevation Model (DEM) in 20 × 20 m scale. A LHASA has been used to provide an indication of where and when landslides may be likely around in the study area.

Results

The result of landslide susceptibility map is presented in Figure 1, which includes the spatial distribution of mean probability for landslide susceptibility across slope units based on 5-fold random cross validation process. The landslide susceptibility map was classified using natural break algorithm in GIS platform. A total of 69.72% of the area was categorized as having a very low susceptibility, 16.01% as

low susceptible, 6.84% as moderate, 4.07% as high and the remaining 3.36% was considered to have very high susceptibility. About 81.51% of landslide data were located in the very-high-susceptibility class, demonstrating the reliability of the map. This map shows the average likelihood of landslide occurrence for different regions.

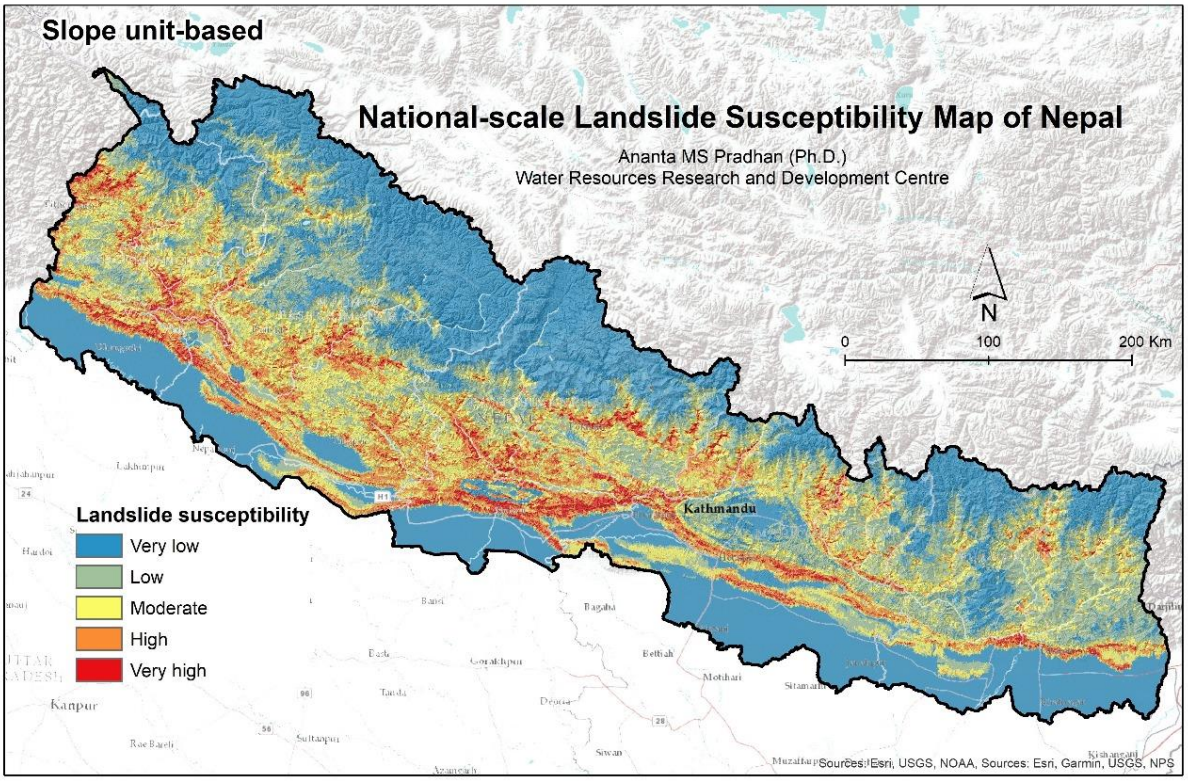

Figure 1. Landslide susceptibilty map of Nepal.

The receiver operating characteristic (ROC) curve was used to evaluate the model and the accuracy of the model was found to be 84%. After preparing the final landslide susceptibility maps, a landslide Nowcast system was developed in Google Earth Engine (GEE) platform and a name “Landslide Hazard Assessment Model LhamNepal) was assign to the developed Application. LhamNepal is an open-access application developed in Google Earth Engine for the rapid characterization of near real time landslide hazard detection to both the scientific and the emergency management communities.

Conclusion

This study significantly advances the field of Landslide Susceptibility Mapping (LSM) by showcasing the potential of advanced machine learning techniques. It underscores the crucial need for precise and interpretable hazard assessments, highlighting their importance in effective disaster management.

References

Kirschbaum, D.; Thomas, S. Satellite-based assessment of rainfall-triggered landslide hazard for situational awareness. *Earth's Future* 6.3 (2018): 505-523.

LANDSLIDE HAZARD MANAGEMENT IN GREECE: THE NATIONAL LANDSLIDE DATABASE AS A MITIGATION TOOL

NATALIA SPANOU [1], EMMANUEL APOSTOLIDIS [1], KATERINA KAVOURA [1], FOTEINI PANAGIOTIDOU [1], IERONYMAKIS VASILEIOS [1], PANAGIOTA KOKKALI [1], NIKOLAOS NIKOLAOU [1], GARYFALIA KONSTANTOPOULOU [1], PANAGIOTIS PASCHOS [1], ALEXANDROS KEPAS [1]
[1] *Hellenic Survey of Geology and Mineral Exploration, Greece;* nspanou@eagme.gr

Introduction

In light of the considerable impact of natural hazards on social, economic, and environmental stability, the comprehension of landslide phenomena represents a fundamental objective of scientific research. The utilisation of a landslide inventory enables the generation of susceptibility or hazard maps. In Europe, landslide inventories are accessible for numerous countries for national purposes, as well as in Greece (Dikau et al 1996, Eechhaut et al 2012, Hervás and Eechhaut 2013). It was deemed appropriate to ensure a representative distribution of events across Europe in order to facilitate the formulation of environmental policy and inform decision-making processes. This was due to the fact that landslides are considered to be one of the eight most significant soil threats in Europe (Gunther et al 2013). It is now well established from a variety of studies that the analysis of landslides supports the collection of existing data and the setting up of a Geographical Information System (GIS), enabling the creation of detailed geodatabases and maps.

The present study offers a comprehensive overview of the national-scale geodatabase of landslides in Greece. This database constitutes the most extensive source of information on landslides in Greece while it was compiled by the Hellenic Survey of Geology and Mineral Exploration (HSGME) following an extended period of documentation of landslide events across the country. The archive spans from the mid-20th century to the present day, continuously incorporating recent events. Currently, a dedicated Landslide Research Team is engaged in first-hand investigation of landslide occurrences, creating detailed reports that analyse the event's characteristics, causes, triggering factors, and consequences. These studies provide sufficient information for the specific characteristics as well as the evolution of landslides, which were then incorporated into the HSGME geodatabase.

Methods

The national landslide database was developed in accordance with the latest European policies and legislation. This geodatabase was constructed allowing the visualization of landslides' geometrical and geospatial features, as well as facilitating the statistical analysis of the data. The database itself is a relational management system meticulously compiled with over 5,500 individual landslide records, each studied in the field and aligned with European Union and United Nations directives on natural disaster risk mapping, fostering international collaboration in mitigating these threats (EC 2006). Access to the landslide geodatabase is currently available to various users within HSGME's local network and it will be made available to the general public via a web GIS platform in the near future. The geodatabase has been designed to accommodate multiple user access, allowing for concurrent or sequential access of different users, each with appropriate editing or reading rights. This configuration ensures immediate access and more rapid data modification, thus facilitating the collective scientific study of landslide phenomena. The geospatial data are organized into feature classes and tables, interconnected through specific relationships. These relationships correspond to information related to general ground failure elements (e.g., date of occurrence, location, source of information), geological elements (geotectonic and geotechnical units of landslide formations), causative factors, observed effects, protection measures,

and more. This structure permits the incorporation of novel geodata, given the inherently dynamic nature of landslides, and guarantees the homogenization of the database through the verification and correction of existing records, including adjustments to the geospatial geometry of current entries.

Results

The formation of a landslide geodatabase provides the opportunity to digitize geospatial data into an incorporated and well-structured digital environment, whose structure is altered based on the user's requirements. The input data are classified, in order to ensure that landslide phenomena are tracked, analyzed, digitalized and presented geospatially, without any temporal limitations, opposed by the registration of a previous time, a lack of digital data, missing values, false correlations between past and present phenomena, as well as the false conclusions about landslide predictions. Based on the structure of the geodatabase, geospatial data offer the opportunity to users of also examining the relationship between landslide distribution and a range of causative factors including geological formations, topography, and hydrological characteristics. Moreover, the digitalization of landslide phenomena via the formation of the geodatabase, represents a new approach for public's awareness regarding landslides and natural hazards. Finally, the distribution of geospatial data, along with the potential for their further exploitation regarding future analysis and study, overcomes the past limitations of data mining and storage, given the instability of analogue data.

Conclusion

The improvement of the national landslide geodatabase marks a significant advancement in the analysis, management and mitigation of landslides in Greece. By digitalizing and structuring extensive geospatial and geological data, this database facilitates improved tracking, analysis, and visualization of landslide occurrences and their characteristics. The implementation of this geodatabase aligns with European policies and enhances accessibility and collaboration among users. Furthermore, this innovative approach not only aids in scientific research and hazard prevention but also promotes public awareness of natural hazards. As a crucial mitigation tool, the database's capability to integrate and analyze diverse data sets paves the way for more accurate predictions and well-informed decision-making, effectively addressing the limitations of previous data collection methods. The data and maps generated by HSGME also serve as a valuable tool for the Civil Protection Authorities.

References

Dikau, R.; Cavallin, A.; Jäger, S. Databases and GIS for landslide research in Europe. *Geomorphology*, 1996, 15, 3–4.

EC 2006 Thematic strategy for soil protection. COM (2006)231 final. Brussels: Commission of the European Communities.

Günther, A.; Reichenbach, P.; Malet, J.-P.; Van Den Eeckhaut, M.; Hervás, J.; Dashwood, C.; Guzzetti, F. Tier-based approaches for landslide susceptibility assessment in Europe. *Landslides*, 2013, 10: 529-546.Van Den Eeckhaut, M.; Hervás, J. State of the art of national landslide databases in Europe and their potential for hazard and risk assessment. Geomorphology, 2012,139–140, 545–558.

Hervás, J.; Van Den Eeckhaut, M. Landslide inventories in Europe and policy recommendations for their interoperability and harmonization, JRC, Publications Office, 2013.

CYCLONE DANIEL'S SCARS: A LANDSLIDE ANALYSIS IN METEORA, GREECE

NATALIA SPANOU[1], KATERINA KAVOURA[1], NIKOLAOS NIKOLAOU[1]

[1] *Hellenic Survey of Geology and Mineral Exploration, Greece;* nspanou@eagme.gr

Introduction

The severe weather event that occurred in September 2023, designated Cyclone Daniel, triggered extensive flooding and landslides across Central Greece. This event provides a unique case study for examining the link between extreme weather and landslide occurrences. This analysis focuses specifically on the Meteora municipality, an area in Greece that was heavily impacted by landslide phenomena triggered by Cyclone Daniel.

Methods

The detailed data on the Meteora landslide occurrences, triggered by Cyclone Daniel, has been subjected to meticulous in-situ investigation and subsequent analysis (Figure 1). The data set comprises information on the location, dimensions, and characteristics of the landslides. A total of 82 phenomena were documented within the municipal boundaries of Meteora. Landslide phenomena encompass a range of processes, including rotational and translational slides, as well as soil and debris flows. Erosions in stream beds are also a common occurrence. Finally, the accumulation of transported materials from the high steric supply of the streams is also a notable phenomenon.

The objective of this analysis is to ascertain the impact of the cyclone's intensity and precipitation patterns on slope stability within this region. Moreover, the efficacy of existing landslide susceptibility maps for the Meteora region has been evaluated. A comparison of these maps with the actual landslide distribution allows for an estimation of their effectiveness for the municipality and the identification of potential areas requiring adjustments.

Figure 1. A number of the impacts of landslides triggered by Cyclone Daniel in the Meteora region.

Results

This study aimed to decipher the mechanisms that precipitate landslides in the Meteora municipality, which was significantly impacted by Cyclone Daniel. The particular meteorological factors that trigger landslide events within the municipality have been identified. Additionally, the accuracy of existing susceptibility maps in predicting landslide locations during extreme weather events has been assessed.

Finally, recommendations for enhanced landslide risk mitigation strategies that are specific to Meteora and have potential applicability to other vulnerable municipalities have been put forth.

Conclusion

Following the conclusion of this study, the most effective protection and mitigation measures were identified as surface water settlement projects, underground water drainage, and, in the case of landslides, a case-by-case approach for the selection of appropriate support works. Additionally, demarcation studies must be conducted to identify and delineate the areas that have been affected or are at risk of being affected. Finally, the maintenance and repair of infrastructure along the road network is essential to ensure the continued functionality and safety of the transport infrastructure, including technical components, bridges and other structures.

Acknowledgements

This study was conducted utilizing the "Landslide Susceptibility Map of Greece," which was developed within the framework of the Operational Program entitled "Competitiveness, Entrepreneurship and Innovation (2015-2020), Project “Studies and researches support to the energy sector, industry and entrepreneurship”, Sub-Project “Susceptibility assessment of landslides in the Greek territory - Volcanic study and risk assessment”, financed by the European Regional Development Fund.

LANDSLIDE MAPPING AND MODEL DEVELOPMENT FROM MULTI-LEVEL REMOTE SENSING TECHNOLOGIES DATA, HRVATSKA KOSTAJNICA CASE STUDY, CROATIA

IVAN KOSOVIĆ[1], LASZLO PODOLSZKI[1], TOMISLAV NOVOSEL[1], TOMISLAV KUREČIĆ[1]

[1] *Croatian Geological Survey, Sachsova 2, Zagreb, Croatia; corresponding author: ikosovic@hgi-cgs.h*

Introduction

Geohazards are a constant threat to human activity in an environment that is constantly changing. Climate changes affect the natural extremes, resulting in rapid temperature changes, flooding, and a high amount of precipitation in a short period. Furthermore, landslides can have several causes, including geological, morphological, physical, and human factors (Alexander 1992). However, they typically have only one trigger. This trigger can often be intense rainfall, earthquake shaking, storm waves, or rapid stream erosion (Varnes 1978). Such unpredictable events can affect slope stability, leading to new landslides and the reactivation of old ones. Predicting the behavior of soil and rock masses during and after extreme events is a crucial yet complex task. Different remote sensing technologies calibrated through local scale datasets can be used and integrated to enhance the knowledge and understanding of the event.

After a rapid temperature change and snowmelt on March 13, 2018, a landslide in Hrvatska Kostajnica destroyed multiple households. The Hrvatska Kostajnica landslide case study introduced a new integrated approach to geohazard research. The research utilized various multi-level remote sensing techniques, and the results were analyzed and integrated to develop a comprehensive landslide model.

Methods

Approaches used in this research included the review of available datasets and the acquisition of new data to develop a landslide model. The new datasets included: 1) remote sensing data, 2) field research, and 3) laboratory data with associated analysis and re-interpretation. The main focus was on acquiring multi-level remote sensing technologies and data such as orthophoto data, unmanned aerial vehicle (UAV) data (Ngadiman et al., 2016), differential interferometric synthetic aperture radar (DInSAR) data (Ferretti et al., 2007), light detection and ranging (LIDAR) data (Jaboyedoff at al., 2012), and geophysical measurements, i.e., electrical resistivity tomography (ERT) data (Loke et al., 2013).

Results

The landslide in Hrvatska Kostajnica covers an area of approximately 300 × 300 m with a maximum height difference of about 60 m (Figure 1). The developed 26 m high detailed geological column at the main scarp revealed that the landslide occurred mainly in the “marly” sediments. Clayey (weathered) limestones were also present at the location, but no clear sliding zone(s) were mapped on the field during geological column development.

The DInSAR data analysis was used in surface displacement behavior trend determination and it indicated that the landslide was a “short and extreme” event rather than a long-term, ongoing, slow slope deformation process. ERT was applied to determine the physical properties of soil and rock, subsurface lithology, groundwater conditions, and geometry of the slide surface. The cross sections within the landslide body (ERT-1 and ERT-2) revealed zones with colluvial materials, in the range of 5–20 Ωm. Below colluvial materials, weathered and interlayered materials are present (with resistivity values in the range of 20–50 Ωm). The “bedrock” on the ERT-1 and ERT-2 is probably a heterogeneous structure (interlayered materials), but not so weathered and with somewhat higher resistivity values (>50 Ωm).

From the available regional data, the area is generally prone to landslides (Podolszki et al., 2022). The preliminary landslide model indicated an affected area of approximately 5 ha with multiple sliding surfaces, the deepest at around 30 m. The multiple datasets acquired in the scope of this research (UAV, DInSAR, LIDAR, and ERT data) and historical orthophotos provided different useful insights that were collectively used to develop a new model of the landslide. ERT results showed that the landslide has

multiple sliding surfaces and that highly deformed materials are present mainly in the main body of the landslide. The sliding surfaces within the landslide body are at depths of around 10–20 m. Additionally, the model identifies a relatively large landslide-endangered zone of approximately 12.5 ha. Based on the characteristics of this particular event (deep-seated with multiple sliding zones) and the collected data, it can be assumed that the the triggering factor was the contemporaneous rapid temperature change driving a sudden snowmelt (~80 cm of snow cover melted) and the Una River flooding (located ~400 m from the landslide and showing a water level ~5 m higher level than usual during the flooding event). These factors probably increased the water pore pressure in the rock mass and the rhythmic changes within the material caused multiple weakened zones. Despite the potential influence of anthropogenic factors in triggering landslides, human activities played little to no role in this instance.

Figure 1. Hrvatska Kostajnica landslide location: A) In the city of Hrvatska Kostajnica near Una River; B) In Croatia, near the border with Bosnia and Herzegovina (red mark on the map)

Conclusion

Field mapping and UAV data collection were performed for the revision of available geological and remote sensing data of the Hrvatska Kostajnica landslide. A new geological column was developed and available remote sensing data were analyzed, namely satellite images and historical orthophotos. New insights about the Hrvatska Kostajnica landslide were gained by LIDAR and geophysical data analysis. From detailed LIDAR data, a precise terrain landslide surface model was developed and used for the cross-section and new landslide map development. These data allowed us to propose a new model of the landslide showing a potential endangered area larger than the area predicted by a preliminary model.

References

Alexander, D. 1992. On the Causes of Landslides: Human Activities, Perception, and Natural Processes. *Environmental Geology and Water Sciences*, Vol. 20, No. 3, pp. 165-1 79.

Ferretti, A.; Monti-Guarnieri, A.; Prati, C.; Rocca, F.; Massonnet, D. InSAR Principles: Guidelines for SAR Interferometry Processing and Interpretation; *ESA Publications*: Auckland, NZ, USA, 2007; ISBN 92-9092-233-8.

Jaboyedoff, M.; Oppikofer, T.; Abellán, A.; Derron, M.H.; Loye, A.; Metzger, R.; Pedrazzini, A. Use of LIDAR in landslide investigations: A review. *Nat. Hazards* 2012, 61, 5–28.

Loke, M.H.; Chambers, J.E.; Rucker, D.F.; Kuras, O.; Wilkinson, P.B. Recent developments in the direct-current geoelectrical imaging method. *J. Appl. Geophys*. 2013, 95, 135–156.

Ngadiman, N.; Kaamin, M.; Sahat, S.; Mokhtar, M.; Ahmad, N.F.A.; Kadir, A.A.; Razali, S.N.M. Production of orthophoto map using UAV photogrammetry: A case study in UTHM Pagoh campus. In *AIP Conference Proceedings*; American Institute of Physics: College Park, ML, USA, 2016.

Podolszki, L.; Kosović, I.; Novosel, T.; Kurečić, T. Multi-Level Sensing Technologies in Landslide Research — Hrvatska Kostajnica Case Study, Croatia. *Sensors*, 22 (2022), 1; 177, 21.

Varnes, D.J. 1978. Slope Movement Types and Processes. *In Special Report 176: Landslides: Analysis and Control* (R.L. Schuster and R.J. Krizek, eds.), TRB, National Research Council, Washington, D.C., pp.12-33.

ASSESSING ROCKFALL HAZARDS POST-WILDFIRES: A CASE STUDY IN EVROS, GREECE

PAVLOS ASTERIOU [1], DIMITRIS SOTIRIADIS [2], ELENI PETALA [3], LABROS KAZELIS [4], EVAGGELOS EVAGGELOU [5], THEOFILOS TZEVELEKIS [6], NIKOS KLIMIS [7]

[1] *Democritus University of Thrace, Department of Civil Engineering, Greece,* pasterio@civil.duth.gr

[2] *Democritus University of Thrace, Department of Civil Engineering, Greece,* dsotiria@civil.duth.gr

[3] *Democritus University of Thrace, Department of Civil Engineering, Greece,* epetala@civil.duth.gr

[4] *Democritus University of Thrace, Department of Civil Engineering, Greece,* labrkaze@civil.duth.gr

[5] *Democritus University of Thrace, Department of Civil Engineering, Greece,* eevange@civil.duth.gr

[6] *Democritus University of Thrace, Department of Civil Engineering, Greece,* thtzebel@civil.duth.gr

[7] *Democritus University of Thrace, Department of Civil Engineering, Greece,* nklimis@civil.duth.gr

Introduction

Following wildfires, rockfalls in forested slopes are expected to increase in occurrence, frequency, and severity, posing a greater hazard to mountainous settlements and infrastructure. Vegetation typically mitigates rockfalls by restricting block movement and absorbing energy through collisions with tree trunks. However, the destruction of vegetation negates this beneficial action, resulting in extended run-out distances and intensified impacts. Moreover, the temperature rise during a wildfire may degrade rock properties, potentially reducing their resistance and increasing the number of unstable blocks. As a result, both the likelihood and consequences of rockfall events, namely the hazard, may heighten. In this paper, we examine these parameters in the Avas site, located in Regional Unit of Evros, Greece, that was heavily impacted by the 2023 wildfire. Figures 1 (a) and (b) illustrates the study area before and after the wildfire, respictevely. The fire started on August 21st, 2023, and burnt more than 800km^2, making it the largest wildfire ever recorded in the EU.

Methods

We deployed to the field to gather all necessary information, including Schmidt hammer hardness, vegetation type, size and density and identified the size and location of previously detached blocks. Then, we composed the geological and vegetation maps of the site. Along with the 2-meter resolution Hellenic Cadastre raster map, we analysed the possible rockfall trajectories in the three-dimensional space using the RockyFor3D (Dorren, 2016) software to evaluate the effect of vegetation. We examined two scenarios: the first with the site's vegetation before the fire, and the second without any vegetation to simulate its destruction after the fire. For each scenario, we analysed cubic blocks with volumes of 1m^3, 0.1m^3 and 0.01m^3, released from the top of the slope. In each analysis, we released 10 blocks from every cell, resulting to a total of 6590 blocks. The vegetation of the study area was measured in patches that remained unburnt. It consists of small Mediterranean scrublands, with a mean density of 6875 stems per hectare and an average stem diameter of less than 5 cm.

Results

First, the findings indicated that the temperature rise did not influence the rock properties, as Schmidt hardness values were similar for both burnt and unburnt rock exposures. This is supported by the fact that even though the branches and leaves of the trees were completely burnt, their stems were only superficially burnt, indicating that the fire passed through the site quickly, resulting in a moderate temperature rise. The analyses with the 1m^3 blocks had similar results to the 0.1m^3 blocks and are not presented hereafter. This is attributed to the fact that this vegetation type has limited capacity to withstand impacts, thus having a limited effect on blocks larger than 0.1m^3. This is in line with Figure 1 (c) and (d), which presents the end positions of the 0.1m^3 blocks in the forested and burnt scenarios, respectively, where the effect of vegetation is negligible. However, when examining Figure 1 (c) and

(e), it is seen that smaller blocks travel less. This is attributed to two reasons: first, larger blocks tend travel longer distances as they are less affected by the irregularities of the slope (Ritchie, 1964 and others), and second, this type of vegetation is more effective in restricting blocks with less energy. For the 0.01m^3 blocks, the destruction of vegetation increases the hazard (Figure 1 (e) and (f)), as more blocks impact the road, especially on its south side.

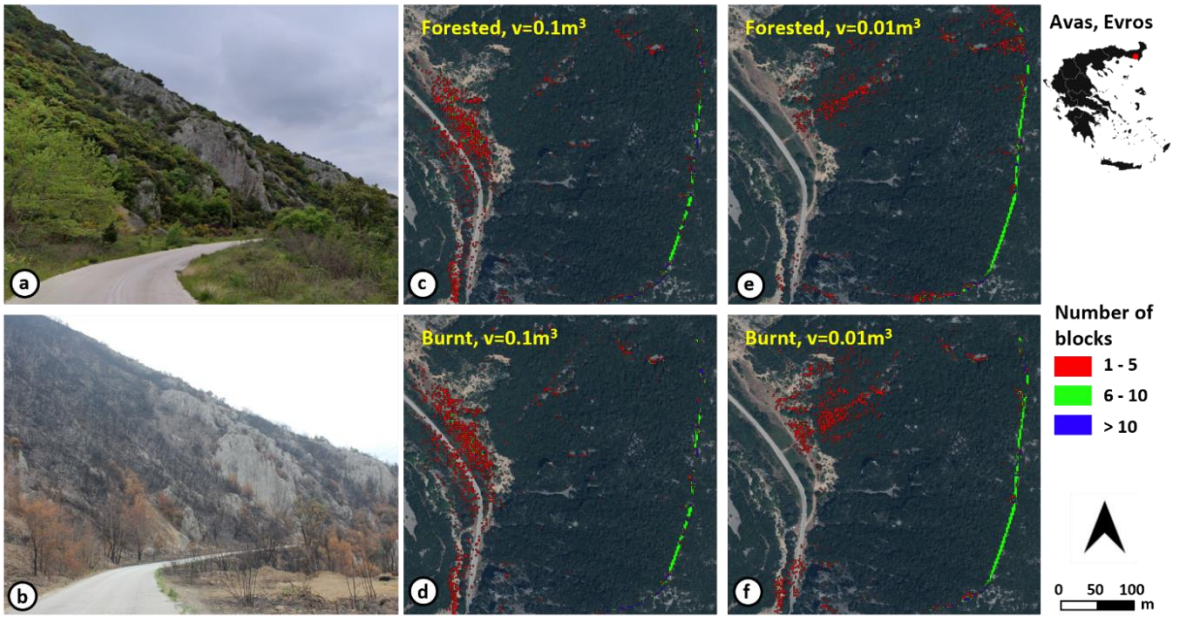

Figure 1. Avas site, (a) before and (b) after the wildfire. Trajectory end points: (c) Forested slope with v=0.1m^3, (d) Burnt slope with v=0.1m^3, (e) Forested slope with v=0.01m^3 and (f) Burnt slope with v=0.01m^3,

Conclusion

The destruction of vegetation due to wildfires increases rockfall hazard as the blocks tend to travel further down the slope. The vegetation type plays a significant role; in Avas study area, the vegetation was weak, primarily affecting small-sized blocks. However, in areas with stronger vegetation, the increase in hazard will be more pronounced for larger blocks. On the other hand, we did not find any evidence that the rock properties degraded from the wildfire in Avas study area.

Following wildfires, various measures are often taken to mitigate the destructive effects of phenomena such as floods, landslides, and others. Although rockfalls may evolve gradually, it is crucial to promptly acknowledge their increased threat. By doing so, rockfall mitigation efforts can be integrated with other early interventions aimed at addressing different consequences. This integrated approach enables a more efficient management of the necessary actions, resulting in cost savings and, ultimately, to the restoration of safety levels to acceptable standards.

Acknowledgement

This project (KE83226) was funded by Democritus University of Thrace under the initiative “DUTh To The People: Actions to Mitigate the Effects of the Devastating Fires in Thrace.”

References

Dorren, L.K.A. *Rockyfor3D (v5.2) revealed – Transparent description of the complete 3D rockfall model*. ecorisQ paper (www.ecorisq.org), 2016.

Ritchie, A. M. *Evaluation of rockfall and its control*. Highway research record 17, pp. 13-28, Washington, USA, 1963.

STREAMLINING ROCKFALL ANALYSIS: A DIGITAL PARADIGM FOR EFFICIENCY, COLLABORATION AND RISK MANAGEMENT

ALKIS GKOUVAILAS [1], İREM AKSULAR [2], S.W.R CHAN [3], H.L.K FU[4], FINLAY LEIBRICK[5]

[1] *Langan Engineering and Environmental Services, United Kingdom,* agkouvailas@langan.com

[2] *AECOM, UAE,* irem.aksular@aecom.com

[3] *AECOM, UAE,* swrachael.chan@aecom.com

[4] *AECOM, Hong Kong,* karen.fu@aecom.com

[5] *AECOM, UAE,* finlay.leibrick@aecom.com

Introduction

Mountains in the Middle East have great geo-heritage value due to their intriguing geological setting. The region envisions leveraging its endowed natural beauty for ecotourism and development, leading to a growing need for rock slope stability and rockfall studies. Given the complexity and scale of projects, combined with their expeditious time frame, it is crucial to carry out these studies efficiently to inform project risk assessment and decision-making for mitigation and master planning in a timely manner.

This paper presents a streamlined workflow for rockfall analysis employed in a recent project close to Riyadh, Kingdom of Saudi Arabia, which successfully achieved the goals outlined above. The proposed development will be situated within a vast landscape featuring desert, plateau, mesas and butte, with encircling cliffs reaching heights of 200 m and spanning over 15 km. This expansive terrain has exhibited signs of historic rock slope instabilities, necessitating detailed geological and geohazard assessments with a focus on rockfall risks. To perform such a comprehensive engineering geological study, an ArcGIS-based paradigm furthering the work of Charalambous and Sakellariou (2007) was implemented, following the workflow shown in **Figure 6**.

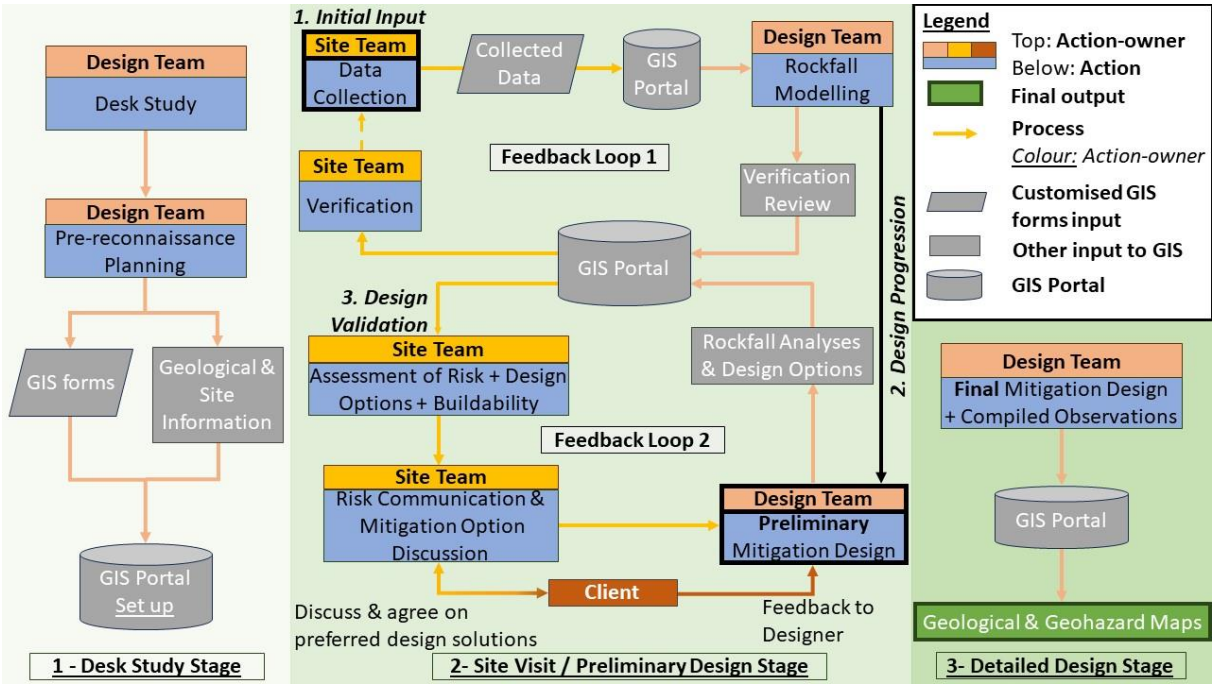

Figure 6. Presented digitalised workflow for rockfall analysis.

Methods

To ensure a focused survey and to develop a better understanding of the site geology and ground conditions, a desk study was carried out through a review of available information. Earlier mapped

geological boundaries and features, slope angle and plot boundary were compiled on ArcGIS for the identification of critical rockfall areas and the formulation of visit routes. The acquired information was pre-loaded through the ArcGIS Online portal, into the ArcGIS Field Map application to be available for offline usage onsite. Moreover, project-specific observation forms were built through ArcGIS Field Map Designers for an expedited and standardised data collection process. These forms, informed by insights from past projects and client feedback, were configured for direct import into rockfall analysis software.

Site data from the geological and geohazard mapping was captured on ArcGIS Field Map, along with geotagged photos for subsequent evaluation. These included observations of geological boundaries, engineering-geological descriptions of soil and rock, and geohazards. Furthermore, an online inventory of historical rockfalls and susceptible areas was integrated as part of the geohazard mapping. It entailed details like originating, impact and termination points, rock block dimensions and shapes, and observed failure mechanisms. All data collected was georeferenced and stored in one central database via the ArcGIS Online portal for usage across different ArcGIS platforms. The integrated acquisition approach allowed the collected data to be shared seamlessly with office designers, enabling the design team to swiftly review it and raise queries or verification requests with the site team while they were still onsite.

In parallel with the field work, designers performed rockfall analysis. Given the terrain complexity, three-dimensional (3D) rockfall modelling was employed through RocFall3®. Input parameters (i.e., coefficients of restitution) were initially assessed based on literature (Gkouvailas, 2014) and then adjusted through back analysis. This was made possible by the streamlined data collection process through which a detailed historical rockfall database was produced. Once the models effectively replicated the historical rockfall events, a series of originating points were placed at all potential initiation locations. Two-dimensional (2D) analyses through RocFall2® were undertaken for critical rockfall trajectories to inform the design of mitigation measures. To facilitate the identification of critical areas and risk assessment, the trajectories were overlaid onto the master plan in the GIS model through a self-developed GIS toolbox. The project site was divided into zones so that rockfall models could be constructed in parallel with the site work. The analysis results (trajectories, kinetic energies, etc.) for the previously mapped areas were shared via the GIS portal with the site team, which enabled real-time validation onsite. Feasibility and applicability of the proposed mitigation were evaluated in the field.

Remote sensing data was utilised to supplement the geological assessment and combined with site observations and rockfall models to create geological and geohazard maps for the project area. Identified risks, their locations and analysis results were incorporated into the project's risk registry. Risks and mitigation measures were communicated to and discussed with the client onsite with the aid of graphics and 3D models to visualise the impact on master planning. This allowed engaged and informed decision-making from the client’s side and provided prompt feedback to the design team.

Results and Conclusion

This digitalised strategy reduced time on site and subsequent data processing. The planned visit with tailored GIS tools promoted targeted surveys with integrative outputs to be fed into rockfall analysis and geological/geohazard mapping. The simultaneity of observation and backend analysis increased the comprehensiveness of inspection and modelling accuracy and improved design efficiency and quality. Additionally, timely, direct, and continuous communication with the client on the site findings, identified geohazards and mitigation solutions optimised the design process and overall project risk management. Considering the proven benefits, this rockfall study blueprint is encouraged for future use.

References

Charalambous, S.; Sakellariou, M. Estimation of rockfall hazard using a GIS-based three-dimensional rockfall simulation model. *Bulletin of the Geological Society of Greece*. 2007, 40 (4), 1934-1946

Gkouvailas, A. Enhanced rockfall analysis based on field experiments in quarries in the UK. *Master Thesis, Imperial College London*, UK, 2014.

GEOMORPHIC EFFECTIVENESS OF FLOOD DISCHARGE AND ITS IMPORTANCE FOR RIVER-BED ENGINEERING CONSTRUCTIONS: A CASE OF THE GODAVARI, INDIA

SUMIT DAS [1], GIANVITO SCARINGI [1]

[1] *Institute of Hydrogeology, Engineering Geology and Applied Geophysics, Charles University, Czech Republic, sumit.das@natur.cuni.cz, gianvito.scaringi@natur.cuni.cz*

Introduction

Floods are a frequent and devastating natural disaster that affects many regions worldwide. While they cannot be fully prevented, adopting suitable strategies can mitigate their geomorphic impact and severity. This is especially true for engineering riverbed constructions in populous areas. Systematic assessments of flood intensity are crucial for effective flood management (Cameron et al., 2000). The impact of a major flood is determined by various factors including the flow's strength, the energy of the stream, the sequence of events, and the shape of the river channel (Miller, 1990; Das 2019). Riverbed constructions such as bridges significantly affect the river's cross-sectional morphology and, therefore, the flood effectiveness. Here, we study the geomorphic impact of floods under typical conditions using a theoretical framework and examine how bridges affect flood dynamics.

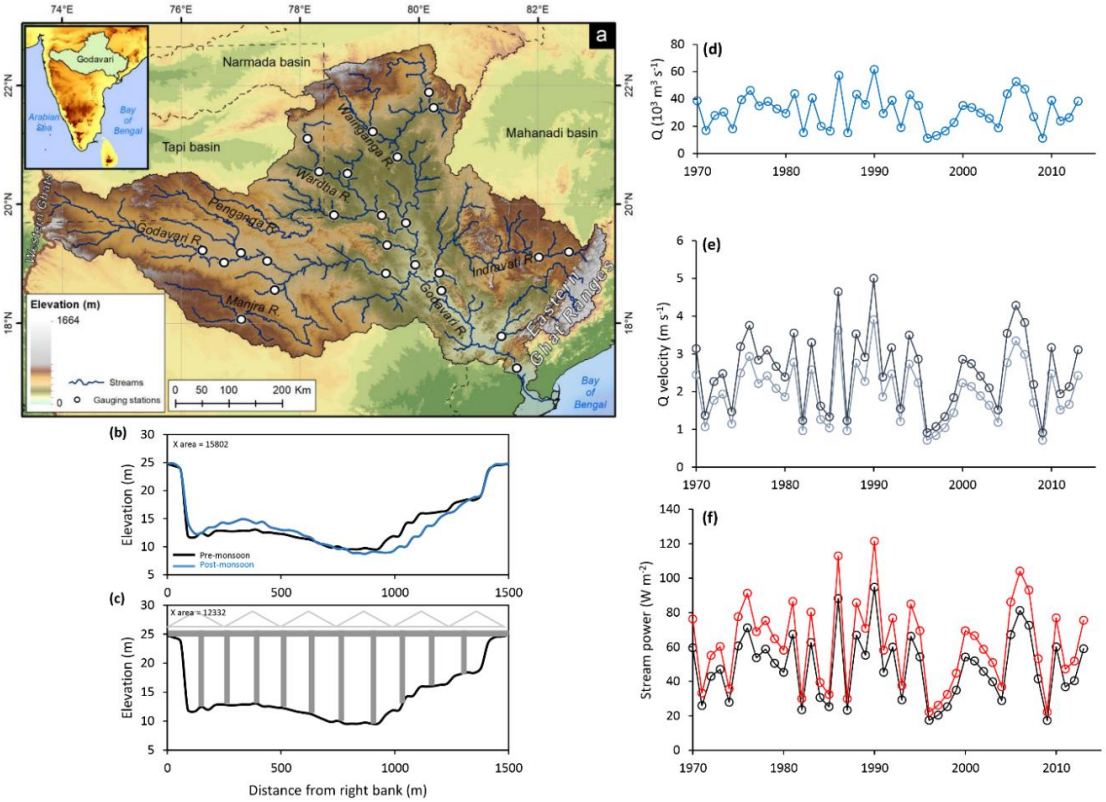

Figure 1. (a) Map of the Godavari basin. (b) Polavaram's river cross-section on the Godavari, and (c) the same section assumed with a bridge comprising 10 pillars of 5 m radius, reducing the area from 15,802 to 12,332 m^2. (d) Yearly fluctuation of peak discharge at Polavaram; (e) changes in peak discharge velocity under normal conditions and with a bridge; (f) stream power variations for both scenarios (black: normal; red: bridge).

Study area and methods

The Godavari basin in Peninsular India has the largest catchment area in the region, spanning over 300,000 km^2 (Fig. 1a). Its rivers flow through three major lithological zones: Deccan basalt in the west, Precambrian Gondwana sedimentary rocks (including sandstone and shale) in the centre, and Archean granite and gneiss in the east. Additionally, the delta region features extensive Quaternary alluvium deposits mixed with moderate-sized gravel and sand.

In this work, ranging from 1970 to 2015, we gathered long-term discharge data and historical cross-

sectional measurements for various gauging stations of the Godavari River from the Central Water Commission (CWC), India. We calculated cross-sectional morphology parameters, namely width, mean depth, area, width-depth ratio, hydraulic radius, and shear stress (τ). We then identified the peak annual discharge as the effective flood for each year to determine the unit stream power (ω) (Leopold et al., 1964). Considering the principle of discharge continuity, we recalculated all parameters under the hypothetical scenario of a bridge being constructed at each cross-section (Fig. 1b & c). This would lead to a notable decrease in cross-sectional area. Given that discharge remains constant across a channel section (theoretically, unless joined by a new tributary), the flood discharge must adjust its flow velocity accordingly. Using historical flood discharge data, we calculated velocities for both standard conditions and with a hypothetical bridge in place, followed by unit stream power computations.
Subsequently, we applied William's (1983) equation to estimate the entrainment potential of various boulder sizes based on the calculated flood stream power in both scenarios. This method's significance lies in evaluating the impact of engineering structures on riverbeds, determining their safety against high floods, and assessing whether such constructions could be severely impacted by flooding.

Results

Our calculations are based on the assumption that the annual peak discharge equates to the bank-full stage for ease of analysis. However, real-world scenarios may differ from this theoretical model. Nevertheless, Table 1 illustrates the cross-sectional parameters for the Polavaram station on the Godavari River. The flood discharge has been recorded ranging from 11×10^3 m^3 s^{-1} in 2009 to an unprecedented 62×10^3 m^3 s^{-1} in 1990, as depicted in Fig. 1d.

Table 1. Computational results of the cross-section geometry and hydraulics.

Parameters	Value
Width (m)	1500
Average depth (m)	10.33
Area (m^2)	15802
Form ratio (Width/Depth)	145.22
Slope (degree)	0.00024
Manning's n	0.024
Boundary shear stress (N m^{-2})	24.29

The terminal gauging station of the Godavari at Polavaram spans 1500 m in width, with maximum and average depths of 15.26 m and 10.33 m, respectively. In evaluating the river cross-sections to understand the flow behaviour, the computed boundary shear stress at this site is 24.29 N m^{-2}. Manning's "n" value, determined by observing channel roughness, bed material, and land use, is 0.024. Under standard conditions, the unit stream power is observed to vary from 17 to 94 W m^{-2}. However, when we simulate the construction of a bridge with 10 pillars, each 5 m in diameter, the stream power increases to 22 to 121 W m^{-2} (Fig. 1f), and the cross-sectional area decreases from 15,802 to 12,332 m^2 (Table 1), assuming a fixed cross-section. In reality, extreme floods can alter cross-sections significantly, and regular assessments of stream power are vital for areas upstream and downstream of dam constructions to prevent potential flood damage to engineering structures and minimize risks to flood-prone areas.

Conclusion

This study offers a theoretical evaluation of flood dynamics in the Godavari River, which is instrumental in safeguarding engineering structures from flood damage and implementing effective flood mitigation strategies for the adjacent areas.

References

Cameron, D.; Beven, K.; Naden, P. *Flood frequency estimation by continuous simulation under climate change (with uncertainty)*. Hydrol. Earth Syst. Sci. 2000, 4, 393–405.

Das, S. *Geospatial mapping of flood susceptibility and hydro-geomorphic response to the floods in Ulhas basin, India*. Remote Sens. App. Soc. Env. 2019, 14, 60-74.

Leopold, L.B.; Wolman, M.G.; Miler, J.P. *Fluvial Processes in Geomorphology*. Freeman, San Francisco, 1964.

Miller, A.J. *Flood hydrology and geomorphic effectiveness in the central Appalachians*. Earth Surf. Process. Landf. 1990, 15, 119–134.

Williams, G.P., *Paleohydrological methods and some examples from Swedish fluvial environments: I. Cobble and boulder deposits*. Geogr. Ann. 1983, 65A, 227–243.

MINING-INDUCED SUBSIDENCE SUSCEPTIBILITY MODELLING OF THE WITWATERSRAND BASIN USING WEIGHTS OF EVIDENCE (WOE) APPROACH IN GIS

S.G. CHILIZA[1], N. MANKAYI[1], M. SEBESHO[1], C. GABAVANA[1], AND G DENNER[1]

[1.] *Council for Geoscience, 280 Pretoria Road, Silverton, Pretoria, 0184, South Africa, msebesho@geoscience.org.za*

Introduction

Mining activities in South Africa have altered the natural environment in numerous ways over the last 120 years. Areas within the Witwatersrand basin located in Johannesburg, Gauteng's East, West Rand and Far West Rand districts, including the KOSH (Klerksdorp-Orkney-Stilfontein-Hartebeesfontein) mining regions, are subjected to ground settlement and surface subsidence due to mining (historical, and current illegal mining) and groundwater dewatering for mining operations to take place (Heath and Engelbrecht, 2011). In response, the Council for Geoscience (CGS) embarked on research seeking to produce land subsidence susceptibility maps that will categorise the abandoned mine areas into zones with varying degrees of subsidence susceptibility driven by previous subsidence inventory data and contributing factors that will aid spatial planning decision making and disaster management.

Methodology

The weight-of-evidence (WoE) statistical approach was selected and used for subsidence susceptibility mapping (Oh & Lee, 2010). This approach computes the conditional probability that an event (in our case, mining-induced subsidence) does or does not belong to a set of mapped causal factors (i.e., conditioning factors). Physical processes known to occur in gold mining settings and the historical perspective of the study area were used to select potential conditioning factors. The WoE theoretical framework was then implemented to objectively assess the relevance of these conditioning and triggering factors.

Broadly, the following steps were completed:

1. Establishment of a comprehensive database/inventory of mining-induced subsidence events (including dewatering for mining).
2. Determination of potential conditioning factors based on geological processes inferred: Proposed conditioning factors were slope, geology, groundwater (dewatered and non-dewatered compartments), faults, and mined-out areas.
3. A probabilistic WoE evaluation of the potential conditioning factors followed by a test of independence of conditioning factors
4. Developing a susceptibility map by combining relevant conditioning factors and validating the map with receiver operating characteristic (ROC) curves.

Results

The results show that groundwater in the form of de-watering has the highest influence on subsidence, with the highest contrast (C value) of 2.33. The geology (dolomitic formations), slope, faults, shaft positions and mined-out areas were found to have weights of 2.08, 1.49, 0.37, 0.63 and 0.42, respectively. The dewatering of Venterspost, Oberholzer, Bank, and Gemsbok-west to allow mining operations has led to the accelerated sinkhole and subsidence occurrences on the Far West Rand, and approximately 1200 events have occurred to date. The mining-induced subsidence susceptibility map for the Far West, West, Central and East Rands of the Witwatersrand goldfields basin is shown in Figure 1. From this map, the analysis of results shows that the actual ground subsidence is in high and very high subsidence susceptibility areas, as confirmed by the AUC method.

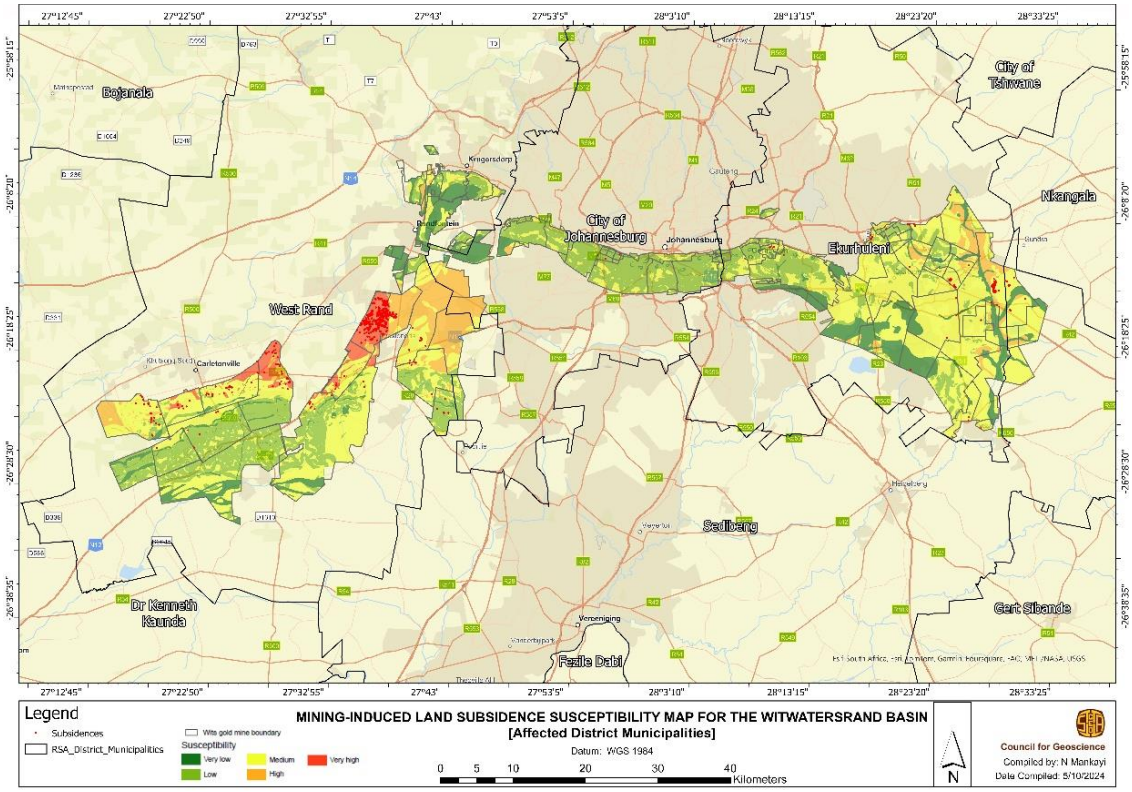

Figure 7: Mining-induced subsidence susceptibility map the Witwatersrand Basin.

Conclusions

The dewatering of dolomite groundwater compartments for mining has been highlighted as the major contributor to the formation of sinkholes and subsidence in the West and Far West Rand areas of the Witwatersrand basin. Therefore, the results presented here must inform future policy and decision-making around dewatering for mining. Given the knowledge, experience and susceptibility modelling results, it is therefore concluded that most of the resources and efforts for monitoring subsidence must be deployed in the Central Rand and parts of the West and East Rands and at all illegal mining hotspots.

References

Heath, H. and Engelbrecht, J. Deformation due to mining activities. Council for Geoscience Internal Report No: 2011-065, 2011

Oh, H. and Lee, S. Assessment of ground subsidence using GIS and the weights-of-evidence model. Engineering Geology, Volume 115, 2010, pp. 36-48.

FOLD-CONTROLLED ROCK SLIDING DETERMINED FROM STRUCTURE AND 2D INSAR PRESENTS A LOW HAZARD: THE CASE OF DUSNJÁRGA, NORTHERN NORWAY

LOUISE M VICK[1], ANDREAS GRUMSTAD[2], CARLY FABER[3], LINE ROUYET[4], SIMEN BEKKEVOLL[5]

[1] *UiT The Arctic University of Norway, Norway, louise.m.vick@uit.no*

[2] *UiT The Arctic University of Norway, Norway, andreas.grumstad@uit.no*

[3] *UiT The Arctic University of Norway, Norway, carly.faber@uit.no*

[4] *NORCE, Norwegian Research Center, Norway, liro@norce.no*

[5] *Troms Fylkeskommune, Norway, simen.bekkevoll@tromsfylke.no*

Introduction

Dusnjárga is a large deforming rock slope in the Kvænangen area of northern Norway. It sits on a peninsular in the Little Altafjord, framed by a series of rock slope deformations (RSD) (Figure 1). These RSD pose a threat to surrounding seaside villages from collapse and tsunami, should they fail. RSDs can creep for up to thousands of years before collapse (McColl & Draebing, 2019), and in some cases may stabilise rather than fail at the end of the creep phase. In remote and alpine cases it is not possible to drill for subsurface information and therefore an interpretation of the mechanics must be made from the surface data. In this work we employ structural data combined with movement from 2D InSAR to assess the kinematics of Dusnjárga to assess the hazard potential of the site.

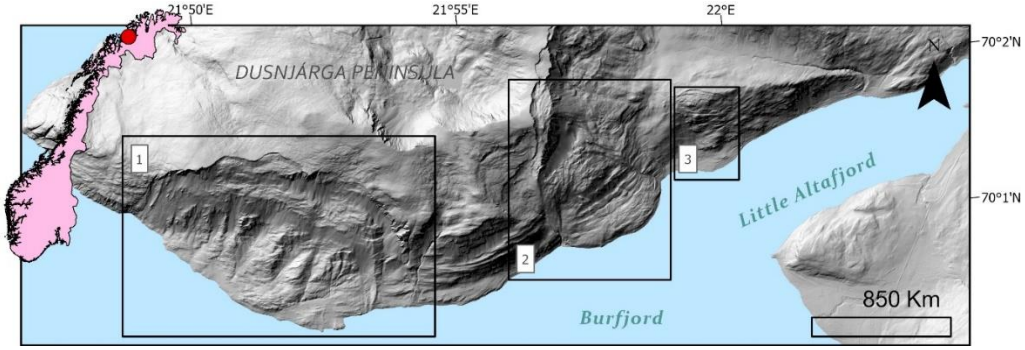

Figure 1. Location map. 1.Vassnestinden RSD, 2. Dusnjárga RSD, 3. Låvan RSD. Inset map with red dot shows generalised location of study area. DEM 2016 series from hødedata.no, sampled at 1m resolution.

Methods

Structural data was collected during summer campaigns in 2019-2021. >3000 structural observations were made, mostly with the FieldMOVE app. InSAR data used in this thesis comes from the public service *InSAR Norway* 2015-19 Copernicus Sentinel-1A and -1B satellite data. 2D InSAR interpolates displacement from two radar geometries to harvest a vector within a profile line (e.g. Frattini et al., 2018). A GIS tool (Lauknes et al., 2020) was used to combine data from overlapping SAR imagery to estimate a combined annual mean velocity. The stable plateau above was used for calibration.

Results

The RSD has a clearly defined detachment limit and coastline toe-bulge, with many scarps and areas of dense fracturing and talus. The slope is comprised of metagrabbro and amphibolite, displaying a range of foliations from weak to strongly pervasive. Some parts of the metagabbro are mylonitised with an intensely planar fabric. The foliation in general dips downslope between 800-150 m asl. Below 150 m, it appears to dip into the slope (Figure 2). The pattern of foliation indicates a large synclinal structure may be present. This is congruent with the displacement vector dip (Figure 2), which shows a movement of the slope downwards from 800 m until ca. 150 m asl, where the slope surface begins to move up and outwards, potentially by slippage along structures associated with the fold.

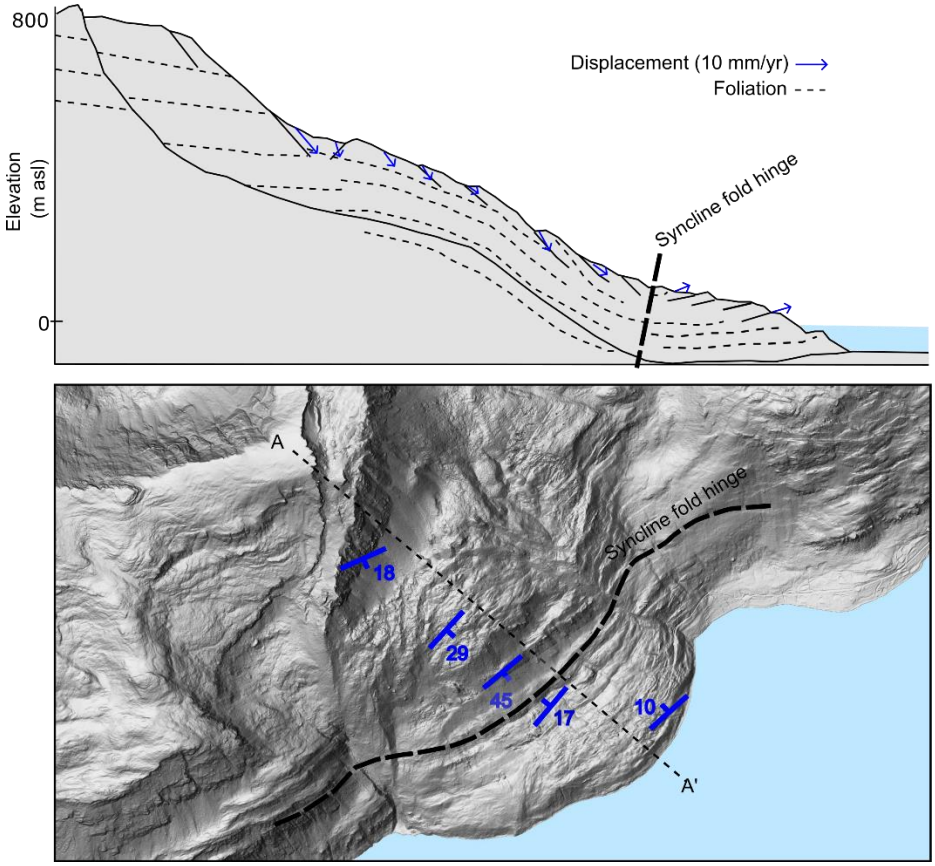

Figure 2. Upper panel: Cross section showing surface morphology, inferred foliation and surface displacement vectors. Lower panel: multiaspect hillshade (from 1 m DEM) showing foliation dip and direction and syncline surface trace.

Conclusion

The combination of structural mapping and 2D InSAR provides insight into the mechanical model of the Dusnjárga RSD. If the basal sliding surface is controlled by a syncline structure, a buckling-style failure (Glastonbury & Fell, 2010) must be considered where friction at the toe cannot be overcome, and transported material becomes imbricated at the toe, after e.g. Braathen et al. (2004). Sudden collapse would therefore not a viable kinematic model. This would render the hazard and subsequently risk to life negligible. Further analysis is planned to model the slope kinematics and strength over time to test this hypothesis.

References

Braathen, A., Blikra, L. H., Berg, S. S., & Karlsen, F. (2004). Rock-slope failures in Norway; type, geometry, deformation mechanisms and stability. Norwegian Journal of Geology, 84(1), 67-88. ISSN 029-196X.

Frattini, P., Crosta, G. B., Rossini, M., & Allievi, J. (2018). Activity and kinematic behaviour of deep-seated landslides from PS-InSAR displacement rate measurements. Landslides, 15(6), 1053-1070. https://doi.org/10.1007/s10346-017-0940-6

Glastonbury, J., & Fell, R. (2010). Geotechnical characteristics of large rapid rockslides. Canadian Geotechnical Journal, 47(1), 116-132. https://doi.org/10.1139/t09-080

Lauknes, T. R., Grahn, J., Rouyet, L., Larsen, Y., Böhme, M., Dehls, J. F., & Kristiansen, L. (2020). Mapping and characterization of unstable slopes with Sentinel-1 multi-geometry InSAR (activity line 2: public sector applications). https://hdl.handle.net/10037/31490

McColl, S. T., & Draebing, D. (2019). Rock Slope Instability in the Proglacial Zone: State of the Art. In Geomorphology of Proglacial Systems (pp. 119-141). https://doi.org/10.1007/978-3-319-94184-4_8

AN EVIDENCE BASED APPROACH TO QUANTIFYING GEOLOGICAL UNCERTAINTY

LUKE JOHNSTONE
AtkinsRealis, England, Luke.Johnstone@AtkinsRealis.com

Introduction

Geotechnical design relies on an analysis informed by an accurate and reliable representation of ground conditions. Here we will focus on 3D digital geological models used to capture ground conditions and inform design. Typically these are comprised of a series of key geological surfaces built from contacts in ground investigation (GI) data (contacts). At the location of the contacts the surface is considered reliable with a high certainty, however between contacts interpretation is necessary and the surface location is inherently uncertain. Uncertainty increases with distance and the more complex or variable the ground conditions are, the more rapidly the uncertainty increases. It is critical to understand and communicate a surface's reliability and its potential variability in areas between contacts or sparsely populated by GI.

Approaches to uncertainty are discussed in guidance such as IAEG C25 (Parry, et al., 2014) however it is rarely quantified and there is no widely accepted framework for its assessment. As a result, surfaces in ground models are described as best estimates and uncertainty is commented on in accompanying reports and risk registers. As digital deliverables, they may be shared and referenced without the accompanying documents, resulting in design decisions divorced from geological advice.

This paper presents an evidence based geostatistical method to quantify the potential variability in a geological surface (quantified uncertainty) based on the distribution of contacts. Quantified uncertainty is calculated as a function of two factors: distance to GI as defined by the distribution of contacts in the XY dimension and geological complexity as defined by the variability of contacts in the Z dimension (elevation).

It is noted that uncertainty in geological models may arise from a number of factors and that not all geological models are focussed on geological surfaces. This methodology is intended to be used as a tool for robust, transparent, and repeatable design decisions in large infrastructure projects, where large teams of geologists examine and interpret geological data, potentially arriving at differing design decisions.

Method

The methodology calculates variables on a grid across the site, then combines these into a quantified uncertainty. The calculation is undertaken using a Grasshopper script in Rhino. The methodology is described as follows and visualised in Figure 1.

Geological Complexity (C): For each grid cell, the standard deviation (*C)* of nearby contacts elevations is calculated. *C* reflects the variability of the geological surfaces in this area, *2*C* is taken as the 95th percentile of the potential variability of the geological surface in that area.

Borehole Influence (I): Following a similar methodology to Lelliott et. al. (2009) the GI zone of influence is modelled using a gaussian function centred on the contact location. The standard deviation of the gaussian function is currently assessed by geological judgement however is the focus of future work.

Quantified Uncertainty (U): The quantified uncertainty for each grid cell is calculated using the formula *U = 2*C*I.*

Case Study and Results

The methodology is applied to a Holocene-Pleistocene sedimentary sequence and used as guidance to set design levels for geological surfaces. The sedimentary sequence contains a range of both anthropogenic, erosional and depositional geological surfaces. To assess the effectiveness of the methodology, the GI data was subsampled then applied as input and test data. This application demonstrates the method's effectiveness in quantifying and communicating uncertainty.

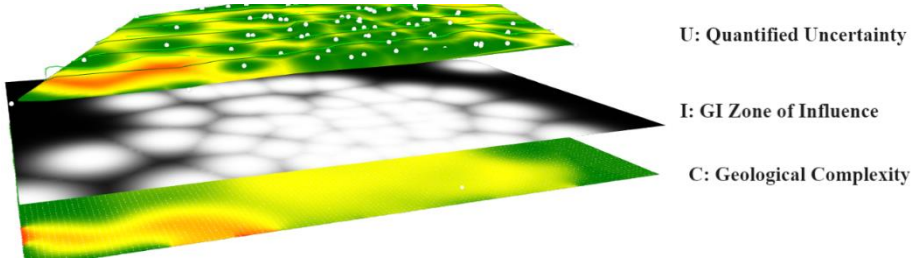

Figure 1. The key compoenents of the methodology visualised as heatmaps

As seen in Figure 1, *C I* and *U* can be displayed as heatmaps, highlighting areas of high risk. The quantified uncertainty can also be displayed as a 95th percentile envelope around a best estimate surface, giving a clear guide on the potential variability of a geological surface (Figure 2).

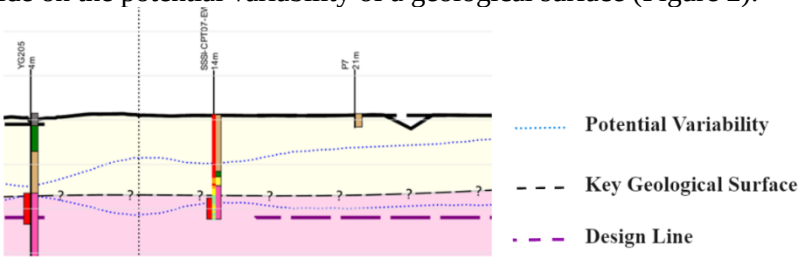

Figure 2. Uncertainty displayed as a 95th percentile envelope

A key weakness of this approach is that it is evidence based and cannot represent hypothesised geological conditions not proven in GI. It is critical that it is used as a decision-making tool paired with a robust conceptual model and geological judgement.

Conclusion

Uncertainty in geological models is a challenging topic often poorly understood and communicated, leading to design decisions disconnected from sound geological judgment. This paper presents a methodology for a systematic, evidence-based approach to quantifying geological complexity. The resulting quantification of uncertainty is clearly communicated, promoting consistent and intelligent design decisions.

References

Fookes, P. (1997). Geology for Engineers: the Geological Model, Prediction and Performance. *Quarterly Journal of Engineering Geology and Hydrogeology, 30*, 293-424.

Lelliott, M. R., Cave, M. R., & Wealthall, G. P. (2009). A structured approach to the measurement of uncertainty in 3D geological models. *Quarterly Journal of Engineering Geology and Hydrogeology*, 95–105. doi:https://doi.org/10.1144/1470-9236/07-081

Parry, S., Baynes, F., Culshaw, M., Eggers, M., Keaton, J., Lentfer, K., . . . Paul, D. (2014). Engineering geological models: an introduction: IAEG Commission C25. *Bulletin of Engineering Geology and the Environment*, 689. doi:10.1007/s100064-014-0576-x

Topic 5

Engineering Geology for the Society

GEOLOGICAL ENGINEERING FOR SOCIETAL & SUSTAINABLE DEVELOPMENT----BANGLADESH A CASE STUDY

ATM SHAKHAWAT HOSSAIN [1]

[1] *Jahangirnagar University, Savar, Dhaka 1342, Bangladesh,, E-mail :* shakhawathos2004@yahoo.com

Abstract

Bangladesh is a South Asian Tropical Monsoonal Country and is facing many climate-related hazards and disasters every year which is a big challenge for the current sustainable development of Bangladesh. Every year casualties due to hazards and disasters are increasing and affecting the food security, livelihood, health, and economic growth of the country. In very recent years Geological Engineering is playing a vital role in managing climate-related issues, challenges, and hazards to become a developed nation by 2041. With the great initiatives of the GoB (Govt. of Bangladesh), several measures have been taken at the policy level to build a sustainable community and a resilient society for all to become the world leader by managing hazards & disasters. Some climate-related hazards, modeling results, hidden ground-related problems, and mitigation measures are presented in this paper to achieve the UN (United Nations) SDG's goals. Renewable & sustainable energy issues and initiatives to reduce the use of carbon emissions will also be discussed. Some examples of recent hazard and disasters and their mitigation measures to reduce rainfall-induced hazard risks are presented as sustainable solutions to reduce slope hazards in the camp area. Role of Geological Engineering certainly can play a vital role in the societal and sustainable development of Bangladesh. Rainwater harvesting technique has been introduced in the temporary shelters of the community dwellers along with low cost drainage system were installed as examples to reduce pore water pressure inside the slopes. These low cost solutions helping the hazard victims to reduce loss and manage water scarcity and sustainability in the investigated area. Suggestions are also recommended to improve the current geoscience and geoengineering-related curricula in the academic institutes including Schools, colleges and Universities to build a smart resilient society and smart Bangladesh to meet the new challenges of the 21st century under the current context of global climate change.

Introduction

Bangladesh is a low-lying country located in South Asia, bordered by India to the north, east, and west, and Myanmar to the south which extends from 20°34' N to 26°38' N latitude and from 88°01' E to 92°41' E. The country's flat topography, location in the Bay of Bengal, and heavy reliance on agriculture make it particularly susceptible to climate-related disasters. According to the Global Climate Risk Index 2021, Bangladesh is the seventh most vulnerable country to climate change in the world. In recent years, the country has experienced several extreme weather events, including cyclones, landslides, floods, and droughts, which have caused significant damage to infrastructure, agriculture, and livelihoods (Climate Vulnerability Index Report, 2023). The average temperature in Bangladesh has been increasing in recent years, with some regions experiencing temperatures above 40 degrees Celsius. Bangladesh experiences a monsoon season from June to September, which is critical for agriculture. However, in recent years, there have been changes in the timing and intensity of rainfall, leading to flooding in some areas and drought in others. Landslides have caused significant damage to infrastructure and have led to loss of life. Besides, sea level rise causing saline water intrusion is another climate driven alarming phenomena for southern region of Bangladesh. All these consequences of climate change significantly affecting the current GDP and threatening sustainability of this developing nation. Geoengineering solutions. Some sustainable geoengineering recommendations are discussed to reduce the hazards and to give benefits to the society & to build a sustainable resilient community.

Methods

The study is followed by Field, Lab methodology and Modeling. Field investigations were conducted in accordance with (British Standard 5930, 1981). Geophysical resistivity test has been conducted according to Wenner array method. Laboratory testing results were analysesd according to (British Standard 1377, 1990 and ASTM method (1974),K.H. Head (1982) & ASTM IS :2720 (Part-12)-1981,

Results

Hossain et al. (2023) discussed that140mm to 280mm of rainfall are sufficient to cause the slope failures in the south eastern folded part of Bangladesh. (Figure 1). Based on all findings some geoengineering sustaianable solutions are recommended to manage climate related hazards and to attain sustainable development of Bangladesh.. Many geoengineering solutions for slope protection, rain water harvesting to reduce water scarcity and water related hazards, climate resilient sustainable housing, new flood level demarcation for sustainable flood resilient infrastructures development in rural and urban areas, renewable energy-based power unit installation, monitoring and EWS installation, the establishment of a National Database are the major recommended geoengineering solutions to fullfill the policy level gap for sustainable development of Bangladesh & to achieve UN SDG's Goals to be a developed nation by 2041.

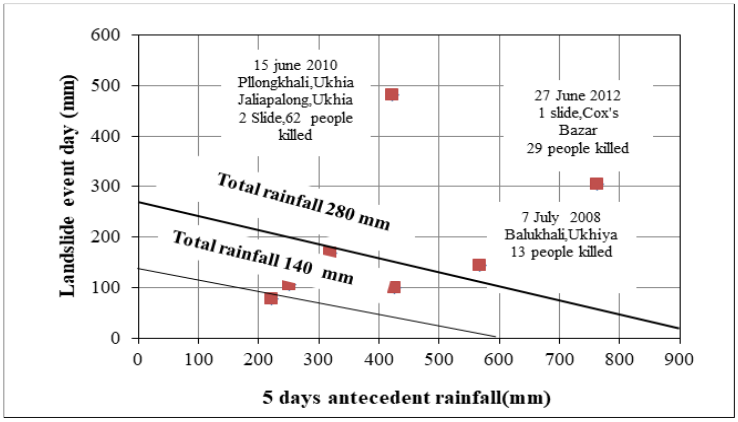

Figure 1: Rainfall Threshold Line of the South Eastern Folded Part of Bangladesh (Hossain et al., 2023)

Conclusion

Geological Engineering certainly can play a vital role in the societal and sustainable development of Bangladesh. Some case study results and Suggestions are also recommended to improve the current geoengineering and geoscience-related curricula in the academic institutes including schools, colleges and Universities to build a smart society and smart Bangladesh and to meet the new challenges of the 21st century under the current context of global climate change.

References

ASTM Standards, 1974. Annual Book of ASTM Standards, Vol 19, 1-643p

British Standard 5930, 1990. Code of practice for site investigations. BS Institution, London.

Hossain, A.T.M.S., Jafrin, S.J., Khan, P. A., Khatun, M., Imam, H., Sayem, M.H., Dutta, T. & Haque, M.E., 2023. The Hidden Geo-hazards In The Rohingya Refugee Camps of Ukhiya, Cox's Bazar, Bangladesh--A Threat For Sustainable Development, Book Volume of IAEG XIV Congress 2023 Chengdu, China, Paper ID: 95. Springer.

Hossain, A.T.M.S., Toll, D.G. & Shushupti, O., 2020. Rainfall Induced Landslide Hazards of Bangladesh: Challenges, Issues and Sustainable Development, International Journal of Scientific & Engineering Research Volume 11, Issue 7, PP. 225-230, DOI: 10.13140/RG.2.2.25981.38884.

THE INTEGRAL ROLE OF ENGINEERING GEOLOGISTS IN DISASTER RISK COMMUNICATION

RANJAN KUMAR DAHAL [1]

[1] *Central Department of Geology, Tribhuvan University, Kirtipur, Kathmandu, Nepal*

Introduction

Disaster Risk Communication (DRC) is the main component in shaping perceptions of disaster risk, influencing preparedness, and impacting decision-making throughout the disaster management cycle. It employs tools like GIS, drones, social media, and early warning systems, with substantial involvement from Engineering Geologists in approaches like hazard mapping and community-based disaster risk reduction.

Effectively communicating disaster risk is vital for saving lives, enhancing preparedness, adaptability, and response capacities of individuals, communities, and institutions, ultimately improving risk management. To achieve this, comprehensive applications of emerging technologies and innovations in disaster risk management by Engineering Geologists are necessary. However, a challenge in DRC arises from restricted data accessibility, often controlled by governmental institutions, leaving engineering geologists in a vulnerable position. Proper data analysis, facilitated by engineering geologists, is crucial for understanding how people live with risk. Data-driven evidence should guide decision-making processes, such as determining evacuations during extreme rainfall warnings. Both data and DRC closely intertwine, influencing individual responses to warnings. Effective best practices for DRC should follow specific rules, including setting clear goals, understanding the audience, considering other sources of information, delivering messages effectively, and using precise and consistent language. In many cases, DRC should be comprehensible, and perception with learning and reasoning associated with DRC should not be neglected afterward, as neglect may lead people to disregard DRC. Engineering geologists must explain disaster risks comprehensively, drawing on geoscience understanding, emphasizing impacts, allowing people to share experiences, being transparent about uncertainties, and avoiding scare tactics. They should also provide options for reducing risk at both individual and community levels, involve stakeholders in planning, and share insights from previous successful implementations.

The extended abstract will focus on the major roles of engineering geologists in the DRC process and provide suggestions on reducing uncertainties. Recognizing risk communication as dynamic and incorporating multi-hazard early warnings can enhance DRC effectiveness in saving lives and improving disaster management.

Multi-hazard early warning systems and DRC

In the context of South Asia, effective multi-hazard early warning systems and disaster risk communication can be achieved through enhanced disaster risk knowledge among local communities and bodies, comprehensive hazard detection, monitoring, analysis, and timely forecasting, efficient warning dissemination, and effective preparedness and response capabilities among the public. Engineering geologists should recognize that risk communication is a dynamic process, not a static outcome, and can be strengthened through multi-hazard early warnings. Effective warning messages should contain five essential elements: the warning source, hazard identification, specific areas at risk, actionable instructions, and guidance on where to seek further assistance, ensuring DRC effectiveness with minimal confusion.

In communicating disaster risks, engineering geologists must explain comprehensively, drawing on geoscience, emphasizing impacts, being transparent about uncertainties, and avoiding scare tactics. They should involve stakeholders, share successful insights, and provide options for risk reduction.

Risk Perception of people

When considering risk perception models, factors such as people's knowledge and understanding of risks, emotional and personal experiences, social amplification of risk, cultural theory, trust, values, gender, education, and ideology play crucial roles (van der Linden, 2017). Dryhurst et al. (2020) found that individuals in major developed countries like the USA, Japan, Germany, South Korea, Sweden, and Italy were less worried about COVID-19. In contrast, people from many developing countries, along with the developed countries of the UK and Spain, were highly concerned about COVID-19 infection. This finding is significant for understanding societal risk perception issues. Numerous studies show that experiential and sociocultural factors explain most of the variance in risk perception models compared to cognition and socio-demographic characteristics. Additionally, during risk communication, people from both developing and developed countries tend to trust governmental activities less and place more trust in non-governmental organizations. The situation is more chaotic in developing countries. For instance, in 2018, the residents of Melamchi Municipality in Nepal were not pleased with the river setback rules imposed by the local government (Figure 1a). However, they experienced severe flood damage in 2021 (Figure 1b). This example illustrates the risk perception of people and the losses they endured despite accurate hazard and risk assessments made by engineering geologists in 2018.

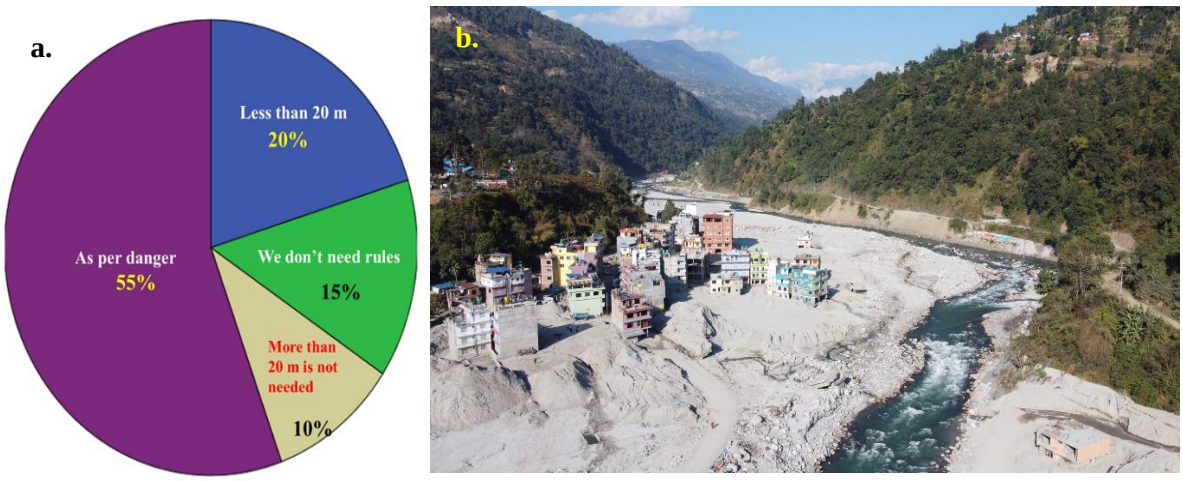

Figure 1. a. People opinion for river set back rules and b. Damaged Melamchi town after 2021 flood which was accurately estimated by engineering geologist in 2018.

Concluding remarks

In fact, the multi-hazard early warning system and disaster risk communication is possible with following activities.

- Enhanced disaster risk knowledge among local people and local bodies (municipalities).
- Detection of hazards, their monitoring, analysis, and forecasting along with communication of possible consequences on time in presence of Engineering Geologists.
- Warning dissemination and communication by effective channels and processes.
- Preparedness and response capabilities of people after warning and getting DRC messages.

Similarly, disaster risk communication (DRC) is a process, not a product, and can be effectively conducted following multi-hazard early warnings, with engineering geologists playing a pivotal role. Effective risk communication requires timely, transparent, dialogic, clear, coherent, empathetic, and proactive processes with the direct involvement of engineering geologists. Additionally, DRC necessitates analysis, planning, credibility, training, and evaluation. Achieving this involves analyzing attitudes and behaviors, understanding and respecting different perspectives, and evaluating effectiveness. There should be coherence between communication, spatial planning, and decision-

making. Moreover, the DRC process must be prepared to address communication paradoxes such as reassurance, efficiency, delegation of responsibility, and ensuring the safety of the people.

References

1. van der Linden S. (2017) Determinants and Measurement of Climate Change Risk Perception, Worry, and Concern, In Nisbet M.C., Schafer M., Markowitz E., Ho S., O'Neill S., and Thaker J. (Eds.), The Oxford Encyclopedia of Climate Change Communication. Oxford University Press, Oxford, UK, Available at SSRN: https://ssrn.com/abstract=2953631 or http://dx.doi.org/10.2139/ssrn.2953631
2. Dryhurst S., Schneider C. R., Kerr J., Freeman A. L. J., Recchia G., van der Bles A. M., Spiegelhalter D. and van der Linden S. (2020) Risk perceptions of COVID-19 around the world, Journal of Risk Research, DOI:10.1080/13669877.2020.1758193(11).

EXPLORING THE EFFECT OF TEMPERATURE ON A CASCADING HAZARD: PROJECTING THE 2021 MELAMCHI FLOOD TO A WARMER CLIMATE

OM PRASAD DHAKAL[1], MARCO LOCHE[1], RANJAN KUMAR DAHAL[2], GIANVITO SCARINGI[1]

[1] *Institute of Hydrogeology, Engineering Geology and Applied Geophysics, Faculty of Science, Charles University, Czech Republic, dhakalo@natur.cuni.cz*

[2] *Central Department of Geology, Tribhuvan University, Nepal*

Introduction

The dependence of the shear strength of geomaterials on temperature may affect the stability of slopes and the propagation of landslides (Scaringi & Loche, 2022). Thermal sensitivity has primarily been observed in pure clays and quartz-clay artificial mixtures. However, evidence exists of significant effects in natural soils, including those from the Melamchi catchment in Nepal, for which weakening has been evaluated at elevated temperatures. Here, we discuss the implications of such evidence in a real-world case study. In 2021, a large-scale disaster occurred in the upper Melamchi catchment (169 km^2), as the outburst of a relatively small glacial lake (~2500 m^3) cascaded down the valley, carrying sediment (>10 Mm^3) with substantial entrainment. The erosion caused slope toe-cutting and numerous landslides, and eventually, the river valley downstream was filled with a thick debris layer (Asian Development Bank, 2021). In the RCP8.5 (worst case) scenario, a 4.9°C warming is expected by the end of the century, with enhanced impact in the alpine Himalayas owing to elevation-dependent warming.

Methods

We incorporated various physical processes (glacial lake outburst, landslides, flood) into a catchment-scale multihazard simulation and compared its result to that of a worst-case scenario, assuming a similar disaster would occur at the end of the century after 4.9°C warming. We developed an input dataset, which we fed to a physically based model – OpenLISEM hazard (van den Bout et al., 2018). The dataset was supplemented by a field campaign during which 71 geotechnical samples were collected and in-situ tests conducted. An engineering geological map of the area was created based on geomorphological interpretation, categorizing the region into soil classes to which geotechnical values derived from the experiments were assigned (cohesion, internal friction angle – IFA, initial moisture content, bulk density, and D50+D90 grain size parameters). Remote sensing sources provided the remaining input rasters. The global elevation product (SRTM) was filtered and interpolated to the desired resolution (20×20 m). Surface parameters were obtained from literature values of the digitally classified (supervised) Sentinel-2 image. Soil depth was modeled using a soil depth model based on the steady-state assumption of soil transport/production. The daily total rainfall from the only station available was used to establish a rainfall intensity equivalent to a 150-year return period flood value using extreme value statistics (Gumbel). Globally available precipitation data from NASA's IMERG (Integrated Multi-satellite Retrievals for GPM) were used to create a design storm with a temporal resolution of 30 min and daily totals based on measured records. Further, 15 landslides were mapped along the river corridor post-disaster during fieldwork. Each landslide was classified according to Varnes, and dimensions, including possible depth to failure, were measured. The landslide volumes were estimated based on their rotational or translational mechanism, and their runout was matched through back analysis. Laboratory-observed changes in IFA due to changes in temperature were assigned to the catchment's spatial domains according to the global clay fraction (SoilGrids250m 2.0, 2021).

Results

The heavy precipitation and the release of landslides during peak discharge facilitated a simulation replicating the Melamchi disaster in 2021. Although the simulation's accuracy based solely on the extent of flooding is not deemed critical, it showed a Kappa value of 0.65. Efforts were primarily focused on calibrating the solids based on data from reports and post-disaster fieldwork. The model underestimated

the solid flow in the absence of fluid, particularly in the upper part of the catchment. Conversely, it overestimated the debris flow height along the lower catchment, especially at the headworks location of the Melamchi water diversion project. The maximum debris flow height simulated at this location was 20 m, compared to the post-disaster visual inspection estimate of ~16 m. The peak water discharge was measured at 442 m³/s with a peak rainfall of ~50 mm/hr across the catchment. For reference, the seasonal peak monsoonal discharge is ~40 m³/sec. Unfortunately, the exceptionally high flood in 2021 was not recorded at the Helambu station because it was swept away by the event. However, the simulation results were consistent with the measured flood height. Given the model's satisfactory fit, we proceeded to simulate the year 2100 scenario, modifying only the IFA. The simulation (**Fig. 1**) indicated an increase in debris flow height along the catchment channel by <1 m. Despite being rather small, this difference, combined with the increased flow velocity, could result in an increased impact pressure of the debris flow. Additionally, longer runout should be simulated owing to the decrease in friction coefficient, but the results remain unclear as the runout of the landslides occurred perpendicular to the river valley and impacted the opposite bank. Finally, the simulation is progressing to incorporate sediment transport during the event, which requires highly calibrated input. The anticipated changes in sediment flux are crucial, as the river is a potential source of drinking water for the people of the Kathmandu Valley.

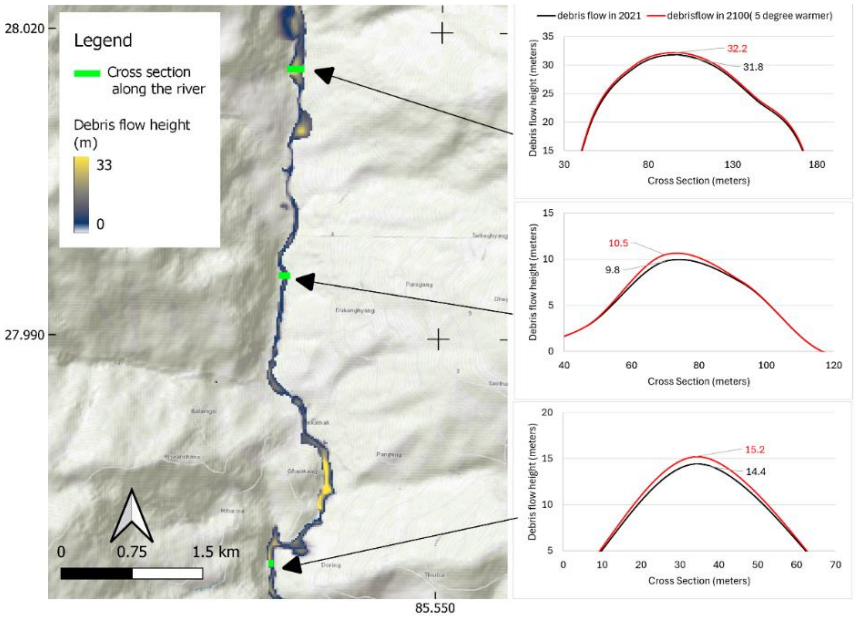

Figure 1. Simulation of the Melamchi disaster (left); back-calculated and projected debris flow heights (right).

Conclusion

We back-analyzed the 2021 Melamchi disaster by incorporating the key processes that occurred during the event. Then, we simulated the same disaster in a worst-case warming scenario (4.9°C increase in temperature) according to the experimentally measured decrease in the soil's shear strength. We evaluated an increase in debris flow height and changes in debris flow velocity, suggesting that further research is needed, particularly in developing a coupled thermo-hydro-mechanical model for catchment scale hazard analysis. Additional experiments are currently underway to clarify thermal effects in natural soils and their potential implications for natural hazard analysis.

References

Asian Development Bank (2021). *Mapping Hazards in Nepal's Melamchi River: Catchment to Enhance Kathmandu's Water Security*. https://dx.doi.org/10.22617/TCS230541-2

Scaringi, G., & Loche, M. (2022). A thermo-hydro-mechanical approach to soil slope stability under climate change. *Geomorphology*, 401, 108108.

van den Bout, B., Jetten, Victor., De Roo, Ad., van Westen, C. J., & Ritsema, Coen. (2018). *OpenLISEM Multi-Hazard Land Surface Process Model*. https://blog.utwente.nl/lisem/

LABORATORY RAINFALL TEST ON PISTON FLOW PHENOMENA INVOLVING PORE AIR PRESSURE IN LANDSLIDE MASS

GEN FURUYA [1], DAICH HABASHITA [2], GONGHUI WANG [3]

[1] *Toyama Prefectural University, Japan, gfuruya@pu-toyama.ac.jp*

[2] *Taisei Corporation, Japan, hbsdit00@pub.taisei.co.jp*

[3] *Kyoto University, Japan, wang.gonghui.3r@kyoto-u.ac.jp*

Introduction

We continuously monitored the 1m-depth-ground temperature and water level of boreholes to clarify the role of groundwater flow in movement of Nishi-Ikawa landslide, a reactivated one on crystalline schist area. The monitoring results show that groundwater in the landslide mass flows in a vein-like pattern and abnormal variation of ground temperature (decreasing in summer and increasing in winter) occurs during heavy rainfall (e.g. Furuya et al., 2021). This suggests that groundwater flows within the slope cannot be explained by the commonly accepted rainfall-infiltration process. We then assumed that this process may result from the piston-flow-like extrusion of groundwater that was recharged more than a decade ago during infiltration processes in heavy rainfall (e.g. Furuya et al., 2022), and pore-air in the infiltration pass may have involved in this process. To examine these assumptions, we conducted indoor experiments, and some results are presented in this study.

Methods

Figure 1 shows a schematic diagram of the experimental apparatus. The landslide slope was modelled by connecting a rubber water hose to two cylindrical pipes with a water head difference of 100 cm between them. To reproduce a slow flow path between the two cylindrical pipes, the rubber water hose was filled with methylcellulose water solution (concentration of 15%), which has been widely used as a viscous pore fluid in centrifuge and other kind of tests (e.g. Stewart et al., 1998). The bottoms of both cylindrical tubes were filled with 10 cm of gravel and saturated with distilled water. On top of the gravel, a specimen (Silica sand: D_{50} = 0.147 mm) was tamped and filled every 10 cm up to the top of the cylindrical tube. Inside the cylindrical tubes, a buried water pressure gauge was placed at the height of 70 cm, a digital barometer was placed at a height of 50 cm from the base, and a pore pressure gauge was placed at the base of the cylindrical tube. Artificial rainfall was applied with a water spray nozzle 200 cm above the top of both cylindrical pipes. The rainfall intensity was 100 mm/h. The initial water content and the number of compaction cycles were changed, and the behaviour of the pore air pressure was monitored under each test condition.

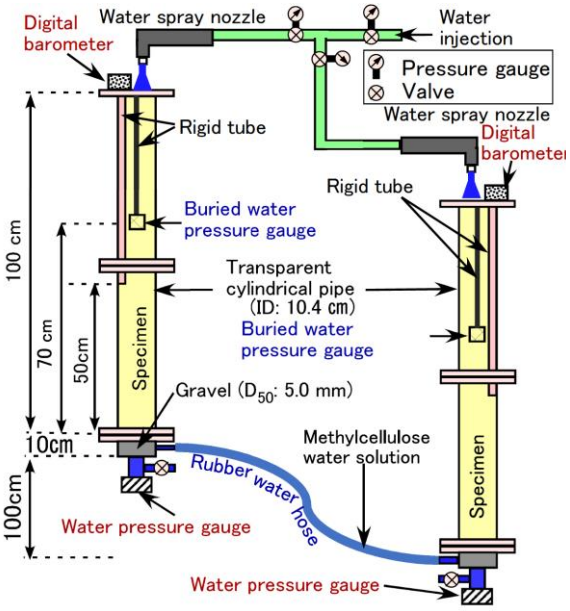

Figure 1. Schematic diagram of the test apparatus

Results

Figure 2 shows the test results. (A) shows the relationship between the water content, the start time of the generating in pore air pressure (based on the start of rainfall) (PAP), and the maximum PAP value under the condition of one tamping cycle (*e*: 1.21-1.24). (B) shows the relationship between the void ratio and the maximum PAP value under 0, 1, and 3 tamping cycles.

In Figure 2(A), the red symbols indicate the relationship between the initial water content and the time at which the PAP increased. It is seen that the higher the initial water, the earlier the starting time of the increase in PAP. The blue symbols show the relationship between the initial water content and the maximum PAP. The initial water content of the specimen was set to 5, 10, 15, and 20%. It is also noticed that the maximum value of PAP during rainfall infiltration is larger for higher initial water content. These results suggest that during rainfall infiltration, the higher the initial moisture content, the more likely the upper part of the specimen will be quikly saturated, and with the descending of wetting front, the air in the pores is less likely to escape into the atmosphere, resulting in a greater increase in the PAP. On the other hand, when the initial moisture content is smaller, it is difficult for the soil layer to be unsaturated, such that the air in the pores escapes more easily into the atmosphere with the descending of wetting front, resulting in a lower increase in the PAP. These results indicate that the moisture condition in the soil before heavy rainfall may influence the rise in pore water pressure due to pore air (pushing out groundwater).

Figure 2(B) shows that the PAP generated during rainfall increases linerly as the void ratio of the specimen decreases with a correlation coefficient of 0.97. This suggests that as the void ratio within the soil layer decreases, the soil's water retention capacity improves during rainfall infiltration (due to increased adsorption water between soil particles), leading to the entrapment of air within the specimen when the pores are filled with adsorption water (acting as a kind of seal). Conversely, when the void ratio is great, the abundance of voids within the specimen allows air to escape, and the wetting front does not descend uniformly, resulting in ineffective air entrapment during rainfall infiltration. Therefore, it is concluded taht the void ratio also plays a role in the increase of pore air pressure.

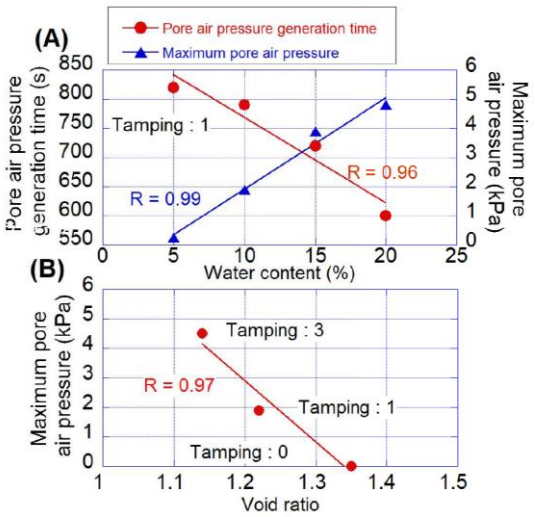

Figure 2. Test results
(A) Relationship between the water content, the start time of the generating in pore air pressure, and the maximum pore air pressure; (B) Relationship between the void ratio and the maximum pore air pressure

Conclusions

When the moisture content of the specimen is greater, air is more easily trapped within the pores during rainfall, leading to a quicker increase in PAP and a greater maximum value of PAP. The lower the void ratio of the specimen, the more adsorption water exists between soil particles, causing the wetting front to act as a sort of seal that traps air, making it easier for PAP to rise.

Acknowledgments

This study was supported by the collaborative research program (2021G-08) of the Disaster Prevention Research Institute of Kyoto University, JSPS KAKENHI (Grant Number JP19H022238).

References

Furuya, G.; Wang, G; Ihara, J.; Suemine, A.; Asai, K. Unravelling the groundwater behaviour in landslide mass during heavy rain by multi-layer ground temperature monitoring, *In Proceedings of the 14th Congress INTERPRAEVENT 2021, Bergen, Norway*, 2021, 5p.

Furuya, G.; Habashita, D.; Win, T.; Wang, G.; Suemine, A. Laboratory rainfall experiments on piston flow phenomena in landslide mass, *Proceedings of the 61st Annual Meeting of the Japan Landslide Society*, 2022, pp. 156-157 (in Japanese).

Stewart, D.; Chen, Y.; Kutter, B. Experience with the use of Methylcellulose as a viscous pore fluid in centrifuge models, *Geotechnical Testing Journal*. 1998, 21 (4), 365-369.

RESILIENCE

ANN WILLIAMS [1]

[1] *Beca Ltd, New Zealand, ann.williams@beca.com*

Introduction

New Zealand experienced widespread flooding and landslides (estimates of circa. 800,000 landslides (GNS 2023)) in early 2023 when cyclones Hale and Gabrielle made land in quick succession, severely impacting the north and east of the North Island. The impacts were such that a National State of Emergency was declared for the third time only, in New Zealand's history (the previous two times were the COVID pandemic and the Canterbury earthquake sequence, all within the last 15 years).

As we begin to see first-hand the impacts of severe weather events on our communities and infrastructure, we find ourselves at the cross-roads of decision making, considering risk and actions to expedite recovery, in the face of climate change. We find ourselves grappling with difficult questions and hard choices to drive resilience in an environment in which circular economy-based design is in its infancy, traditional warning and response systems are not effective across regions (early warning – to what effect?), traditional design and construction approaches are too slow, and government finances are stretched to imbalance.

The Cyclone Gabrielle Example

Unprecedented rainfall triggered a landslide that took out a 120 m long section of state highway (SH) 25A, a principal access between the west and east coasts of the Coromandel Peninsula, North Island, New Zealand. Three remedial options were considered: go around, build up from the valley floor with MSE walls, or bridge. A bridge option was selected because of the higher reliability of construction time (not lower cost) in the face of likely further rainfall and saturated deeply weathered volcanic soils. Construction began in June 2023 and the highway was re-opened about 10 months from the date that landsliding occurred, about half the time a bridge of this type would take to design and construct. This was achieved by collaboratively applying an existing bridge design (consultants and contractors working together) which allowed available materials, including repurposed steel plates for bridge beams that had been imported for another project, to be diverted for immediate use. Currently value is equated with lowest cost, but real value (increased tourism spend and GDP in the region) was achieved through faster return to service without compromising design or quality of materials (INZ 2024).

Figure 1. Upper left: landslide impacting SH25a. Upper right: bridge solution under construction (photograph from Waka Kotahi NZ Transport Agency)

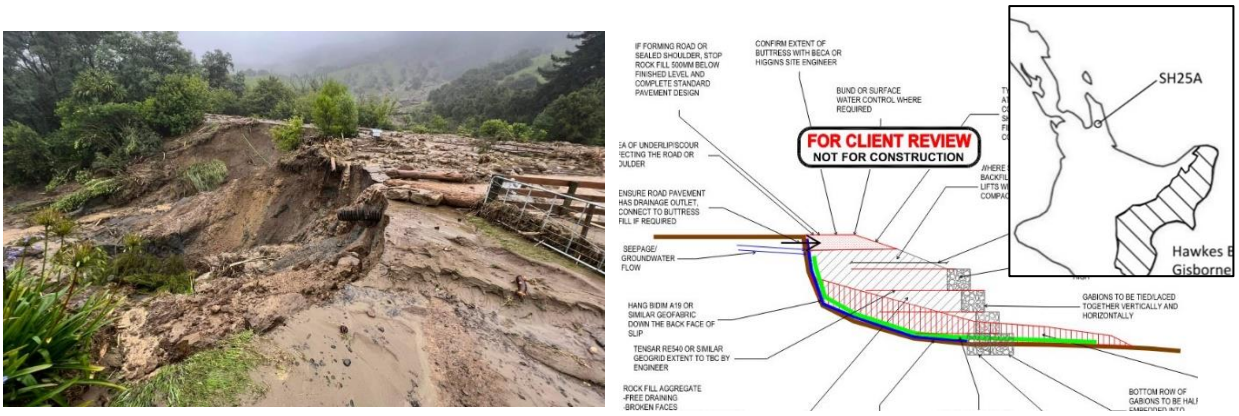

Figure 2. Example slip and standard design remediation from SH5, Hawkes Bay region (shaded on inset map).

Flooding and loss of State Highways and bridges (several sections of SH2, SH5, SH38, SH550 and SH51) was widespread across the Hawkes Bay region with links in and out of the region, power, phone and internet cut off. There were hundreds of similar underslip sites, and it rapidly became clear that there is a difference in needs between new build and emergency works or so-called "resilience" works. Applying traditional processes and standards is time consuming and costly, with repairs getting held up by options studies. Developing standard designs across a road corridor and standard design details across a region, applied by contractors with engineering geological and geotechnical support, allowed access routes to be opened up and a collaborative approach to temporary and permanent works solutions established. Pre-agreement of design life, factor of safety and departures from code were key factors in re-establishing links, noting that stretches of the highways remain vulnerable to future weather events.

Discussion

Climate resilience can be defined as "the ability to anticipate, prepare for and respond to the impacts of a changing climate, including the impacts that we can anticipate and the impacts of extreme events..." (MfE 2022). Understanding the risk of climate related instability requires understanding the hazard and its probability (e.g., AGS 2007a, GNS 2023), but climate change increases uncertainty giving us a decreasing ability to predict the impacts, which are complex. Politicians use slogans like "build back better" and "resilient infrastructure", but there is a mismatch of expectation between infrastructure owners, insurers, designers and the public around what "resilience" means. Understanding the interdependencies between infrastructure networks is key to resilience – the resilience of one infrastructure sector often depends on the resilience of others. We need to ask ourselves which highways must perform and which we can allow to fail and repair more frequently? The examples demonstrate that we need to apply scenario testing, options analysis, and adaptive planning now, before the next extreme weather event makes landfall. We need to develop standard methods of assessment and tools to provide comparable judgements around response across a network.

References

AGS (Australian Geomechanics Society) *Guidelines for Landslide Susceptibility, Hazard and Risk Zoning for Land Use Planning*, 2007a.

GNS Science (Institute of Geological and Nuclear Sciences) *Hazard Risk Management Framework,* 2023.

INZ (Infrastructure New Zealand) *SH25a Taparahi Bridge Case Study*, February 2024. Available online: https://infrastructure.org.nz/wp-content/uploads/2024/02/Infrastructure-NZ-SH25A-Taparahi-Bridge-Case-Study-DIGITAL.pdf.

MfE (Ministry for the Environment) *Aoteoaroa New Zealand's First National Adaptation Plan* 2022.

FAILURE MECHANISMS OF SOFT ROCK CLIFFS DUE TO SEA WAVE MOTION: A NUMERICAL INSIGHT

PIERNICOLA LOLLINO [1], GIOACCHINO FRANCESCO ANDRIANI [1]

[1] *Department of Earth and Environmental Sciences, University of Bari Aldo Moro, Italy, piernicola.lollino@uniba.it*

Introduction

The evolution of soft rock coastlines is mainly related to natural factors, as for example the environmental weathering processes as well as the impact of strong wave loading. Severe sea storms and intense rainfalls are seen to increase in intensity and frequency, according to the worldwide acknowledged climate change, which is recognized to be particularly intense in the last years. Wave impact stress during energetic sea storms can represent the triggering factors of coastal instability processes, giving rise to the development of rock mass failures and consequent coastal retreat (Gong et al. 2018; Lollino et al. 2021). Concerning the impact of wave action on rocky cliffs, wave impact are supposed to induce fatigue processes in soft rocks, so that, after several wave storms, with repeated loading applied to the cliff, rock starts to fail with the generation of macro-discontinuities that tend to propagate upslope to involve the whole cliff. In this perspective, some authors have also demonstrated through laboratory tests the effect of fatigue processes on soft rocks (Cerfontain & Collin 2018; Li et al. 2001). Numerical analyses have also become important tools to investigate the response of slopes and coastal cliffs under the effects of specific predisposing, preparatory and/or triggering factors (Perrotti et al. 2019; Amorosi et al. 2019). In this work, the recent evolution of a soft rocky coastal stretch on the Italian southern Adriatic sector is analysed. To investigate the most important contributing factors to coastal evolution, a numerical finite element analysis focusing on an ideal soft calcarenite rock cliff has been carried out. In particular, the role of impact loading due to strong sea motion, in accordance with the typical sea storm features in the area, is analyzed.

Methods

In order to investigate the role of wave action at the toe of soft rocky cliffs, a finite element model representing typical geometrical features of the cliffs outcropping along the south-eastern coastlines of the Apulia region has been developed. The cliff is 12 m high and is affected by a wave height of 3 m. The sea wave is simulated by means of a trapezoidal loading function, with a maximum value of 300 kPa. The behavior of the calcarenite rock is analyzed by means of an elasto-plastic constitutive model, with a Mohr-Coulomb strength envelope, with $c' = 200$ kPa and $\phi' = 30°$. A tension cut-off with a tensile strength of 160 kPa is also assumed. The boundary conditions are the standard ones, with total fixities at the bottom of the model and null displacement along the external vertical sides. A gravity loading condition is assigned at the beginning of the analysis in order to initialize the stress state of the rock mass.

Results

The numerical results indicate that strong wave impacts can induce plastic shear strains at the toe of the cliff, from which failures can propagate upwards involving the whole cliff. In particular, Figure 1 shows the concentration of plastic points at the toe of the cliff, along with the quite remarkable horizontal displacements resulting from the application of wave impact loading. A large number of analysis, adopting different assumptions in terms of material properties and wave loading impact have been also carried out to investigate the role of such features.

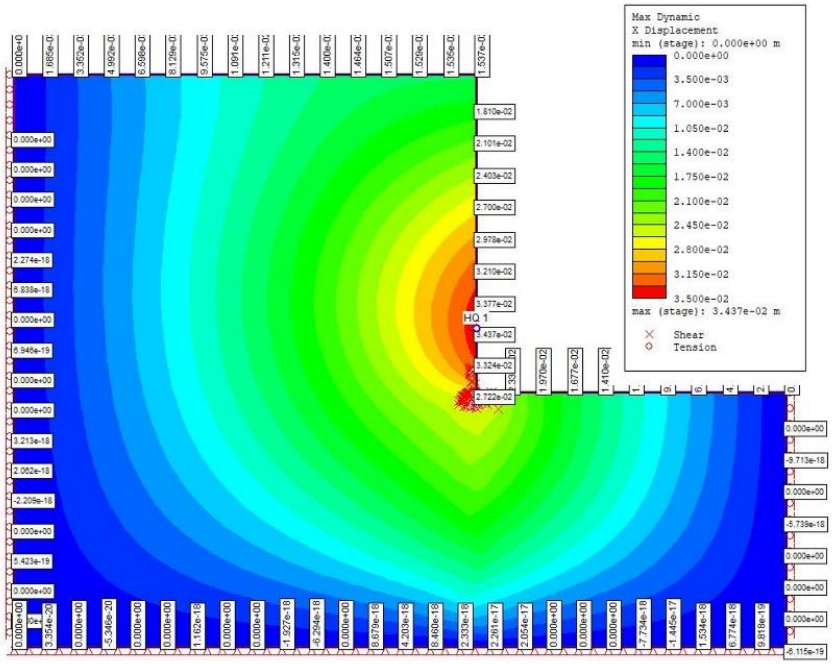

Figure 1. Horizontal displacements and plastic points calculated as an effect of wave impact.

Conclusion

The numerical analysis has highlighted the impact of wave loading as a triggering factor to induce failure in the soft rock cliffs. Although using a simple constitutive model, some interesting results have been achieved in this perspective. More sophisticated constitutive models need to be applied in order to verify the effect of rock fatigue in the generation of cliff failure, even ad lower wave impact levels.

References

Amorosi, A.; Rollo, F., Gagliardini, L. *The analysis of weak rock block behaviour by an advanced constitutive model*. CNRIG, La Ricerca Geotecnica per la Protezione e lo Sviluppo del Territorio, Lecco. 2019.

Cerfontaine, B.; Collin, F. *Cyclic and fatigue behaviour of rock materials: review, interpretation and research perspectives*. Rock Mech. & Rock Engng. 2018, 51: 391-414. Doi: /10.1007/s00603-017-1337-5.

Gong, B.; Wang, S.; Sloan, S.W.; Sheng, D.; Tang, C. *Modelling coastal cliff recession based on GIM-DDD method*. Rock Mech. & Rock Engng. 2018, 51: 1077-1095. Doi: 10.1007/s00603-017-1382-0.

Li, N.; Chen, W; Zhang, P; Swoboda, G. *The mechanical properties and a fatigue-damage model for jointed rock masses subjected to dynamic cyclical loading*. Int. J. Rock Mechanics & Min. Sci. 2001, 1071-1079.

Lollino, P.; Pagliarulo, R.; Trizzino, R.; Santaloia, F.; Pisano, L.; Zumpano, V.; Perrotti, M.; Fazio, N.L. *Multi-scale approach to analyse the evolution of soft rock coastal cliffs and role of controlling factors: a case study in south-eastern Italy*. Geomatics, Natural Hazards and Risk. 2021, 12(1). Doi: 10.1080/19475705.2021.1910351.

Perrotti, M.; Godone, D.; Allasia, P.; Baldo, M.; Fazio, N.L.; Lollino, P. *Investigating the susceptibility to failure of a rock cliff by integrating Structure-from-Motion analysis and 3D geomechanical modelling.* Remote Sensing 2019, 12, 3994, doi: 10.3390/rs12233994.

THE IMPORTANCE OF TOPOGRAPHIC POSITION ON LANDSLIDE FORMATION NEAR KUTINA

DAVOR POLLAK [1], NINA HEĆEJ [2], IRIS BOSTJANČIĆ [3], VLATKO GULAM [4]

[1] *Croatian geological survey, Sachsova 2, 10000 Zagreb, Croatia;,* davor.pollak@hgi-cgs.hr

[2] *University of Bergen, Faculty of Mathematics and Natural Sciences, Allégaten 41, 5007 Bergen, Norway,* nina.hecej@uib.no

[3] *Croatian geological survey, Sachsova 2, 10000 Zagreb, Croatia;,* iris.bostjancic@hgi-cgs.hr

[4] *Croatian geological survey, Sachsova 2, 10000 Zagreb, Croatia;,* vlatko.gulam@hgi-cgs.hr

Introduction

This research analyses possible preferred topographic positions of landslides in the research area. Namely, the landslide inventory (created for the safEarth and RESPONS-a Interreg IPA CBC projects) in the southwest slopes of Mt. Moslavačka gora revealed grouping of landslide locations in grapelike clusters around gullies and water courses (Pollak at al., 2022). That observation is further analysed here on the updated landslide inventory which now contains more than 1700 landslides within an area of almost 130 km^2.

The topographic position and landform analysis of the research area is done using Topographic Position Index (TPI).

Methods

This research explores typical landforms in the terrain and topographic position of landslides in the natural environment. The analysis are based on LiDAR-derived DEM (with a resolution of 0.5x0.5 m) and geological map in the scale 1:300 000 (HGI, 2009).

Firstly, DEM derivates (slope angle map, hillshade, contour map) and orthophoto was used to build very detailed landslide inventory. The same DEM was used to compute Topographic Positioning Index (TPI) for the whole research area. TPI compares the elevation of each cell in a DEM to the mean elevation of a specified neighbourhood around that cell (Weiss, 2001).

Although TPI calculations are very straightforward in ArcMap software, the analysis are done with caution. Namely, TPI values are highly scale dependant and determined by neighbourhood (window) size. Small neighbourhood (window) determine small hills and valleys, while large neighbourhoods capture larger-scale features like mountain ranges and plateaus (Jennes, 2006). Therefore, neighbourhood size should be appropriate for the morphology of the terrain, phenomenon being analysed and the purpose of the analysis.

The TPI results also depend on neighbourhood geometry. The application provides several neighbourhood types (circle, annulus, wedge, rectangle), but the authors believe that circular shape is most appropriate for our analysis. A circular neighbourhood is composed of cells whose cell centres fall within certain radius from the focal cell.

Results

Regarding general geomorphological characteristics, the flattest terrain is typical for delluvial, proluvial and of course alluvial sediments and regions.

Loose or poorly cemented deposits (M_6^2, M_7 and Pl_1) have well developed drainage network with frequent gullies and ridges in between. That enables the formation of relatively steep natural slopes in between them, which frequently sets preconditions for many slope instabilities (landslides) in the region. The contrast are loess sediments which usually don't have ridges and gullies detected.

Deep, steep and frequent gullies are found in migmatites and granites (Pz-Mz) and well-cemented sediments (M_4 and $M_{2,3}$).

In this study, TPI values are used to differentiate four topographic positions:

1. Ridge – highly positive TPI values represent locations that are higher than the surroundings, at or near top of the hill or ridge;
2. Gulley – very negative TPI values indicate positions which are lower than average of the surroundings, at or near the bottom of the valley
3. Upper slope – moderately positive TPI values
4. Lower slope - moderately negative values

Since TPI values are highly scale dependent, several neighbourhood sizes were tested (100, 250 and 500 m). Among them, a neighbourhood radius of 250 meters provides the most realistic positioning of named topographic classes in the research area.
The analysis indicates that landslide polygons are dominantly positioned on the lower slope for all tested scales (Figure 1). It can also be seen that neighbourhood circle with a radius of 250 m puts greater emphasis on the lower slope as the location for most of the landslide polygons, which corresponds to the nature of these landslides.

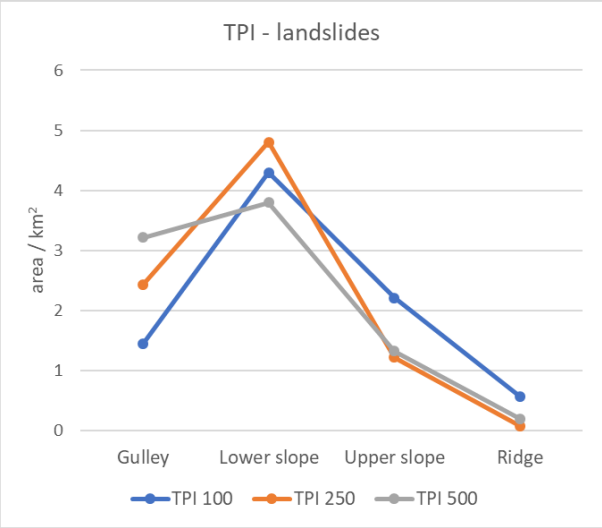

Figure 1. Topographic positions of landslides based on TPI values calculated for neighbourhood sizes of 100, 250 and 500 m.

Conclusion

The topographic analysis unambiguously proves the assumption that landslides in the research area are strongly related to the network of incised watercourses. Given that the great majority of landslides occur at lower slopes and at the edges of gullies, it is obvious that erosional activity of surface waters plays important role in landslide initiation, alongside common factors such as slope angle and pore pressure. This means that further studies should promote TPI as an important factor in detailed landslide susceptibility mapping.

References

HGI. Geological map of the Republic of Croatia, M: 1 : 300 000. *Croatian Geological Survey, Zagreb, Croatia.* 2009

Jenness, J.. Topographic Position Index (tpi_jen.avx) extension for ArcView 3.x, v. 1.3a. *Jenness Enterprises. Available at: http://www.jennessent.com/arcview/tpi.htm* .(assessed January 2006)

Pollak, D.; Hećej, N.; Grizelj, A. Landslide inventory and characteristics, based on LiDAR scanning and optimised field investigations in the Kutina area, Croatia. *Geologia Croatica*. 2022, 75/1, 83-99. https://doi.org/10.4154/gc.2022.02

Weiss, A. Topographic position and landforms analysis. *In: Poster presentation, ESRI user conference, San Diego, CA*. 2001.

ENGINEERING GEOLOGY FOR THE SOCIETY: EXAMPLES FROM ZAGREB CITY AREA, CROATIA

LASZLO PODOLSZKI [1], TOMISLAV NOVOSEL [1]

[1] *Croatian Geological Survey, Croatia,* lpodolszki@hgi-cgs.hr, tnovosel@hgi-cgs.hr

Introduction

Sustainable development relies on adequate planning for which reliable and quality data is needed. From detailed and up to date data, usable and practical thematic maps can be developed and used in geohazards assessment and urban planning. Geohazards include a variety of phenomena but in this paper the focus is on the conducted engineering geological studies in Zagreb city area (~641 km^2) by Croatian Geological Survey with emphasis on the development of geological and seismic zonation(s) (Miklin et al., 2019), detailed engineering geological maps (Miklin et al., 2007), landslide inventories (Miklin et al., 2018) and terrain stability and zonation maps (Podolszki and Terzić, 2023). These studies cover time span of more than 20 years and the aim of these studies were to improve the geohazards management and sustainable development of the Zagreb city metropolitan area.

Methods

In the Zagreb city area numerous researches and studies were conducted during the last decades, but the relevant data regarding the aspect of engineering geology and geohazards are relatively scarce. Still, there are valuable studies/data in which detailed data about engineering geological properties (Miklin et al., 2007), landslides (Miklin et al., 2018), ground type of sediments (according to Eurocode 8, Miklin et al., 2019) and geological zoning (Podolszki and Terzić, 2023) can be found. Detailed data for the part of the research area (~175 km^2, ~25% of Zagreb city area), gives insight regarding the landslide locations and type of sediments present in the ~1/4 of the Zagreb city area. Still, it must be emphasized that for the rest of the Zagreb city area (~3/4), detailed investigations are needed.

Results

Developed detailed engineering geological maps provide information about physical and mechanical properties of materials and about characteristic surface processes and phenomena for the area (geohazards, with emphasis on landslides), including the information about lithology, stratigraphy, and tectonics and as such they should be considered as standard for other areas in Croatia (Miklin et al., 2007; Miklin et al., 2018). Within seismic and geological micro zonation for the part of the Zagreb city area the geological, geotechnical, geophysical and seismic characteristics of the research area were compiled and addressed (Miklin et al., 2019). Ground type determination and description was performed and the research results were also presented on developed seismic zonation map in accordance with Eurocode 8 in scale of 1:25,000 where areas of equal soil amplification relative to the bedrock were depicted (Miklin et al., 2019). Finally, based on available geological data and small-scale maps, geozonation of Zagreb city area was conducted and a new map in scale of 1:100,000 was developed (Podolszki and Terzić, 2023). Although the developed map gives insight into geological conditions for the whole area of Zgareb city and differs four zones with six geological complexes, the developed map is a small-scale map. It can be used as guideline towards seismic risk assessment as characteristic phenomena (geohazards) for each geological complexes are defined and a ground type assessment according to Eurocode 8 is given (Podolszki and Terzić, 2023). Still, for direct use in urban planning the developed map needs to be upscaled to scale 1:25,000 (or more) with detailed (geo)data (currently non-existent or non-available for the whole research area).

Conclusion

To conduct the aforementioned studies relatively large funding was required and interdisciplinary teams of researchers throughout the years. Still, once collected detailed and quality (engineering geological) data remains as constant value as base for further updates and analysis. On the other hand, it is a never-ending process: as new data and techniques become available and/or the research area goes through changes/development – there is always room for the improvement of the developed thematic engineering geological maps (in wider sense). The best way to cope with geohazards and urbanization at Zagreb city area (or any other area) is to conduct geo-researches periodically and interdisciplinary with new technologies applied and up-to-date methodology. By adopting that approach green, safe and sustainable development can be reached.

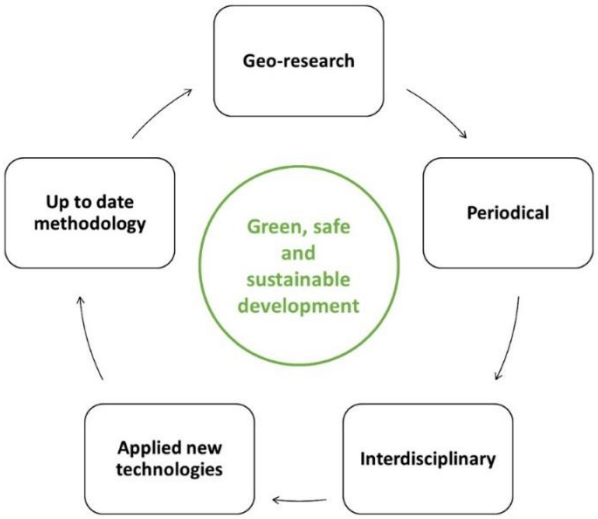

Figure 1. Never-ending process (cycle) of geo-research towards green, safe and sustainable development.

References

Miklin, Ž.; Mlinar, Ž.; Brkić, Ž.; Hećimović, I. Detaljna Inženjerskogeološka Karta Podsljemenske Urbanizirane Zone Mjerila 1:5000 (DIGK-Faza I) [Detailed Engineering–geological Map of Podsljeme Urban Area in Scale of 1:5000 (Phase I)—In Croatian]. Croatian Geological Survey, Zagreb, Croatia, 2007, Books 1-4, 44 maps.

Miklin, Ž.; Novosel, T.; Podolszki, L. Seizmička i geološka mikrozonacija dijela grada Zagreba – Knjiga 1 [Seismic and geo-logical microzonation for the part of the Zagreb city area – Book 1—In Croatian]. Croatian Geological Survey, Zagreb, Croatia, 2019, 1-178, 1 map.

Miklin, Ž.; Podolszki, L.; Novosel, T.; Sokolić, Ž.; Ofak, J.; Padovan, B.; Zailac, K. Detaljna Inženjerskogeološka Karta Podsljemenske Urbanizirane Zone Mjerila 1:5000 (DIGK-Faza II)[Detailed Engineering–geological Map of Podsljeme Urban Area in Scale of 1:5000 (Phase II)—In Croatian]. Croatian Geological Survey, Zagreb, Croatia, 2018, Books 1-6, 41 maps.

Podolszki, L.; Terzić, J. Procjena potresnog rizika grada Zagreba – Geološki elaborat [Zagreb city seismic risk assessment – Geological report—In Croatian]. Croatian Geological Survey, Zagreb, Croatia 2023, 1-49, 1 map.

INTEGRATION OF LOCAL RELIEF INTO SMALL-SCALE LANDSLIDE SUSCEPTIBILITY MAPPING

IRIS BOSTJANČIĆ [1], GULAM VLATKO [2], POLLAK DAVOR [3]

[1] *Croatian geological survey, Croatia, ibostjancic@hgi-cgs.hr*

[2] *Croatian geological survey, Croatia, vgulam@hgi-cgs.hr*

[3] *Croatian geological survey, Croatia, dpollak@hgi-cgs.hr*

Introduction

Landslide susceptibility maps (LSMs) provide insight into the spatial likelihood of landslides occurring (Fell et al., 2008). The scale of these maps depends on their intended use and the size of the investigated area. Small-scale LSMs, covering areas over 10,000 km^2 at scales smaller than 1:100,000, inform policy makers and the general public (Cascini, 2008). However, creating such maps for large areas presents challenges concerning the consistency and quality of available landslide inventories and input data from which geo-environmental conditioning factors are derived.

Geological characteristics significantly affect landslide occurrence, with slope angle often serving as the primary indicator of the stability of certain areas. Consequently, lithology and slope are commonly incorporated into small-scale LSMs. However, slope is strongly influenced by the resolution of the digital elevation model (DEM) from which it is derived. Since the derivation of small-scale LSMs implies a coarser DEM resolution, in this study, slope is substituted with local relief, which measures the difference between the highest and lowest elevations in an area (Smith, 1935), indicating the potential energy for mass movement.

Methods

The study area encompasses the entire northern and eastern continental part of Croatia, covering 29,785.5 km2. It generally belongs to the Pannonian Basin System, covered with numerous geological units. While Neogene and Quaternary deposits, varying from marls and carbonate rocks to various clastic sediments, are predominantly exposed on the surface, Pre-Neogene basement rocks are locally exposed on the slopes or cores of the mountains within the study area.

To test the applicability of local relief in landslide susceptibility assessment, two scenarios are evaluated, using geological units and slope as the conditioning factors in the first scenario (LSM1) and geological units and local relief in the second scenario (LSM2). Geological units are obtained from a 1:300,000 scale Geological Map of the Republic of Croatia (HGI-CGS, 2009), while slope and local relief are derived from a 25 m resolution DEM based on a 1:25,000 scale topographical map using Arc GIS tools (Slope and Focal statistics). To calculate local relief, the Range statistics type is used with a defined neighborhood distance of 1,200 m.

Four different sources of landslide inventories, containing a total of 1,003 landslides, are utilized. Three inventories are synthesized from historical geological maps, namely, the Engineering Geological Map of SFRY at a scale of 1:500,000 (Čubrilović et al., 1967), the Kutina sheet of the Basic geological map of the Republic of Croatia at a scale of 1:100,000 (Crnko, 2014), and a draft field geological maps at a scale of 1:25,000. This data forms the training dataset for modelling the LSMs. A landslide inventory from the publicly accessible web portal "Report a Landslide" (https://www.hgi-cgs.hr/prijava-klizista/) is used as the testing dataset to validate the LSMs' performance.

The Frequency Ratio (FR) method is employed to assess landslide susceptibility. Using 765 landslides from training dataset, FR weights are calculated, normalized, and assigned to each factor category. By summing the weights of conditioning factors, a landslide susceptibility index (LSI) is calculated. Finally,

to enable the zonation of the study area according to zones of similar landslide susceptibility, LSI values are reclassified into 4 landslide susceptibility zones (LSZs): (1) low, (2) moderate, (3) high, and (4) very high. In both scenarios, the Natural Break classification is used to define LSZs, enabling consistent LSI classification and clear comparison of LSMs. LSM1 and LSM2 are adjusted for small-scale presentation and are resampled to a resolution of 150 m. The accuracy of LSMs is evaluated through relative landslide density (RLD), which is calculated as the ratio between the percentage of the number of landslides within each LSZ and the percentage of the area of a certain susceptibility zone. RLD is calculated using both the training (765) and testing (238) landslide datasets to test the model effectiveness (i.e., success rate) and the model accuracy (i.e., predictive rate), respectively.

Results

The final results of this study, the effectiveness and accuracy of the LSM1 and LSM2 models, are represented in Table 1. It can be observed that for both LSMs, the RLD increases towards the very high LSZ. Specifically, the number of landslides and RLD for LSM2 for both training and testing datasets are larger within very high LSZ compared to LSM1. Also, the number of landslides and RLD for LSM2 are smaller within the low LSZ compared to LSM1.

Table 1. Number of landslides and Relative landslide density (RLD) within each landslide susceptibility zone for derived LSM1 and LSM2 models.

LSZ	LSM1 Area (%)	LSM2 Area (%)	LSM1 (a)		LSM2 (a)		LSM1 (b)		LSM2 (b)	
			Landslide No. (%)	RLD	Landslide No. (%)	RLD	Landslide No. (%)	RLD	Landslide No. (%)	RLD
Low	60	52	5.36	0.09	0.78	0.01	15.97	0.26	7.56	0.14
Moderate	11	14	15.42	1.48	5.36	0.40	13.87	1.33	16.39	1.21
High	15	19	27.58	1.84	33.33	1.77	33.61	2.24	33.19	1.76
Very high	14	15	51.63	3.61	60.52	3.99	36.55	2.55	42.86	2.83

Notes: (a) Training landslide datset, (b) Testing landslide dataset.

Conclusion

The presented results confirm that integrating local relief into small-scale LSMs is justified. The higher RLD in the very high LSZ for LSM2 indicates a better alignment with observed landslide occurrences. Moreover, the reduced number of landslides in the low LSZ for LSM2 suggests a more accurate exclusion of stable areas from high-susceptibility zones. This highlights the effectiveness of using local relief for more accurate landslide susceptibility mapping in large areas.

References

Cascini, L. Applicability of Landslide Susceptibility and Hazard Zoning at Different Scales. *Engineering Geology*. 2008, 102, 164–177.

Crnko, J. *Osnovna geološka karta Republike Hrvatske 1:100 000, list Kutina L 33-94 [Basic Geological Map of the Republic of Croatia 1:100 000, Kutina sheet – in Croatian]*. HGI-CGS, Zagreb, 2014.

Čubrilović, P.; Palavestrić, L.; Nikolić, T. *Inženjerskogeološka karta SFR Jugoslavije 1:500 000 [Engineering-Geological Map of SFR of Jugoslavia 1:500 000 – in Croatian]*. Savezni geološki zavod, Beograd, 1967.

Fell, R.; Corominas, J.; Bonnard, C.; Cascini, L.; Leroi, E.; Savage, W.Z. Guidelines for Landslide Susceptibility, Hazard and Risk Zoning for Land Use Planning. *Engineering Geology*. 2008, 102, 85-98.

HGI-CGS (Croatian Geological Survey). *Geološka karta Republike Hrvatske 1:300.000 [Geological Map of the Republic of Croatia at a scale of 1:300,000 – in Croatian]*. HGI-CGS, Zagreb, 2009.

Smith, G-H. The Relative Relief of Ohio. *Geographical Review*. 1935, 25/ 2, 272-284.

ENGINEERING GEOLOGY: A CORNERSTONE OF INFRASTRUCTURAL AND ECONOMIC ADVANCEMENT IN ALGERIA

BOULABEIZ MAHREZ [1], DASSAMIOUR MOHAMED [2], AOUIDANE LAICHE [3], AGAGUENIA SIHAM [4]

[1] *Khenchela university, Algeria, E-mail: mboulabeiz@univ-khenchela.dz*

[2] *University of Constantine 1, Algeria, E-mail: mohamed.dassamiour@umc.edu.dz*

[1] *Khenchela university, Algeria, E-mail: aouidane.laiche@univ-khenchela.dz*

[3] *Oum ElBouaghi University, Algeria, E-Mail: sihamagaguenia@univ-oeb.dz*

Introduction

Algeria, the largest country in Africa, is strategically important due to its vast territory of 2,381,741 square kilometers and diverse borders with seven nations. As the world's 10th largest country and Africa's 10th most populous country with over 46 million people, Algeria is a major player in global energy markets. In 2022, it was the 16th largest oil producer, the 10th largest natural gas producer and the 7th largest natural gas exporter worldwide (Belgacem Tahchi, 2024). The energy sector is central to Algeria's economy, with hydrocarbons accounting for 60% of budget revenue and 98% of export revenue in 2016. The country's rich hydrocarbon, natural gas and mineral resources highlight the critical role of engineering geology in resource exploration, assessment, and efficient utilization. Engineering geology's importance in Algeria's development has been increasingly recognized

Algeria geology

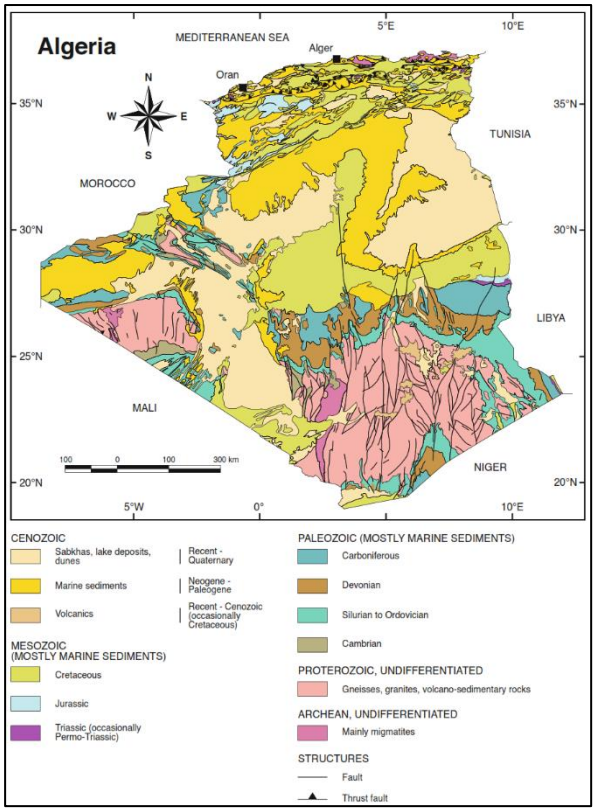

Fig. 1 Geological overview of Algeria (modified after Fabre et al, 1978)

Algeria's geology can be divided into three contrasting tectono-stratigraphic domains (Thomas Schlüter, 2006)(Fig. 1) : 1.The West African craton generally consists of a Precambrian granitized basement; 2.The eastern limit of the West African Craton borders the Tuareg shield; 3.and In the north, beginning from Tangier in Morocco through northern Algeria to Tunis in Tunisia, a folded chain extends the entire length of the Maghreb.

Economic Geology

The production of hydrocarbons is the cornerstone of Algeria's mineral sector, and contributes the majority of the country's export revenue. Although the government promotes a diverse but relatively small-scale metal production, the majority of Algeria's iron ore is comes from the Ouenza mine, whose iron content ranges from 53 to 60%. Additional iron ore mining takes place in Bou Khadra. Lead and zinc mining, which is largely artisanal, is conducted in the Oued Amizour area, while the El Abed Mine near the Algerian-Moroccan border yields between 10,000 to 15,000 metric tons of zinc concentrates annually. In addition, Algeria accounts for about 10% of global mercury production. is an important Paleozoic oil and gas region, and has significant fields such as Hassi Messaoud, with 8 billion barrels of oil, and Hassi R'Mel, with 50 trillion cubic feet of gas and 2 billion barrels of crude oil. The majority of hydrocarbon resources are concentrated in the Bechar-Timimoun, Illizi, and Ghadames Basins, and are mainly contained in structures associated with Caledonian and Hercynian tectonic movements.

Given Algeria's diverse and complex geological landscape, engineering geology plays a transformative

role beyond its essential functions. It contributes significantly to the country's infrastructural and economic progress and serves as a driving force for progress and development. The impact of discipline is particularly evident in addressing the challenges posed by Algeria's unique geological features while harnessing its natural resources for sustainable growth.

Engineering Geology in Algeria

The passage details the evolution of engineering geology in Algeria after independence in 1962. Initially focused on oil exploration, the field diversified to address national needs by creating Sonatrach S.P.A., now the largest oil and gas company in Algeria and Africa. The company operates in exploration, production, pipeline transportation, transformation, and marketing of hydrocarbons and by-products. Training specialists and adopting new technologies like 3D seismic imaging marked the 1970s-1990s. Since the 2000s, the field has embraced sustainability, environmental concerns, and the exploration of resources beyond oil and gas. Furthermore, numerous organizations now work in the engineering geology field, such as ALGEOS, LNHC, GIEC, and INGEO International. Algeria's universities have been instrumental in driving the nation's progress in engineering geology. This critical field underpins infrastructure and economic development. By establishing specialized programs, universities like institutions in Algiers, Annaba, and Oran have trained generations of skilled professionals. This reflects Algeria's goal to maximize and diversify resource use while fostering national expertise.

Infrastructure Development:

Engineering geology plays a crucial role in Algeria's infrastructure development, particularly in planning, designing, and constructing major projects such as highways, railways, and urban areas. This is achieved by ensuring structural stability and mitigating geological hazards.

Algeria boasts one of Africa's densest road networks, with 112,696 km of roads, including 29,280 km of highways and over 4,910 engineering structures (Logistic cluster, 2024). A notable 1,216 km stretch connects Annaba in the east to Tlemcen in the west. Since 2010, Algeria has implemented two five-year programs (2010-2014 and 2015-2019) aimed at economic recovery and reducing hydrocarbon dependence. These programs, with a public investment of $286 billion, focus on major rail, road, and water projects (Laridji, M.A et al, 2021).

Engineering geology is vital for achieving sustainable development objectives by:

1. Optimizing infrastructure design and implementation, considering local geological conditions to ensure longevity and hazard resistance.
2. Assessing and mitigating geological risks to safeguard populations and infrastructure.
3. Contributing to economic diversification, reducing reliance on hydrocarbons.

As a cornerstone of Algeria's development strategy, engineering geology ensures sustainable, environmentally responsible, and future-oriented economic growth.

Conclusion

Engineering geology is a cornerstone of Algeria's infrastructural and economic progress. Through comprehensive site investigations, responsible resource management and the use of innovative techniques, engineering geologists make a significant contribution to the country's development. As Algeria continues its growth trajectory, the role of engineering geology will remain essential. These qualified professionals ensure the safety and sustainability of important projects and drive the country's progress.

References

Fabre T., Freulon T.M. Pharuaien has stromatolites northwest of the Hoggar // C.R. Acad. Sci.– p 1962.– 254.

Laridji, M.A; Maliki, S.B. Transport Infrastructure Spending in Algeria: State of the Art. *Review MECAS.* 2021, 17. 1, 125-137

Logistic cluster, Available online: 2.3 Algeria Road Network Assessment | Digital Logistics Capacity Assessments (logcluster.org) (accessed on 5 July 2024).

Schlüter, T. Geological Atlas of Africa; Springer: Berlin/Heidelberg, Germany, 2006; p. 272.

Tahchi, B. Algerian gas to strengthen energy security of the European Union: Policy, capacity and strategy, *Energy Reports* 2024, 11, 3600-3613

Topic 6

Geological and Geotechnical Challenges in Urban Development and Construction

COASTAL AREAS UNDER THE THREAT OF LAND SUBSIDENCE AND FLOODING - THE CASES OF MESSOLONGHI AND AITOLIKON, GREECE

NIKOLAOS ANTONIADIS[1,2], STAVROULA ALATZA[3], CONSTANTINOS LOUPASAKIS[2], CHARALAMPOS (HARIS) KONTOES[3]

[1] *Delft University of Technology, Faculty of Civil Engineering and Geosciences (N.Antoniadis-1@student.tudelft.nl)*

[2] *National Technical University of Athens (NTUA), School of Mining and Metallurgical Engineering, Department of Geological Sciences (nikosantoniadis@mail.ntua.gr, cloupasakis@metal.ntua.gr)*

[2] *National Observatory of Athens (NOA), Institute for Astronomy, Astrophysics, Space Applications and Remote Sensing, Operational Unit "BEYOND Center of Earth Observation Research and Satellite Remote Sensing" (alatza@noa.gr, kontoes@noa.gr)*

Introduction

The current study aims to investigate the driving mechanisms of surface deformation occurring in the coastal cities of Messolonghi and Aitolikon in Greece (Figure 1). Low-rate surface displacements have been reported along these sites, often resulting in building damages. Messolonghi occupies a flat lowland and is founded on Quaternary alluvial deposits consisting of fine grain sediments (clays, silts, and sands). Drillings performed in the city of Messolonghi identified organic clay horizons containing a significant amount of plant remains and are characterized as soft to moderately stiff (SPT values 1-14 and compression index of up to 0.42) [1], [2], [3]. The second city, Aitolikon, initially consisted of 4–5 very small islands, which were later connected by fishermen using wooden piles and earth fills. Over the years, continuous fillings were added and the irregularly shaped island of Aitolikon with a 300 m in diameter was created.

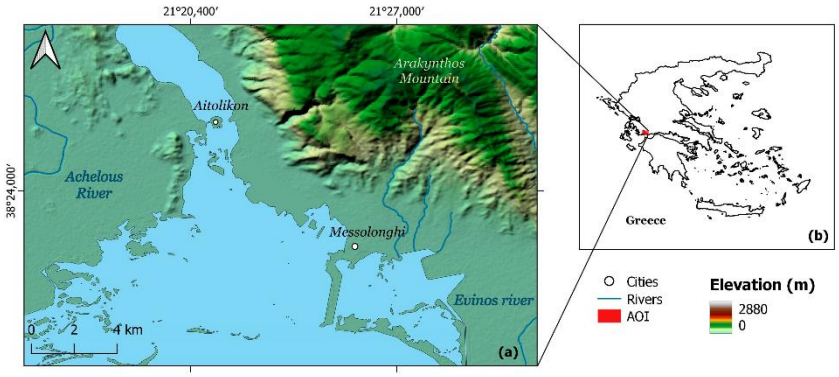

Figure 8. (a) The cities of Messolonghi and Aitolikon & (b) Location of the study area.

Methods

To fully determine the phenomena occurring in these areas, results from the satellite data processing were examined together with geological, geotechnical, hydrogeological, precipitation, sea level rise, and field trip data and thus a more accurate interpretation of the phenomenon was achieved. The parallelized Persistent Scatterers Interferometry PSI (P-PSI) processing chain, developed in the Operational Unit BEYOND Center for EO Research and Satellite Remote Sensing of the National Observatory of Athens (NOA) [4], was implemented in Sentinel-1 SLC images, for a 7-year period, to perform a time-series analysis of the Line of Sight and vertical displacements from both the descending and ascending satellite passes, in the affected areas. The estimated LOS displacements verified the land subsidence phenomena in both sites. The results were correlated with the vertical deformations acquired from the European Ground Motion Service [5].

The effect of global warming and climate change is also evident in Messolonghi and Aitolikon. Both areas have experienced an increased frequency and volume of precipitation, sea level rise as well as floods. The data from the tide gauges of Katakolon and Patras [6], as well as the Representative Concentration Pathway (RCP) [7] and Shared Socioeconomic Pathways (SSP) scenarios [8] were used to estimate the projected sea level rise as well as the areas that will be flooded by 2100. Precipitation data was obtained from the automatic weather stations' NOANN network of the National Observatory of Athens (NOA) [9] and were statistically processed and analyzed in correlation with the recorded deformations. Finally, Corine's land use map for 2006 [10] and 2018 [11] were

used. A correlation between the increase in the area used for residential and commercial purposes in Eastern Messolonghi with the increase in the rate of subsidence in the same part was found.

Results - Conclusion

The recorded subsidence in the east part of Messolonghi indicate a mean rate of −5mm/yr. The estimated subsidence rates increase towards the coastline and numerous buildings are affected. In the city of Aitolikon, maximum deformation values reach a mean rate of −4 mm/yr. The highest deformations are observed in the south part of the Island, where Vaso Katraki Museum is located (mean values of -4.5 mm/year). In the north part of the town, significant damages to buildings have been recorded. In both sites, the main factor contributing to the deformations is the load by external buildings imposed on the normally consolidated clay formations. In Messolonghi, most buildings are constructed with mat foundations, and only a few have spread footings. The difference in the type of foundation is attributed to the improvement of the Greek Code for Seismic Resistant Structures. Moreover, the foundation type also varied based on the nature of the formations encountered during construction. Deformation patterns are manifested primarily in buildings constructed with spread footings. Moreover, due to the constant increase in the sea level and the increased precipitation rates, the groundwater level fluctuates throughout the year, leading to the reactivation of the primary consolidation. Overall, in both sites, the situation is expected to worsen over the next few years because of the gradual subsidence of the sites and the increase in the mean precipitation rates and sea levels caused by climate change.

References

[1] I. Lemesios, “Environmental Hydrogeological Survey of the Horizons of the Wider Area of the Municipality of Messolonghi in Relation to Its Natural Healing Resources,” Master Thesis, University of Patras, Patras, 2008. Accessed: Jun. 05, 2023. [Online]. Available: https://hdl.handle.net/10889/823

[2] Hellenic Survey of Geology & Mineral Exploration (HSGME), “Geotechnical investigation of the foundations for the construction of worker’s households in the areas of Messolonghi-Aitolikon I, II-Agrinio,” 2020.

[3] N. Douveas, D. Kavadia, and P. Papadopoulou, “Geotechnical foundation conditions of Mesologion swimming pool center,” *Bulletin of the Geological Society of Greece*, vol. 40, no. 4, p. 1644, Jan. 2007, doi: 10.12681/bgsg.17068.

[4] I. Papoutsis, C. Kontoes, S. Alatza, A. Apostolakis, and C. Loupasakis, “InSAR Greece with Parallelized Persistent Scatterer Interferometry: A National Ground Motion Service for Big Copernicus Sentinel-1 Data,” *Remote Sens (Basel)*, vol. 12, no. 19, p. 3207, Oct. 2020, doi: 10.3390/rs12193207.

[5] “EGMS White Paper.” Accessed: Jun. 10, 2023. [Online]. Available: : https://land.copernicus.eu/user-corner/technical-library/egms-white-paper

[6] Flanders Marine Institute (VLIZ) and Intergovernmental Oceanographic Commission (IOC), “Sea level station monitoring facility.” Accessed: Jun. 06, 2023. [Online]. Available: http://www.ioc-sealevelmonitoring.org

[7] Climate Change Knowledge Portal, “Greece - Sea Level Rise.” Accessed: Sep. 25, 2022. [Online]. Available: https://climateknowledgeportal.worldbank.org/country/greece/impacts-sea-level-rise

[8] NASA, “Sea Level Projection Tool – NASA Sea Level Change Portal.” Accessed: Sep. 27, 2022. [Online]. Available: https://sealevel.nasa.gov/ipcc-ar6-sea-level-projection-tool

[9] K. Lagouvardos *et al.*, “The automatic weather stations NOANN network of the National Observatory of Athens: operation and database,” *Geosci Data J*, vol. 4, no. 1, pp. 4–16, Jun. 2017, doi: https://doi.org/10.1002/gdj3.44.

[10] European Environment Agency (EEA), “European Union, Copernicus Land Monitoring Service ,” 2006. Accessed: Jun. 11, 2023. [Online]. Available: https://land.copernicus.eu/pan-european/corine-land-cover/clc-2006

[11] European Environment Agency (EEA), “European Union, Copernicus Land Monitoring Service,” 2018. Accessed: Jun. 11, 2023. [Online]. Available: https://land.copernicus.eu/pan-european/corine-land-cover/clc2018

EVALUATING THE EFFECTIVENESS OF LANDSLIDE MITIGATION MEASURES USING MCDA METHODS AND SNAP SOFTWARE

CONSTANTINOS NEFROS[1], CONSTANTINOS LOUPASAKIS [1], GIANNA KITSARA [2] AND CHRISTOS GIANNAKOPOULOS [2]

[1] Laboratory of Engineering Geology and Hydrogeology, School of Mining and Metallurgical Engineering, National Technical University of Athens, 15780, Zografou, Athens, Greece; kostasnefros@central.ntua.gr (C.N.); cloupasakis@metal.ntua.gr (C.L)

[2] Institute for Environmental Research and Sustainable Development, National Observatory of Athens, 15236, Athens, Greece; gkitsara@noa.gr (G.K.); cgiannak@noa.gr (C.G.)

1 Introduction

Landslides can be caused by either natural or anthropogenic factors, such as road construction. On the other hand, human actions such as mitigation measures can also stabilize a slope, preventing a landslide. Multi-Criteria Decision Analysis (MCDA) methods and Geographical Information Systems (GIS) are widely applied for conducting the Landslide Susceptibility Assessment (LSA) of an area. In this process, the mitigation measures are usually not taken into consideration or are notably underestimated (Nefros and Loupasakis, 2022), as there is high uncertainty regarding their effectiveness (Kamal et al., 2023). Remote Sensing techniques, such as Persistent Scatterer Interferometry (PSI), are widely used for monitoring ground movements, providing evidence even for slow-moving landslides. Thus, PSI and GIS can be used to update the LSA of the Area of Interest (AOI) by incorporating the effective stabilization measures taken after the initial assessment. The main objective of this study is to highlight the potential of using MCDA methods with GIS and remote sensing techniques to provide an up-to-date LSA. Critical regions of the road network of Chania, a regional unit (RU) in Crete Island, Southern Greece, were examined as a case study area.

2 Data and Methods

During this study, the Analytical Hierarchy Process (AHP) was applied to the Chania RU. Experts were used to evaluate the most critical landslide causal factors along with their contribution–weight. The SentiNel Application Platform (SNAP), an open-source tool that enables Persistent Scatterer Interferometry (PSI) analysis through the extension of Stanford Method of Persistent Scatterer (StaMPS) software package (Foumelis et al., 2018), was used to analyze Sentinel-1 images and provide evidence about terrain movements in critical regions in the AOI. These regions of the road network were primarily affected by recent extreme precipitation events occured in February 2019, and mitigation measures had been established by civil protection authorities.

3 Results

First, the AHP was applied and the LSA for Chania RU was conducted. Subsequently, the most critical regions of the Chania RU road network were identified. Using SNAP software, PS time series were examined before and after the application of the mitigation measures. In regions where the velocities of the PS movements were below the threshold of 2 mm/year, it was indicated that the applied mitigation measures were effective and the slope was stabilized (Figure 1). Consequently, the susceptibility map was relatively updated for these regions.

Fig.1. PS velocities of the examined area

4 Conclusion

As was revealed, human activities can considerably affect the landslide susceptibility of a region. In this direction, GIS and Remote Sensing techniques can contribute to updating the LSA by providing valuable information about the effectiveness of the mitigation measures already applied and identifying the newly most susceptible regions, where mitigation measures are insufficient and urgent actions must be adopted by authorities. Thus, LSA emerges as a dynamic process that needs to be regularly updated.

References

Foumelis, M.; et al., (2018). "Esa Snap - Stamps Integrated Processing for Sentinel-1 Persistent Scatterer Interferometry," IGARSS 2018 - IEEE International Geoscience and Remote Sensing Symposium, Valencia, Spain, 2018, pp. 1364-1367, doi: 10.1109/IGARSS.2018.8519545

Kamal, A.S.M.M.; Hossain, F.; Ahmed, B. et al. (2023). Assessing the effectiveness of landslide slope stability by analysing structural mitigation measures and community risk perception. Nat Hazards 117, 2393–2418, https://doi.org/10.1007/s11069-023-05947-6

Nefros, C.; Loupasakis, C. (2022). Introducing a geospatial database and GIS techniques as a decision-making tool for multicriteria decision analysis methods in landslides susceptibility assessment. Bulletin of the Geological Society of Greece, 59(1), 68–103. doi: 10.12681/bgsg.29038

EXPERIMENTAL METHOD FOR TESTING THIXOTROPIC PROPERTIES OF SOILS

WIKTOR STOŁOWSKI [1], ALEKSANDER SACZKA [1], KLAUDIA SEKUŁA [1]

[1] *AGH University of Cracow, Poland, wstolowski@student.agh.edu.pl, oleksaczka@student.agh.edu.pl, klaudia.sekula@agh.edu.pl*

Introduction

Currently, there is no reliable and commonly used method of detecting thixotropic characteristics in soil samples. The complexity of soil behaviour under various loading and environmental conditions further complicates the development of such methods. Disturbing a thixotropic structure of soil causes it to change its plasticity index and in extreme cases leads to soil liquefaction. Thixotropic plasticization can be induced by various dynamic actions. For instance, vibrations emitted by tracked vehicles, conveyor belts, and heavy machinery during construction activities can alter the soil structure. Furthermore, pile driving and drilling operations, particularly impact drilling, exert significant stress on the soil, exacerbating the risk of plasticization. These activities generate complications such as unexpected settlements or shifts in foundation stability, leading to additional costs and delays in construction projects.

Methods

To develop a methodology for determining thixotropic properties, soil samples were collected for subsequent testing. The samples were taken from locations with previously encountered cases of thixotropic soils exhibiting varying intensities of these properties. Several soil characteristics were identified and measured, including natural water content, bulk density, plastic limit, liquid limit, and the grain size analysis. Once collected, the soil samples underwent comprehensive laboratory analysis to identify and measure several critical soil characteristics. First, the natural water content of each sample was determined. This measurement is crucial because the amount of water present in the soil directly affects its thixotropic properties [Ren et al. 2021]. Water content influences the plasticity of the soil and its ability to change state under applied stress.

Determining bulk density, which is the mass of soil per unit volume, helped assess the the compaction level of the soil. This property is important because it affects the strength and behavior of the soil under load [Bao et al. 2019]. Higher bulk density typically indicates a more compact and less porous soil structure, which may affect its ability to exhibit thixotropic behavior.

In addition to bulk density, the plastic limit of the soil was tested. The plastic limit is the minimum water content at which the soil transitions from a semi-solid state to a plastic state. This parameter is vital for understanding the consistency of the soil and its potential to become more pliable when water content is present. Similarly, the liquid limit of the soil was determined. The liquid limit represents the maximum water content at which the soil changes from a plastic state to a liquid state. This measurement is important for identifying the point at which the soil begins to exhibit fluid-like properties, which is a key aspect of thixotropy [Monge et al. 1998].

Furthermore, grain size analysis was performed. This involved examining the mineral composition and particle size distribution, including the proportions of sand, silt, and clay. The fraction composition affects the mechanical and hydraulic properties of the soil, influencing its behavior under various environmental conditions [Zhang et al. 2017, Wang et al. 2021].

By investigating these parameters, a comprehensive understanding of the physical characteristics of the soil that contribute to its thixotropic properties was achieved. This detailed analysis provided the foundation for developing a robust methodology to assess the risk of thixotropy in different field conditions. Such a methodology is essential for geotechnical engineering and geological risk management, enabling better prediction and mitigation of thixotropic soil behavior in construction and land development projects.

Simultaneously, work was undertaken on the construction of a device that would enable the determination of thixotropic properties of the soil. This device has the ability to apply vibrations of

various frequencies and amplitudes in such a way as to best simulate the actual factors causing the soil to liquefy under the influence of vibrations. The soil sample for testing is prepared in such a way as to reproduce the density and natural water content occurring in-situ at the place of sampling.
The methodology being developed is intended to ensure the possibility of measuring the amount of liquefaction immediately after the sample is subjected to vibrations.

Results

The expected results anticipate the creation of an apparatus that enables the study of thixotropic soils under conditions similar to natural ones. The main objective of this apparatus is to achieve correlation between laboratory results.

Conclusion

There is still no methodology that simultaneously determines the properties of thixotropic soils. However, by creating an apparatus that induces soil liquefaction, this goal seems increasingly feasible and achievable.

The research was financed by the AGH University of Krakow, Excellence Initiative – Research University.

References

Ren, Y.; Yang, S.; Andersen, K. H.; Yang, Q.; Wang, Y. Thixotropy of soft clay: A review, *Engineering Geology*. 2021, 287, 106097.

Baoa, X.; Jina, Z.; Cuia, H; Chena, X.; Xieb, X. Soil liquefaction mitigation in geotechnical engineering: An overview of recently developed methods, *Soil Dynamics and Earthquake Engineering.* 2019, 120, 273–291.

Monge, O.; Chassagneux, D.; Mouroux, P. Methodology for liquefaction hazard studies: new tool and recent applications, *Soil Dynamics and Earthquake Engineering*. 1998, 17, 415–425.

Zhang, X. W.; Kong, L. W.; Yang, A. W.; Sayem, H. M. Thixotropic mechanism of clay: A microstructural investigation, *Soils and Foundations*. 2017, volume 57, issue 1, pages 23-25.

OPTIMIZING URBAN MANAGEMENT, PLANNING, AND RESILIENCE THROUGH AN ENGINEERING GEOLOGICAL DATABASE: THESSALONIKI'S EXPERIENCE

ALIKI KOKKALA[1], VASSILIS MARINOS[2], GEORGE PAPATHANASIOU[1], ANTONIS MOURATIDIS[1]

[1] *Aristotle University of Thessaloniki, Greece, kokkalaaliki@gmail.com*

[1] *Aristotle University of Thessaloniki, Greece, gpapatha@geo.auth.gr*

[1] *Aristotle University of Thessaloniki, Greece, amourati@geo.auth.gr*

[2] *National Technical University of Athens, Greece, marinosv@civil.ntua.gr*

Introduction

The research introduces an advanced engineering geological database, based on the Tunnel Information and Analysis System-TIAS (AGS, 1999; Marinos et al., 2013), a pivotal tool for managing extensive geological and engineering geological data. Derived from hundreds of boreholes and numerous geotechnical investigations, the database facilitates the engineering geological assessment and classification within Thessaloniki's urban area in northern Greece. The focus is on the Quaternary and Neogene age sediments and fill deposits, aiming to mitigate geological uncertainties and geotechnical challenges for safe urban planning. The study underscores the importance of big data management in understanding geological heterogeneity, subsurface variations, engineering geological conditions, geological hazards, and early-stage infrastructure design considerations.

Methods

The research integrates various software, scientific tools and coding techniques to analyze, correlate, and present data. Key outputs include detailed thematic maps, statistical plots, two-dimensional and three-dimensional models, and an updated engineering geological map of the Thessaloniki basin (Figure 1). These outputs provide insights into the spatial distribution of geological formations, physical and mechanical parameters, as well as the redefinition of geological contacts (Kokkala and Marinos, 2022).

Results

The research results propose new, precise ranges of values, detailed by depth and region, for physical, mechanical and hydraulic parameters of the geomaterials examined. Furthermore, examples of specific database applications are created, with emphasis on the investigation and assessment of the engineering geological evaluation based on geohazards (liquefaction and settlement) and type of engineering project (urban tunneling and construction of major foundations).

Conclusion

This research transforms primary data into critical insights, emerging as an essential tool for both researchers and practitioners in the realm of geohazard mitigation and urban planning. It showcases the significant benefits of advanced methodological approaches in enriching the understanding and management of geological and engineering geological data, fostering improved strategies for urban protection and infrastructure design.

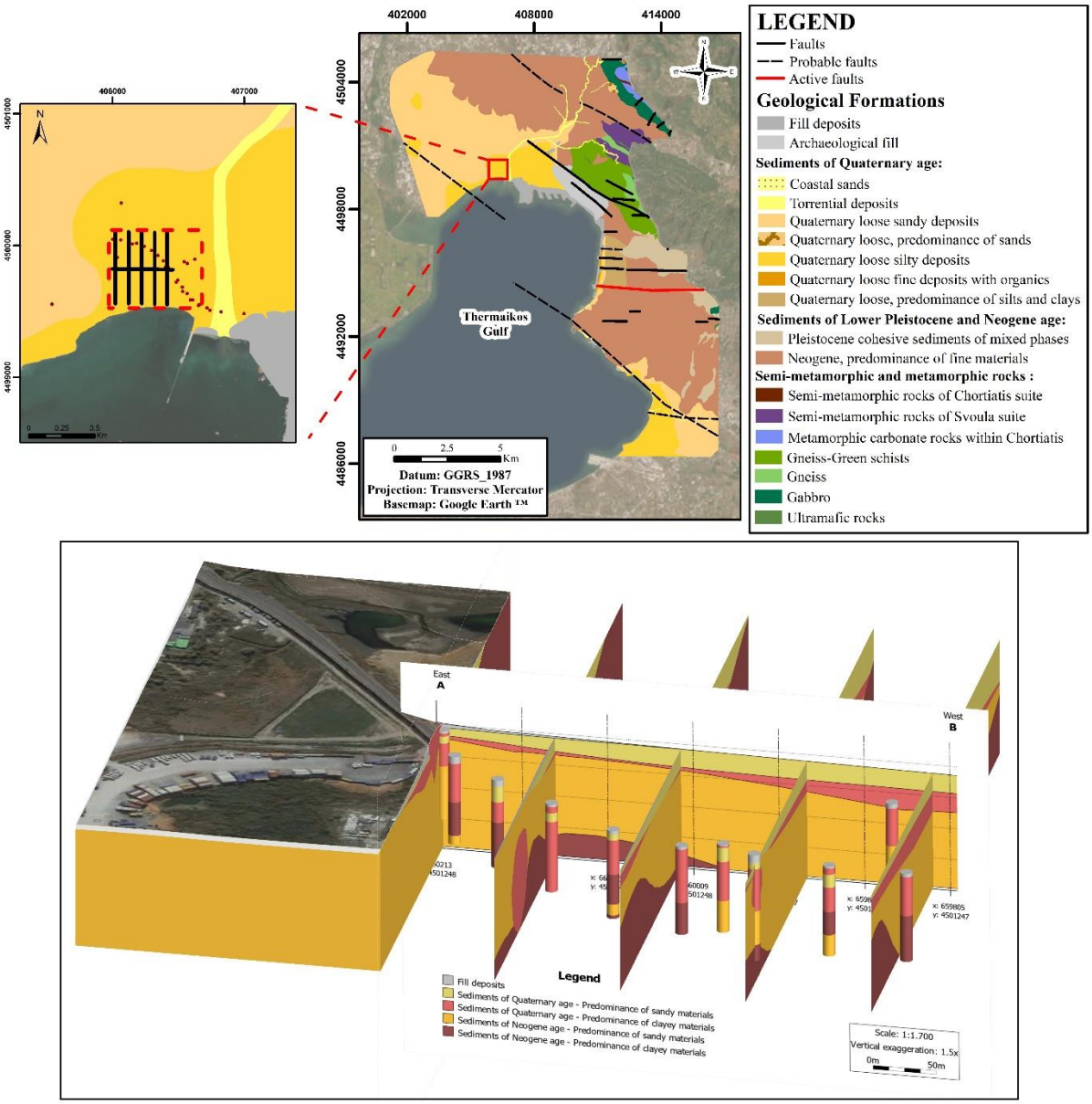

Figure 1. Updated engineering geological map of Thessaloniki city accompanied by a 3D geological model of a specific area (modified by the authors from Rozos et al. 1998).

References

Association of Geotechnical and Geoenvironmental Specialists (AGS). 1999. Electronic Transfer of Geotechnical and Geoenvironmental Data, 3rd edition

Kokkala, A. and Marinos, V. 2022. An engineering geological database for managing, planning and protecting intelligent cities: The case of Thessaloniki city in Northern Greece. Engineering Geology, 301, 106617, https://doi.org/10.1016/j.enggeo.2022.106617

Marinos, V., Prountzopoulos, G., Fortsakis, P., Koumoutsakos, D., Korkaris, K. and Papouli, D. 2013. Tunnel information and analysis system: a geotechnical database for tunnels. Geotech. Geol. Eng, 31, 891–910, https://doi.org/10.1007/s10706-012-9570-x

Rozos, D., Apostolidis, E. and Hadzinakos, I., 1998. Engineering-Geological Map of the Wider Thessaloniki Area, 1:25.000 Scale. I.G.M.E, Athens

FORMATION OF TALUS DEPOSITS IN SOFT ROCK MASS AND ITS IMPACT TO INFRASTRUCTURE: SOME EXAMPLES OF LOW COST MITIGATION MEASURES

GORAN VLASTELICA [1], PRIMOŽ JELUŠIČ [2], PREDRAG MIŠČEVIĆ [1], BOJAN ŽLENDER [2]

[1] *University of Split, Faculty of Civil Engineering, Architecture and Geodesy; Matice hrvatske 15, 21000 Split, Croatia; goran.vlastelica@gradst.hr, predrag.miscevic@gradst.hr*

[2] *University of Maribor, Faculty of Civil Engineering, Transportation Engineering and Architecture, Smetanova 17, 2000 Maribor, Slovenia; primoz.jelusic@um.si, bojan.zlender@um.si*

Introduction

The weathering of flysch rock masses which consist mainly of soft rock causes significant erosion of the surface of cuts and slopes (Vlastelica et all, 2018a), as well as it is one of key factors of successive shallow landslides and repeating rockfalls which are generated from harder layers due to differential erosion (Miščević and Vlastelica, 2014). Detached and eroded material is usually deposited at the bottom of the slope where it forms a talus that occupies useful space (Figure 1).

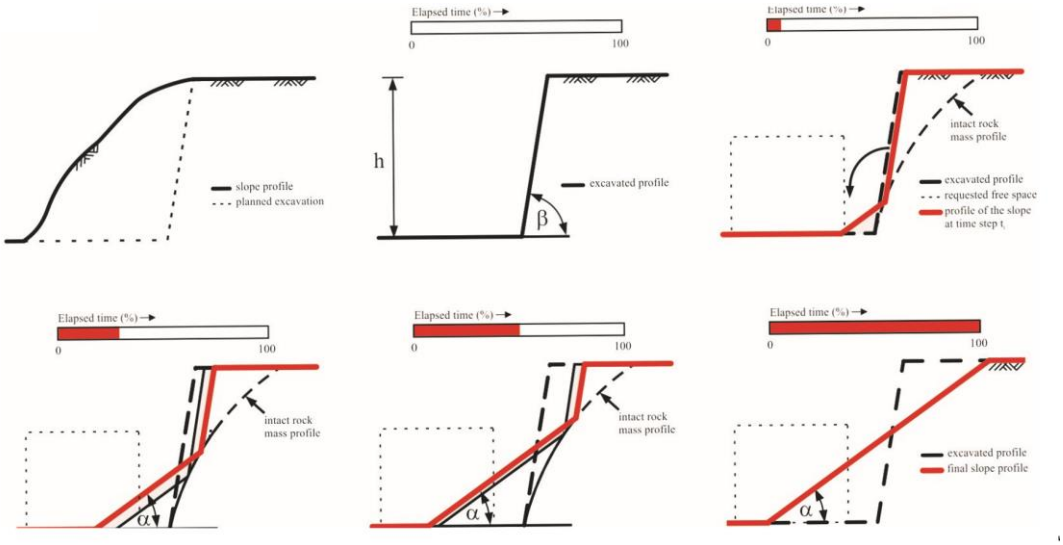

Figure 1. Formation of a steep slope from the initial time to its final transformation. Jelušič et all (2024)

If the talus material is just removed, the weathering and erosion process is further accelerated, leading to possible collapse of the whole slope. The usability of the area in front of the slope is most often required due to necessary infrastructure, buildings, or other reasons. Therefore, if the weathered material is not removed and the slope should not move too far away from the initial wall, a barrier in the form of a retaining wall must be constructed to limit the area in which the slope material is deposited.

Some of the typical low cost mitigation measures which can be used to form the barrier are: reinforced concrete wall, gabion gravity retaining wall and geosynthetic reinforced soil wall (Figure 2). These solutions are presented in detail in Jelušič et all (2024), are compared under functional, cost and environmental aspects (Vlastelica et all, 2016; Vlastelica et all, 2018b).

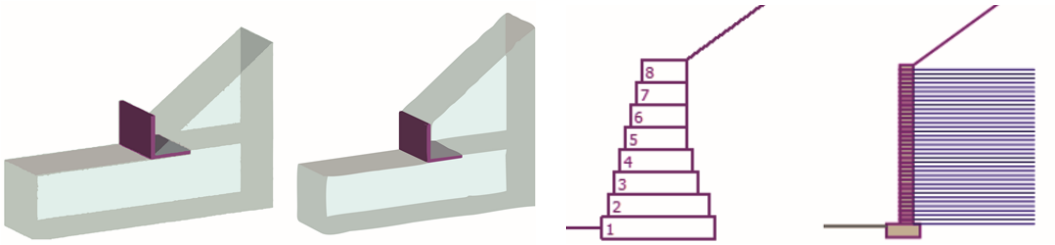

Figure 2. The retaining wall subjected to earth pressure, as a result of scree accumulation. Jelušič et all (2024)

Methods

The time dependent accumulation of scree behind the retaining wall is used as input for dimensioning of the retaining wall. The retaining wall must be verified in accordance with Eurocode standards (EN 1997-1) therefore the five main conditions were defined in the form of five geotechnical constraints: Condition 1: bearing capacity failure; Condition 2: position of resultant (eccentricity); Condition 3: sliding failure; Condition 4: wall overturning; Condition 5: global stability analysis. Each retaining wall is subjected to earth pressure, as a result of the scree accumulation, as shown in Figure 2. It should be noted that each retaining wall is analyzed separately at any selected time *t*. (Jelušič et all, 2016)
A simple analytical model (Jelušič and Žlender, 2020) for a retaining wall is used, that takes into account the position, time, and inclination of the retaining wall (Jelušič et all, 2024). The result of the analysis is the position and geometry of the retaining wall, which should be optimal from various points of view, such as technical, functional, cost or environmental aspects. All walls are dimensioned to optimize costs.

Discussion and conclusion

Permanent solutions that achieve high level of safety (such as complete slope stabilization i.e. with geotechnical anchors or nails) is not affordable for most users, or there is not sufficient amount of funds to cover all endangered areas. Therefore, to use some low cost mitigation measures and recommendations that would reduce damage to infrastructure and reduce the risks of using the space is better than not to use any at all. The added value of low cost mitigation measures is the use of the benefits of the natural process. The previously eroded - softer material can be used to reduce damage to the retaining walls or barriers or reduce the need for it, and the use of construction activities can be highly reduced (reduced material transport, thus the reduced CO_2 footprint).
It should be noted that in cases when low cost mitigation measures are applied, the whole area of the slope which corresponds to final slope profile (from the barier to the top of the slope in lower right profile on Figure 1) has to be inaccessible for people (or used only at their own risk) because of constant danger of potential rockfalls and landslides.
In highly urbanized area it is not acceptable to leave this kind of slopes unattained. It can lead to infrastructure damage and it can be hazardous for people, especially in cases when there are houses or infrastructure on the top of the slope. In this cases more elaborate and permanent measures should be used. Slope transformation is not limited only to change of the slope profile, also the mechanical properties of the material (rock mass) itself are degraded. This should also be taken into account for any future usage of the slope area.

References

Jelušič, P.; Žlender, B.; Dolinar, B. NLP Optimization Model as a Failure Mechanism for Geosynthetic Reinforced Slopes Subjected to Pore-Water Pressure. *Int. J. Geomech.* 2016, *16*, no 5.

Jelušič, P.; Žlender, B. Determining optimal designs for geosynthetic-reinforced soil bridge abutments. *Soft Comput.* 2020, *24*, 3601–3614.

Jelušič P, Vlastelica G, Žlender B. Sustainable Retaining Wall Solution as a Mitigation Strategy on Steep Slopes in Soft Rock Mass. *Geosciences*. 2024; 14(4): 90.

Miščević, P.; Vlastelica, G. Impact of weathering on slope stability in soft rock mass. *J. Rock Mech. Geotech. Eng.* 2014, 6, 240–250.

Vlastelica, G.; Miščević, P.; Fukuoka, H. Monitoring of vertical cuts in soft rock mass, defining erosion rates and modelling time-dependent geometrical development of the slope. *Rock Mechanics and Rock Engineering: From the Past to the Future.* Ulusay, R. et al. (eds.), 2016, 1249-1254.

Vlastelica, G.; Miščević, P.; Štambuk Cvitanović, N.; Glibota, A. Geomechanical aspects of remediation of quarries in the flysch: Case study of abandoned quarry in Majdan, Croatia. *Geomechanics and Geodynamics of Rock Masses: EUROCK 2018*, CRC Press, 2018, 679-684.

Vlastelica, G.; Miščević, P.; Štambuk Cvitanović, N. Durability of soft rocks in Eocene flysch formation (Dalmatia, Croatia). *Eng. Geol.* 2018b, 245, 207–217.

INIO – A GLOBAL INSAR SERVICE, PROVIDING GEOTECHNICAL ANALYSIS FROM SPACE

GEORGIA KARADIMOU [1], DYRE DAMMANN [2], REGULA FRAUENFELDER [3], MALTE VÖGE [4]

[1] *Kongsberg Satellite Services, Norway, georgia.karadimou@ksat.no*

[2] *Norwegian Geotechnical Institute, Norway, dyre.dammann@ngi.no*

[3] *Norwegian Geotechnical Institute, Norway, regula.frauenfelder@ngi.no*

[4] *Norwegian Geotechnical Institute, Norway, malte.voege@ngi.no*

Introduction

Synthetic Aperture Radar Interferometry (InSAR) is a technique that enables observations of ground motion from space with millimeter-scale precision. The Norwegian Geotechnical Institute (NGI) and Kongsberg Satellite Services (KSAT) launched a designated and scalable commercial InSAR service, Inio, in 2024. This comprehensive land monitoring service is unique, combining extensive expertise within earth observation and geotechnical engineering. It ensures maximum benefits from land monitoring while saving costs and mitigating risk via assessments of ground stability and risk.

Infrastructure like bridges, roads, railroads, tunnelling, hydro dams and mine tailings, can be monitored to detect geohazards such as creep and subsidence, to track ground movements, evaluate project impacts and help monitor risk to operations as well as surrounding areas. Subsiding cities, or geological and natural hazards affecting populations, can be continuously monitored and assess risks to the built environment.

Methods

Differential InSAR (D-InSAR) is a class of advanced, multi-temporal microwave remote sensing techniques that are used to determine relative surface deformations in the line-of-sight (LOS) direction of a sensor, by extracting the phase difference from pairs of SAR images of the same area acquired at different points in time. There are several unique algorithms that fall under the differential InSAR umbrella; each with certain advantages and disadvantages, depending on the application. A key aspect of InSAR processing is to identify pixels that provide a stable and coherent backscatter over the entire measurement period. Non-coherent pixels, e.g. affected by vegetation, are masked out. Coherent scatterers are divided into point-scatterers (PS), where a single point-like object is responsible for most of the backscatter within the pixel, and distributed scatterers (DS), where the backscatter is evenly distributed from within across the whole pixel. While PS are most common in urban areas, rural areas are mostly covered by DS. Many processing techniques focus on either PS or DS, however, combined PS-DS processing approaches have been developed as well (see e.g. Raspini et al 2022).

An increasing number of SAR satellites, both public and commercial, provide a constantly growing archive of data for InSAR analyses, which allows for detailed deformation analyses on almost every place on earth. Capturing data for many years into the past, in some places going back to the beginning of the 1990^{s}, provides a unique opportunity to map structural integrity of important infrastructure over long periods of time. The large footprint of the SAR images enables the tracking of spatial variations in ground movement over many kilometers.

Results

For the last few decades, InSAR has been applied to challenging often remote environments, or hard to monitor. Inio has been focused on both stability of the ground and the stability of industry operations and enhancing societal safety (see Figure 1). Past projects included applications in the areas of tailings dams, tunneling, urban infrastructure, landslides, Carbon capture and storage (CCS) and ground water pumping induced subsidence (see, e.g., Vöge et al 2012, Vöge et al 2015, and Vöge et al 2022).

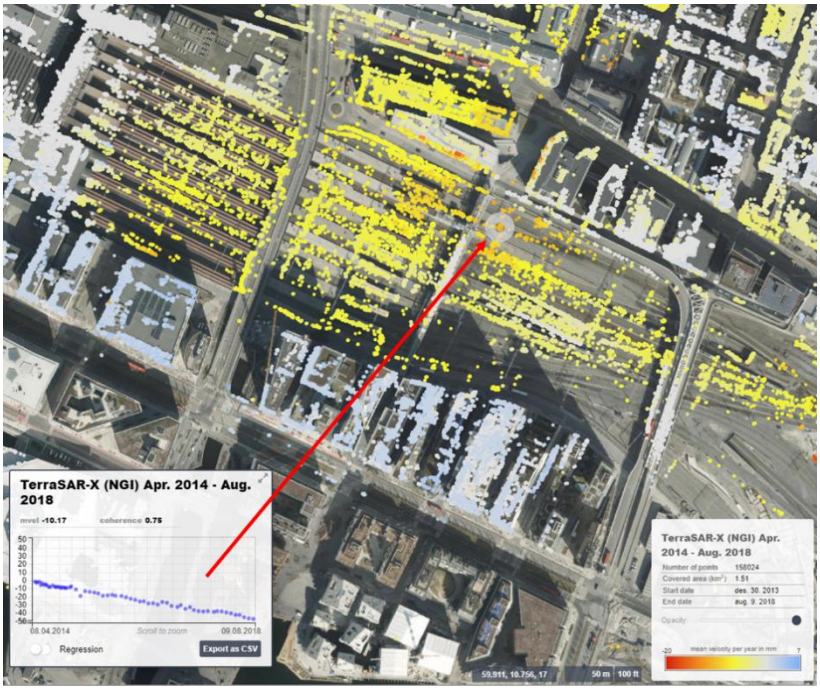

Figure 9: Example of InSAR measurements over the track area of Oslo Central Station. Color-coded measurement points show the mean ground velocity between Apr. 2014 and August 2018. The time-series shows the displacement history for the same period. The data was processed from a TerraSAR-X image stack in staring spotlight mode (resolution <1m) using a Permanent Scatterer algorithm. (see https://insarkart.ngi.no/malte/oslospublic)

Another example is the time-series analyses performed over the Feijão Mine tailings dam in Brazil, with line-of-sight displacements averaged over time, issuing a velocity map for the period May 2015-January 2019 just before the failure on 25 January 2019. In the centre of the dam face, a small part appeared to show an increased downward movement on 17 December 2018. This acceleration could indicate a possible precursor of the upcoming failure. The mean velocity at this smaller part was -9.93 mm/year.

Conclusion

The use of InSAR is on a rapid increase along with elevated access to satellite data and stakeholder awareness of the technology. Industries and communities all over the world are facing challenging conditions for operations and installations as well as rapid environmental change. InSAR has large untapped potential to help cost-effectively map deformation and prioritize stabilization measures and maintenance to mitigate risk at places. Inio is enabling maximum use and benefit of InSAR worldwide.

References

Raspini, F.; Caleca, F.; Del Soldato, M.; Festa, D., Confuorto, P.; Bianchini, S. 2022. Review of satellite radar interferometry for subsidence analysis. Earth-Science Reviews 235 (2022) 104239

Vöge, M.; Frauenfelder, R.; Larsen, Y. Displacement monitoring at Svartevatn dam with interferometric SAR, *2012 IEEE International Geoscience and Remote Sensing Symposium*, Munich, Germany, 2012, pp. 3895-3898, doi: 10.1109/IGARSS.2012.6350561.

Vöge, M.; Frauenfelder, R.; Ekseth, K.; Arora, M. K.; Bhattacharya, A.; Basin, R. K. 2015. The use of SAR interferometry for landslide mapping in the Indian Himalayas, *Int. Arch. Photogramm. Remote Sens. Spatial Inf. Sci.,* XL-7/W3, 857–863, https://doi.org/10.5194/isprsarchives-XL-7-W3-857-2015.

Vöge, M.; Boulanger-Martel, V.; Salazar, S.; Frauenfelder, R.; Nujaim, M.; Pabst, T. 2022. Satellite-based radar interferometry for monitoring ground surface deformation of filtered tailings storage facilities in continuous permafrost regions. *75th Canadian Geotechnical Conference, Calgary, Alberta, Canada,* 2022.

flysch: Case study of abandoned quarry in Majdan, Croatia. *Geomechanics and Geodynamics of Rock Masses: EUROCK 2018*, CRC Press, 2018, 679-684.

Vlastelica, G.; Miščević, P.; Štambuk Cvitanović, N. Durability of soft rocks in Eocene flysch formation (Dalmatia, Croatia). *Eng. Geol.* 2018b, 245, 207–217.

Topic 7

Environmental Geology and Geotechnical Engineering for Natural Resource Management

EXPERIMENTAL STUDY ON TURBIDITY CURRENTS TRANSPORTING MICROPLASTICS IN DIFFERENT CANYON TOPOGRAPHIES

YANG LU [1], XIAOLEI LIU [2]

[1] *Shandong Provincial Key Laboratory of Marine Environment and Geological Engineering, Ocean University of China, China, luyang2017@163.com*

[2] *Shandong Provincial Key Laboratory of Marine Environment and Geological Engineering, Ocean University of China; Laboratory for Marine Geology, Qingdao Marine Science and Technology Center, China, xiaolei@ouc.edu.cn*

Introduction

Nowadays, plastics or microplastics in the marine environment has gain lots of attention due to their harm to marine ecosystems and human health (Kane et al., 2019). Previous studies have focused more on the plastic distribution around the sea surface, but the physical process of transport and burial of plastics in the deep oceans remains unclear. Given that most of these plastics (probably 99%) are buried in the deep oceans and the turbidity currents are proposed to be the main carrier for plastic transport (Pohl et al., 2020), it is necessary to understand how the turbidity currents transport the plastics and make them buried in the seabed.

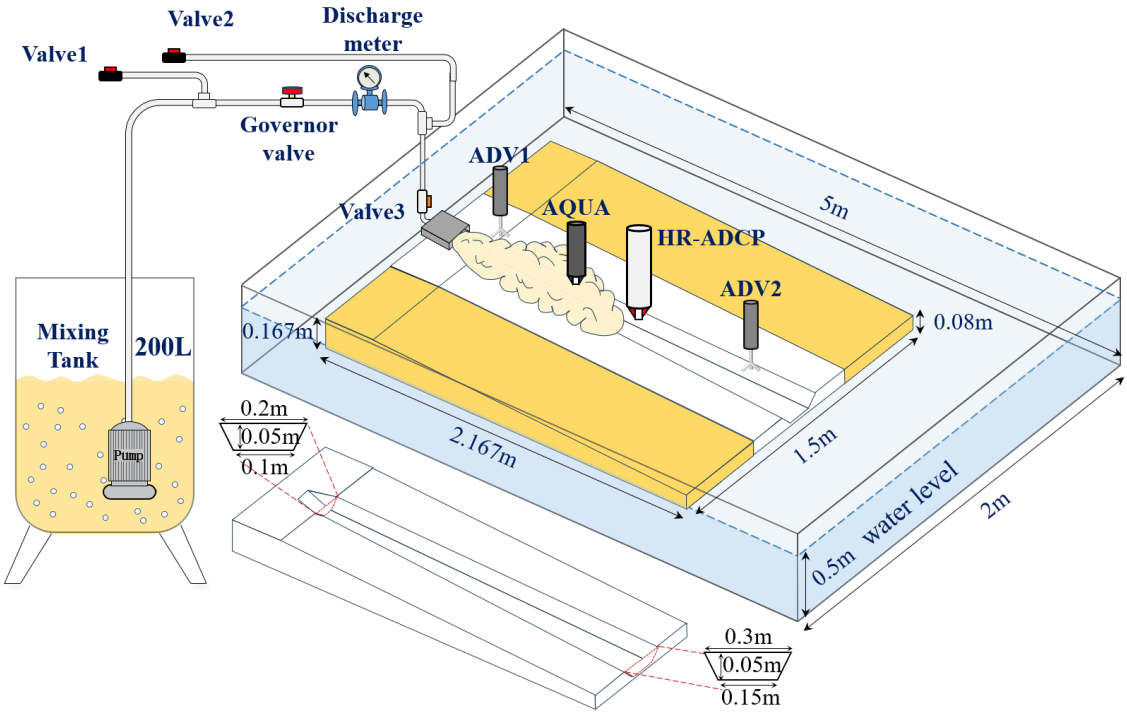

Figure 1. Experimental apparatus of turbidity currents transporting microplastics in the canyon topography

Methods

Based on the Froude scaling approach (Straub et al., 2008), we designed a series of experiments on turbidity currents transporting microplastics in different canyon topographies. The turbidity currents are composed of kaolin clay, quartz and fresh water, and the canyon topography is set to be straight or sinuous. These experiments were carried out in a water tank with high-resolution and high-frequency acoustic measuring instruments equipped (Figure 1), including the acoustic Doppler velocimeter (ADV), suspended sediment profiler (AQUA), and the high-resolution acoustic Doppler current profiler (HR-ADCP).

Results

The preservation rate of microplastics in canyons can reach up to 87.69%. Results show that the topography is an important factor affecting the deposition of microplastics, specifically, the canyon sinuosity increases the preservation rate. The preferential deposition zone of microplastics is located at the lee side of the wavy sediment deposits in the canyon head (Figure 2). Additionally, changes in flow rate and concentration of turbidity currents regulate the preservation rate and the distance between microplastic-enriched area and canyon head.

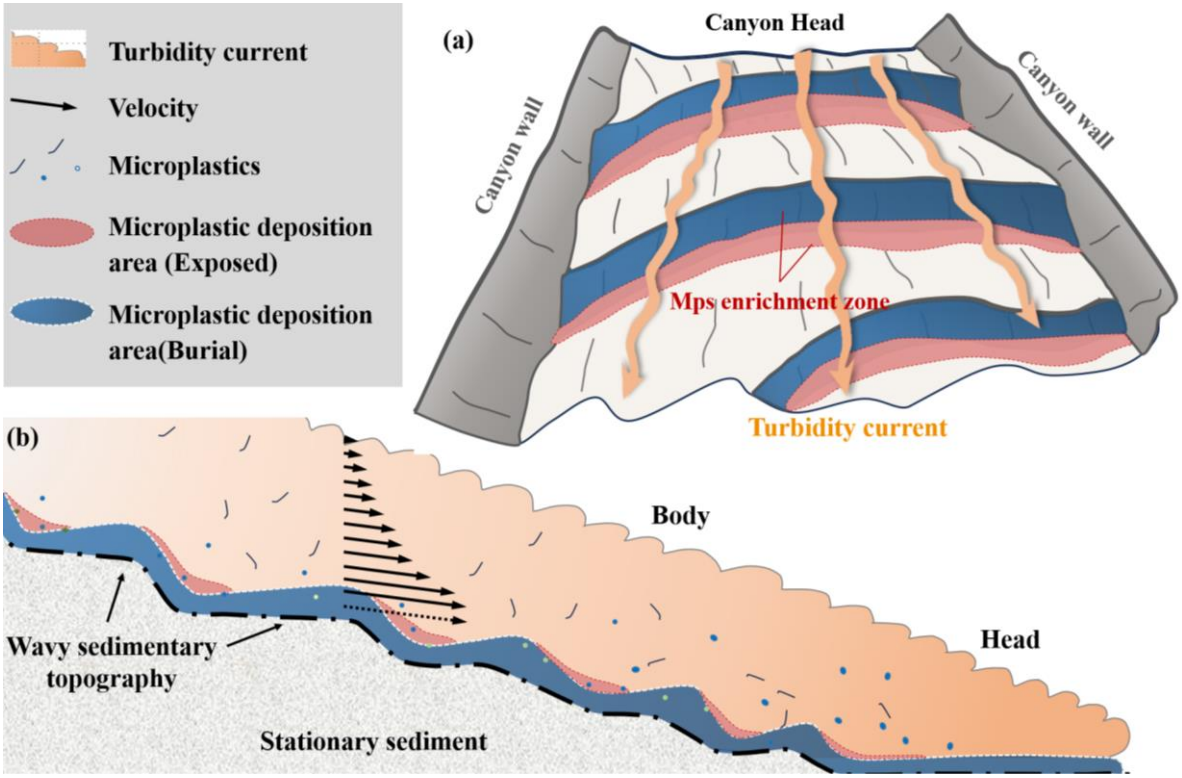

Figure 2. Schematic diagram showing the mechanism of microplastic deposition on the wavy deposits

Conclusion

This study adopts an experimental approach to investigate the migration and deposition characteristics of microplastics in different canyon topographies. The properties of turbidity currents and canyon sinuosity comprehensively determine the ultimate fate of microplastics transported in canyons. This study can provide valuable insights into evaluating the possible effects of plastics on marine environments and ecosystems.

References

Straub, K. M.; Mohrig, D.; McElroy, B.; Buttles, J.; Pirmez, C. Interactions between turbidity currents and topography in aggrading sinuous submarine channels: A laboratory study. *GSA Bulletin*, 2008, 120(3-4), 368-385.

Kane, I. A.; Clare, M. A. Dispersion, accumulation, and the ultimate fate of microplastics in deep-marine environments: A review and future directions. *Frontiers in Earth Science*, 2019, 7, 00080.

Pohl, F.; Eggenhuisen, J. T.; Kane, I. A.; Clare, M. A. Transport and burial of microplastics in deep-marine sediments by turbidity currents. *Environmental Science & Technology*, 2020, 54: 4180-4189.

MULTI-HAZARD ASSESSMENT OF SOIL EROSION AND LANDSLIDE SUSCEPTIBILITY IN THE DRAINAGE BASIN OF THE PINIOS DAM IN GREECE

MARIA MICHALOPOULOU[1], SPYRIDON LAINAS[1], NIKOLAOS DEPOUNTIS[1]

[1] *Department of Geology, Laboratory of Engineering Geology, University of Patras, 265 04 Patras, Greece*
maria_michalopoulou@ac.upatras.gr

Introduction

Soil erosion is a critical natural phenomenon that could be characterized as a hazard due to its varying intensity across different regions (Depountis et al., 2020), which frequently leads to surficial or shallow landslides, posing substantial risks to human lives, infrastructure, and the natural environment with substantial socio-economic impacts. In EU countries, 1 billion tons of soil are lost annually due to erosion, with Greece ranking among the top three Mediterranean countries, alongside Italy and Spain, exhibiting the highest recorded soil erosion rates (Panagos et al., 2020). Especially in Western Greece the phenomenon of erosion is more intense and for this reason the present research focuses on the southern part of the Pinios dam drainage basin, which is particularly vulnerable to soil erosion and landslides (Lainas et al., 2021; Michalopoulou et al., 2022). The steep terrain, the geological conditions, the poor soil cover, the intense rainfall patterns, as well as wildfires that have occurred during the previous decades, have significantly contributed to the area's increased susceptibility to soil erosion and landslides. Taking these factors into account, a modelling approach using the Revised Universal Soil Loss Equation (RUSLE) and the Landslide Susceptibility Index (LSI) was applied to identify areas prone to erosion and landslides within the study area. The aim of this study is to provide valuable insights into the spatial distribution and the severity of soil erosion and landslides by investigating their correlation and the combined effect of dominant causal factors that play a major role in their activation. Establishing a multi-hazard approach towards the identification of areas with the highest susceptibility can be considered a fundamental step in establishing mitigation strategies at local and regional levels.

Methods

This study focuses on two main hazards that prevail in the research area of the Pinios dam drainage basin, which are the soil erosion and landslide occurrence. To assess the soil erosion analysis, the RUSLE model was used by incorporating the parameters of rainfall-runoff erosivity, soil erodibility, slope length and steepness, land cover management, as well as support practices. The Rainfall-Runoff Erosivity Factor (R) was calculated based on the mean annual precipitation. The Soil Erodibility Factor (K) was assessed by using the methodology by Wischmeier and Smith (1978) in the prevailing geological formations and the Slope Length and Steepness Factor (LS) was estimated using the Calsite method and a DEM with 5m accuracy. The Cover Management Factor (C) was estimated using the Corine Land Cover (CLC) database (2018 version), and finally, the Support Practice Factor (P) was assigned a unity value because of the lack of available data on the management practices implemented in the study area. The multiplication of the above factors, using ArcGIS Pro v.3.3.1, led to the creation of an annual soil erosion map of the study area in tonnes/ha/year. The landslide susceptibility was estimated by applying the Frequency Ratio (FR) method. The FR is a statistical method that can been used to analyze the relationship between the distribution of landslides and contributing factors (geology, precipitation, slope and land-use). When the FR value is above unity it indicates a positive correlation between the landslide occurrence and the specific class of the contributing factor, suggesting higher landslide susceptibility. Based on the FR values for each category of the contributing factors, the LSI was calculated as the sum of the corresponding FR values.

Results

The results of this study demonstrate that areas with the highest erosion potential are predominantly located along the steep valley sides of the Pinios River and its tributaries. In terms of landslide susceptibility, areas most prone to landslides are characterized by slope angles between 15° and 45°, mean annual precipitation ranging from 600 to 1000 mm, geological conditions dominated by Pleio-

Pleistocene sediments, and agricultural land primarily consisting of complex cultivation, along with agricultural land with areas of natural vegetation. The most prone to erosion areas were the ones where the soil erosion rate was higher than the mean value estimated by the RUSLE model. Similarly, the most prone to landslides areas were areas with LSI values higher than the mean LSI value. The identification of the areas prone to the examined hazards is showed in Figure 1.

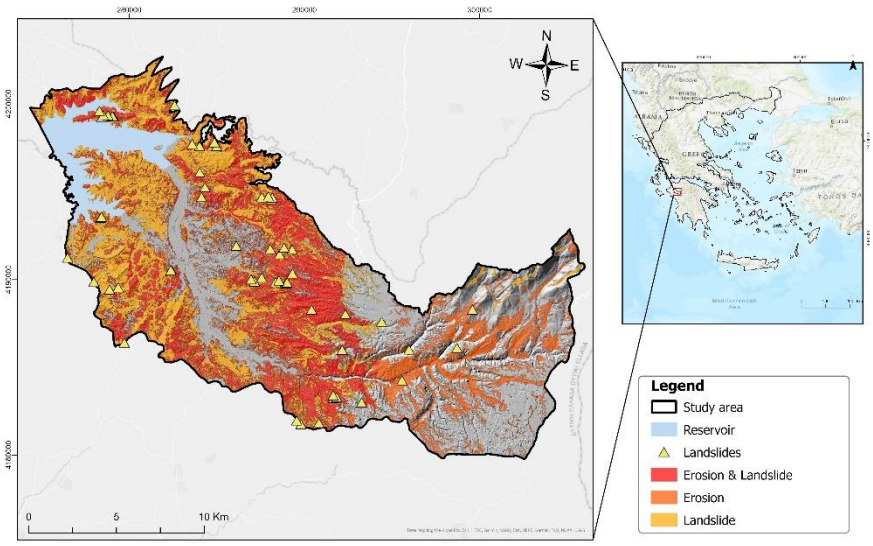

Figure 1. The multi-hazard map of the research area regarding to soil erosion and landslides.

Conclusions

This research method allowed to develop a multi-hazard map by integrating both soil erosion and landslide susceptibility. By utilizing GIS, regions with high erosion potential were superimposed with those highly susceptible to landslides. The percentage of the areas prone to soil erosion is equal to 33.94%, while the corresponding percentage regarding landslides is equal to 48.06%. The combined assessment of both hazards showed that the total percentage of the research area that can be affected by them is equal to 22.00%. Considering that under specific geological conditions soil erosion and shallow landslides are phenomena with similar generation patterns, combined triggering and effect, this approach has facilitated the identification of areas prone to soil erosion and landslide occurrence (multi-hazard approach) which is crucial for the implementation of suitable preventative measures and effective strategies by the state authorities, especially towards the assessment of the sustainability of the dam reservoir.

References

Depountis, N., Michalopoulou, M., Kavoura, K., Nikolakopoulos, K., & Sabatakakis, N. (2020). *Estimating soil erosion rate changes in areas affected by wildfires*. ISPRS International Journal of Geo-Information, 9(10), 562.

Lainas, S., Depountis, N., & Sabatakakis, N. (2021). *Preliminary Forecasting of Rainfall-Induced Shallow Landslides in the Wildfire Burned Areas of Western Greece*. Land, 10(8), 877.

Michalopoulou, M., Depountis, N., Nikolakopoulos, K., & Boumpoulis, V. (2022). *The significance of digital elevation models in the calculation of LS factor and soil erosion. Land*, 11(9), 1592.

Panagos, P.; Ballabio, C.; Poesen, J.; Lugato, E.; Scarpa, S.; Montanarella, L.; Borrelli, P. *A Soil Erosion Indicator for Supporting Agricultural, Environmental and Climate Policies in the European Union*. Remote Sens. 2020, 12, 1365.

Wischmeier, W.H.; Smith, D.D. *Predicting Rainfall Erosion Losses, a Guide to Conservation Planning; Agriculture Handbook No. 537*; US Department of Agriculture, Science and Education Administration: Washington, DC, USA, 1978.

DAMAGE EVOLUTION OF GRANITE-ENCASED- CONCRETE STRUCTURE UNDER STEPWISE CYCLIC TRIAXIAL LOADING

XIN YU [1], SHENGWEN QI [1], JOHN KEMENY [2], YUYE TAN [3], WEIDONG SONG [3], SONGFENG GUO [1], BOWEN ZHENG [1]

[1] *Institute of Geology and Geophysics, Chinese Academy of Sciences, Beijing, China,* yuxin@mail.iggcas.ac.cn, qishengwen@mail.iggcas.ac.cn, guosongfeng@mail.iggcas.ac.cn, *zhengbowen@mail.iggcas.ac.cn*

[2] *University of Arizone, Tucson, US, kemeny@arizone.edu*

[3] *University of Science and Techenology Beijing, Beijing, China,* tanyuye@ustb.edu.cn, *songwd@ustb.edu.cn*

Introduction

Rock-encased-backfill (RB) structures are common in underground mining engineering, for example in the cut-and- fill and stoping methods. To understand the effects of cyclic excavation and blasting activities on the damage of these RB structures, a series of triaxial stepwise-increasing-amplitude cyclic loading experiments was conducted with cylindrical RB specimens (rock on outside, backfill on inside) with different volume fractions of rock (VF = 0.48, 0.61, 0.73, and 0.84), confining pressures (0, 6, 9, and 12 MPa), and cyclic loading rates (200, 300, 400, and 500 N/s). The damage evolution and meso-crack formation during the cyclic process were analysed with results from stress-strain hysteresis loops, acoustic emission events, and post-failure X-ray 3D fracture morphology.

Methods

Cylindrical RB specimens were prepared to represent the underground structure between rock and backfill during the backfilling process. The rock used in this study was granite, the most important ore-bearing rock mass of the Shangshan Island Gold Mine located in Shandong province, China. The backfill consisted of tailings from the same mine, 52.4-grade cement, and distilled water. The physical and chemical properties of the tailings are detailed in Yu et al. (2021, 2024). The test process and experiment can be seen in Fig. 1.

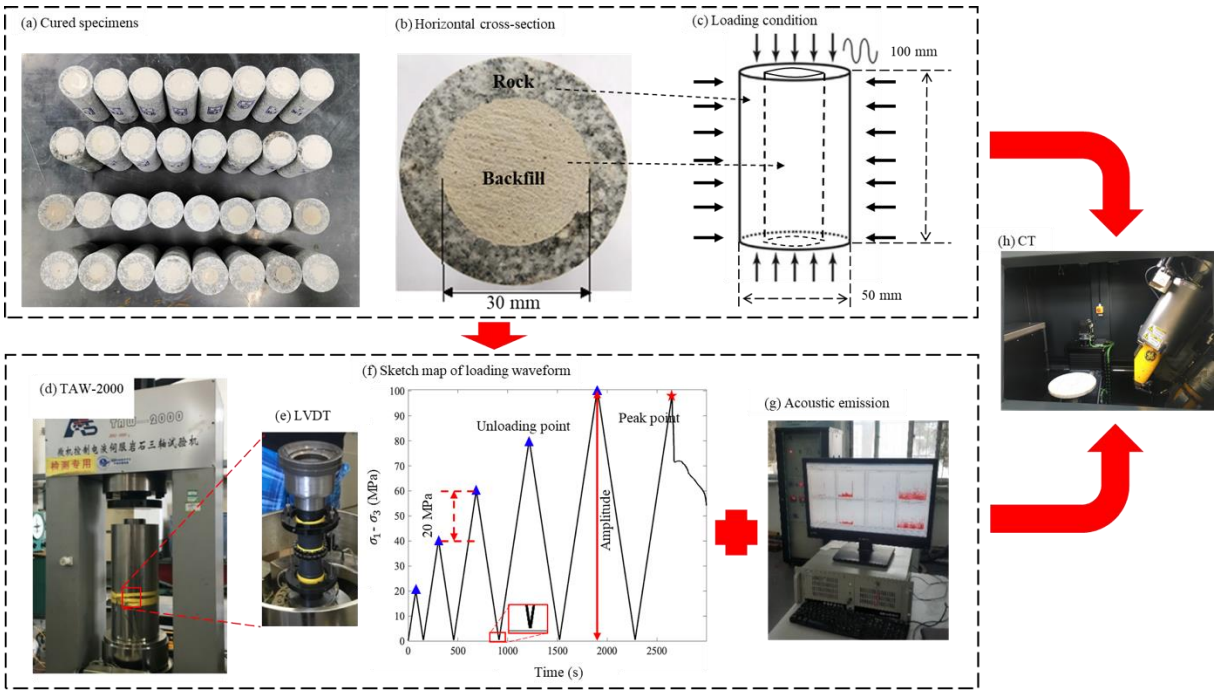

Figure 1. Rock-encased-backfill specimen (RB) and the experimental procedure.

Results

The results showed significant differences between cyclic and monotonic loadings of RB specimens, particularly with regard to the generation of shear microcracks, the development of stress memory and strain hardening, and the contact forces and associated friction that develops along the rock-backfill interface. One important finding is that as a function of the number of cycles, the elastic strain increases linearly and the dissipated energy increases exponentially. Also, compared with monotonic loading, the cyclic strain hardening characteristics are more sensitive to rising confining pressures during the initial compaction stage. Another finding is that compared with monotonic loading, more shear microcracks are generated during every reloading stage, but these microcracks tend to be dispersed and lessen the likelihood of large shear fracture formation. The transition from elastic to plastic behavior varies depending on the parameters of each test (confinement, volume fraction, and cyclic rate), and an interesting finding was that the transformation to plastic behavior is significantly lower under the conditions of 0.73 rock volume fraction, 400 N/s cyclic loading rate, and 9 MPa confinement (Figure 2). All the findings have important practical implications on the underground mining stability management.

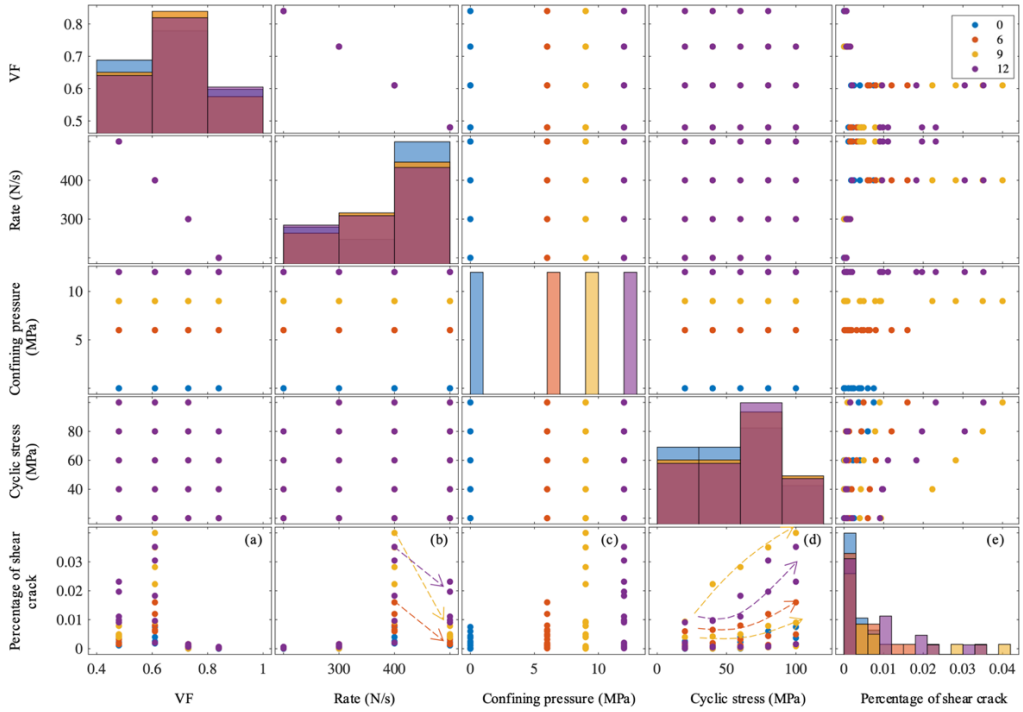

Figure 2. Relationship of VF, cyclic loading rate, confining pressure, cyclic stress, and percentage of shear crack.

Conclusion

The work presented here is unique and builds upon many studies of single material samples under monotonic and cyclic loadings, and bi-material samples under monotonic loading. As far as we know, this is the first comprehensive set of tests on rock encased backfill samples under cyclic loading.

References

Yu, X., J. Kemeny, J. Li, W. Song, and Y. Tan. 3D Observations of Fracturing in Rock-Backfill Composite Specimens Under Triaxial Loading, *Rock Mechanics & Rock Engineering*. 2021, 54(12), 6009-6022.

Yu, X., Y. Tan, W. Song, J. Kemeny, S. Qi, B. Zheng, and S. Guo. Damage evolution of rock-encased-backfill structure under stepwise cyclic triaxial loading, *Journal of Rock Mechanics and Geotechnical Engineering*. 2024.

HYDROGEOCHEMICAL MODELLING OF $CaCO_3$ SCALING FROM THE SERPENTINIZATION-DRIVEN HYPERALKALINE SRPINGS

VLADIMIR ŠARABA[1], TATJANA TRTIĆ-PETROVIĆ[2], TANJA PETROVIĆ PANTIĆ[3]

[1] *Laboratory of Physics, Vinča Institute of Nuclear Sciences, National Institute of the Republic of Serbia, University of Belgrade, Belgrade, Serbia, vladimir.saraba@vin.bg.ac.rs*

[2] *Laboratory of Physics, Vinča Institute of Nuclear Sciences, National Institute of the Republic of Serbia, University of Belgrade, Belgrade, Serbia, ttrtic@vin.bg.ac.rs*

[2] *Department of Geotechnics and Hydrogeology, Geological Survey of Serbia, Belgrade, Serbia, tanjapetrovic.hg@gmail.com*

Introduction

The serpentinization-driven hyperalkaline springs (HAS), with a pH value over 11.0 (Dragišić & Živanović, 2014) and mainly of Ca^{2+} - OH^- genetic type, are globally rare groundwater occurrences, with potential application in bottling, spa treatments and medical balneotherapy (Spahić et al., 2023). The carbonate minerals at HAS is typical of serpentinization in the worldwide peridotite massifs (Falk et al., 2016) and mineral scaling can affect serious operational problems in engineering geological investigations, such as membrane pores blockage and impairment of equipment functionality (Cao et al., 2022). This study is focused on the application of hydrogeochemical modelling to access the possibility of $CaCO_3$ scaling from the selected 4 HAS, designated as White Waters (WW-1, WW-2, WW-3 and WW-4, respectively), in the Mokra Gora area of the Zlatibor mountain of western Serbia belonging to the Dinaric ophiolite belt terrane in the central section of Balkan Peninsula (Nikić et al., 2013). The geographic position and geological composition of the wider research area is shown in Figure 1.

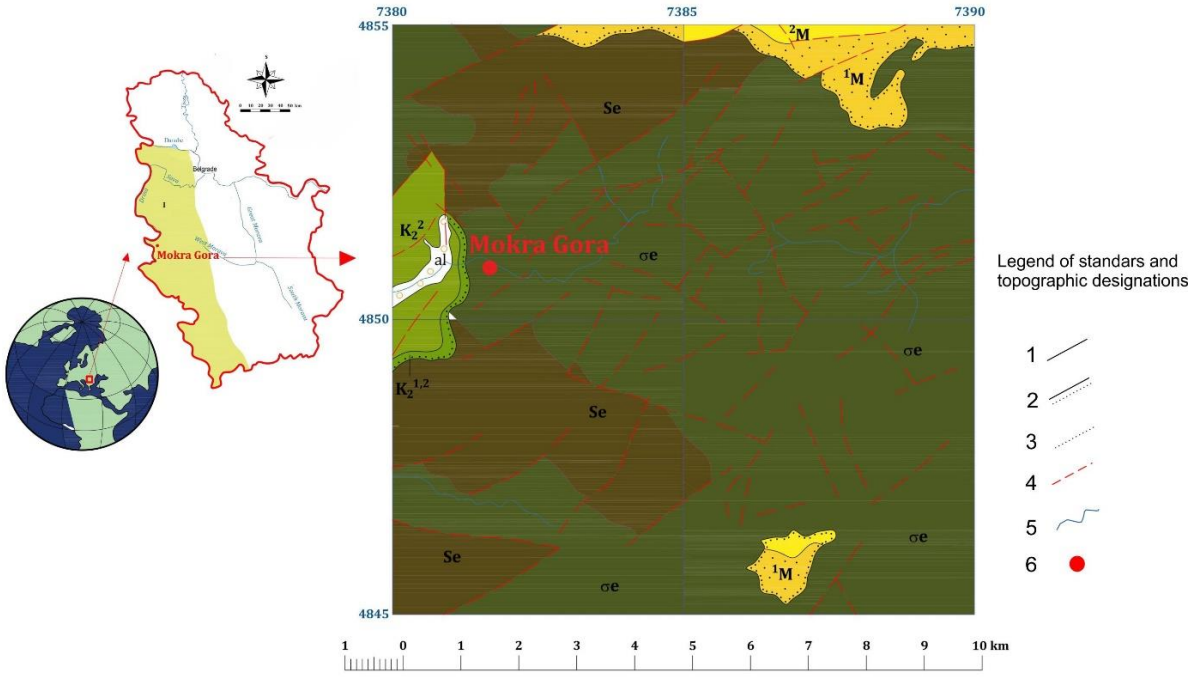

Figure 1. Schematic representation of geographic position and geological setting of the wider research area of Mokra Gora (Ciric et al., 2023; Mojsilović et al., 1978). Geological legend: I - Inner Dinarides of western Serbia; al – Alluvium; ^{2}M – Marlstones and dolomites; ^{1}M – Conglomerates and weakly cemented sandstones; K_2^2 – Layered and sandy-marly limestones and marlstones; $K_2^{1,2}$ - Conglomerates, sandstones, claystones and oolitic iron ores; Se – Serpentinite; σe – Harzburgite. Legend of standard and topographic designations: : 1 - Normal boundary: determined; 2 - Erosional or tectonic-erosive boundary (determined); 3 – The boundary of gradual lithological transition; 4 – Fault: assumed; 5 – River; 6 – Mokra Gora research area.

The investigated occurrences originate from the wide Jurassic supra-custal on-land ophiolites, which are cumulates of mafic plus ultramfic origin and serpentinized peridotites (Spahić et al., 2023), and appear as linear ascending serpentinization-driven springs in the Kamišna River valley (Dragišić et al., 1999).

Methods

Hydrogeochemical modelling, using the program WATCH updated to version 2.4. website (Iceland Water Chemistry Group, 2010), was conducted to determine the saturation index (SI) for calcite in order to assess the possible precipitation of given mineral (SI>0) from the examined HAS. Additionally, we calculated the Langelier Saturation Index (LSI) to predict the $CaCO_3$ scaling (LSI>0) from the studied HAS. The SI and LSI were calculated based on the previously determined physico-chemical properties of the investigated HAS. The values of SI, LSI<0 show that saturation of $CaCO_3$ has not been reached from the examined HAS, while the SI, LSI≈0 indicates equilibrium between $CaCO_3$ and the investigated groundwaters.

Results and discussion

The WATCH program indicated the possible precipitation of calcite, taking into account that the positive SI values were linked with all examined HAS, i. e. 1.47 for WW-1, 1.42 for WW-2, 1.68 for WW-3 and 1.94 for WW-4 occurrence, respectively. This program is mostly used to explain the chemical composition of deep formation and geothermal fluids (Ma et al., 2023) and the HAS of Mokra Gora area discharges from the deep fractured zones (Dragišić et al., 1999). Also, the LSI confirmed the possible scaling of $CaCO_3$ from all investigated HAS, bearing in mind the LSI values of 1.3 for WW-1 and WW-3, 1.2 for WW-2 and 2.0 for WW-4 occurrence, respectively. The LSI is the most widely used index in the water field (Ozair et al., 2012), whereby this index was also applied to predict the $CaCO_3$ scaling from the selected HAS. The uptake of CO_2 in the zones of emergence of HAS contribute to the precipitation of $CaCO_3$, wherefore the HAS may have an environmental significance in terms of CO_2 storage (Spahić et al., 2023). Also, at high pH values, the CO_3^{2-} is dominant compared to HCO_3^- (Dragišić & Živanović, 2014), which is conducive to $CaCO_3$ scaling and aragonite is more commonly occurring as bottom deposits, while calcite as surface film (Spahić et al., 2023). Bearing in mind the foregoing, the main limitation of the program WATCH includes the impossibility of calculating the SI for aragonite, in order to access whether it can be precipitated from the investigated HAS, since it is possible to determine the SI only for minerals available with the WATCH program, such as calcite.

Conclusion

The results of the program WATCH and the LSI index consistently indicate the possibility of $CaCO_3$ scaling from the investigated 4 HAS, whereby hydrogeochemical modelling can be applied in engineering geological investigations for the prognosis of risk of the development of chemical clogging process of underground installations.

References

Cao, Z.; Hu, Y.; Zhao, H.; Cao, B.; Zhang, P.; Sulfate mineral scaling: From fundamental mechanisms to control strategies. *Water Research*, 2022, 222, 118945. https://doi.org/10.1016/j.watres.2022.118945

Ciric, M.; Šaraba, V.; Budin, C.; de Boer, T.; Nikodinovic-Runic, J.; Polyurethane-Degrading Potential of Alkaline Groundwater Bacteria. *Microbial Ecology*, 2024, 87(1), 21. https://doi.org/10.1007/s00248-023-02338-z

Dragišić, V.; Tišma, R..; Milenić, D.; Miladinović, B.; Potkonjak, B.; Špadijer, S.; Hiperalkalne mineralne vode Srbije. *In International Conference "Water for the 21st century*, 611-618; Water Technology and Sanitary Engineering Association, Belgrade, 1999.

Dragišić, V.; Živanović, V. *Opšta hidrogeologija*. University of Belgrade, Faculty of Mining and Geology, 2014.

Falk, E. S.; Guo, W.; Paukert, A. N.; Matter, J. M.; Mervine, E. M.; Kelemen, P. B. Controls on the stable isotope compositions of travertine from hyperalkaline springs in Oman: Insights from clumped isotope measurements. *Geochimica et Cosmochimica Acta*, 2016, 192, 1-28.

Iceland Water Chemistry Group. *The chemical speciation program WATCH, version 2.4. website*. ÍSOR - Iceland GeoSurvey, Reykjavik, 2010. https://en.isor.is/software/

Ma, S.; Yang, Y.; Lei, X.; Yue, B. Water scaling predication for typical sandstone geothermal reservoirs in the Xi'an Depression. *Energy Geoscience*, 2023, 100182. https://doi.org/10.1016/j.engeos.2023.100182

Mojsilović, S.; Baklaić, D.; Đoković, I.; *Geological map of Serbia 1:100000 – Titovo Užice*. Belgrade: Federal Geological Society, 1978. Available from: https://geoliss.mre.gov.rs/prez/OGK/RasterSrbija/OGKWebOrig/listovi.php?karta=Titovo_Uzice

Nikić, Z.; Sreckovic-Batocanin, D.; Burazer, M.; Ristic, R.; Papic, P.; Nikolic, V. A conceptual model of mildly alkaline water discharging from the Zlatibor ultramafic massif, western Serbia. *Hydrogeology Journal*, 2013, 21(5), 1147-1163. 10.1007/s10040-013-0983-2

Ozair, G. An overview of calcium carbonate saturation indices as a criterion to protect desalinated water transmission lines from deterioration. *Nature, Environment and Pollution Technology*, 2012, 11(2), 203-212. ISSN: 0972-6268

Spahić, D.; Nikić, Z.; Mukherjee, S.; Dokmanović, P. Discovery of hyperalkaline waters in the ophiolites of western Serbia: Environmental considerations for carbon capture and sequestration. *Geoenergy Science and Engineering*. 2023, 212319. https://doi.org/10.1016/j.geoen.2023.212319

INVESTIGATION OF THE ABSORBING PROPERTIES OF MODIFIED SANDY SOIL TO CREATE A GEOCHEMICAL BARRIER FOR STORAGE LANDFILLS MUNICIPAL SOLID WASTE

ALEXANDRA KOVALEVSKAYA [1], TATYANA MALIKOVA [2], IRINA RODKINA [3]

[1] *Lomonosov Moscow State University (MSU), Russian Federation, alexa.kovalevskaya@mail.ru*

[2] *Lomonosov Moscow State University (MSU), Russian Federation, malikovatv@my.msu.ru*

[3] *Lomonosov Moscow State University (MSU), Russian Federation, irina-rodkina2007@yandex.ru*

Introduction

Lead compounds may be among the hazardous components of municipal waste. Clay soils and organic substances have the best absorption capacity in relation to Pb, while sandy soils are practically unable to absorb it. Therefore, the development of a technique for creating a geochemical barrier against lead based on modified sandy soil is promising.

The aim of the work is to study the absorption capacity of sandy soils with the addition of a clay substance and an organic binder (starch) in relation to lead. During the work, the pH and Eh of the selected filtrate were also measured to identify patterns between the values obtained and the amount of lead absorbed by the soil.

Methods

To study the absorbing properties of the modified sandy soil, a model soil was created based on Lyubertsy sand J_3V_2 (the fraction content of 0.5-0.25 mm is 50%, 0.25-0.10 mm - 48%, 0.10-0.05 mm - 2%), kilic clay and organic binder (starch) in a ratio of 10:1:1. The study was conducted by dynamic filtering. A solution of $Pb(NO_3)_2$ lead nitrate with a concentration of Pb 1.25 g/l was passed through a 10 cm thick model soil in the filtration column. The filtrate was sampled in 100 ml every 2 hours and 48 minutes. For the accuracy of the obtained values, tests were carried out on three samples.

The determination of pH and Eh solutions was carried out potentiometrically on the pH-150 device in accordance with GOST R 51232-98: reference electrode EVP-1M4, measuring electrode ESL-45-11, the steepness of the electrode function 58.25.

The zero charge point of the soil pH_{ZPC} – is the pH value at which the total charge of the surface of the soil particles is zero. In this work, pH_{ZPC} was determined for modified sandy soil both before and after the filtration process to compare the pH_{ZPC} values before and after lead ion sorption. The acid-base method was used to determine the pH_{ZPC} value titration of soil against the background of electrolyte solutions of different concentrations, described by T.A. Sokolova and S.J. Trofimov. HNO_3 acid and KOH alkali were used as titrants, and NaCl solutions with concentrations of 0.5 M, 0.1 M and 0.01 M were used as an electrolyte.

The cation exchange capacity of the soil was determined for model soil (sand, clay, starch) and for sand modified only with kilic clay. The determination was carried out according to the method described by E.V. Arinushkina, based on saturation of the soil with sodium ion, followed by its determination by the gypsum method.

The concentration of lead in solutions was determined using the Quantum Z.ETA atomic absorption spectrometer, manufactured by NPO KORTEK, Moscow. The method of atomic absorption spectrometry (AAS) is based on the phenomenon of resonant absorption of light by free atoms (atomic vapor) of the element being determined.

Results

Based on the measured pH values of the filtrate, a relationship between the pH and the amount of filtrate selected was revealed. After a certain amount of time, the pH of the filtrate decreases from 7-8 to 5-6 units, which corresponds to the pH of the initial solution $Pb(NO_3)_2$, which indicates the completion of the Pb absorption process by the soil. There was no correlation between the Eh values of the filtrate and its selected amount, which is probably due to the activity of living organisms trapped on the ground or in the filtration column.

The pH_{ZPC} values of 8.5 before absorption and 6.25 units after absorption correspond to the measured pH values of the filtrate and the general behavior of the soil during Pb absorption.

The measurement of soil CEC showed that the absorption of lead by the model soil does not depend on its CEC value (0.07 mg-eq/100 g for the entire model soil and model soil excluding starch), therefore, lead sorption does not occur in the exchange complex of the soil, but in more durable centers.

According to the results of measuring the concentration of Pb absorbed by the model soil, an absorption capacity value of 1.96 mg/g was obtained. At the same time, the created soil with a capacity of 10 cm retained Pb with a concentration of 1.25 g/l for 35.5 hours. The maximum amount of lead absorbed by clay and starch is 11.76 mg/g, which is much less than the values obtained by studying the absorption capacity of similar soils under static sorption conditions (on average 48.24 mg/g).

Conclusion

Thus, in this work, the absorption capacity of sandy soil modified with clay soil (montmorillonite) and organic binder (starch) in relation to lead was studied. A relationship was revealed between the pH value of the solution and the amount of absorbed lead under dynamic sorption conditions (absorption of Pb ions by the soil leads to a change in the pH of the filtrate). Determination of the Eh values of the filtrate showed that the Eh value is probably influenced by living organisms. The obtained pH_{ZPC} values satisfy the general pattern of pH solution behavior. According to the measurement of the cation exchange capacity, it was found that the absorption of lead cations does not depend on the value of the soil cation exchange capacity (0.072 mg-eq/100g for a mixture of sandy and clay soil and 0.069 mg-eq/100g for a mixture of sandy soil, clay soil and starch), therefore, the absorption of lead occurs with the formation of more durable complexes. The maximum amount of lead absorbed by such a soil at an initial concentration of lead in a solution of 1.25 g/l is 1.96 mg/g. The maximum amount of absorbed lead without taking into account the mass of sand (absorption by clay and starch) is 11.76 mg/g, which is much less than the values obtained by studying the absorption capacity of similar soils under static sorption conditions (on average 48.24 mg/g according to A.I. Kovalevskaya).

References

Arinushkina E.V. Manual on chemical analysis of soils. Moscow: MSU, 1971.

Kovalevskaya A.I. Creation of sorption barriers against lead on the basis of clay soils modified with organic binders: abstracts of the international conference «Lomonosov-2022», section «Ecological geology». – M., 2022.

Sokolova T.A., Trofimov S.J. Sorption properties of soils. Adsorption. Cationic exchange. Tula: Vulture and K, 2009.

DISTRICT-SCALE SEASONAL UNDERGROUND THERMAL ENERGY STORAGE: CHALLENGES AND OPPORTUNITIES IN THE CZECH REPUBLIC

GIANVITO SCARINGI[1], JAN JERMAN[1], TOMÁŠ KADLÍČEK[1], DAVID MAŠÍN[1], JAN NAJSER[1], JAKUB ROHÁČ[1]

[1] *Institute of Hydrogeology, Engineering Geology and Applied Geophysics, Faculty of Science, Charles University, Czech Republic, gianvito.scaringi@natur.cuni.cz*

Introduction and motivation

Energy geostructures (EGS) and shallow underground thermal energy storage (UTES) systems are receiving considerable attention from the research community and policymakers thanks to potential energy savings and the consequent reduction in energy expenditures and carbon emissions. The feasibility, design, and challenges related to UTES systems, in combination with EGS but also independent from them, are thus being explored extensively (Loveridge et al., 2020). UTES systems can mitigate the high temporal variability of renewable energy sources (RES), such as photovoltaics, solar thermal, and wind energy, which are affected by seasonality and local weather conditions (Lyden et al., 2022). In fact, as far as non-industrial consumption is concerned, over half of the energy demand is used for indoor heating and climatisation (Connolly, 2017). However, a fundamental offset exists between the time functions of energy production from RES and consumption (Fig. 1). This creates imbalances in the energy grid, with overproduction during daytime in summer months and increased needs in wintertime, resulting in high and volatile prices of electricity.

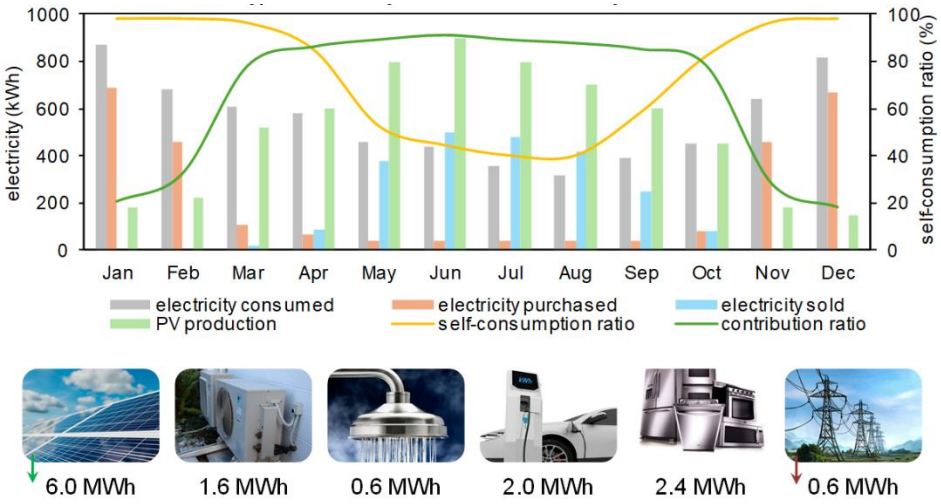

Figure 1. Typical electricity balance for a new family house in the Czech Republic.

UTES can mitigate this imbalance by storing excess energy in the form of heat underground (Yang et al., 2021) and subsequently retrieving it when it is needed, with considerable efficiency (Zymnis & Whittle, 2014). In the urban environment, with possible constraints in terms of available space, the spatial domain of UTES may intersect the areas of influence of building foundations and other underground infrastructures. This occurrence can also be intentional when foundations are themselves equipped with heat exchangers, such as in EGS. This specific design can be economically advantageous thanks to the double function (static and thermal) absolved by the structural elements. However, it also brings challenges as it triggers a coupled THM response in the ground-structure interaction. Further challenges relate to the upscaling of the design to serve not a single building but an entire district, where the energy needs and productions of the individual buildings (not only residential) are combined, with increased efficiency. While EGS with UTES are being studied extensively in other European countries (Aresti et al., 2024), the Czech Republic has been lagging behind. Here, no implementations of EGS with UTES exist, neither at the building nor at the district level. Besides regulatory complications, this stems from a lack of knowledge of the multiphysical long-term THM ground response to cyclic thermal

loading, as well as from an insufficient understanding of the interaction with other RES and the associated challenges. Thanks to a grant we received from the Czech Ministry of Education, Youth and Sport (INTER-EXCELLENCE II programme, INTER-COST sub-programme, project no. LUC24143), we are taking the opportunity to realign ourselves to the international community and increase our readiness for the domestic adoption of these technologies. Our medium-term goal is to become a national reference and attract funding for applied research towards practical implementation.

Methods and Expected Outcomes

We aim to exploit our expertise in THM experiments and modelling and combine it with thermodynamic-based, multi-scale, and time-dependent knowledge of soil behaviour to enhance our understanding of the ground response through targeted experiments and the development of a modelling framework for UTES. In particular, we plan to incorporate a micro-structural representation of soil behaviour into a double-scale hypoplastic framework (Mašín, 2017) and introduce time- and rate-dependent formulations (Jerman & Mašín, 2020) of constitutive equations describing experimentally observed responses, such as thermal creep and plastic strain accumulation under cyclic loading (Pico & Mašín, 2024). Based on the developed framework, we will produce numerical implementations, which we will calibrate according to realistic boundary conditions determined from building practices, soil types, and climate scenarios in the Czech Republic. We will optimise these implementations to produce a numerical proof-of-concept of district-scale UTES, which will be the basis for follow-up applied research in cooperation with the industry.

Conclusion

Energy geostructures and underground thermal energy storage systems pose considerable engineering geological challenges and motivate substantial research. However, the Czech Republic has been lagging behind in the development of such solutions. We aim to exploit the opportunity of a newly funded project to bring advancements and make our country competitive in the implementation of solutions that considerably increase the usability of renewable energy and reduce the carbon footprint of buildings.

References

Aresti, L., et al. (2024). Energy Geo-structures: a review of their integration with other sources and its limitations. *Renewable Energy*, 230, 120835.

Connolly, D. (2017). Heat Roadmap Europe: Quantitative comparison between the electricity, heating, and cooling sectors for different European countries. *Energy*, 139, 580–593.

Jerman, J., Mašín, D. (2020). Hypoplastic and viscohypoplastic models for soft clays with strength anisotropy. *Int. Journal for Numerical and Analytical Methods in Geomechanics*, 44(10), 1396-1416.

Loveridge, F., McCartney, J.S., Narsilio, G.A., Sanchez, M. (2020). Energy geostructures: A review of analysis approaches, in situ testing and model scale experiments. *Geomechanics for Energy and the Environment*, 22, 100173.

Lyden, A., Brown, C.S., Kolo, I., Falcone, G., Friedrich, D. (2022). Seasonal thermal energy storage in smart energy systems: District-level applications and modelling approaches. *Renewable and Sustainable Energy Reviews*, 167, 112760.

Mašín, D. (2017). Coupled thermohydromechanical double-structure model for expansive soils. *Journal of Engineering Mechanics*, 143(9), 04017067.

Pico, M., Mašín, D. (2024). Coupled thermo-hydro-mechanical hypoplastic model for partially saturated fine-grained soils under monotonic and cyclic loading. *Computers and Geotechnics*, 172, 106447.

Yang, T., Liu, W., Kramer, G.J., Sun, Q. (2021). Seasonal thermal energy storage: A techno-economic literature review. *Renewable and Sustainable Energy Reviews*, 139, 110732.

Zymnis, D.M., Whittle, A.J. (2014). Numerical Simulation of a Shallow Geothermal Heating/Cooling System. Proceedings of the Geo-Congress 2014, pp. 2767–2776.

Topic 8

Advances in Geological Modelling for Engineering Applications

COMBINED IMPACT OF INHERENT AND STRESS-INDUCED ANISOTROPY ON ROCK PERMEABILITY AND SLOPE STABILITY: ODA'S EQUATION SOLUTION AND FLAC3D SIMULATION ANALYSIS

CHIA-HUEI TU[1], JIA-JYUN DONG[2], ALVIAN RIZKY YANUARDIAN[3], JIA-YI WU[4]

[1] *Graduate Institute of Applied Geology, National Central University, Taiwan, tu_758594520@hotmail.com*

[2] *Graduate Institute of Applied Geology, National Central University, Taiwan, jjdong@geo.ncu.edu.tw*

[3] *Graduate Institute of Applied Geology, National Central University, Taiwan, alvian.ry@gmail.com*

[4] *Graduate Institute of Applied Geology, National Central University, Taiwan, jweek44@gmail.com*

Introduction

The joints within the rock mass can also become pathways for groundwater flow, and pore water pressure can reduce the effective stress and shear strength of potential sliding surfaces. Groundwater can accelerate rock weathering and reduce strength, all of which negatively impact the stability of rock slopes. Oda (1985) selected appropriate boundary conditions based on analytical conditions, defined system boundaries, and considered saturated groundwater flow in mountainous areas, classifying groundwater flow systems into small-scale, medium-scale, and large-scale types. Wyllie and Chris (2004) assumed that the slope material is composed of sedimentary material, suggesting that horizontal permeability might be higher than vertical permeability. This indicates that permeability anisotropy has a certain degree of influence on slope pore water pressure and the steady-state flow system of groundwater. Dong et al. (2006) used an equivalent concept to explore the impact of permeability anisotropy on the distribution of pore water pressure in rock slopes. Furthermore, pore water pressure affects the shear strength and effective stress of potential sliding surfaces, further influencing slope stability. However, secondary fractures and stress-induced permeability anisotropy in the rock mass have not yet been considered. Therefore, further research is needed on the influence of joint orientations in the rock mass or joint closures due to stress on the stability of jointed rock slopes (Dong et al., 2012).

Methods

This study discusses the impact of two conditions on slope stability: inherent joints and stress-induced anisotropic permeabilities. A numerical model of a rock slope was designed using FLAC3D, and the stress field was solved through gravity equilibrium. The stress data from the model grid were imported into Oda's equation to calculate the anisotropic permeability tensor. This tensor was then substituted back into the FLAC3D model to solve for the pore water pressure distribution, and the slope stability was analysed using the shear strength reduction method. In Condition 1, we assumed that the permeability is influenced by the distribution of multiple sets of joints. This study reflected the degree of difference in joint density in each direction using the coefficients $D_{X'X'}$, $D_{Y'Y'}$, and $D_{Z'Z'}$ of the fabric tensor, and assumed a higher density for joints parallel to the slope surface (bedding parallel joints). In Condition 2, we considered the directionality of the principal stress distribution, with the maximum principal stress parallel to the slope surface and the minimum principal stress perpendicular to the slope surface. Various stress ratios (maximum principal stress/minimum principal stress = 1 to 5) were also assumed.

Results

Assuming a homogeneous isotropic analysis as the control group, the results are shown at the top of Figure 1. Figures 2(b) and 1(a) (middle) display permeability tensor distributions for Condition 1 ($D_{Z'Z'}$ =0 to 4) and Condition 2 (stress ratios = 1 to 5). Without considering stress direction, the minimum permeability tensor remains horizontal, while it aligns parallel to the slope when stress ratio is considered. Figure 2(a) shows permeability coefficient variations. For Condition 1 (blue line), the maximum permeability tensor increases with $D_{Z'Z'}$, while the minimum decreases. For Condition 2 (orange line), both increase with stress ratio. Figure 2(b) indicates that Condition 1 has a greater impact on permeability anisotropy than Condition 2, with a maximum value of 7 times versus 1.44 times.

Figure 1(b) presents pore pressure distributions for isotropy, Condition 1 ($D_{Z'Z'}$ =4), and Condition 2 (stress ratio = 5). Pore pressure distribution is significantly influenced by permeability anisotropy; Condition 2 shows little difference from isotropy due to lower anisotropy. Figure 2(c) shows safety factor results, mirroring trends in Figure 2(b). For Condition 1, the safety factor increases with anisotropy, while for Condition 2, it converges. Figure 1(c) illustrates maximum shear strain increments for isotropy, Condition 1 ($D_{Z'Z'}$ =4), and Condition 2 (stress ratio = 5). Higher shear strain increments occur at the slope toe, especially in Condition 1 with higher permeability anisotropy. However, the safety factor for Condition 1 is also relatively larger.

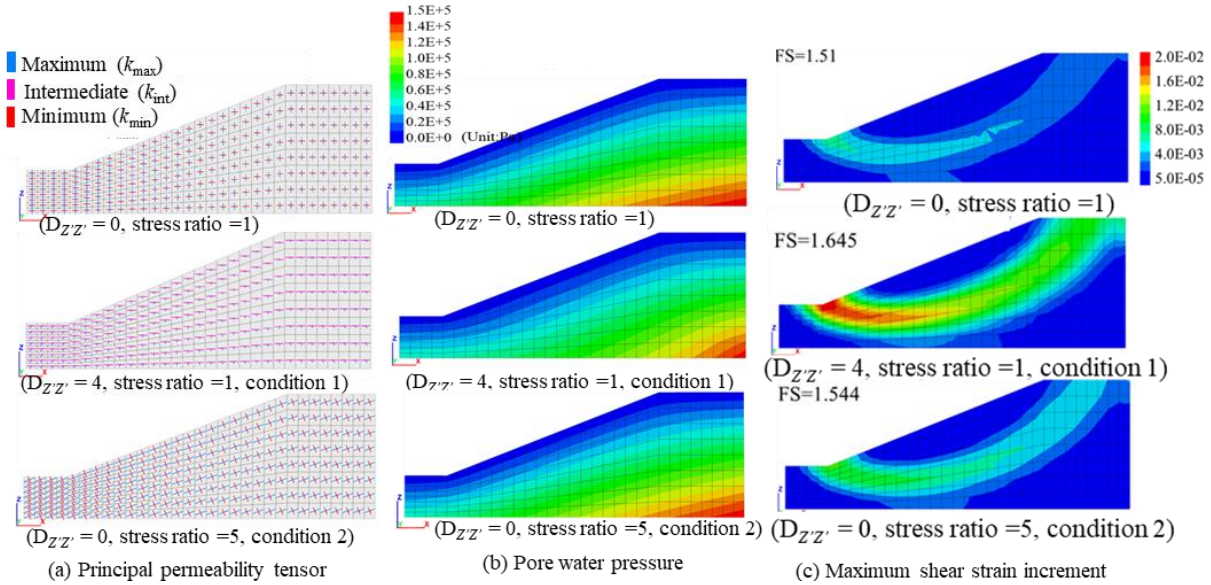

Figure 1. The distribution of permeability tensors, pore water pressure, and maximum shear strain increment for each condition.

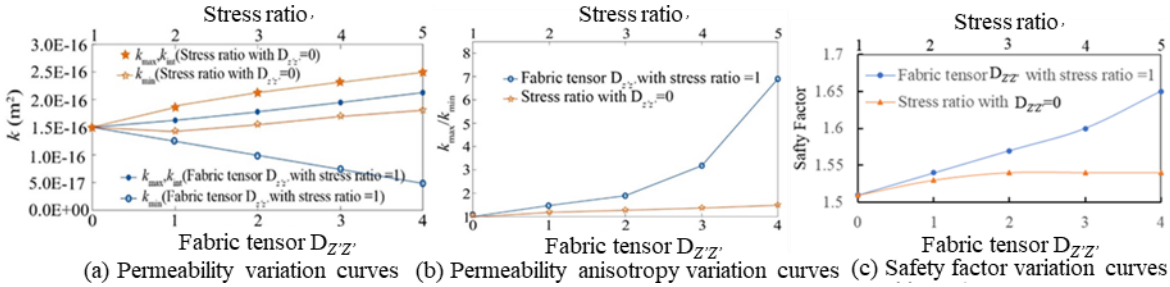

Figure 2. The permeability variation curves, permeability anisotropy variation curves, and safety factor variation lines for each condition.

Conclusion

This study simplified the analysis by treating stress and joint distribution as separate conditions. It aimed to compare their impact on permeability anisotropy. Results suggest that joint distribution has a stronger influence on permeability anisotropy when stress isn't considered. However, in Condition 2, where joint distribution remains constant, changes in permeability anisotropy are minimal.

References

Dong, J.J.; Tu, C.H.; Lee, W.R.; Jheng, Y.J. Effects of hydraulic conductivity/strength anisotropy on the stability. *Computers and Geotechnics*. 2012, 40, 147-159.

Dong, J.J.; Tzeng, J.H.; Wu, P.K.; Lin, M.L. Effects of anisotropic permeability on stabilization and pore water pressure distribution of poorly cemented stratified rock slopes. *International Journal for Numerical and Analytical Methods in Geomechanics*. 2006, 30(15), 1501-1600.

Oda, M. Permeability tensor for discontinuous rock masses. *Geotechnique*. 1985, 35(4), 483-495.

Wyllie, D.C.; Chris, M. *Rock Slope Engineering Civil and Mining*, In: Hoek, E. & Bray, J.W., Eds., Rock Slope Engineering, London, 2004.

MULTI-TEMPORAL EVALUATION OF LANDSLIDES IN A DAM RESERVOIR AREA WITH THE INTEGRATION OF MULTIPLE METHODS

TÜMAY KADAKCİ KOCA [1]

[1] *Muğla Sıtkı Koçman University, Geological Engineering Department, Türkiye, tumaykoca@gmail.com*

Introduction

The landslides in the reservoir area of dam sites necessitate profound geological and geotechnical investigations since any mass movement after dam construction may cause catastrophic damage to the engineering project. Detailed geological and geotechnical investigation of reservoir slopes and generating engineering geological models and a time-dependent mechanical approach are crucial for hazard mitigation. To date, several research have evaluated the stability of the reservoir slopes separately by the combination of field works and numerical or limit equilibrium models (Luo et al. 2019; Kafle et al. 2022). On the other hand, some of them studied with the combination of field works and remote sensing techniques (Iqbal et al. 2017; Gan et al. 2019). In general, extensive laboratory testing on rock/soil material is lacking. On the contrary, laboratory testing has been combined with numerical or limit equilibrium models to determine the stability conditions in several studies (Sun et al. 2016; Wang et al. 2022). To the best of author's knowledge, there is no multi-temporal study on the stability of reservoir slopes with the combination of different field investigations, laboratory tests, and remote sensing techniques. This study therefore aims to (i) determine the topographical evolution over time (ii) construct an engineering geological model explaining the mechanism of the landslides (iii) estimate the volume and sliding rate of landslides (iv) determine the role of triggering factors (e.g., seismic activity, heavy rainfall, wildfire) in the Miocene sedimentary rock slopes in the reservoir area.

Methods

A multi-method approach was adapted to achieve the scope of this study. Firstly, field investigations such as borehole logging, discontinuity measurement according to ISRM (2007), and geophysical survey (MASW and ERT) were performed. Secondly, laboratory works such as static and cyclic mechanical testing (uniaxial compressive and shear tests) have been performed under dry and water-saturated conditions. Afterward, photogrammetric analyses by using multi-temporal (1953-2017) aerial photographs in conjunction with the back analyses of numerical models were conducted. The purpose of using the photogrammetric results in the back analyses is to simulate the real slopes more accurately. photogrammetric displacement-based back analyses of the failed slopes have been performed by utilizing the finite element method (FEM). Numerical modeling of slopes is a useful tool to corroborate or develop the interpretation of slope behavior; however, a proper evaluation of the field observations, geological and hydrological data, as well as the physical, mechanical, and deformation properties of the rock mass is the key issue for realistic slope model. In this manner, static and cyclic laboratory tests and in-situ tests were performed.

Results

Initially, geological cross-sections passing through landslides were constructed to illustrate the main geostructural features and lithological units in the study area (Figure 1). Afterward, an engineering geological model (EGM) was constructed for the landslides in the study area based on the inferences from field observations, geophysical investigations, cored boreholes, photogrammetric analysis, and stereographic projection. The EGM provided a good understanding of the mechanism and possible time-dependent response of soil and rock units (Kadakci Koca 2021). Soil and rock materials have been depleted from the four slopes between 1953 and 2012 with an average mobilization rate of 2.06 x104 m^3/year. Hence, the landslides in the study area can be characterized by continuous movement with fluctuations in sliding rate (2012-1995: $1.37x10^4$ m^3/year, 1995-1953: $2.34x10^4$ m^3/year) due to different triggering factors. The seismic activity in 1969 was found to be the most significant triggering factor, inducing the largest material movement. It is also apparent that after the wildfire occurred in 1988, the cohesive strength of vegetation roots was lost and therefore the erosional process accelerated and

through a long period it promoted an overall decrease in shear strength in the soil mantle and the weathered and weak rock layers. Rainfall events, principally after the wildfire facilitated the transportation of granular material and played a great role in decreasing the cohesion and internal friction angle of the soil mantle and rock units.

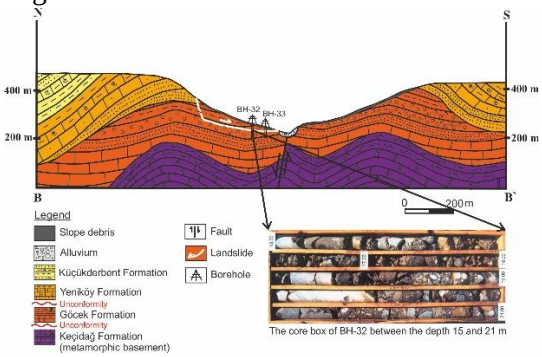

Figure 1. The geological setting of the reservoir slopes (revised from Kadakci Koca and Koca 2019)

Conclusion

The topographical evolution between 1953 and 2017 together with the mechanical and structural evolution of rock and soil units derived from back analyses gave the insight to understand the multi-temporal evolution of slope materials in a geotechnical manner. In addition, the determined fluctuations in movement rates were attributed to factors such as precipitation, fire incidents, and seismic events. However, a shorter period of differential DEMs that coincide pre-event and post-event is required for a more precise estimation of triggering factors. Hence, the landslides due to the triggering factors can not be evaluated as co-event or post-event. Overall, the study sheds light on the complex interplay of geological, hydrogeological, and geotechnical factors influencing landslide dynamics, providing valuable insights for future risk mitigation strategies in similar environments.

References

Gan, B.; Yang, X.; Zhou, J. GIS-based remote sensing analysis of the spatial-temporal evolution of landslides in a hydropower reservoir in southwest China. *Geomatics, Natural Hazards and Risk.* 2019, 10(1), 2291-2312.

International Society for Rock Mechanics (ISRM). R. Ulusay; J. A. Hudson, (Eds.). *The complete ISRM suggested methods for rock characterization, testing and monitoring: 1974-2006*. Kozan Ofset: Ankara, Türkiye, 2007.

Iqbal, J.; Tu, X.; Xu, L. Landslide Hazards in Reservoir Areas: Case Study of Xiangjiaba Reservoir, Southwest China. *Natural Hazards Review*. 2017, 18(4), 040170009.

Kadakci Koca, T. *Multi-Temporal Stability Investigation of Landslides in Çağlayan Dam Reservoir Area*. Ph.D. Thesis, Dokuz Eylül University, İzmir, Türkiye, 2021.

Kadakci Koca, T; Koca, M.Y. Volume estimation and evaluation of rotational landslides using multi-temporal aerial photographs in Çağlayan dam reservoir area, Turkey. *Arabian Journal of Geosciences.* 2019, 12, 140.

Kafle, L.; Xu, W.; Zeng, S.; Nagel, T. A numerical investigation of slope stability influenced by the combined effects of reservoir water level fluctuations and precipitation: A case study of the Bianjiazhai landslide in China. *Engineering Geology*. 2022, 297, 106508.

landslide in the Three Gorges Reservoir region under the combined effect of reservoir water level fluctuation and rainfall. *Engineering Geology*. 2016, 205, 133-145.

Luo, S.; Jin, X.; Huang, D. Long-term coupled effects of hydrological factors on kinematic responses of a reactivated landslide in the Three Gorges Reservoir. *Engineering Geology*. 2019, 261, 105271.

Sun, G.; Zheng, H.; Huang, Y.; Li, C. Parameter inversion and deformation mechanism of Sanmendong

Wang, W.; Wang, P.; Zhang, Z. Study on gravel soil strength degradation and its influence on the slope stability in reservoir bank fluctuating zone. *Engineering Failure Analysis*. 2022, 134, 105980.

3D-NUMERICAL SIMULATION OF GEOMECHANICAL FRACTURE PROCESSES IN THE VICINITY OF DEEP GEOTHERMAL DRILLINGS IN SE BAVARIA, GERMANY

JUSTIN MATTHEIS[1], CATHARINA DREXL[2], PATRICIA AMBOS[3], KUROSCH THURO

[1] *Technical University of Munich, Chair of Engineering Geology, Germany, justin.mattheis@tum.de*

[2] *Technical University of Munich, Chair of Engineering Geology, Germany, catharina.drexl@tum.de*

[3] *Technical University of Munich, Chair of Engineering Geology, Germany, patricia.ambos@tum.de*

[4] *Technical University of Munich, Chair of Engineering Geology, Germany, thuro@tum.de*

Introduction

In SE Germany, the well-known hydro-geothermal reservoir in the North Alpine Foreland Basin (NAFB) provides a suitable renewable source for domestically and industrially demanded heat (Agemar et al., 2014). However, the reservoir, i.e., carbonates reaching up to 5 km deep below the surface, shows widely known heterogeneity. Its varying hydraulic and mechanical properties constitute risks for the efficient planning and execution of these wells. Increasing the understanding of subsurface processes is a crucial task to significantly expand the share of geothermal heat supply in the heating sector. Besides the acting stress conditions, the geomechanical behavior of these deep wells is highly dependent on mechanical rock mechanical properties and the orientation of discontinuities such as faults and joints.

Methods

3D-numerical models are created using the hybrid FDEM code "Irazu" (Geomechanica Inc., Canada) to investigate the fracture process zone around a vertical wellbore, dissected by oblique joint sets. Mattheis et al. 2023 defined three typical lithologies for the carbonate reservoir and assigned typical rock mechanical parameters. Additional fracture energy testing by Ambos (2024), according to the experiments described in Kuruppu et al. (2014, mode I) and Bahrami et al. (2020, mode II) led to updated values for the "Limestone" and "Dolostone" material and completes the material parameters used for the simulations in Tab. 1. All other numerical parameters were kept at a default, and the stress tensor for the investigated depths of three to five kilometers was calculated after Potten (2020). In contrast to previous 2D FDEM models (Mattheis et al. 2023, Stockinger 2022) the three-dimensional stress tensor could be applied. The discontinuity (DFN) properties and orientations were adopted from Stockinger (2022). The model is initialized with the in-situ stress state and after 50% of timesteps the borehole excavation is simulated by reduction of the cores Young's modulus. In total, 18 3D models were simulated (nine with and nine without DFN).

Table 1. Experimentally determined material parameters used in the numerical models.

Material	Density	Young's modulus	Poisson's ratio	Tensile Strength	Cohesion	Coefficient of friction	Fracture Energy I	Fracture Energy II
	ρ_b [g/m^3]	E [GPa]	ν [-]	σ_t [MPa]	c [MPa]	μ [-]	G_{CI} [N/m]	G_{CII} [N/m]
Limestone	2.61[2]	42.96[2]	0.15[2]	5.60[2]	18.00[4]	0.6[4]	28.04[3]	133.00[1]
Strong Limest.	2.63[2]	49.44[2]	0.14[2]	10.10[2]	31.00[4]	0.6[4]	48.50[1]	243.90[1]
Dolostone	2.67[2]	52.96[2]	0.09[2]	10.10[2]	20.00[4]	0.6[4]	25.24[3]	111.90[3]

Notes: [1] after Mattheis et al. (2023); [2] after Potten (2020); [3] after Ambos (2024), [4] estimated by Irazu

Results

In general, fractured elements (= generated fractures) appear for all materials and originate from the wellbore wall. With increasing depth and, therefore, stress magnitude, the fractures penetrate deeper into the rock mass. As shown in Figure 1, the integrated joint sets weaken first, as their frictional and cohesive properties are lowest in the rock mass. Wedge-shaped breakouts form the wellbore wall and are in the direction of the least principal stress (Shmin). Although most of the fractures form after the excavation, especially near the joints, fracturing also occurs before due to the time-dependent, stepwise

reduction of Young's modulus before excavation. The "Limestone" constitutes the weakest material, and the "Strong Limestone" showed the most minor extent of fracturing, being the toughest material. A sensitivity study showed that the fracture energy parameters influence the occurring fracture pattern the most.

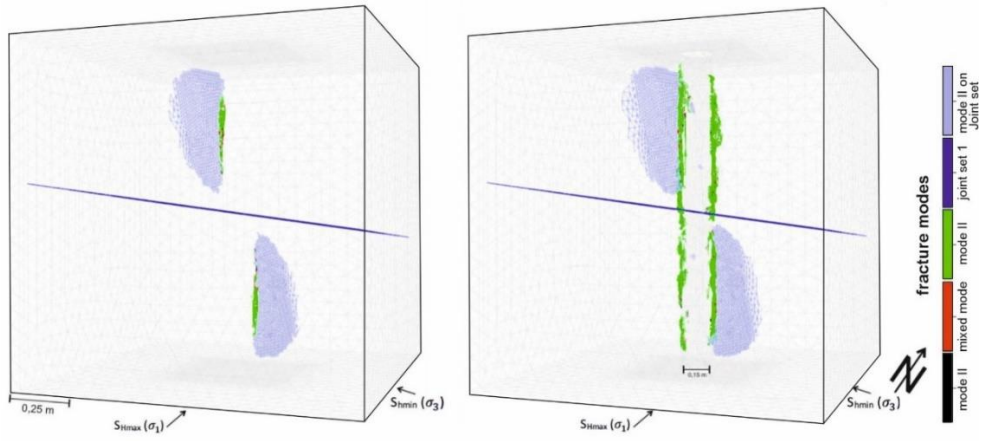

Figure 2. Fracture formation and occuring fracture modes of material "dolostone" with joint sets in 5 km. left: fracturing shortly before excavation, right: fractures after excavation, modified after Ambos (2024)

Conclusion

The modeled results show the importance of constraining the numerical results with experimentally determined input parameters, as especially the fracture energies vary significantly depending on the rock type and are, additionally, two of the most essential input parameters controlling the model's stability. The 3D-numerical models show potentially problematic scenarios regarding breakout formation and show that in-situ stresses, lithologies, and DFNs control fracture propagation. In contrast with the 2D results from Mattheis et al. 2023, it was found that discontinuities in the rock mass promote breakouts and increased fracture propagation and thus have a negative influence on borehole stability. Also, the 3D-modeled scenarios produced generally fewer fractures than the models of Mattheis et al. (2023). Expanding the models to more diverse scenarios, including deviated wells and further comparison of 2D and 3D results, is necessary to understand the subsurface conditions around the deep geothermal wells and is, thus, the subject of future work.

References

Agemar, T.; Weber, J.; Schulz, R. Deep Geothermal Energy Production in Germany. *Energies*, 2014, 7(7), 4397–4416.

Ambos, P. *Dreidimensionale geotechnische FEMDEM Modellierung eines Bohrlochs in einem tiefgeothermalen Reservoir des süddeutschen Molassebeckens*. unpubl. Master's Thesis, Technical University of Munich, Munich, 2024.

Bahrami, B.; Nejati, M.; Ayatollahi, M.; Driesner, T.; Bahramit, B. Theory and experiment on true mode II fracturing of rocks. *Engineering Fracture Mechanics*, 2020, 240(1).

Kuruppu, M.D.; Obara, Y.; Ayatollahi, M.R.; Chong, K.P.; Funatsu, T. ISRM-Suggested Method for Determining the Mode I Static Fracture Toughness Using Semi-Circular Bend Specimen. *Rock Mechanics and Rock Engineering*, 2014, 47(1), 267–274.

Mattheis, J.; Drexl, C.; Potten, M.; Stockinger, G.; Thuro, K. Borehole stability in geothermal reservoirs - A combined laboratory and numerical approach. 2023*, Proceedings of the 15th ISRM Congress 2023 & 72nd Geomechanics Colloquium*.

Potten, M. *Geomechanical characterization of sedimentary and crystalline geothermal reservoirs*. Ph.D. Thesis. Technical University of Munich, Munich, 2020.

Stockinger, G. *Fracturing in Deep Boreholes*. Ph.D. Thesis. Technical University of Munich, Munich, 2022.

VIRTUAL OUTCROP RECONSTRUCTION FOR HYDROGEOLOGICAL PARAMETRIZATION (DARUVAR, CROATIA)

IVAN KOSOVIĆ [1], MARCO POLA [1], JOSIP TERZIĆ [1], KOSTA URUMOVIĆ [1], STAŠA BOROVIĆ [1], TIHOMIR FRANGEN [1], MIRJA PAVIĆ [1], BOJAN MATOŠ [2], IVICA PAVIČIĆ [2], ANDREA BISTACCHI [3], SILVIA MITTEMPERGHER [3], STEFANO CASIRAGHI [3], GABRIELE BENEDETTI [3]

[1] *Croatian Geological Survey, Sachsova 2, Zagreb, Croatia; corresponding author: ikosovic@hgi-cgs.hr*

[2] *University of Zagreb, Faculty of Mining, Geology and Petroleum Engineering, Pierottijeva 6, Zagreb, Croatia*

[3] *University of Milan – Bicocca, Department of Earth and Environmental Sciences, Piazza della Scienza 4, Milano, Italy*

Introduction

Geothermal resources are crucial within the ongoing green energy transition because they are renewable sources of energy and raw materials. Site-specific plans based on geological and hydrogeological reconstructions are required for their preservation. Deep carbonates host important geothermal resources (Goldscheider et al., 2010), and Croatia is rich in such geothermal resources. The occurrence of thermal waters in the town of Daruvar (Figure 1A) has been extensively investigated. Thermal springs (temperatures of 38-50°C) are the outflow area of an intermediate scale hydrothermal system hosted in a fractured Mesozoic carbonate aquifer (Kosović et al., 2024). In this research, structural analyses, hydrogeological investigations, and discrete fracture network (DFN) modeling were conducted for the structural and hydrogeological characterization of the Daruvar thermal aquifer.

Methods

- Structural investigations were conducted NE of Daruvar (red square in Figure 1A) where the carbonate rock complex is exposed. They included the measurement of the main discontinuity sets and the photogrammetric reconstruction of delineated outcrops. The digital outcrop model allowed collecting a large dataset of discontinuities for the statistical analysis of their geometry (e.g., Bistacchi et al., 2020).
- Hydrogeological investigations allowed to quantify the porosity (Φ) and permeability (k) of the thermal aquifer based on the well log and pumping test of a 190 m deep well in Daruvar. Well logging was conducted after the drilling in 2008, while the pumping test was performed in 2022. The results were analyzed using classical approaches for the interpretation of pumping tests (Hantush, 1961).
- DFN modeling was used to constrain the hydrogeological parametrization of the aquifer. A model at the scale of the carbonate aquifer explored by hydrogeological investigations (Figure 1B) was constructed and calibrated using the results of structural and hydrogeological analyses.

Results

702 images were acquired resulting in a sub-cm digital outcrop model of 0.2 km^2. Virtual structural analysis depicted two dominant systems of discontinuities dipping towards N241°of 65° and N296° of 75 that reflected measured bedding and fracture sets from field investigations. A highly fractured section of the outcrop, likely similar to the intensely fractured aquifer, was selected for the statistical analysis of the geometrical features of the discontinuity sets to derive the input parameters for the DFN modeling.

Using the results of caliper log, a section of the well with tight walls was considered as representative of the natural aquifer condition. The resulting Φ from the neutron log was from 0.03 to 9.1% (average = 2.7%). The k was calculated using transmissivity values from the pumping test analyses and literature (Borović et al., 2019). Different aquifer thicknesses (investigated thickness, saturated thickness, thickness of fracture corridors) were considered resulting in a k from 7.4 to 122.8 D (average = 46 D).

The two discontinuity sets identified by structural investigations were reproduced into the DFN model. The model calibration mostly explored the discontinuity aperture. This parameter was not measured on the field because it would not be representative of the aquifer situation at depth due to the surficial relaxation of the rock mass. The result of the calibration was a linear and power correlation of the aperture with Φ and k, respectively. Considering the average Φ of the aquifer, the calibrated aperture value was 3 mm obtaining a k value of 1.5×10^5 D. Such high k was interpreted as connected to the Φ

used for the calibration, which represents the total Φ. Fluid flow is influenced by the effective Φ, which is at least an order of magnitude lower than total Φ in carbonate aquifers. This difference was accounted for by testing a "dual aperture" approach. Considering the experimental dataset, a Φ of 0.2% (10th percentile of the distribution) was tested. It resulted in a calibrated fracture aperture of 0.22 mm obtaining a k of 60.5 D (Figure 1C), comparable with the experimental dataset.

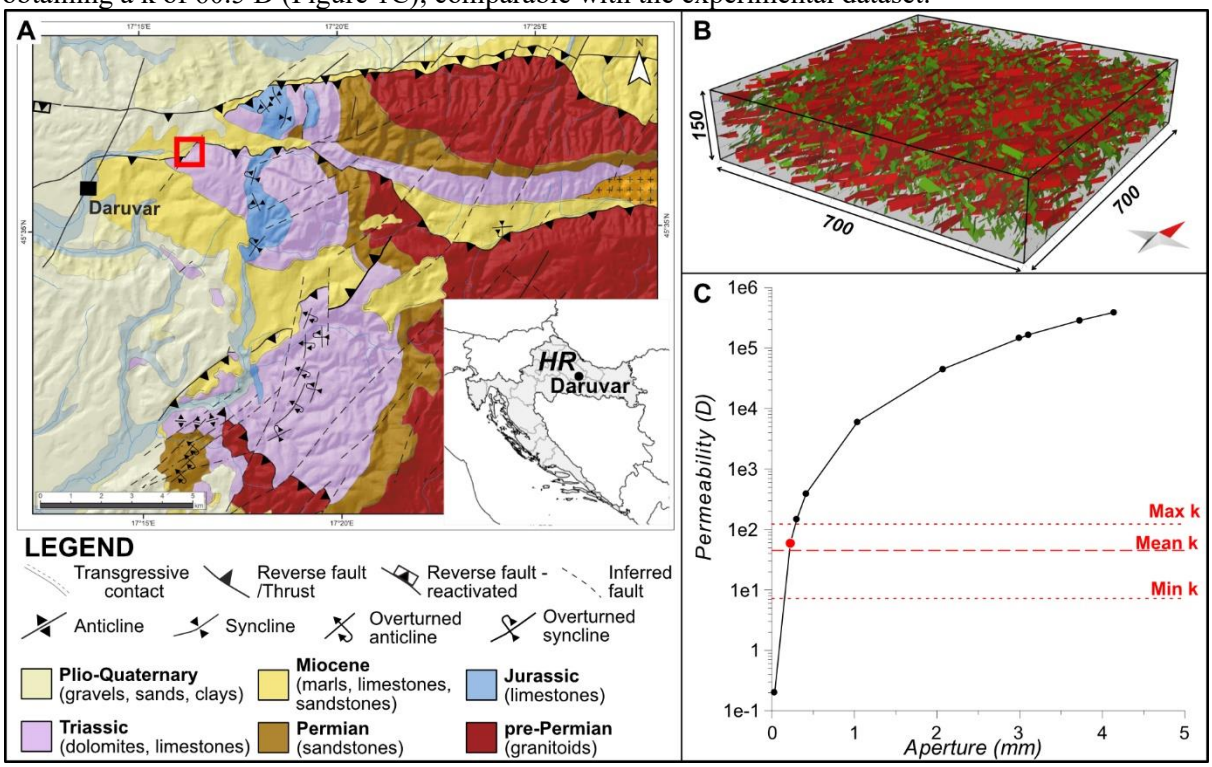

Figure 1. (A) Simplified geological map. (B) Aquifer scale DFN model. (C) The best DFN model (aperture of 0.22 mm) resulted in comparable calibrated and experimental permeability values (red dot and lines).

Conclusion

The obtained results highlight the importance of integrating structural and hydrogeological approaches to investigate fractured aquifers. Structural data can be used to determine the architecture of the fracture network in the rock mass, while hydrogeological investigations supported by numerical modeling calibrated from structural results can provide a solid hydrogeological parametrization of the aquifer.

Acknowledgments

This research was funded by the HyTheC project of HRZZ, grant number UIP-2019-04-1218.

References

Bistacchi, A.; Mittempergher, S.; Martinelli, M.; Storti, F. On a new robust workflow for the statistical and spatial analysis of fracture data collected with scanlines (or the importance of stationarity). *Solid Earth*, 2020, 11, 2535–2547

Borović, S.; Pola, M.; Bačani, A.; Urumović, K. Constraining the recharge area of a hydrothermal system in fractured carbonates by numerical modelling. *Geothermics*, 2019, 82, 128–149.

Goldscheider, N.; Mádl-Szőnyi, J.; Erőss, A.; Schill, E. Review: Thermal water resources in carbonate rock aquifers. *Hydrogeology Journal*, 2010, 18(6), 1303–1318

Kosović, I.; Matoš, B.; Pavičić, I.; Pola, M.; Mileusnić, M.; Pavić, M.; Borović, S. Geological modeling of a tectonically controlled hydrothermal system in the southwestern part of the Pannonian basin (Croatia). *Frontiers in Earth Science*, 2024, 12, 1401935.

Hantush, M.S. Aquifer Tests on Partially Penetrating Wells. *Journal of the Hydraulics Division*, 1961, 87, 171–195.

SURFACE GEOPHYSICAL INVESTIGATION OF NATURAL THERMAL SPRING AREA IN DARUVAR, CROATIA

MARCO POLA [1], IVAN KOSOVIĆ [1], JOSIP TERZIĆ [1], KOSTA URUMOVIĆ [1], BOJAN MATOŠ [2], STAŠA BOROVIĆ [1]

[1] *Croatian Geological Survey, Sachsova 2, Zagreb, Croatia, mpola@hgi-cgs.hr*¸

[2] *University of Zagreb, Faculty of Mining, Geology and Petroleum Engineering, Pierottijeva 6, Zagreb, Croatia, bojan.matos@rgn.unizg.hr*

Introduction

Renewable geothermal resources play an important role in the green global energy transition. A key factor for estimating the potential of a geothermal resource is a detailed reconstruction of the architecture of the aquifer and the geological setting in the outflow area favoring the upwelling of thermal waters. Croatia is rich in geothermal resources and the occurrence of thermal waters in Daruvar city has been extensively investigated (e.g., Borović et al., 2019; Kosović et al., 2023). This research focuses on the local scale reconstruction and modeling of the geological setting of the Daruvar thermal spring area using an integrated geophysical approach based on electrical resistivity tomography and both active and passive seismic methods.

Methods

Electrical resistivity tomography (ERT) was employed to delineate the structural and lithological properties of the Daruvar spring area. Eight profiles were acquired using an electrical imaging system in 2021 and 2022. Field apparent resistivity data were inverted into 2D resistivity subsurface models reconstructing the geometries of lithologies and structures in the subsurface (Loke et al., 2013). An integrated approach based on the active multichannel analysis of surface waves (MASW) and the passive horizontal-to-vertical spectral ratio (HVSR) methods was applied to map the thickness of the Quaternary cover. The center of the MASW seismic profile was located where the 6 stations of HVSR measurement were conducted. The seismic impedance contrast between bedrock and unconsolidated Quaternary sediments creates a peak in the H/V curve (ratio of horizontal to vertical seismic noise spectra), which was used to estimate the thickness of the alluvial cover (Nakaruma, 2019). The thickness calculation depends on the vertical distribution of the surface waves' velocity, which was assessed using the MASW approach for a site-specific reconstruction (Park et al., 1999).

Results

The spatial distribution of resistivity shows relatively low values from 10 to 150 Ωm (Figure 1). Based on the stratigraphic logs of the wells, three resistivity layers/geological units were identified (Figure 1): (1) the Quaternary alluvial cover with resistivity ranging between 30 and 50 Ωm (layer 1); (2) the Neogene sediments with resistivity values of 10-30 Ωm (layer 2); and (3) the Triassic dolomites that were divided in a compact layer with resistivity ranging from 70 to 150 Ωm (layer 3a) and a fractured layer characterized by resistivity values of 20-30 Ωm (layer 3b). Furthermore, sharp lateral variations in the resistivity distributions were observed. They were generally marked by low resistivity anomalies and were interpreted as fracture zones along the faults (dashed red lines in Figure 1). The high secondary porosity of the fracture zones, which was connected to their intense fracturing, and the occurrence of thermal waters decreased the bulk resistivity of the rock mass.

The obtained results allowed us to reconstruct the architecture and geological properties of the Daruvar thermal spring area. The Quaternary cover has a thickness of 5 to 15 m increasing northward and eastward. Its thickness and geometry were confirmed by the seismic investigations. Neogene deposits are generally found below the Quaternary alluvial cover, except for the central part of the study area where the Triassic dolomites are found at the surface. Two main faults border southward and eastward the thermal spring area juxtaposing the highly permeable Triassic dolomites with the low permeable Neogene deposits. This lateral contrast fosters the rising of the thermal waters forming a shallow thermal resource in the Daruvar area. The main outflow of the Daruvar thermal springs, represented by the Antunovo vrelo, Blatna kupelj, and Ivanovo vrelo springs (A, B, and I, respectively, in Figure 1), occurs

within the interaction zone of the faults imaged through ERT. Faults are associated with highly permeable damage zones that represent a preferential pathway for the circulation of thermal fluids. The connected fault zones enhance the upwelling of thermal waters resulting in the occurrence of the thermal springs with water temperature up to 48°C (Borović et al., 2019).

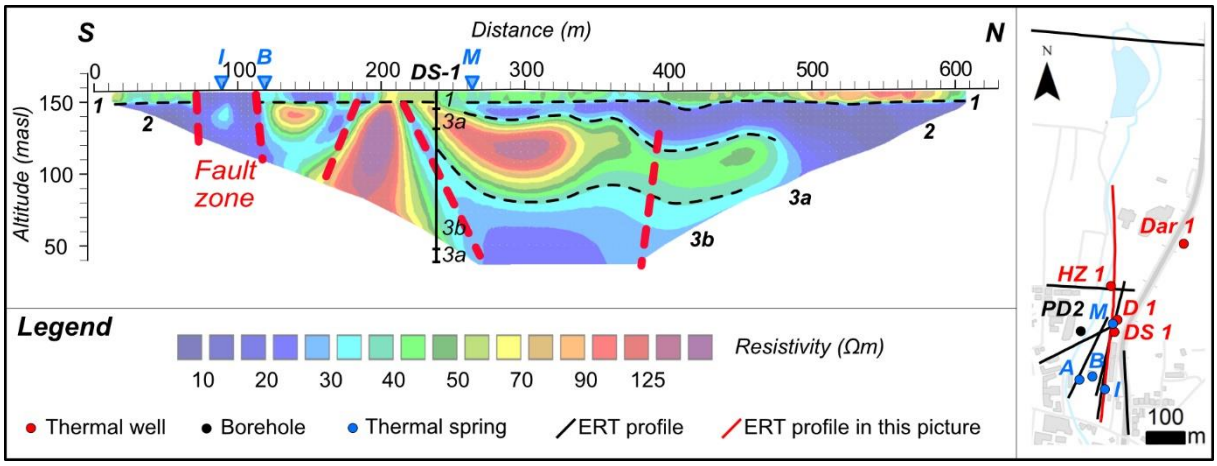

Figure 1. Inverse resistivity model of an ERT profile (red line in the map) conducted with 10 m spacing between electrodes. It shows a general overview of the resistivity distribution in the Daruvar spring area. Dashed red lines indicate fault zones characterized by low resistivity values. The map shows the traces of ERT profiles (black lines) and the locations of springs and boreholes (dots) used for the geological reconstruction.

Conclusion

This research focused on the reconstruction of the geological and structural settings of the Daruvar thermal spring area using different geophysical methods. Their joint interpretation completed with the stratigraphic logs of exploitation wells and boreholes allowed the reconstruction of the vertical and horizontal distributions of lithological units and proved the occurrence of faults deforming the bedrock in the Daruvar area. The local fault and fracture networks permit a quick upwelling of thermal fluids resulting in thermal springs with temperatures up to 48°C. This work proves that a cost-effective geophysical approach could be used to investigate shallow geothermal systems hosted in fractured carbonate rocks.

Acknowledgments

This research was funded by the HyTheC project of HRZZ, grant number UIP-2019-04-1218.

References

Borović, S.; Pola, M.; Bačani, A.; Urumović, K. Constraining the recharge area of a hydrothermal system in fractured carbonates by numerical modeling. *Geothermics*, 2019, 82, 128–149.

Kosović, Ivan; Briški, Maja; Pavić, Mirja; Padovan, Božo; Pavičić, Ivica; Matoš, Bojan; Pola, Marco; Borović, Staša. Reconstruction of Fault Architecture in the Natural Thermal Spring Area of Daruvar Hydrothermal System Using Surface Geophysical Investigations (Croatia). *Sustainability*, 2023, 15; 12134, 22.

Nakamura, Y. What Is the Nakamura Method? Seismol. Res. Lett. 2019, 90, 1437–1443.

Park, C.B.; Miller, R.D.; Xia, J. Multichannel Analysis of Surface Waves. Geophysics 1999, 64, 800–808.

3D RANDOM FIELD MODELLING OF SUBSURFACE STRATIGRAPHY AND GEOTECHNICAL PARAMETERS IN THE TAIPEI BASIN: IMPLICATIONS FOR MAPPING V_{S30}

STEFAN CHRISTOPHER NICHOLAS[1], JIA-JYUN DONG[2], YU-CHEN LU[3]

[1] PhD Candidate, Graduate Institute of Applied Geology, National Central, University, Taiwan, stefan_nicholas@hotmail.co.uk

2 Professor, Graduate Institute of Applied Geology, National Central, University, Taiwan, jjdong@geo.ncu.edu.tw

3 Postdoc, Graduate Institute of Material Sciences and Engineering, National Central, University, Taiwan, erwin92302101@hotmail.com.

Introduction

Seismic hazards are a significant challenge in Taiwan, especially in the Taipei Basin, which is particularly vulnerable due to site effects and its high population density. Covering an area of around 243 km², the Taipei Basin's top 30 meters mainly consists of alternating layers of sand and clay from the Sungshan Formation, and in some areas towards the basin margins, the underlying Jingmei Formation, which is composed of alluvial gravel. The average shear-wave velocity of the upper 30 meters of the ground (V_{S30}) is commonly used to assess site effects (Anderson et al. 1996; Park and Elrick 1998; Huang et al. 2007; Tsai et al, 2021), caused by soft alluvial sediment overlying hard rock, resulting in amplified shear-waves and intensified ground motion (Kuo, 2011). This creates the need for an accurate regional scale V_{S30} map for the Taipei Basin. Previous studies on V_{S30} mapping in the Taipei Basin have primarily relied on interpolation methods, such as Kriging, to generate V_{S30} maps (Lee and Tsai, 2008). However, these approaches often overlook the impact of geological and geotechnical model uncertainty on V_{S30} estimation, resulting in maps that may not fully capture the spatial variability of geological and geotechnical properties. To address this issue, we utilised a stratigraphic based geo-property random field model (SGRF) (Lu et al., 2024) to produce probabilistic stratigraphic and geotechnical parameter models and assess the associated uncertainties. In the SGRF model, stochastic Markov random field (SMRF) (Li et al., 2016; Wei and Wang, 2022; Lu et al., 2024) provides the probabilistic framework for the geological model. After the geological model is established, geotechnical parameter models for unit weight and void ratio are developed using fractional Brownian motion (fBM). These models are subsequently used to generate shear-wave velocity models, which are then employed to calculate V_{S30}. After multiple realisations, the mean and standard deviation of V_{S30} is used quantify the spatial variability and uncertainty.

Methods

The workflow for this study is outlined in Figure 1. First, data from 6,804 boreholes was collected and screened, including stratigraphic configurations, unit weight, and void ratio. Following this, an initial geological model was simulated utilizing SMRF theory (Li et al., 2016; Wei and Wang, 2022; Lu et al., 2024). This involves establishing a neighbor system and simulation order, followed by performing Markov Chain Monte Carlo (MCMC) simulations to produce multiple potential realizations of the subsurface stratigraphy, enabling the quantification of uncertainty through the principle of information entropy. Bayesian machine learning calibrates the parameters of the SMRF model based on the probability of correctly predicting soil layers in observation wells from each MCMC simulation (Lu et al., 2024). Subsequently, geotechnical parameter models are simulated using fractional Brownian motion (fBM). This starts with determining the spatial probability of geotechnical parameters within a neighbor system based on the geological model. Once the neighbor system, spatial probability, simulation order, and standard deviation spatial matrix have been established, MCMC simulations are then performed. Statistical values of geotechnical parameters for each soil layer from each MCMC simulation are used with Bayesian machine learning to calibrate parameters of fBM. Shear-wave velocity (Vs) models are calculated using Vs estimation functions that correlate vertical effective stress (calculated from the unit weight models and groundwater level data) and void ratio to Vs for different soil types. The mean and standard deviation of Vs across the Taipei Basin are then calculated after 500

realisations. Finally, a V_{S30} distribution map is created based on the mean Vs in the top 30 m of the ground, and the V_{S30} uncertainty is compared to the geological model uncertainty.

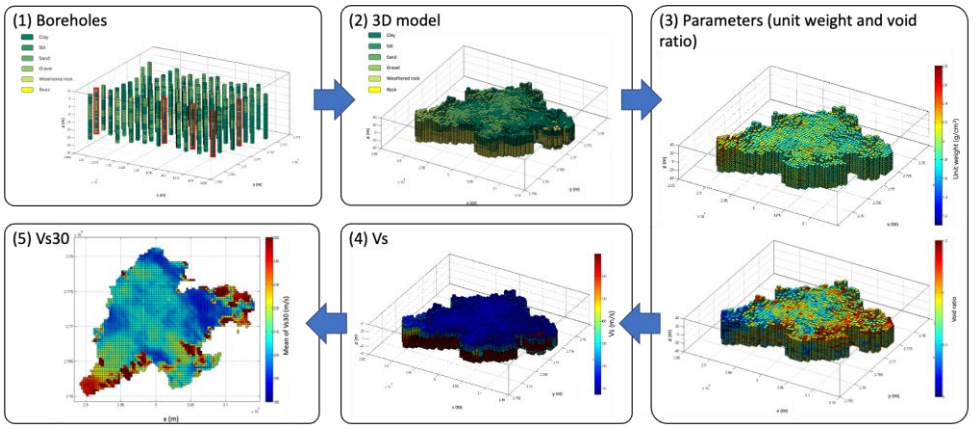

Figure 1. Research workflow; (1) digitalize borehole data, (2) generate 3D Markov random field-based geological model, (3) create geotechnical parameter models using Fractional Brownian Motion, (4) generate shear wave velocity (Vs) models using estimation functions that correlate Vs to void ratio and vertical effective stress, (5) produce V_{S30} map for the Taipei Basin.

Results

According to the results, the majority of the region's V_{S30} values range from approximately 190 to 220 m/s, which aligns with measured V_{S30} values from strong motion stations within the basin. While at the southern and eastern boundaries of the study area, V_{S30} values rise to around 250 m/s, which is also observed in the measured data. Compared with previous V_{S30} maps within the Taipei Basin, such as by Lee and Tsai 2008, our results show a similar trend but with key differences in more localised areas. For example, our study identifies larger low V_{S30} areas (<180 m/s) in the north and northeast of the basin, which are critical for seismic hazard assessments. The results also show that the shear-wave velocity distribution is closely correlated to the different geological layers, and areas with higher geological model uncertainty also exhibit higher uncertainty in V_{S30}. This is shown in Figure 2, where the average information entropy in the top 30 m of the ground ($I_{E,30}$), which is used to quantify the uncertainty in the geological model, is compared to the standard deviation of the V_{S30} map.

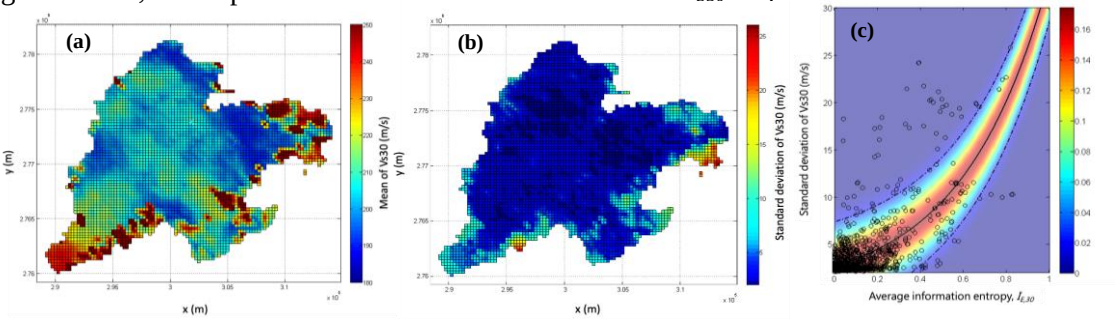

Figure 2. (a) Mean of V_{S30} in the Taipei Basin after 500 realisations, (b) standard deviation of V_{S30} in the Taipei Basin after 500 realisations, (c) relationship between uncertainty in the geological model and standard deviation of V_{S30}.

Conclusion

This study utilises a probabilistic framework to estimate V_{S30} in the Taipei Basin, while considering the spatial distribution of geological layers and geotechnical parameters. The findings emphasize the critical importance of considering geological model uncertainty when calculating V_{S30}, Furthermore, the random field method offers several advantages over traditional geostatistical methods by directly considering the spatial distribution characteristics of the subsurface stratigraphy.

References

Anderson, J. G., Lee, Y., Zeng, Y., and Day, S. (1996). Control of strong motion by the upper 30 meters, Bull. Seismol. Soc. Am. 86, 1749–1759.

Huang, M. W., Wang, J. H., Ma, K. F., Wang, C. Y., Hung, J. H., and Wen, K. L. (2007). Frequency-dependent site amplifications with f ≥ 0:01 Hz evaluated from the velocity and density models in Central Taiwan, Bull. Seismol. Soc. Am. 97, 624–63

Kuo, C. H., Wen, K. L., Hsieh, H. H., Chang, T. M., Lin, C. M., & Chen, C. T. (2011). Evaluating empirical regression equations for VS and estimating VS30 in northeastern Taiwan, Soil Dynam. Earthq. Eng. 31, 431–439.

Lee, C. T., and Tsai, B. R. (2008). Mapping VS30 in Taiwan, Terr. Atmos. Ocean. Sci. 19, 671–682.

Li, Z., Wang, X., Wang, H., and Liang, R.Y. (2016). Quantifying stratigraphic uncertainties by stochastic simulation techniques based on Markov random field, Eng. Geol. 201, 106–122.

Lu, Y. C., Chien, W. Y., Nicholas, S. C., Dong, J. J., Juang, C. H., and Tien, Y. M. (2024). Three-dimensional probabilistic geological and geotechnical property modeling. Geotech 2024 (TGS), 26-28 Aug., Tainan, Taiwan.

Park, S., and Elrick, S. (1998). Predictions of shear-wave velocities in southern California using surface geology, Bull. Seism. Soc. Am. 88, 677– 685.

Tsai, C. C., Kishida, T., & Lin, W. C. (2021). Adjustment of site factors for basin effects from site response analysis and deep downhole array measurements in Taipei, Eng. Geol. 285, 106071.

Wei, X., and Wang, H. (2022). Stochastic stratigraphic modeling using Bayesian machine learning, Eng. Geol. 307, 106789.

FROM DATA TO DEPTHS: A JOURNEY INTO 3D GEOLOGICAL MODELLING

LUCIE BAUDOUY [1], ANNA FIORAVANTI [1], CEDRIC DUVAIL [1]

[1] *Ginger CEBTP, France,* c.duvail@groupeginger.com

Introduction

In this extended abstract, we present the general methodology employed by our geological consulting team to deliver 3D geological models to our clients across various thematic areas. Our approach involves applying agile methods, utilizing disparate data of varying quality and sources, to provide cost-effective and time-efficient models that meet the study's requirements.

Methods

The development of a 3D subsurface model is a multifaceted process that demands a structured approach. The methodology encompasses several critical stages, each contributing to the accuracy and utility of the final model. Herein, we present an outline of the essential steps involved in this process.

The foundation of any reliable 3D subsurface model lies in the comprehensive collection and meticulous preparation of relevant data. Geological maps, field surveys, borehole logs, and geophysical survey results constitute the primary data sources. The precision of these data sets directly impacts the quality of the model, requiring rigorous validation and calibration to ensure their reliability and coherence.

Identifying the geological units to be represented in the model is a critical task. This step requires a detailed analysis of the collected data to discern the various geological formations present within the study area. The differentiation of these units is based on their lithological, structural, and geotechnical characteristics, which are essential for constructing an accurate and functional model. The clear identification and delineation of these units is imperative for the subsequent modelling processes.

The prepared data are then imported into specialized 3D modelling software, such as Leapfrog Works. This stage involves ensuring that the data is correctly formatted and compatible with the software's requirements. The integrity of the data during importation is essential, as any discrepancies or errors can propagate through the modelling process, potentially compromising the model's accuracy.

After the data import, the next step is the creation of the 3D subsurface model by constructing a three-dimensional representation of the subsurface geological units. The software employs advanced interpolation techniques to generate continuous surfaces that define the boundaries between different geological formations. This step is iterative, with continuous refinements made to improve the fidelity of the model based on the input data.

The verification and adjustment stage is critical for ensuring the model's accuracy. This involves comparing the model's output with the original field data and making necessary adjustments to rectify any inconsistencies. The use of validation techniques, such as cross-validation with independent data sets, enhances the reliability of the model. This stage may require multiple iterations to achieve a model that accurately represents the subsurface conditions.

Results

Geological modelling enables spatial visualization and representation of geological units and formation geometries. This approach is important for engineers and infrastructure designers to better understand the nature and distribution of geological materials in subsurface environments. It also facilitates the estimation of physical properties distribution such as strength, permeability, and density, which are essential for assessing the mechanical behaviour of materials and incorporating these parameters into structural design.

By modelling various geological units and considering their geotechnical characteristics, geological modelling also assesses geotechnical risks associated with urbanization and infrastructure development (Fioravanti and Ricard, 2022). It helps identify potentially problematic areas, such as zones prone to landslides, differential settlements, or underground cavities (Duvail *et al.* 2021).

Groundwater management benefits significantly from geological modelling by enhancing understanding of groundwater reservoirs' geometries and distributions (Duvail *et al.* 2018).

Moreover, geological modelling provides essential input data for simulating site effects in seismic hazard assessment (Fioravanti and Ricard, 2024). It predicts local amplification phenomena of seismic

intensity, duration, and damage caused by seismic waves, critical for siting facilities like power plants, dams, or storage facilities that require precise identification of the depth to bedrock.
Lastly, it aids in estimating the nature of rocks for excavation, contributing to effective planning, material re-employment and management of underground infrastructure.

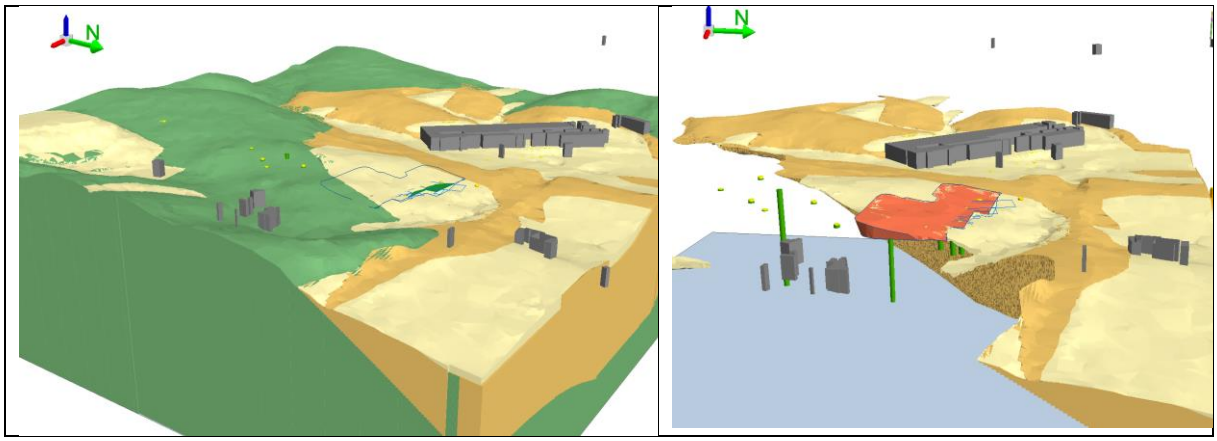

Figure 1. Example of a geological model built to estimate the volume of different materials (soft sediments versus bedrock) to be excavated (Duvail *et al.* 2022)

Conclusion

Our comprehensive methodology for developing 3D geological models showcases the integration of diverse data sources through agile and cost-effective practices. By systematically collecting, preparing, and validating geological, geotechnical, and geophysical data, we ensure the creation of accurate and reliable subsurface models. These models are indispensable tools for engineers and infrastructure designers, providing significant insights into the spatial distribution and physical properties of geological units. They also play a vital role in assessing geotechnical risks, managing groundwater resources, and evaluating how a site's geologic conditions will respond to seismic shaking. Additionally, our models optimize survey campaigns by identifying the most relevant areas for data collection, ensuring that survey efforts are both efficient and effective. Ultimately, our approach facilitates informed decision-making and enhances the planning and management of various infrastructure projects. The geological model also constitutes a useful and comprehensive discussion support between the various stakeholders and decision-makers. As we continue to refine our techniques and incorporate new data, our models will become even more precise, further supporting the successful execution of diverse geotechnical and engineering studies.

References – Few examples of main projects

Fioravanti A., Ricard B., Le Havre Wind turbines factory Extension B115, *Siemens Gamesa Renewable Energy* - France – 2024

Duvail C., Baudouy L., Fioravanti A., Update of the Cadarache geological model around the INB56 facility, France, 2022

Fioravanti A., Ricard B., Technip – Eastman - Saint Jean de Folleville, Construction of a new plant on the banks of the Seine, *Eastman Sequel project*, France, 2022

Duvail C., Baudouy L., Fioravanti A., 3D modelling of the salt cavities of la Madeleine, *Rhodia Chimie*, France, 2021

Duvail C., Baudouy L., Fioravanti A., 3D geological modelling for the management of the aquifers in Argens valley (Var). *Syndicat de l'Eau du Var Est (SEVE)*, France 2018

Topic 9

Geo-Aspects of Earthquake Engineering

DETAILED STUDY OF A LATERAL SPREADING FOLLOWING THE 2020 PETRINJA EARTHQUAKE (M_W = 6.4) - KUPA RIVER (CROATIA)

NGUYEN LAURA [1], MOIRIAT DENIS [1], GÉLIS CÉLINE [1], HÜRTGEN JOCHEN [2], BENZ-NAVARETTE MIGUEL [3], MRAVLJA BRUNO [4], LUONG TUAN ANH [3], REIFFSTECK PHILIPPE [5], JOSEPHINE LOUIS KIM [2], BAIZE STEPHANE [1], BELIĆ NIKOLA [6], MASLAČ JOSIPA [6], WACHA LARA [6], KORDIĆ BRANKO [6] AND MARKUŠIĆ SNJEŽANA [4]

[1] IRSN, France, *laura.nguyen@irsn.fr*; *denis.moiriat@irsn.fr*; *céline.gelis@irsn.fr*; *stephane.baize@irsn.fr*

[2] RWTH Aachen University, Germany, *j.huertgen@nug.rwth-aachen.de*; *kim.josephine.louis@rwth-aachen.de*

[3] Sol Solution, France, *mbenz@sol-solution.com*; *taluong@sol-solution.com*

[4] University of Zagreb, Faculty of Science, Croatia, *bruno.mravlja@gfz.hr; markusic@gfz.hr*

[5] Gustave Eiffel University, France, *philippe.reiffsteck@univ-eiffel.fr*

[6] HGI-CGS, Croatia, *nbelic@hgi-cgs.hr*; *jmaslac@hgi-cgs.hr*; *lwacha@hgi-cgs.hr*, *bkordic@hgi-cgs.hr*

Introduction

The Petrinja earthquake in Dec. 2020 caused extensive liquefaction occurrences with a lot of sand blows and cracks in the alluvial plain of the Kupa river and, in some of its meanders, local ground subsidence and lateral spreading. All these features are located in flat areas close to the riverbanks in the youngest alluvial terrace (Holocene). From the ground surface, these sediments correspond to 2 m thick clayey silts (Unit 1) overlying different sands at least 3 m thick (Unit 2) and then gravels (Unit 3). Hydraulically, Units 2 and 3 are water-saturated by the alluvial aquifer of the Kupa. All the sand blows correspond to poorly graded sands with silts (SP-SM or SM) and originate from sand bars developped in the convex parts of meanders and buried between 3 and 6 m below the surface (Luong et al., 2023).

This work focuses on one convex meander whose sedimentary aggradation geometries are well highlighted by the DEM image with 0.5 m resolution (points bars, Fig. 1A). Its southern part (site D1) presents alignments of sand blows still observable in 2022, while its northern part (site D2) shows a distribution of long open fissures up to more than 90 m from the bank, reflecting a lateral movement towards the river channel. Only a few traces of sand blows can still be seen on D2 site in 2022.

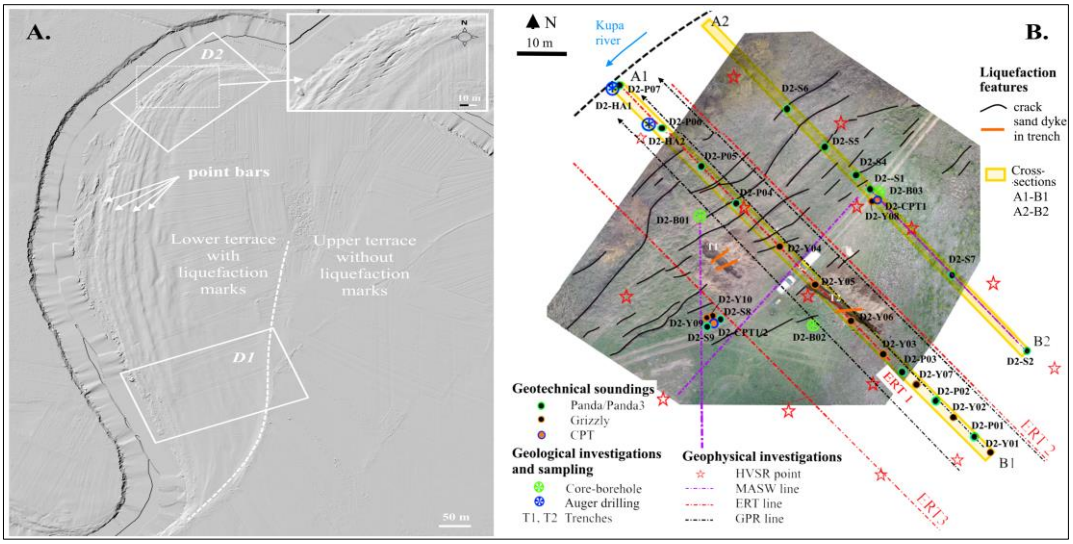

Figure 1. A. Digital Elevation Model (DEM) of site D and B. Location of investigations at site D2

This sliding of non-liquefable layers over liquefied material at depth depends on many factors including the thickness and depth of the liquefied layer (Bunn & Gillins, 2015). In order to identify the causes and mechanisms of this lateral spreading, geotechnical and geophysical investigations were carried out at sites D1 and D2 between Sept. 2022 and March 2024 (Fig. 1B).

Methods

Given the geological context, the guiding idea was to intersect the structures by carrying out cross-sections perpendicular to the Kupa riverbanks (Fig. 1B). We prospected up to a depth of 15 m which is the maximum depth known for surface liquefaction occurrence (Huang & Yu, 2013). Geophysical measurements such as Ambient noise measurements (HVSR), Multichannel Analysis of Surface Waves (MASW), Ground Penetrating Radar (GPR) and Electric Resistivity profiles (ERT) were carried out notably to highlight the geometries of structures at depth. They supplement geotechnical soundings (Dynamic Cone Penetrometer Tests DCPT) and core-boreholes in order to build a detailed model of this lateral spreading. Four trenches for observations and sampling and shear vane tests in cohesive soils also allow to underline the differences between D1 and D2 sites. The results of three Cone Penetrometer Testing (CPT) implemented in 2024 (Fig. 1B) have not yet included in the analysis.

Results

Whatever D1 or D2 sites, the limits at depth between the sedimentary units (Units 1 to 3) show large undulations along a cross-section (Fig. 2) with the same wavelength as those of the points bars at the surface (Fig. 1A). However, this sedimentary organisation in sub-horizontal layers is disturbed locally by subvertical rises of liquefied materials within the Units 1 and 2 (clearly identified on ERT profiles). Above sand blows or sand dykes in trenches, the HVSR measurements reveal a high frequency peak between 4 and 6 Hz. The combination with the Vs measurements (MASW) between 100 and 150 m/s in Unit 1 and 2 (Fig. 2) tends to pinpoint a strong contrast at the bottom of Unit 2 and presumably due to liquefaction of the layers overlying this contrast.

Unlike D1, the site D2 would have presented during the ground shaking a continuous and thicker liquefied layer in the Unit 2 (Fig. 2) allowing lateral movement of non-liquefiable layers above it. All the sandy materials in this liquefied layer are prone to liquefaction with grain sizes close to those of sand blows or sand dykes sampled in the trenches. Their soil resistance (q_d < 2 MPa) and their low shear wave velocity (Vs < 150 m/s) also correspond to loose to very loose sediments. Moreover, the undrained cohesion of the silty cover of Unit 1 at site D2 (~75 KPa) lower than that measured at the site D1 (~125 KPa) must have facilitated fracturing as a result.

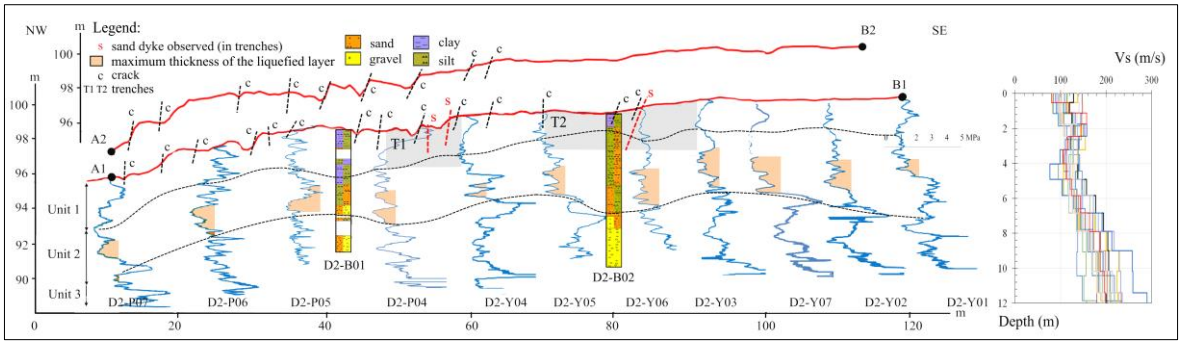

Figure 2. Site D2 - Geotechnical cross-section of a lateral spreading (location on Fig. 1B)

Conclusion

This work sets out the conditions that led to the occurrence of a lateral spreading (site D2) during the Petrinja earthquake in a convex part of a meander of the Kupa river and underlines the notable differences with an adjacent area with only alignments of sand blows at its surface (site D1).

References

Bunn, M.D. and Gillins, D.T., 2015. Assessing lateral spread analysis in areas prone to great and long-duration earthquakes." USGS Report Award G14AP00067.

Huang, Y. and Yu, M., 2013. Review of soil liquefaction characteristics during major earthquakes of the 21st century, Natural Hazards, 65(3): 2375-2384.

Luong, T.A. et al. 2023. Use of the new dynamic cone penetrometer for the study of soil liquefaction along the Kupa (Croatia), Proceedings of the 9th Conf. Croatian Geotech., May 4- 6., ISBN: 978-953-48525-2-1, 101-110.

MACROSEISMIC DATA TO CHARACTERIZE LOCALIZED TOPOGRAPHICAL DAMAGE PATTERNS IN NORTHERN CROATIA AFTER 2020 ZAGREB AND PETRINJA EARTHQUAKES

DAVOR STANKO [1], IVICA SOVIĆ [2], SNJEŽANA MARKUŠIĆ [2]

[1] University of Zagreb, Faculty of Geotechnical Engineering, Varaždin, Croatia; davor.stanko@gfv.hr

[2] University of Zagreb, Faculty of Science, Department of Geophysics, Zagreb, Croatia, sovic@gfz.hr; markusic@gfz.hr

Introduction

On 22 March 2020, Zagreb was hit by the strongest earthquake since 1880 with a magnitude of 5.5 (Markušić et al. 2020). The intensity of VII-VIII °EMS-98 was observed near the epicentral area. In the same year, on 29 December 2020, the wider Petrinja area was hit by a destructive earthquake of magnitude 6.2 with an observed intensity of VIII °EMS (Markušić et al. 2021) in the epicentral area (Figure 1). A considerable part of the reported damage (intensity VI according to EMS classification) to churches, museums, cultural and older buildings and houses in Northern Croatia occurred in topographical areas (marked in Figure 1).

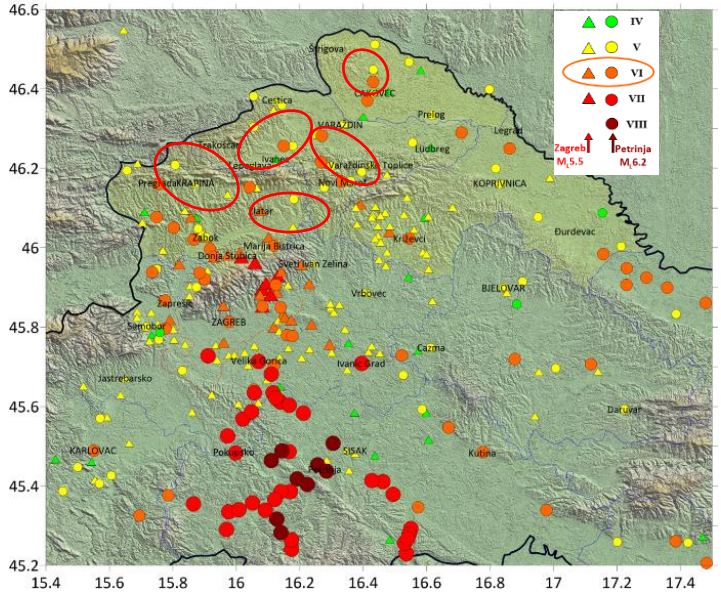

Figure 1. Macroseismic data from 2020 Zagreb and Petrinja earthquakes. (Source of data: Ivica Sović, Seismological Survey of Croatia at University of Zagreb, Faculty of Science, Department of Geophysics)

Methods

Relevant macroseismic observations and data for the study region are compiled from the most recent events of 2020. Macroseismic data (archives, church records) from historical earthquakes in this region, i.e., Međimurje M5.1 in 1738, Great Zagreb M6.3 in 1880, Mt. Ivanščica M4.7 in 1982, Kraljev Vrh M4.9 in 1990 and Ludbreg-Kalnik M4.7 in 1993 are also collected to analyze possible differences between stratigraphic and topographic macroseismic intensity observations and the associated impact on damage.

Results

Table 1. shows the macroseismic observations of the most recent events of 2020 in Northern Croatia with a classification of damage according to the EMS98 scale. For example, in Trakošćan Castle, which was built on a topographic peak, slight damage was observed in the form of diverging thin cracks that formed in places that are important for the load-bearing capacity of the masonry vaults (Markušić et al. 2021b). The first damage to the Chapel of St. Margarete in Kapelščak was also detected in March 2020, and new damage with internal and external cracks appeared after December 2020. The Diocese of

Varaždin has closed numerous churches that were damaged in those two earthquakes. It is worth mentioning that several places (e.g., Trakošćan, Klenovnik, Kraljev Vrh, Koprivnički Bregi, Ludbreg, Kalnik, Novi Marof, Krapina) were also damaged by relatively moderate earthquakes in 1982, 1990 and 1993. Historical earthquakes provide a deep insight into the consequences, and new findings from recent events are helpful in mitigating the consequences of future earthquakes, especially in topographic areas.

Table 1. Some topographic locations with reported damage from earthquakes in 2020 with damage classification according to the EMS98 scale (based on data provided by the Conservation Departments of Varaždin and Krapina)

County	Site / Object	EMS98 damage 2020 earthquakes	Historical earthquake damage
Međimurje	Kapelščak - Chapel of St. Margarete	K2	1738
	Štrigova - Church of St. Jerome	K2	1738, 1880
Varaždin	Klenovnik Castle (Hospital)	K2	1982
	Maruševec - Church of St. George	K3	1982
	Trakošćan Castle	K2	1880, 1982
	Natkrižovljan – Church of St. Barbara	K2	1880
Koprivnica-Križevci	Novi Marof – Castle Erdody (Hospital)	K2	1880, 1982, 1993
	Koprivnički Bregi – Church of St. Rok	K2	1993
	Gornji Dubovec - Church of St. Margaret	K3	1993
	Laz Bistrički - St. Andrije Church	K2	1880
Hrvatsko Zagorje	Slani Potok - The Chapel of St. Fabian and St. Sebastian	K4	1880
	Sveti Ivan Zelina - Museum	K2	1880
	Chapel of the Blessed Virgin Mary in Strmec	K4	1880, 1990
	Klanjec – Parish church of the annunciation of the Blessed virgin Mary	K2-K3	1880, 1990
	Gornje Jesenje - The Church of St.John	K3	1880, 1982
	Kraljev Vrh - Three Kings Church	K2	1880, 1990

Conclusion

When it comes to historical and recent earthquakes, what matters from an engineering and societal perspective is the damage and cost, regardless of whether it was caused by a single earthquake or a main/aftershock. From a seismological point of view, even small improvements in the definition of the main seismological parameters of an earthquake that are relevant for a given area (e.g., location of the epicenter, earthquake magnitude) and the definition of local soil conditions are very important. It is of great importance to understand these effects on seismic hazard and risk in order to ensure better mitigation, prevention and reduction of earthquake disasters in the affected stratigraphic and topographic areas.

Acknowledgments

This work was supported by the Croatian Science Foundation under the project “Seismic ground motion amplification induced by topographic irregularity in Northern Croatia” [HRZZ-IP-2022-10-1296].

References

Markušić, S., Stanko, D., Korbar, T., Belić, N., Penava, D., Kordić, B., *The Zagreb (Croatia) M5.5 earthquake on 22 March 2020,* Geosciences, 10 (2020), 7; 252, 21. doi: 10.3390/geosciences10070252

Markušić, S., Stanko, D., Penava, D., Ivančić, I., Bjelotomić Oršulić, O., Korbar, T., Sarhosis, V. *Destructive M6.2 Petrinja Earthquake (Croatia) in 2020—Preliminary Multidisciplinary Research,* Remote sensing, 13 (2021a), 6; 1095, 29. doi: 10.3390/rs13061095

Markušić, S., Stanko, D., Penava, D., Trajber, D., Šalić, R. *Preliminary observations on historical castle Trakošćan (Croatia) performance under recent ML ≥ 5.5 earthquakes,* Geosciences, 11 (2021b), 11; 461, 17. doi: 10.3390/geosciences11110461

ACCOUNTING FOR SITE EFFECTS IN THE ASSESSMENTS OF SUSCEPTIBILITY TO CO-SEISMIC SLOPE FAILURES IN HILLTOP TOWNS OF THE SOUTHERN APENNINES

FLAVIANA FREDELLA [1], VINCENZO DEL GAUDIO [2], NICOLA VENISTI [3], PAOLA CAPONE [4], JANUSZ WASOWSKI [5].

[1] *Dipartimento di Scienze della Terra e Geoambientali, Università degli Studi di Bari "Aldo Moro"– Bari, Italy, flaviana.fredella@uniba.it*

[2] *Dipartimento di Scienze della Terra e Geoambientali, Università degli Studi di Bari "Aldo Moro"– Bari, Italy, vincenzo.delgaudio@uniba.it*

[3] *Dipartimento di Scienze della Terra e Geoambientali, Università degli Studi di Bari "Aldo Moro"– Bari, Italy, nicola.venisti@uniba.it*

[4] *Dipartimento di Scienze della Terra e Geoambientali, Università degli Studi di Bari "Aldo Moro"– Bari, Italy, paola.capone@uniba.it*

[5] *Consiglio Nazionale delle Ricerche – Istituto di Ricerca per la Protezione Idrogeologica – Bari, Italy, j.wasowski@ba.irpi.cnr.it*

Introduction

This study reports some advances in a procedure for a regional scale identification of slopes potentially susceptible to earthquakes-induced landslides. The Daunia Mts. (south-eastern Appennines, Italy) were chosen to test the procedure because of i) the widespread presence of marginally stable slopes consisting of clay-rich flysch materials, ii) the presence of active seismogenic sources in the surrounding areas and iii) the large amount of relevant data made available by ongoing seismic microzonation studies. The tested procedure derives from an approach for a probabilistic estimate of the basic resistance demand expressed through the quantity $(A_c)_x$ (Del Gaudio et al., 2003). This parameter represents the critical acceleration a_c that a slope must have to keep the probability of exceeding a critical threshold x of Newmark displacement D_N within a pre-defined probability (e.g. 10% in 50 years). The calculation of $(A_c)_x$ is based on empirical relations linking D_N to a_c and to Arias Intensity (Arias, 1970), the latter used as a measure of seismic shaking energy.

Methods

In this study we focused on the first step of a three-stage procedure consisting of: i) estimating the resistance demand $(A_c)_x$ placed by local seismicity on the slope; ii) comparing it to the actual slope resistance a_c and iii) classifying slope susceptibility to seismically induced failures, based on differences between $(A_c)_x$ and a_c.

For implementing stage (i), we first updated basic maps of $(A_c)_x$ obtained in previous works for Daunia Mts., using the latest version of tools for seismic hazard assessment and adopting x = 10 cm as critical threshold of D_N for earth slopes. Compared to previous studies, however, we intend to integrate the calculation of the resistance demand by taking into account the site amplification of ground shaking, which can occur on slopes, especially where softer materials overlie a stiffer substratum. For an expeditious estimate of the site amplification, we utilize the ambient noise analysis recordings acquired during the seismic microzonation conducted in Daunia urban and peri-urban areas. Data already processed with a standard method (Nakamura, 1989) are now reanalysed with a more recent technique (HVIP - Del Gaudio, 2017), which provides estimates of the ellipticity of Rayleigh waves as function of frequency. These estimates show peak values of horizontal to vertical ratios of ground motion amplitude (H/V) at resonance frequencies. Such estimates are expected to be more stable and better correlated to the local amplification factor.

At this stage, site effects are incorporated through a simplified calculation of local seismic response, adopting 1D models of site conditions. These models are based on stratigraphies derived from pre-existing boreholes and results of previous geophysical investigations, integrated with purposely

conducted geological surveys and ambient noise data inversion in terms of velocity vertical profiles (Figure 1).

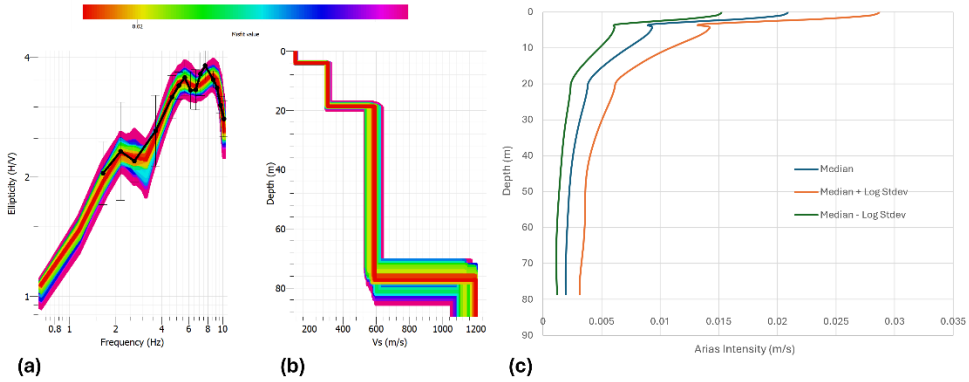

Figure 1. Steps to estimate amplification factors of Arias intensity from 1D site response modelling using ambient noise data: (a) fit between experimental and theoretical curve of Rayleigh wave ellipticity and (b) the corresponding Vs profile obtained using the software DINVER (Wathelet, 2005) for data inversion; (c) Arias intensity vertical profile obtained with the code STRATA (Kottke et al., 2013) to calculate the amplification factor.

Results

The new estimates of $(A_c)_{10}$ resulting from database update give an increase of 50% (from 0.04 to 0.06 g) of their maximum values, which is strongly influenced by the redefined geometry of the seismogenic zones. The first estimates of the site response effect on 16 sites of 3 municipalities show amplification factors in terms of Arias intensity between 3 and 7, which would imply a further increase of the resistance demand in terms of slope critical acceleration by a factor of between 2 and 4.

Conclusion

In view of identifying potential areas of criticalities related to slope destabilization in regional seismic scenarios, the results of the first tests show the importance of incorporating site amplification effects in the calculation of the slope resistance demand placed by the regional seismicity. As next step we intend to evaluate, in estimating the site amplification influence on slope resistance demand, the uncertainties related to the use of simplified 1D models of site condition, by comparing these estimates with the results of 2D/3D modelling. Furthermore, we intend to verify the possibility of extending expeditious estimates of site amplification on slope stability under seismic shaking through empirical relationships providing expected amplification factors, directly based on the results of ambient noise analysis.

References

Arias A. A measure of earthquake intensity, *in Seismic Design for Nuclear Power Plants, R. J. Hansen (ed), MIT Press, Cambridge, Massachusetts.* 1970, 438-483.

Del Gaudio V.; 2017: Instantaneous polarization analysis of ambient noise recordings in site response investigations. *J. Geophys. Int.* 2017. 210, 443-464.

Del Gaudio V.; Pierri P.; Wasowski J. An Approach to Time-Probabilistic Evaluation of Seismically Induced Landslide Hazard. *Bulletin of the Seismological Society of America*. 2003, 93, 2, 557-569.

Kottke R.; Wang X.; Rathje E. Technical Manual for Strata. *Geotechnical Engineering Center, - University of Texas*. 2013, 89 pages.

Nakamura Y. A method for dynamic characteristics estimation of subsurface using microtremor on the ground surface. *Q. Report Railway Tech. Res. Inst.* 1994**,** 30, 25-33.

Wathelet, M. Array recordings of ambient vibrations: surface-wave inversion, PhD thesis, Liège University, Belgium. 2005.

ASSESSING THE LIQUEFACTION EJECTA POTENTIAL BASED ON CPTu; CASE STUDY PINIADA VALLEY, GREECE

GEORGE PAPATHANASSIOU [1], LYDIA GOERLOK [1], SOTIRIS VALKANIOTIS [2], MARIA TAFTSOGLOU [2]

[1] *Aristotle University of Thessaloniki, Greece,* gpapatha@geo.auth.gr

[2] *Democritus University of Thrace, Greece*

Introduction

The 2021 Damasi, Greece earthquake Mw=6.3 triggered numerous liquefaction phenomena at the Piniada Valley. The liquefaction features were reported during a field survey conducetd few hours after the event along the Piniada Valley. They were classified as sand craters, as singular features as well as aligned ones, and ground fissures, from where a mixture of water and fine sandy and silty material was ejected, and lateral spreading phenomena. According to eyewitnesses, the phenomena, occurred during the March 3rd mainshock, locally caused mixed fluid fountaining as high as 1 m from the topographic surface. The total area covered by the ejected material (sand blow) at Piniada Valley was estimated as 0.0325 km^2, approximately 0.5% of the zone that is delimited by the village Piniada, to the north, and the present-day river channel of river Pinios, to the south (Papathanassiou et al. 2022).

This area is covered by Holocene sediments deposited along the meandering fluvial system of Pinios. The characteristic evolution of Pinios River dictates the depositional process of the sediments and contributed to the lateral and vertical heterogeneity of the surficial soil material. That was clearly shown during the 2021 event since liquefaction phenomena preferred to concentrate in specific location forming clusters of liquefaction-induced ground disruption such as sand boils, craters and ground fissures. In addition, it is highlighted that within a short distance, the severity of ejecta was totally different. The goal of this study is to investigate the liquefaction potential of a selected area located within a point bar, based on data provided by Cone Penetration Tests with pore water pressure measurement (CPTu).

Methods

On March 2024, a campaign focusing on the conduction of CPTu in selected sites at Piniada valley took place. The goal of this campaign was to investigate the liquefaction potential of a selected area of 400m^2 located within a point bar deposit. Thus, it was decided to perform 6 CPTu up to a depth of 15 meters in an distance of 15 among them ((Fig. 1); 3 on areas of liquefaction manifestations (CPTu1, CPTu2 and CPTu4) and 3 on non-liquefiable sites (CPTu3, CPTu5 and CPTu6).

Figure 2. Locations of CPTu tests. View of ejecta captured by the UAV-campaign conducted few days after the event (Papathanassiou et al. 2022)

Results

The data provided by the in-situ tests were proceed with the Cliq software deveoloped by Geologismiki and the liquefaction Potential Index (LPI) per site was computed. As it is shown in figure 2, the LPI values of CPTu varies depending the methodogy applied for the computation. In addition, based on the

classification suggested by Iwasaki et al. (1978) and the methology proposed by Boulanger and Idriss (2014), the LPI values (>10) of CPTu1, CPTu2, CPTu3 and CPTu4 indicates that surface manifestations should be expected to be triggered by the Damasi 2021 event of M6.3 and of PGA value equal to 0.3g. On the contrary, for the sites where the CPTu5 and CPTu6 were conducted, the liquefaction potential is lower compared to the others sites.

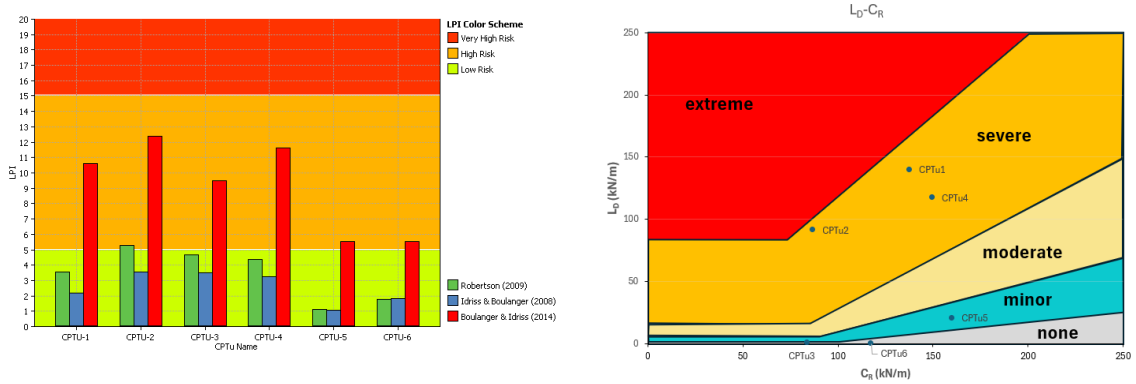

Figure 2. Left. LPI values of CPTu tests. **Right**. CPTu on the diagram of Liquefaction Ejecta Demand (L_D)-Crust Resistance (C_r).

In addition, the liquefaction ejection severity procedure was applied (Hutabarat and Bray 2022) aiming to examine the accuracy of this recently suggested method. The outcome (Fig. 2) is that CPTu1, CPTu 2 and CPTu4 are plotted in the area described as severe ejecta cases, while the CPTu3 and CPTu6 as none ejecta one. The area where the CPTu5 conducted is considered as an area of minor ejecta severity.

Conclusion

Between these two approaches there is mismatch for CPTu3 which was classified as high liquefaction potential area, based on LPI approach, and as a none ejecta case based on the methodology of "ejecta severity". Following the post-earthquake mapping of liquefaction phenomena triggered by Damasi 2021 event (Papathanassiou et al. 2022), the site where the CPTu3 was conducted is classified as a non-liquefaction surface manifestation one. Thus, in this case the ejecta severity approach, recently proposed by Hutabarat and Bray (2022), succesfully predict the real case scenario. On the other hand, the case of CPTu5 was classified as a minor ejecta site which is not in agreement with the results of the conducted survey, where liquefaction phenomena were not reported.

In addition, it could be stated that though the fact that all the area is surficial characterized as point bar deposits, the expected vertical and lateral heterogeneity of the soil stratigraphy could be the main reasons for this differentiation regarding the liquefaction manifetsation even in a distance of few meters.

Acknowledgment

The CPTu campaign was funded by the Research Committee of Aristotle University of Thessaloniki.

References

Hutabarat, D., Bray, J. Estimating the Severity of Liquefaction Ejecta Using the Cone Penetration Test. Journal of Geotechnical and Geoenvironmental Engineering 2022. 148. 04021195. 10.1061/(ASCE)GT.1943-5606.0002744.

Papathanassiou G., Valkaniotis S., Ganas Ath., Stampolidis A., Rapri D., Caputo R., 2022. Floodplain evolution and its influence on liquefaction clustering: the case study of March 2021 Thessaly, Greece, seismic sequence, Engineering Geology, 2022, 298, 106542

Iwasaki, T, Tatsuoka, F., Tokida, K, and Yasuda, S. A Practical Method for Assessing Soil Liquefaction Potential Based on Case Studies at Various Sites in Japan, 2nd International Conference on Microzonation for Safer Construction Research and Application, 1978, 885-896

NATIONAL SCALE EARTHQUAKE SUSCEPTIBILITY MAPPING UTILIZING EXPLAINABLE ARTIFICIAL INTELLIGENCE IN THE NEPAL HIMALAYA

SUCHITA SHRESTHA[1], ANANTA MAN SINGH PRADHAN [2], TAE-SEOB KANG [3]

[1] *Department of Mines and Geology, Ministry of Industry, Commerce and Supplies, Government of Nepal, Lainchour, Kathmandu, Nepal, suchitashrestha@gmail.com*

[2] *Ministry of Energy, Water Resources and Irrigation, Government of Nepal, Nepal, anantageo@hotmail.com*

[3] *Division of Earth Environmental System Science, Pukyong National University, Busan 48513, Republic of Korea, tskang@pknu.ac.kr*

Introduction

Nepal is situated in one of the world's most earthquake-prone areas due to its position in a geologically intricate zone where the Indian tectonic plate meets the Eurasian plate. The continuous convergence of these plates results in frequent seismic activity, with shifts along fault lines often leading to powerful earthquakes in the region. Most of the casualties and damage from past and recent earthquakes in Nepal are due to the country's vulnerable infrastructure (Gautam & Chaulagain, 2016). Nepal is undergoing significant annual population growth, rapid urbanization, and extensive infrastructure development. Unfortunately, this rapid development, often without adherence to earthquake codes, has heightened the region's earthquake risk. The seismic activity observed in recent decades underscores the potential for future earthquakes to impact this densely populated area. This study was focus on enhancing spatial probability mapping using explainable artificial intelligence (XAI). Traditional seismic hazard zone (SHZ) methods typically rely on statistical analyses of historical earthquake data, which can be limited in scope. XAI offers a solution by integrating diverse geological, geomorphological, and geophysical data, thereby expanding the analytical framework. Unlike traditional methods like probabilistic seismic hazard analysis, which often involve complex mathematical models and algorithms, XAI employs machine learning (ML) algorithms designed to generate transparent and interpretable outcomes. This makes it more accessible for scientists, engineers, and policymakers to grasp the underlying factors influencing seismic hazard assessments.

Methods

The earthquake catalog encompasses data from all historical earthquake events within the study area, regardless of their sources, magnitude scales, recording agencies, or event sizes. Geo-related covariates are important in earthquake studies because they can help identify areas that are likely to experience earthquakes. Previous studies on earthquake hazards and probabilities derived several relevant factors for earthquake probability assessments. Elevation (Elv), topographic position index (TPI), magnitude density (MagDen), depth density (DepDen), fault proximity (FaultProx), fault density (FaultDen), and “tectonic zone” covariates are crucial factors that contribute significantly to the assessment of earthquake probability. The rise of AI has been meteoric in recent years, promising transformative changes across various industries. However, the increasing reliance on black-box machine learning (ML) models for critical predictions has raised concerns about the opacity of their decision-making processes. This lack of transparency has sparked a demand among stakeholders for more understandable AI systems (Nguyen et al., 2021). Explainable AI (XAI) aims to address this challenge by developing ML techniques that are not only accurate but also interpretable. When applying XAI techniques alongside modeling approaches such as Random Forest (RF) and Extreme Gradient Boosting (XGB), the objective is to create models that retain high accuracy while providing clear explanations of their reasoning.

Results

We utilized a set of seven geo-related covariates to develop two predictive models: Random Forest (RF) and Extreme Gradient Boosting (XGB). Among these covariates, "tectonic" was a categorical factor.

The values of all seven covariates were numerically encoded in a spreadsheet, with earthquake and non-earthquake cases designated as the target outcomes. Numeric values representing earthquake probability were assigned to distinct datasets. These forecasted values, confined within the 0 to 1 range, can be interpreted as probabilities. Figure 1a illustrates the distribution of earthquake probability values obtained using the RF model, while Figure 1b depicts the earthquake probabilities generated by the XGB model across the Nepalese Himalayas.

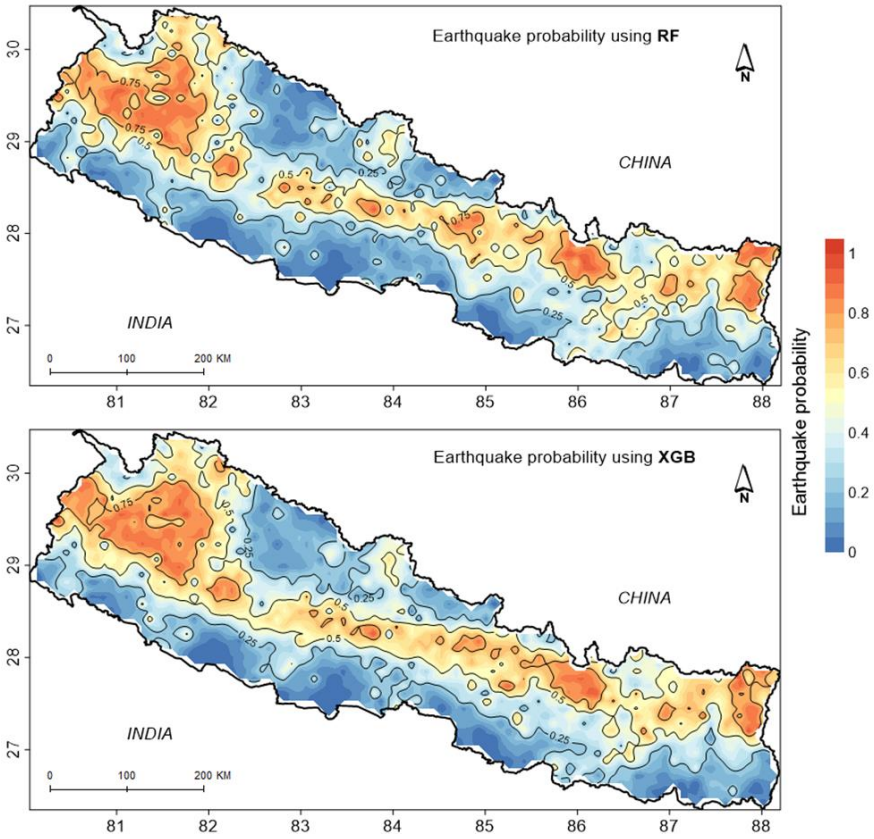

Figure 1. Earthquake probability map of Nepal generated by the a) random forest (RF) and b) extreme gradient boosting (XGB) models.

In the overall process, 1,710 earthquake and non-earthquake instances were analyzed. The RF model accurately classified 801 out of 855 earthquake events and 800 out of 855 non-earthquake events. In comparison, the XGB model correctly identified 765 earthquake events and 741 non-earthquake events. The misclassification indices, determined using a confusion matrix, indicate an uncertainty of 6.37% for the RF model and 11.93% for the XGB model.

Conclusion

The RF model exhibited excellent predictive performance with an AUC of 0.79, while the XGB model demonstrated an AUC of 0.76, indicating a strong goodness-of-fit. For future studies, we recommend exploring the impacts of additional geo-related covariates and incorporating findings from precursor studies to enhance the accuracy of earthquake probability assessments.

References

Gautam, D.; Chaulagain H Structural performance and associated lessons to be learned from world earthquakes in Nepal after 25 April 2015 (MW 7.8) Gorkha earthquake. *Engineering Failure Analysis 68:222–243* (2016).

A GEOLOGICAL AND GEOPHYSICAL INTERPRETATION OF GRAVEL LIQUEFACTION SITE EFFECTS FOLLOWING THE Mw 6.4 PETRINJA (CROATIA) EARTHQUAKE

NIKOLA BELIĆ[1], GIUSEPPE DI GIULIO[2], MAURIZIO VASSALLO[2], SARA AMOROSO[2,3], KYLE ROLLINS[4], GABRIELE TARABUSI[2], LUCA MINARELLI[2], MARKO ŠPELIĆ[1], RADOVAN FILJAK[1], LARA WACHA[1], KOSTA URUMOVIĆ[1], AND TOMISLAV KUREČIĆ[1]

[1] *Croatian Geological Survey, Dept. of Geology, Zagreb, Croatia, nbelic©hgi-cgs.hr*

[2]*INGV Istituto Nazionale di Geofisica e Vulcanologia, Roma, Italy, giuseppe.digiulio@ingv.it*

[3]*Univ. of Chieti-Pescara, Dept. of Engineering and Geology, Pescara, Italy, sara.amoroso@unich.it*

[4]*Brigham Young University, Dept. of Civil and Construction Engineering, Provo UT, USA, rollinsk@byu.edu*

Introduction

In December 2020, the city of Petrinja in Central Croatia was struck by a Mw 6.4 earthquake. Liquefaction, coseismic ruptures, lateral spreading, landslides, and other natural phenomena were found up to 20 km from the earthquake epicenter (Maslač et al 2024; Baize et al. 2022; Pollak et al. 2021). Among more than 170 sand-ejecta occurrences, six sites stand out with gravel as the liquefaction material. This distinction encouraged an international team of scientists and engineers to perform an extensive geotechnical investigation (Amoroso et al. 2023). In this work we bring a geological and geophysical interpretation for Site 2, located in the centre of the investigated area (Fig. 1).

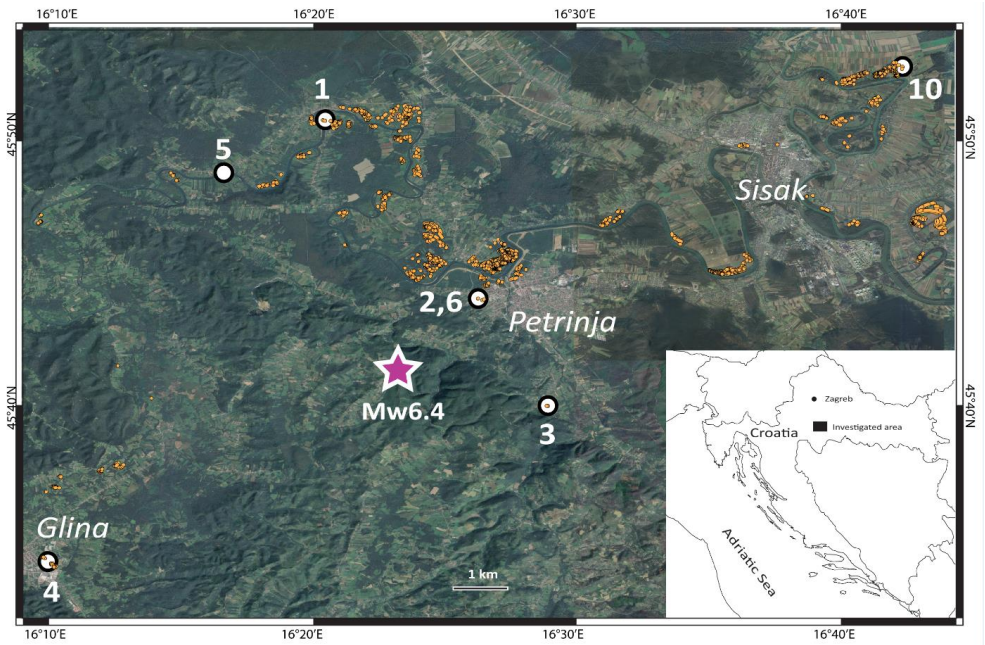

Figure 1. Map of the investigated area: Orange stripes represent liquefaction traces mapped based on the aerial and satellite images (Baize et al. 2022), and the white dots represent the investigated sites.

Methods

Geophysical survey comprised both active and passive investigations. For the active survey (MASW method), we used 48 to 72-point linear arrays of vertical 4.5 Hz geophones, recording 1.5 s signal increments at a sampling rate of 8000 Hz. A 5 kg sledgehammer was used to reproduce forward and reverse shot records to retrieve shear-wave velocity (Vs) profiles (Amoroso et al. 2023; Rollins et al. 2024). For the passive survey (HVSR method), we recorded ambient noise (up to a few hours at each site) using 2D arrays with 20 to 46 seismic nodes, with a sampling rate of 250 Hz. The recordings were

used to compute the surface-wave dispersion curves and horizontal-to-vertical noise spectral ratio (H/V curve), and then to derive site resonance frequencies, important for detecting the presence of seismic contrasts in the subsoil profiles (Di Giulio et al. 2021).

Results

The results from the geophysical surveys were jointly used to perform the inversions and define shear-wave velocity (Vs) profiles (Park et al. 2007). For data processing and interpretation, we used Geopsy software (Wathelet et al. 2020). At most sites we have recorded fundamental resonance frequency (f_0) of 4 Hz and first-order resonance frequency (f_1) of 0.3 Hz. At Site 2, f_0 corresponds to the seismic contrast between layers with modelled share wave velocity (Vs) of 60 and 200 m/s, and f_1 corresponds to the seismic contrast between layers with modelled share wave velocity (Vs) of 200 and 550 m/s (Fig. 2 a). Shear-wave velocity in the first 30 m (Vs_{30}) was calculated at 272 m/s.

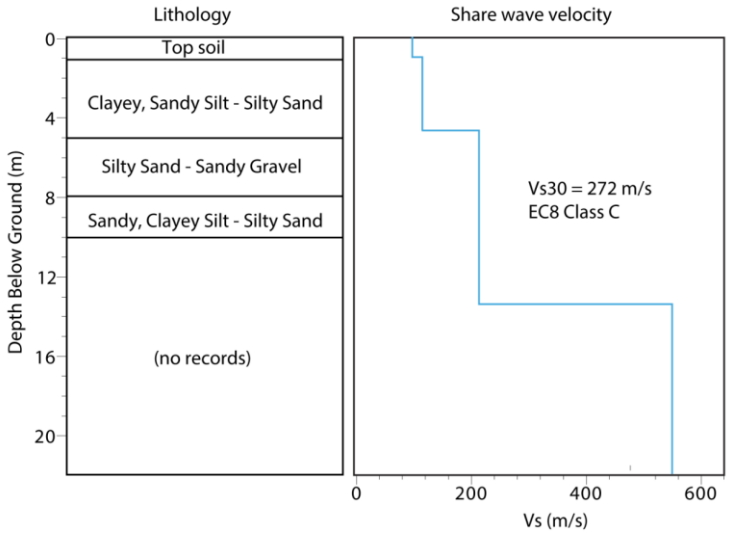

Figure 2. (a) Lithological profile derived from geotechnical borehole at Site 2 (left) in comparison to the Vs30 profile for the 0-20 m interval (right).

Conclusion

Based on the comparison between lithostratigraphic description of geotechnical borehole, and modelled shear-wave velocity (Vs) profiles at Site 2, we conclude that the seismic contrast at the fundamental resonance frequency f_0 corresponds to the lithological boundary between clayey silty sand – sitty sand, and, silty sand – silty gravel, recorded at 5 m in the geotechnical borehole. The bottom layer (5 – 8 m from the surface) is, most probably, the source for the liquefaction material. The seismic contrast at the first order resonance frequency f_1 corresponds to the deeper lithological boundary, which was not reached by geotechnical drilling in 2022. Recorded seismic contrasts can be verified to lithological profiles at the borehole site. Further geophysical measurements, and estimated share wave velocity models can extend the geological interpretation to a larger investigation area.

Acknowledgements

Funding for this work was provided by Progetti di Ricerca Libera INGV 2021 (Istituto Nazionale di Geofisica e Vulcanologia) “Liquefaction Assessment of Gravelly Deposits (LAGD; 9999.816): historical data analyses and in situ testing at Italian trial sites to develop innovative methods”, by the Geotechnical Extreme Events Reconnaissance (GEER) organization, by Brigham Young University (Provo, Utah) and by the University of Ferrara (Ferrara, Italy). This support is gratefully acknowleged; however, the opinions, conclusions, and recommendations in this paper do not necessarily represent those of the sponsors.

References

Amoroso, S., K. M. Rollins, G. Di Giulio, L. Wacha, K. Urumović, D. Faieta, R. Filjak, D. Fontana, S. Lugli and M. Manuel. 2023. Geotechnical and geophysical tests following the 2020 earthquake-induced liquefaction phenomena. In Proceedings of the 2nd Croatian Conference on Earthquake Engineering - 2CroCEE. Zagreb, Croatia. https://doi.org/10.5592/CO/2CroCEE.2023.21

Baize, S., Amoroso, S., Belić, N., Benedetti, L., Boncio, P., Budić, M. Cinti, F.R., Henriquet, M., Jamšek Rupnik, P., Kordić, B., Markušić, S., Minarelli, L., Pantosti, D., Pucci, S., Špelić, M., Testa, A., Valkaniotis, S., Vukovski, M., Atanackov, J., Barbača, J., Bavec, M., Brajkovič, R., Brčić, V., Caciagli, M., Celarc, B., Civico, R., De Martini, P.M., Filjak, R., Iezzi F., Moulin, A., Kurečić, T., Métois, M., Nappi, R., Novak, A., Novak, M., Pace, B., Palenik, D. and Ricci T. 2022. Environmental effects and seismogenic source characterization of the December 2020 earthquake sequence near Petrinja, Croatia. Geophysical Journal International, 230(2): pp. 1394–1418. https://doi.org/10.1093/gji/ggac123

Di Giulio, G., Cultrera, G., Cornou, C., Bard, P.Y. and Al Tfaily, B. 2021. Quality assessment for site characterization at seismic stations. Bulletin of Earthquake Engineering 19(12): 4643-4691. https://doi.org/10.1007/s10518-021-01137-6

Maslač J., Belić, N., Budić, M., Cinti, F.R., Kordić, B., Pantosti, D., Pucci, S., Špelić, M., Amoroso, S., Minarelli, L., Valvano, C. (2024). Earthquake Geology Studies in Croatia: active faults and seismic potential project Map portal, GISCloud, https://app113450.giscloud.com

Park, C. B., Miller, R. D., Xia, J. and Ivanov, J. 2007. Multichannel analysis of surface waves (MASW)-Active and passive methods. The Leading Edge 26: 60-64. https://doi.org/10.1190/1.2431832

Pollak, D., Gulam, V., Novosel, T., Avanić, R., Tomljenović, B., Hećej, N., Terzić, J., Stipčević, J., Bačić, M. and Kurečić, T. 2021. The preliminary inventory of coseismic ground failures related to December 2020 – January 2021 Petrinja earthquake series. Geologia Croatica: Journal of the Croatian Geological Survey and the Croatian Geological Society 74(2): 189-208. https://doi.org/10.4154/gc.2021.08

Rollins, K., Amoroso, S., Walburger, A., di Giulio, G., Belić, N., Urumović, K., Filjak, R., Minarelli, L., Tarabusi, G., Stanko, D., Markušić, S., Marenghi, L., & Vassallo, M. (2024). Liquefaction assessment at gravel sites in Croatia based on V s and DPT blow count. Proceedings of the 7th International Conference on Geotechnical and Geophysical Site Characterization, Barcelona, 18 - 21 June 2024

Topic 10

In the Path of Progress AI Innovations in Landslide and Engineering Geological Research

ON THE DEEP-SEATED BEDROCK LANDSLIDE TRIGGERED BY THE 2018 HOKKAIDO EASTERN IBURI EARTHQUAKE: A CASE STUDY

GONGHUI WANG[1], SHENGSHAN WU[2], ISSEI DOI[3], GEN FURUYA[4], NAOKI WATANABE[5]

[1] *Disaster Prevention Research Institute, Kyoto Univ., Kyoto, Japan, E-mail: wang.gonghui.3r@kyoto-u.ac.jp*

[2] *Graduate School of Science, Kyoto Univ., E-mail: wu.shengshan.35v@st.kyoto-u.ac.jp*

[3] *Disaster Prevention Research Institute, Kyoto Univ., Kyoto, Japan, E-mail: doi.issei.5e@kyoto-u.ac.jp*

[4] *Toyama Prefectural Univ., Japan, E-mail: gfuruya@pu-toyama.ac.jp*

[5] *Research Institute for Natural Hazards and Disaster Recovery, Niigata Univ., Japan, E-mail: jibanken@cc.niigata-u.ac.jp*

Introduction

The 2018 Hokkaido Eastern Iburi Earthquake, registering at a magnitude of 6.7 and striking at 3:08 on September 6th, prompted a significant number of landslides, resulting in a lot of casualties. While most slides occurred on tephra slopes and were shallow, there were instances of bedrock landslides, notably one in the Horonai area（referred to as the Horonai landslide in this study). This particular landslide exhibited translational movement, with materials shifting approximately 350 meters along a gently sloping bedding plane of about 6 degrees. Field examination revealed that the displaced materials suffered high-speed movement. To investigate the initiation and movement mechanisms of this landslide, we installed seismometers across the affected area to study the seismic response. Geological and geomorphological surveys were conducted on the landslide site, with soil samples taken from layers adjacent to the sliding surface. Subsequent undrained ring shear tests were performed on these samples to analyze their static and dynamic shear behavior. Based on the results, the initiation and movement mechenisms of this deep-seated bedrock landslide were discussed.

Horonai landslide and methods

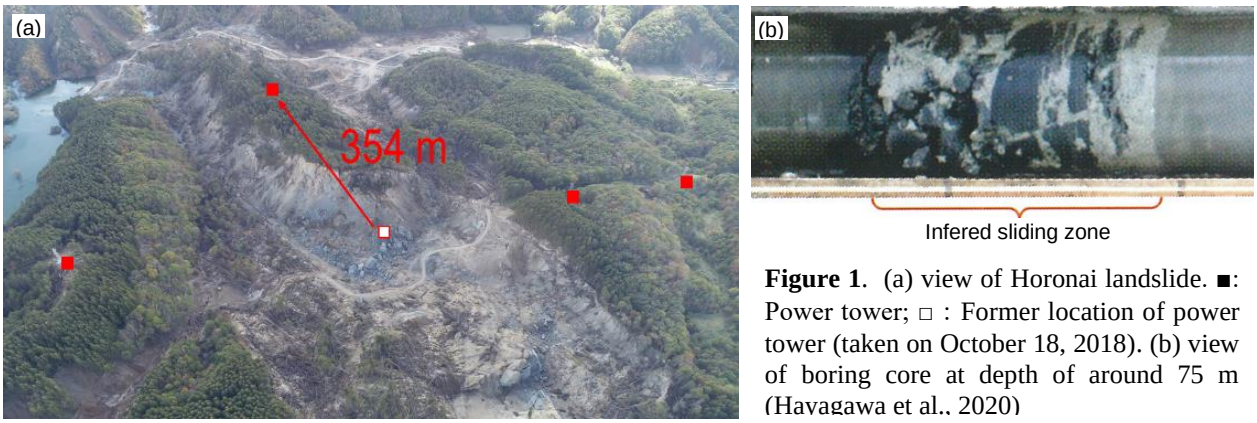

Figure 1. (a) view of Horonai landslide. ■: Power tower; □ : Former location of power tower (taken on October 18, 2018). (b) view of boring core at depth of around 75 m (Havagawa et al., 2020)

Horonai landslide was the largest rockslide caused by the above mentioned earthquake. The bedrock around the landslide site consists of the Kemusi Formation, which includes siliceous to hard mudstone and glauconitic sandstone. The bedding planes at the landslide site dip approximately 10° towards the south to southeast. The landslide body is composed of interbedded sandstone and mudstone, predominantly muddy, with thin layers of calcareous concretions and tuffaceous sandstone. The landslide movement was translational with the sliding surface being formed along the bedding planes (Hayakawa et al., 2020). Additionally, the main block of the landslide body moved en masse while retaining the original rock structure. The landslide is about 1200 m in length and 400 m in width. The displaced mass traveled about 350 m along the slope, damming the river on the toe part and forming a large scale natural dam. The boring surveys revealed a crushed sandy layer (about 15 cm thick) around a depth of 75.15 to 75.30 m, which was inferred to be the sliding surface (Fig. 1b). Core observations

near the sliding layer showed fractures in the upper soil layer, with sandy soil from the sliding layer intruding into these fractures. These phenomena suggest that during the earthquake, the tuffaceous sandstone near the sliding surface was crushed and liquefied, resulting in the rapid and long runout of the displaced mass. But why and how the shear failure along this layer had been triggered remain unclear. To clarify these questions, we conducted field surveys, collected soil samples from the sandstone and mudstone layers, and examined their shear behavior under different test conditions. We installed seismometers at different locations of the landslide, and then analyzed the possible coseismic response of the slope based on the recorded earthquake waves.

Results

As shown in Fig. 2a, the static shear tests showed that high pore-water pressure (PWP) could be built up within the sandy materials in saturated states, although in this test water leakage occurred during the undrained shearing. However, as shown in Fig. 2b, the sample taken from mudstone layer did not show significant buildup of PWP. It is noted that this test was conducted by applying the possible seismic shear loading during the main shock of the earthquake that was estimated by assuming an infinitely long slope of 6 degrees with a soil layer thickness of about 52 m, and by using the seismic wave data recorded at a nearby observation station during the main shock. Fig. 2b shows that although displacement occurred in the soil layer due to the application of dynamic shear stress, no continuous movement occurred in the soil layer after the seismic shear stress ended. Therefore, it is inferred that shear failure won't be triggered within the mudstone layer. Analysis on the seismic waves recorded the installed seismometers revealed that resonance during the main shock might have occurred, resulting in larger ground motion and then enabling the shear failure along the sandy layer of the bedrock.

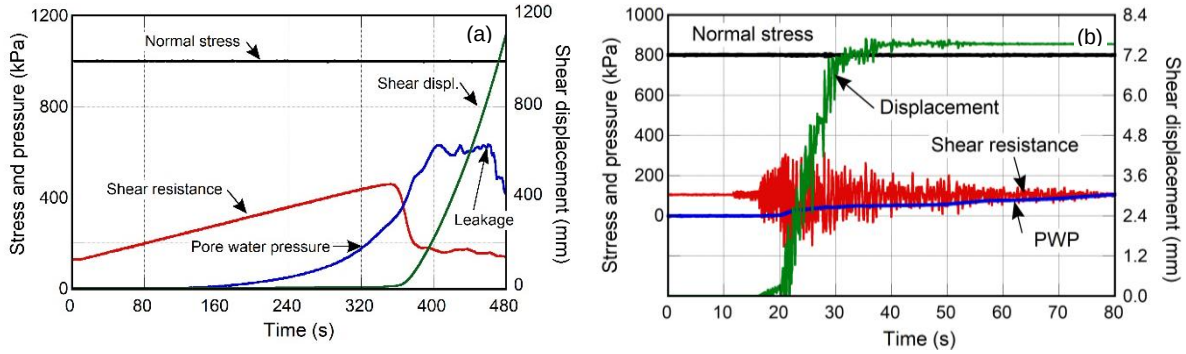

Figure 2. Undrained ring shear tests on samples taken from sandstone (a) and mudstone layers

Conclusion

During the 2018 Hokkaido Eastern Iburi earthquake, a large-scale rockslide occurred in the Hidaka Horokawa area, characterized by interbedded sandstone and mudstone formations. It is believed that this rockslide involved rapid and long-distance translational movement along a low-angle (about 6°) sliding surface parallel to bedding planes. The main block of the sliding mass had a thickness of about 80 m, and the slip plane was formed within the interbedded sandstone and mudstone layers, where liquefaction phenomena were observed. The resultss of shear tests revealed taht sandy layers in saturated state may suffer from buildup of high PWP and localized liquefaction phenomaon, and then enable the rapid long runout of dispaced landslide material. The soil layers along mudstone may not suffer from liquefaction behavior, although it has smaller peak shear strengh. Ground motion stronger than those recorded during the main shock in a nearby seismic station may occured in the landslide area, enabling the occurence of shear failure along the boundary between the sandstone and mudstone.

References

Hayakawa, T.; Shimizu, R.; Teraguchi, K.; Ishizaki, H.; Tajika, A.; Kizaki K. The Hidaka Horokawa Rockslide." In ***Landslide Disasters Caused by the 2018 Hokkaido Eastern Iburi Earthquake***. Hokkaido University Press, 2020, pp. 164-176.

POINT CLOUDS AND MACHINE LEARNING IN ROCK SLOPE MODELING

IOANNIS FARMAKIS [1], JEAN D. HUTHCINSON [1], NICHOLAS VLACHOPOULOS [2]

[1] *Department of Geological Sciences & Engineering, Queen's University, Canada*, i.farmakis@icloud.com

[2] *Department of Civil Engineering, Royal Military College, Canada*

Introduction

"When we open our eyes on a familiar scene, we form an immediate impression of recognizable objects, organized coherently in a spatial framework" (Treisman & Gelade 1980). This quote defines in simple terms the biological process of creating our "model" of the scene. This "model" is often the primary source of information that our cognitive perception relies on to develop intelligence. Today, with the available computational power and the ever-increasing level of digitization, the digital imitation of the biological "modelling" mechanisms is not only a very interesting and appealing exercise, but it is also achievable. Despite the practical challenges in replicating the biological sight-perception mechanisms in rock slope management, the process can be conceptualized as two distinct phases. The first phase translates into the transformation of reality to the "digital model" with the use of sensors to play the role of the eye and create computer-usable inputs. The second phase includes the evolution of the digital model to an "intelligent model". This involves processes for both the efficient representation of semantics and extraction of knowledge within digital rock slope replicas as well as the exploitation of the generated data to achieve autonomy and predictability (Figure 1).

Today in rock slope management we are able to leverage slope-scale point clouds utilizing various reality capture devices. These techniques provide large amounts of data that allow for site-specific digital modelling that would reliably represent the 3D complexity of a rock slope. This turn towards slope-scale knowledge extraction from point clouds signifies the conquest of the first phase in rock slope modelling evolution scheme (Figure 1). However, there is still the need to improve the capabilities of our models and achieve intelligence through automation. The analysis of these data is often limited to daunting time-consuming manual processing for the extraction of meaningful information to support the "intelligent model" phase. If we consider point clouds as digital reality assets, a whole new field of intelligent applications becomes available with the integration of Machine Learning (ML). The reflection to go from human-centered processes to autonomous data-driven workflows at slope-scale motivate our research to develop automation and Artificial Intelligence (AI) to speed-up inference processes.

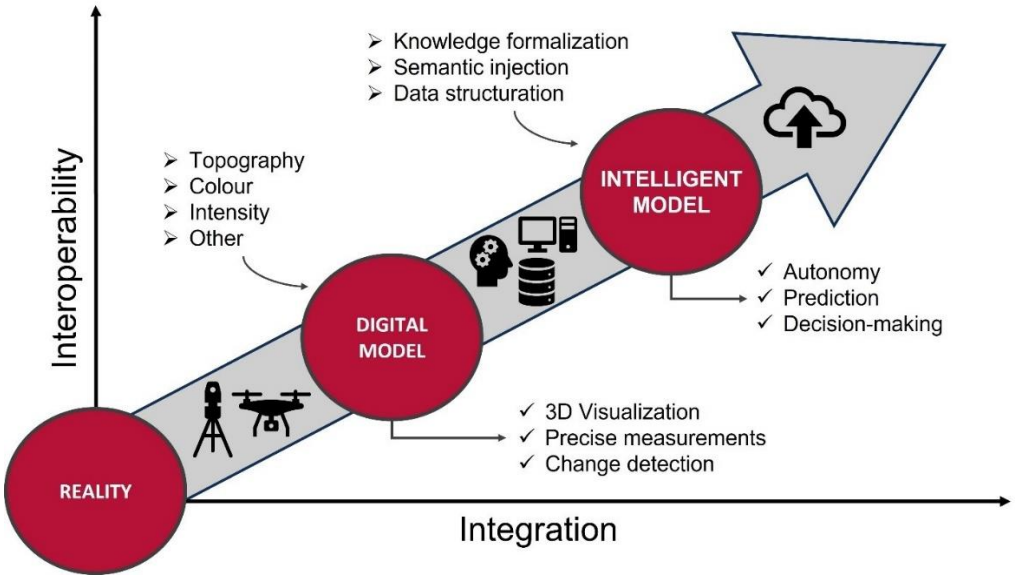

Figure 1. Schematic representation of the evolution of rock slope modelling through digital transformation and artificial intelligence.

Methods

In this work, we showcase ML integration into rockfall monitoring workflows for the development of AI able to automate data analysis and simulate processes as vision problems. We employ deep artificial neural network (ANN) architectures to tackle rockfall detection and slope-scale rockfall susceptibility modeling (RSM) based on long-term LiDAR-based monitoring data.

Deep neural network architectures for 3D point cloud learning are developed for rockfall detection based on a 5-year change detection database consisting of more than 8,000 rock slope clusters of identified change for training, with scanning intervals ranging from 5 days to 6 months. The models are tested on the 536 clusters from the two last data acquisitions to simulate the real monitoring situation and subsequently on the most frequent of the campaigns to increase the probability of working with single-event clusters.

We also explore the potential of simulating the conceptualization of slope-scale rockfall susceptibility modelling using computer power and AI. Three different types of 3D geometric learning neural networks are employed to interpret high-resolution digital observations capturing the rock slope evolution via long-term, LiDAR-based 3D differencing.

Results

The ML models are tested on real case examples from different rock slope settings in Canada and England and are successfully integrated into dynamic rockfall database population processes within the monitoring program. The best-performing rockfall detection model achieves an accuracy of about 89% and 84% on the last and shortest campaign, respectively. The optimized deep learning models are further evaluated on a geologically different rockfall database achieving almost 93% accuracy in a location where discrete geomorphologic features such as steep rock outcrops and erosion channels are present. Our novel slope-scale RSM apporoach leads to effective development of local susceptibility indicators from local geometry and learning from recent rockfall activity. The resultant models produce slope-wide rockfall susceptibility maps in high resolution, producing up to 75% agreement with validated occurrences.

Conclusions

The results indicate clear potential for our AI to develop engineering geological perception and learn from recent rockfall activity based on 3D computer vision. The study shows that although it is challenging to achieve generalization in rockfall detection, site-specific training of the proposed deep learning architecture can lead to high-level performance and support further advancements in rockfall risk management. Our novel approach shows that treating RSM as a vision problem enables AI-based, data-driven RSM at very high resolution. Our results imply that the DL models are able to develop a perception of rock slope geometry and the location of critical blocks, thereby imitating a field expert who deterministically assesses rockfall susceptibility in a qualitative manner based on their knowledge and experience but perhaps lacks empirical data to inform their analysis.

References

Treisman, A. M., & Gelade, G. (1980). A feature-integration theory of attention. *Cognitive Psychology*, *12*(1), 97–136. doi: 10.1016/0010-0285(80)90005-5.

Farmakis, I., DiFrancesco, P-M., Hutchinson, D.J., Vlachopoulos, N. 2022. Rockfall detection using LiDAR and deep learning. *Engineering Geology*. 309:106836. (12 pp.) doi: 10.1016/j.enggeo2022.106836.

Farmakis, I., Bonneau, D., DiFrancesco, P-M., Hutchinson, D.J., Vlachopoulos, N. 2022. Rockfall monitoring using LiDAR and AI: Opportunities and challenges. *11th International Symposium of Field Monitoring in Geomechanics 2022. Imperial College, London, UK, 4-7 September*.

Farmakis, I., Hutchinson, D.J., Vlachopoulos, N., Westoby, M., Lim, M. 2023. Slope-scale rockfall susceptibility modelling as a 3D computer vision problem. Remote Sensing, 15(11): 2712. (19 pp.) doi: 10.3390/rs15112712.

EFFECTIVE ROCKFALL RISK MITIGATION TECHNIQUES BASED ON DIACHRONIC CLOSE-RANGE REMOTE SENSING DATASETS. CASE STUDY: KALYMNOS ISL. WORLD-RENOWNED CLIMBING TERRAIN (GREECE)

EMMANUEL VASSILAKIS [1], ALIKI KONSOLAKI [1], KOSTANTINOS SOUKIS [1], JOHN LIALIARIS [2], SPYRIDON MAVROULIS [1], EVELINA KOTSI [1], EFTHYMIOS LEKKAS [1]

[1] *National and Kapodistrian University of Athens, Greece, evasilak@geol.uoa.gr*

[2] *Geodesign PPC, Greece, lialiarisj@gmail.com*

Introduction

Kalymnos Island features extensive vertical limestone cliffs that span throughout the entire onshore area, establishing it as one of the world's premier locations for sports climbing. Drawing thousands of tourists and climbers annually, Kalymnos captivates with its unparalleled natural beauty and unique geomorphological relief. The absence of vegetation and the prevalence of large limestone vertical cliffs contribute to a distinctive geological setting, showcasing detached boulders throughout the island and positioning it as an ideal site for studying rockfall events worldwide. To investigate this peculiar geological landscape, contemporary close-range remote sensing techniques such as UAS images photogrammetric processing, terrestrial LiDAR point clouds, and high-resolution satellite imagery within a GIS platform are employed. This integrated approach facilitates the creation of detailed terrain models and enables the identification of spatial boulder distribution on the downslope areas of steep carbonate cliffs. Moreover, the diachronic study of the detected high-risk locations delineated the surface changes at the foot of the steep slopes where several back analyses were performed. Utilizing these quantitative techniques provides valuable information for designing protective measures for the stability of the slopes, highlighting the safe climbing routes for the athletes and the infrastructure at the cliff bases. Strategies involve anchoring individual rock blocks, removing unsafe rock masses, and implementing restraining nets or dynamic rockfall barriers at strategic locations along the route trail to mitigate risks effectively.

Methods

The methodology was based on the synergy of equipment in different working levels, depending on the type of the covered area and the scale of study, which varies at each location. Most of these sites are large and wide areas with numerous fallen boulders on the downslopes beneath the vertical cliffs, which needed to be mapped. In such cases, several planned UAS flights were conducted, and thousands of accurately georeferenced images were acquired, due to the use of Network RTK methods (Panagiotopoulou et al. 2020).

At specific locations where larger scale observations needed to be made, such as cliffs which are used for sports climbing, the point clouds were generated by using terrestrial LiDAR equipment. Several bases were established for covering the entire cliff from different angles, as the roughness is generally quite high and the ‘shadow’ effect during the data acquisition could produce holes within the datasets (Vassilakis and Konsolaki, 2022). The bundling of the point clouds acquired from the different bases, was made possible since the proposed methodology includes the establishment of a dense network of Ground Control Points, which were measured with RTK-GNSS equipment for gaining actual coordinates. After merging the partial scans and combining them into a single point cloud, the methodology continues with further processing including filtering and noisy points removal. Moreover, the final product is combined with the point cloud that was generated after the photogrammetric processing.

The same procedure is repeated either once a year, before the climbing season starts or after extreme weather events or earthquakes with nearby epicentres. The multitemporal datasets are co-registered and compared with each other, with several algorithms such as M3C2, C2C DoD etc. (Bernard et al. 2021) and we were able to point out locations where several safety measures should be taken, either by

constructing them or by removing rock blocks that were about to fall, potentially after the next catastrophic event. The methodology is completed by exporting the results into file formats that can be imported in several geotechnical or discontinuity recognition software for further interpretation.

Results

The results and the produced 3D models were utilized to determine areas susceptible to different failure types. The assessment of rock stability at several climbing sites by combining innovatively high-accuracy equipment, sophisticated techniques, and research methods could lead to hazard identification in great detail. Additionally, the results may be seriously considered by the local authorities for the maintenance and/or re-design the climbing routes, as well as for certifying them as "safe climbing".

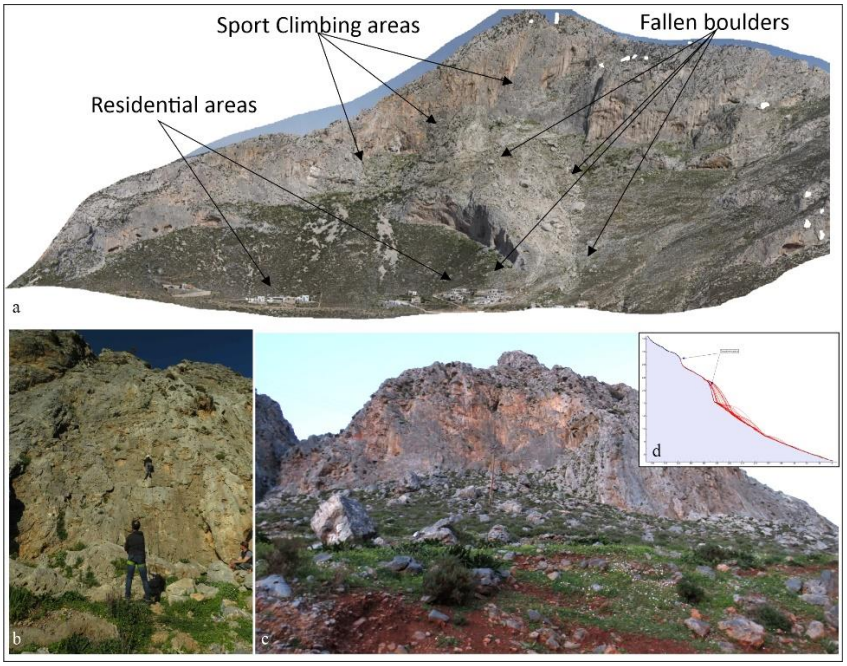

Figure 1. (a) A very typical part of Kalymnos Isl. as visualized after the photogrammetry processing of UAV images. The methodology involves TLS equipment to be used for the data acquisition at high risk climbing sites (b), whereas UAS image acquisition is suggested for wider areas where rockfalling is a continous phenomenon (c). The point cloud data are used for detailed topography cross section, which are imported into rockfalling simulation software (d).

Conclusion

The highly accurate products, including detailed elevation models and ortho-geo-referenced images, are the valuable outcomes of these kinds of workflows. It is widely accepted that the sophisticated simulation software, used for designing safety measures, needs as highly accurate input data as possible. Therefore these close-range remote sensing methodologies are ideal for producing such datasets.

References

Bernard, T.G.; Lague, D.; Steer, P. Beyond 2D landslide inventories and their rollover: synoptic 3D inventories and volume from repeat lidar data. *Earth Surface Dynamics.* 2021, 9, 1013-1044.

Panagiotopoulou, S.; Erkeki, A.; Antonakakis, A.; Grigorakakis, P.; Protopapa, V.; Tsiostas, G.; Vlachou, K.; Vassilakis, Emm. Evaluation of Network Real Time Kinematics contribution to the accuracy/productivity ratio for UAS-SfM Photogrammetry. *In Proceedings of the 2020 European Navigation Conference (ENC)*, Dresden, Germany, 23-24 November 2020.

Vassilakis, E.; Konsolaki, A. Quantification of cave geomorphological characteristics based on multi source point cloud data interoperability. *Zeitschrift für Geomorphologie*. 2022, 63, 265-277.

UNVEILING COASTAL CLIFF VULNERABILITIES BY INTEGRATING LIDAR, UAS, AND AI TECHNOLOGIES. CASE STUDY: NAVAGIO SHIPWRECK BEACH, ZAKYNTHOS (GREECE)

ALIKI KONSOLAKI [1], EMMANUEL VASSILAKIS[1], EFSTRATIOS KARANTANELLIS[2], EVELINA KOTSI[1], EFTHIMIOS LEKKAS[1]

[1] *National and Kapodistrian University of Athens, Greece, alikikons@geol.uoa.gr*

[3]*University of Michigan, Ann Arbor, USA, stratis@umich.edu*

Introduction

Coastal cliffs are one of the cases of steep terrains naturally vulnerable to a range of erosional processes, with rockfalls emerging as one of the most prevalent and hazardous. Although predicting rockfall occurrences remains challenging due to multi-faceted triggering factors such as extreme weather events, seismic activity, erosion, and human actions, technological advancements offer promising avenues for developing more robust and effective risk assessment methodologies. Light Detection and Ranging (LiDAR), photogrammetry from Unmanned Aerial System images, and satellite imagery, coupled with the evolution of artificial intelligence, have revolutionized the field of rockfall assessment by enabling precise detection and quantification of 3D topographic changes, offering insights into rockfall dynamics (Abellán, A., et al. 2010).

Methods

There are many methods applied, considering the advancing study of rockfalls. DEM of Difference (DoD) (Li et al., 2024), Adaptive Cloud-to-Cloud (AC2C) (Huang et al., 2022) and Multiscale Model-to-Model Cloud Comparison (M3C2) (Lague et al., 2013) are some of the most utilized and consistent methods for 3D change detection analyses. The latter as the most insighted has various applications in estimating changes in a 3D spatial environment (DiFrancesco et al.,2020). In relation to the other methods, M3C2 is a direct 3D point cloud comparison, that computes 3D distances along the normal direction of the topographic surface, allowing better capture of subtle changes on steep surfaces (Bernard et al., 2021).

The “U” shaped vertical cliffs of “Navagio” shipwreck in Zakynthos, Greece were chosen as case study for applying the above-mentioned methodology. In a time-frame of three years (2020-2023), multiple UAS surveys and a TLS survey (in 2023) have been carried out, providing us valuable data for the detection of possibly loosened rocks. During the UAS surveys we managed to succeed the high precision Direct Georeferencing (DG), taking advantage of the Network Real Time Kinematics, which does not necessarily require Ground Control Points (GCPs). Moreover, we enhanced the methodology by using the Post Processing Kinematics (PPK) approach, including GNSS permanent station’s RINEX data within the procedure, along with the establishment of pseudo GCPs succeeding a perfect co-registration of the datasets (<5mm).

After the co-registration, we applied the M3C2 algorithm by isolating patches of significant topographic change using the statistical model accounting for point cloud roughness, density, and registration error (Figure 1). The efficiency of this workflow was tested by comparing a UAS and a TLS survey of the same day.

Results

In total, three simulations were performed by applying the M3C2 algorithm: (P1) a UAS-UAS comparison of 2020 – 2023 surveys, (P2) a UAS-TLS comparison of 2020 – 2023 surveys, and (P3) a UAS-TLS comparison of the same period (July 2023). P1 and P2 were registered by Gaussian noise with mean 0 and a standard deviation of 0.04 m and 0.12 m respectively. The point cloud was divided in three segments as the orientation changes significantly. The final spatial level of detection (LoD) based on our data process was 0.2 m meaning all features larger than this LoD are recognizable and valid. The P3 simulation served as a validation procedure, leveraging the high accuracy and detail of the

TLS data to verify the UAS change detection analysis.

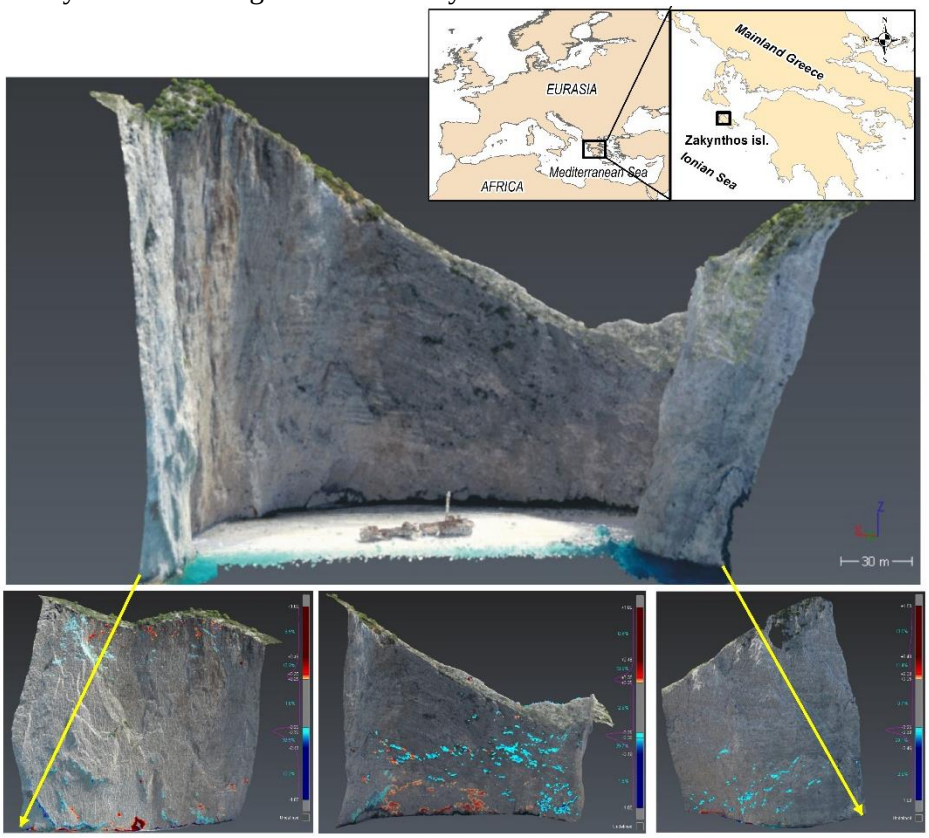

Figure 1. The results of the processing of the Navagio beach cliff with the M3C2 algorithm. The color scale shows the calculated 3D changes, with blue areas indicating erosional areas whereas red areas indicating depositional areas. The bottom row figures represent the three segments.

Conclusion

This study applies cutting-edge methodologies that enhance our understanding of slope stability and monitoring in tectonically active coastal areas. The presented approach can be a useful, efficient and transferable tool that can significantly benefit risk-mitigation efforts for the design of protection measures by expanding applications to other sites with similar geological and geomorphological properties worldwide.

References

Abellán, A., Calvet, J., Vilaplana, J. M., and Blanchard, J. Detection and spatial prediction of rockfalls by means of terrestrial laser scanner monitoring. *Geomorphology*, 2010. 119(3), 162-171.

DiFrancesco, P.-M., Bonneau, D., and Hutchinson, D. J. The Implications of M3C2 Projection Diameter on 3D Semi-Automated Rockfall Extraction from Sequential Terrestrial Laser Scanning Point Clouds. *Remote Sensing*, 2020. 12(11), p. 1885.

Huang, H., Ye, Z., Zhang, C., Yue, Y., Cui, C., and Hammad, A. Adaptive Cloud-to-Cloud (AC2C) Comparison Method for Photogrammetric Point Cloud Error Estimation Considering Theoretical Error Space, *Remote Sensing,* 2022. 14(17), p. 4289.

Lague, D., Brodu, N., and Leroux, J.: Accurate 3D comparison of complex topography with terrestrial laser scanner: Application to the Rangitikei canyon (NZ), *ISPRS J. Photogramm. Remote Sens.*, 2013. 82, 10–26.

Li, P., Li, D., Hu, J., Fassnacht, F. E., Latifi, H., Yao, W., Gao, J., Chan, F. K. S., Dang, T., and Tang, F. Improving the application of UAV-LiDAR for erosion monitoring through accounting for uncertainty in DEM of difference. *CATENA*, 2024. v. 234, p. 107534.

ADVANCING LANDSLIDE MAPPING: INTEGRATING MACHINE LEARNING AND OBJECT-BASED ANALYSIS WITH UAV-DERIVED DATA

EFSTRATIOS KARANTANELLIS [1], VASSILIS MARINOS [2], EMMANUEL VASSILAKIS [3]

[1] *University of Michigan, USA, stratis@umich.edu*

[2] *National Technical University of Athens, Greece, marinosv@civil.ntua.gr*

[2] *National and Kapodistrian University of Athens, Greece, evasilak@geol.uoa.gr*

Introduction

We find ourselves in an ever-evolving environment, where the past fifty years have marked a pivotal moment in scientific thinking. This shift is particularly evident in the scientific approach to analyzing natural-induced hazards. Geohazards annually contribute significantly to loss of life and property, with mass movements standing out as widespread occurrences globally. The study of extreme events and their repercussions on landscape stability is a critical area in environmental research. In this paper, we showcase the advancements in the integration of Artificial Intelligence (AI) and Remote Sensing (RS) for improved landslide assessments, leveraging developments in Earth Observation (EO) data analysis. We highlight the application of Object-Based Image Analysis (OBIA), which have not traditionally been tailored for landslide studies but have proven effective in this context. The framework enables the translation of complex real-world landslide scenarios into analyzable objects through segmentation algorithms, applying subsequent classifications via rule-based or advanced Machine Learning (ML) algorithms. We demonstrate how ML has the potential to revolutionize geoscience data analysis and address major societal concerns presented by landslide hazards by tapping into the vast reserves of geoscience data. ML algorithms, particularly Random Forest (RF), integrated into an Object-Based Image Analysis (OBIA) workflow, demonstrated adaptability for sub-zone landslide mapping on a local scale. Given the increasing frequency of extreme meteorological events driven by climate change, the integration of UAV datasets, Structure from Motion (SfM), and advancements in OBIA and AI can respond effectively by enabling precise and accurate analysis of landslide and rockfall failures. Our results affirm that rotational landslides and their thematic sub-zones were adequately recognized and mapped through the ML procedure.

Methods

Understanding the large deviations in landslide mechanisms is of paramount importance for providing long-term landslide mitigation in a region. However, this task is challenging and quite poorly addressed in the literature because landslide failures are often highly variable in space and time due to their stochastic and episodic characteristics. While engineering geological assessment is a fundamental task in landslide characterization, unstable slopes can pose a high level of risk to geoscientists employing traditional field reconnaissance (landslide mapping, discontinuity measurements, Schmidt hammer test, etc.) due to difficult accessibility and safety concerns. In addition to the exploitation of an optimal data collection and analysis procedure for landslide characterization, the presented study also addressed methodological questions related to the reproducibility and efficiency of the developed object-based workflows (figure 1) for different landslide scenarios, considering the sensitivity of the selected attributes (morphometric, spectral, contextual, and spatial) (Karantanellis et al., 2021).

The two created dataset structures were processed distinctly following the same workflow for segmentation and classification during object-based analysis. Two major challenges exist in the OBIA process: first, the determination of optimal parameters for image segmentation, and second, the selection of suitable features and thresholds for classification. Consequently, the selection of appropriate segmentation parameters is a challenging task, and they are often estimated subjectively through trial and error. Several studies have proposed automated approaches for objectively estimating the scale parameter (SP) value for multi-resolution segmentation (MRS). The Estimation of Scale Parameter 2 (ESP 2) (Drăguţ et al., 2014) was employed to identify statistically relevant object levels for a set of input layers by evaluating the relative changes in local variance for a predefined scale spectrum. Second, trial and error tests based on expert's prior site knowledge have been explored on both input structures

("RGB" and "RGB+DSM").

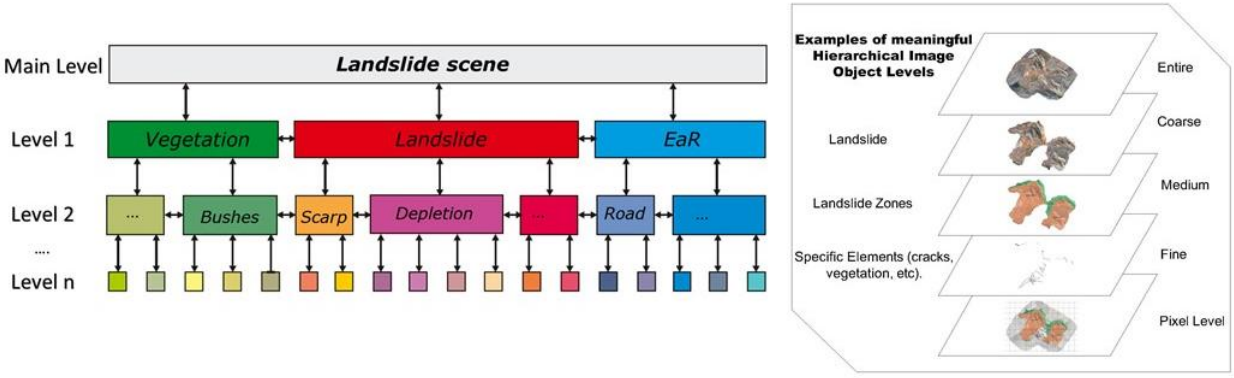

Figure 1. Object-based hierarchical landslide levels for segmenting and classifying datasets.

Results

The combination of object-based analysis and knowledge-based classification provided a robust framework for landslide classification, as it enabled the extraction of both spectral semantic and spatial features, allowing for a more comprehensive characterization of the landslide sites. This comprehensive approach contributes to a more accurate and detailed understanding of the landslide phenomena, improving the overall quality of the classification results. To assess the transferability of the developed workflow, the most efficient classification configuration determined from the previous tests (input data structure: RGB+DSM, SP: 100, and shape/color weight: 0.6) was applied to another landslide, which constitutes a similar failure in the wider region under the same landslide characteristics as the previous one (geological, lithological, failure type). The test site is a landslide failure that occurred in an open-pit mine of coal in northern Greece. Transferability is critical in image classification, and it was conducted to test its efficiency in the proposed study. To ensure consistency in the implementation approach, the study applied identical object features and processes for both segmentation and classification. Considering the extracted F1 metrics, the RF model for the RGB+DSM structure illustrated the best classification agreement.

Conclusion

Landslide phenomena represent natural scenes of complex and heterogeneous character. Such natural processes can be better understood by analyzing them with OBIA as this approach mimics the way how humans recognize patterns. In conclusion, this study employed a novel approach for landslide classification using OBIA and ML techniques. The selection of an appropriate method, i.e. an expert-based or ML approach, depends on the availability of training data and the scope of the study. Expert-based methods are more flexible and adaptive for site-specific landslide mapping than ML, which requires a large amount of training data. This suggests that the knowledge-based approach can be applied to similar failure mechanisms. By using OBIA for site-specific landslide assessment, sub-zones of rotational landslides could be effectively identified with high precision. A limitation is the need for prior knowledge of the site under investigation to optimally adapt the ruleset. Future research should focus on improving automated sub-zone classification for different landslide types. In addition, the integration of deep learning and OBIA for landslide susceptibility mapping using UAV datasets is highly proposed for future consideration.

References

Drăguţ L., Csillik O., Eisank C., Tiede D., "Automated parameterisation for multi-scale image segmentation on multiple layers", ISPRS Journal of Photogrammetry and Remote Sensing, Volume 88, 2014, Pages 119-127, ISSN 0924-2716, https://doi.org/10.1016/j.isprsjprs.2013.11.018.

Karantanellis E., Marinos V., Vassilakis E., and Hölbling D.. 2021. "Evaluation of Machine Learning Algorithms for Object-Based Mapping of Landslide Zones Using UAV Data" *Geosciences* 11, no. 8: 305. https://doi.org/10.3390/geosciences11080305

ENVIRONMENTAL SEISMOLOGY WITH AI

WEI-AN CHAO [1], MING-WAN HUANG [2], COLLAB RESEARCH GROUP [1]…

[1] *Department of Civil Engineering, National Yang Ming Chiao Tung University, Hsinchu 30093, Taiwan vvnchao@nycu.edu.tw*

[2] *He Yu Engineering Consultant Co. Ltd., Taichung 407201, Taiwan, mwhuang05@gmail.com*

Introduction

A seasonal climate, frequent typhoon and high earthquake activity links to interaction between the evolution of mountain landscape and the physical/chemical erosion processes is an important scientific issue in Global, especially for the active orogenic belt region. Recently, the environmental seismology has been widely applied to study the surface processes, such as landslide, debris flow, rockfalls and fluvial processes, which would be helpful to clarify the aforementioned scientific issue. This study presents four topics about the environmental seismology using AI algorithms: (1) Rapid coseismic landslide susceptibility assessment using Newmark analysis and decision-tree (DT) algorithm, (2) An automatic machine-learning classifier using riverine seismic signals: flooding, debris flooding and debris flow, (3) Seismic classifier by deep neural network (DNN) for early warning of post-failure landslides and (4) A wavelet scattering network using seismic records of a single station for roadside rockfall recognition. Aforementioned studies not only provide a better understanding of earth surface processes in the context of climatic and tectonic forcing but also reduce the social impact of of geohazards.

Methods

Decision Tree (DT, Ahmadi et al., 2018) algorithms is a supervised machine-learning model with simplicity, flexibility and high interpretability, which are adopted to train two DT models: coseismic landslide susceptibility model and a classifier of water-and-sediment events. Five features (peak ground acceleration, peak ground velocity, epicentral distance, source-to-station azimuth, strike) and two labels (YES: landslide, NO: non-landslide) for coseismic landslide model. For clarifying water-and-sediment events (FD: flooding, DFD: debris flow flooding, DF: debris flow), peak value of power spectral density and signal-to-noise ration are crucial parameters for source recognition.

In case of DNN model for early warning of post-failure landslides, VGG16 architecture (Simonyan and Zisserman, 2015), which comprising 16 convolution layers and 3 dense layers, was used. 224 × 224 pixel RGB images are created by combining two 112 × 224 RGB single-station spectrogram as model inputs. The convolutional layers used a fixed filter size of 3 × 3 pixels with a stride of 1 pixel. Spatial pooling was performed using max pooling with a 2 × 2 pixel window and a stride of 2. We replaced the flattened layer with global average pooling. A softmax activation function is used for the final layer, while all other layers used the rectified linear unit (ReLU) activation function. For training, we set the epoch to 150, batch size to 128, learning rate to 0.001, and stochastic gradient descent (SGD) as the optimizer.

Finally, a scattering network (Seydoux et al., 2020) performs convolution and pooling on the three-component seismic records to extract multiscale wavelet scattering coefficients. For feature extract, the pricipal components analysis (PCA) is used. Subsequently, we cluster the primary features using unsupervised learning algorithm of K-means. Cluster events are eathquake, rockfall and background noise.

Results

Figure 1 shows two DT models for coseismic landslide and water-and-sediment events, which result the accuracy rate larger than 0.8. Results of the PCA decomposition for primary and secondary features and K-means clustering of six events are shown in Figure 2.

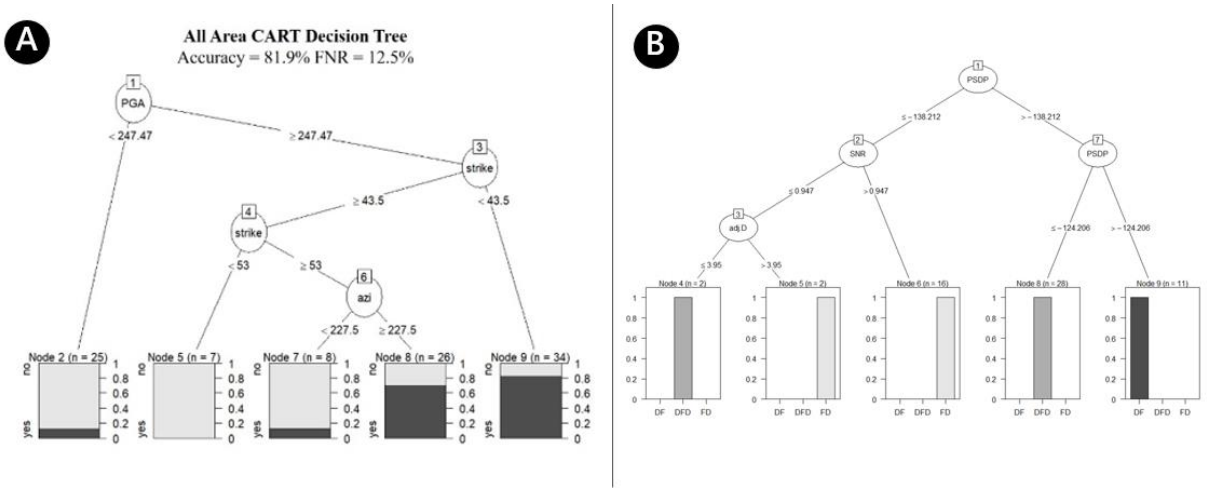

Figure 1. Resulted DT models of (A) coseismic landslide and (B) water-and-sediment events.

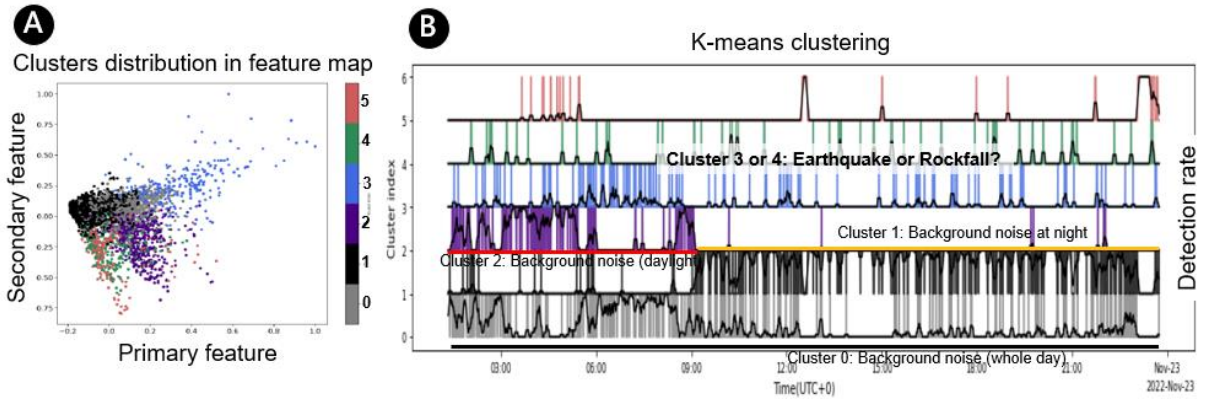

Figure 2. (A) Map of primary and secondary features based on scattering coefficients. (B) K-means result obtained from one-day single seismic station with detection rate for each of the 6 clusters.

Conclusion

Both of supervised and unsupervised machine-learning algorithms applied this study can provide information such as seismic source identification and coseismic landslide prediction, which would be very helpful for geohazard early warning and monitoring system.

References

Ahmadi, E.; Weckman, G. R.; Masel, D. T. Decision making model to predict presence of coronary artery disease using neural network and C5. 0 decision tree. *Journal of Ambient Intelligence and Humanized Computing*. 2018, 9, 999-1011. https://doi.org/10.1007/s12652-017-0499-z

Seydoux, L.; Balestriero, R.; Poli, P.; Hoop, M.; Campillo, M.; Baraniuk, R. Clustering earthquake signals and background noises in continuous seismic data with unsupervised deep learning. *Nature Communications*. 2020, 11:3972, https://doi.org/10.1038/s41467-020-17841-x.

Simonyan, K.; Zisserman, A. Very deep convolution networks for large-scale image recognition. Published as a conference paper at ICLR 2015.